João Antônio Pires Alves

A deterministic and stochastic analysis of wind turbines

TESE DE DOUTORADO

DEPARTAMENTO DE ENGENHARIA MECÂNICA

Programa de pós-graduação em Engenharia Mecânica

Rio de Janeiro
March 2016

Pontifícia Universidade Católica
do Rio de Janeiro

João Antônio Pires Alves

A deterministic and stochastic analysis of wind turbines

TESE DE DOUTORADO

Thesis presented to the Programa de Pós-Graduação em Engenharia Mecânica of the Departamento de Engenharia Mecânica do Centro Técnico Científico da PUC–Rio, as partial fulfillment of the requirements for the degree of Doutor em Engenharia Mecânica.

Advisor: Prof. Rubens Sampaio Filho

Rio de Janeiro
March 2016

Pontifícia Universidade Católica
do Rio de Janeiro

João Antônio Pires Alves

A deterministic and stochastic analysis of wind turbines

Thesis presented to the Postgraduate Program in Engenharia Mecânica of the Departamento de Engenharia Mecânica do Centro Técnico Científico da PUC–Rio, as partial fulfillment of the requirements for the degree of Doutor em Engenharia Mecânica. Approved by the following commission:

Prof. Rubens Sampaio Filho
Advisor
Departamento de Engenharia Mecânica-PUC-Rio

Prof. Hans Ingo Weber
Departamento de Engenharia Mecânica-PUC-Rio

Prof. Roberta de Queiroz Lima
Departamento de Engenharia Mecânica-PUC-Rio

Prof. Thiago Gamboa Ritto
Universidade Federal do Rio de Janeiro

Prof. Fernando Alves Rochinha
Universidade Federal do Rio de Janeiro

Prof. Márcio da Silveira Carvalho
Coordinator of the Centro Técnico Científico
Pontifícia Universidade Católica do Rio de Janeiro

Rio de Janeiro , March 23rd, 2016.

João Antônio Pires Alves

Mechanical Engineer since 1988. Obtained the Master Degree in the field of numerical analysis using Finite Element Method in 1992 at PUC-Rio. Engineer at the Laboratório de Metrolgia Dimensional of the Instituto Nacional de Metrologia, Qualidade e Tecnologia (Inmetro) since 1995, working on improvements of standards calibration and parts measurements using Coordinate Measuring Machine techniques.

Bibliographic data

Pires Alves, João Antônio

A deterministic and stochastic analysis of wind turbines / João Antônio Pires Alves; advisor: Rubens Sampaio Filho — 2016.

172 f. : il. ; 30 cm

1. Tese (Doutorado em Engenharia Mecânica) - Pontifícia Universidade Católica do Rio de Janeiro, Rio de Janeiro, 2016.

Inclui bibliografia

1. Engenharia Mecânica – Teses; 2. Dinâmica;; 3. Carregamento randômico;; 4. Estruturas flexíveis;; 5. Turbinas eólicas.; I. Sampaio Filho, Rubens. II. Pontifícia Universidade Católica do Rio de Janeiro. Departamento de Engenharia Mecânica. III. Título.

CDD: 621

To my wife and our children.

Acknowledgments

Above all, the author must to thank to his wife for her understanding and love, as well as, to his parents who have always encouraged and supported him sometimes facing great difficulties. He is also grateful to all colleagues from Instituto Nacional de Metrologia, Qualidade e Tecnologia - Inmetro, particularly Marcos M. de Souza, José C. V. de Oliveira, Paulo R. G. Couto, Luis H. Paraguassu, Luis H. B. Vieira, Wellington S. Barros, Davi A. Brasil, Dimas B. Teixeira and Renato N. Teixeira. Also, many thanks to Carlos Eduardo Gonzales Baldi.

The author would like to express his gratitude to all of those professors who, since the beginning of his student life, inspired and contributed in a great amount to his formation. It is not possible to list all of them but they are fully represented by talented people like Prof. Carlos Alberto Almeida, Prof. José L. de França Freire, Prof. Hans I. Weber, Prof. Maurício N. Frota, Prof. Ivan F. M. de Menezes, Prof. Márcio da Silveira Carvalho, Prof. Luiz F. A. Azevedo, Prof. Arthur M. B. Braga and Prof^a. Roberta de Q. Lima from PUC-Rio. The author is specially grateful to Prof. Rubens Sampaio Filho and would like to express his admiration and respect. His comprehensive knowledge on Mechanics, a remarkable talent to transmit its concepts, his integrity and seriousness (and sometimes, his patience) really counted in the development of this work. It was an honour to take part of his group at the Laboratório de Dinâmica e Vibrações and to have him as advisor.

Finally, the author gratefully acknowledges the support of Pontifícia Universidade Católica do Rio de Janeiro and of the National Institute for Metrology, Quality and Technology - Inmetro.

Abstract

Pires Alves, João Antônio; Sampaio Filho, Rubens (Advisor). **A deterministic and stochastic analysis of wind turbines**. Rio de Janeiro, 2016. 172p. Doctoral Thesis — Departamento de Engenharia Mecânica, Pontifícia Universidade Católica do Rio de Janeiro.

This thesis presents a dynamic analysis of a three-blade wind turbine with tubular cross section under deterministic and stochastic concentrated and distributed loads including those caused by wind and by sea currents. Variations in soil conditions are allowed, being modeled as linear axial and torsional springs installed at the base of the tower. The random loading is due to the action of the wind on the turbine blades. The symmetries involved allow the tower to be modeled as having four separated and superimposed structural behaviors: a beaming spatial (lateral motion), a shaft (torsional) motion and a bar (axial) motion. Finite elements are used for approximating the dynamic of the tower and then a reduced model is constructed using a basis of finite dimension of the structure eigenvectors. The other turbine components, namely, the nacelle, the shaft and the blades are modeled as rigid bodies whose links are imposed by constraints functions. An algorithm based on Newmark method was developed to integrate the system of equations in time. Velocities, accelerations, forces and torques as well as the resulting stresses are obtained for several configurations.

Keywords

Dynamics; Random loads; Flexible structures; Wind turbines.

Resumo

Pires Alves, João Antônio; Sampaio Filho, Rubens. **Uma análise determinística e estocástica de turbinas eólicas**. Rio de Janeiro, 2016. 172p. Tese de Doutorado — Departamento de Engenharia Mecânica, Pontifícia Universidade Católica do Rio de Janeiro.

Este trabalho apresenta uma análise dinâmica de uma turbina eólica com torre tubular e com rotor de três pás sob carregamentos determinísticos e estocásticos, concentrados e distribuídos, dentre eles os provocados pelo vento e por correntes marinhas. Variações nas condições do solo são permitidas sendo simuladas como molas axiais e torcionais lineares instaladas na base da torre. Os carregamentos aleatórios são devidos à ação do vento sobre as pás da turbina. As simetrias envolvidas permitem que a torre seja modelada como quatro elementos estruturais distintos e superpostos: uma viga com movimento espacial (dois movimentos laterais independentes), um eixo (movimento de torção) e uma barra (movimento axial). Elementos finitos são utilizados para a aproximação da dinâmica da torre, sendo então construído um modelo reduzido, utilizando uma base de dimensão finita com autovetores da estrutura. Os demais componentes da turbina, nacele, eixo e pás são modelados como corpos rígidos. Todos os componentes são agrupados e para modelar seus vínculos são impostas equações de restrição. Um algoritmo baseado no método de Newmark foi desenvolvido para integrar o sistema de equações no tempo. Velocidades, acelerações, forças e torques são obtidos para diversas configurações.

Palavras–chave

Dinâmica; Carregamento randômico; Estruturas flexíveis; Turbinas eólicas.

Contents

List of Figures

List of Tables

Nomenclature

$[\bar{\bar{H}}]$	Eigenvectors matrix
$[\bar{G}]$	Matrix equal to $2[\bar{E}]$
$[\mathbb{J}_h]$	Derivative of $\{\mathbb{G}_h\}$ with respect to $\{\breve{q}\}$
$[\mathbb{J}_{nh}]$	Derivative of $\{\mathbb{G}_{nh}\}$ with respect to $\{\breve{q}\}$
$[\mathbb{K}_h]$	Overall scale factors matrix
$[\mathbb{P}_h]$	Overall penalty factors matrix
$[\mathbb{P}_{nh}]$	Overall non-holonomic penalty matrix
$[\mathfrak{H}]$	Triangular matrix resulting for decomposition of $[S^0]$
$[\mathfrak{K}_{red}]$	Tangent matrix for reduced model
$[\mathrm{J}_b]$	Tensor of inertia of a body
$[\mathtt{J}_{tip}]$	Total matrix of inertia at the tip of the tower
$[\tilde{\mathbb{J}}_{nh_{red}}]$	Approximated derivative of the non-holonomic constraints for reduced model
$[\tilde{\mathbb{M}}_{red}]$	Approximated mass matrix for reduced model
$[A_b]$	Transformation matrix for a body
$[B_b]$	Matrix equals to $[\frac{\partial}{\partial\{\Theta_b\}}[A_b]\{\bar{r}_b\}]$
$[C^e]$	Element damping matrix
$[C_t]$	Tower damping matrix
$[E]$,$[\bar{E}]$	Matrices that compose matrix $[A]$ ($[A] = [E][\bar{E}]^T$)
$[G]$	Matrix equal to $2[E]$
$[H]$	Shape matrix for finite element formulation
$[H^e]$	Element interpolation matrix
$[I]$	Identity matrix
$[J_h]$	Derivative of the holonomic constrain vector with respect to $\{\mathrm{q}\}$
$[J_{nh}]$	Derivative of the non-holonomic constrain vector with respect to $\{\dot{q}\}$
$[K^e]$	Element stiffness matrix
$[k_h]$	Holonomic scale factor matrix for a body
$[K_t]$	Tower stiffness matrix

$[M^e]$	Element mass matrix
$[M_b]$	Mass matrix for body b
$[M_n]$	Nacelle mass matrix
$[M_s]$	Shaft mass matrix
$[M_t]$	Tower mass matrix
$[m_{\Theta\Theta}]$	Sub-matrix of body mass matrix $[M_b]$
$[M_{b_i}]$	Blade i mass matrix
$[m_{R\Theta}]$	Sub-matrix of body mass matrix $[M_b]$
$[m_{RR}]$	Sub-matrix of body mass matrix $[M_b]$
$[m_{RU}]$	Sub-matrix of body mass matrix $[M_b]$
$[m_{UU}]$	Sub-matrix of body mass matrix $[M_b]$
$[p_h]$	Holonomic penalty factor matrix for a body
$[R^0(\tau)]$	Cross correlation matrix
$[S^0]$	Cross spectral density matrix for a Gaussian stationary random process
$\alpha_b(r)$	Angle of attack at r position
$\bar{l}$	Length scale for coherence
$\bar{V}$	Body volume
Δp	Drop in pressure
δW	Total increment of virtual work
δW_e	Total increment of virtual work made for external forces
δW_i	Total increment of virtual work made for the elastic forces
$\epsilon_{xx}(x,y,z), \gamma_{xy}(x,y,z)$	Axial and shear strains
κ_y, κ_z	Shape factors
$\lambda_b(r)$	Speed ratio at r position
λ_b	Tip speed ratio
$\mathbb{K}_{nh}$	Overall non-holonomic scale factor matrix
Ω	Rotor speed
ω_a	Rotational speed of the wind
$\phi_i(x), \psi_i(x)$	i^{th} elements of the base of the eigenvector functions

ρ	Density of the tower
ρ_a	Density of the air
ρ_f	Density of the fluid
$\sigma_b(r)$	Solidity at r
Coh	Coherence function
f	Frequency
I	Turbulence intensity
l	Length scale for spectrum function
θ_{b_0}	Blade pitch
$\theta_b(r)$	Blade pitch at r position
Θ_i	Euler parameters ($i = 0, \cdots, 3$)
ϑ	Angle for body positioning
$\{\bar{\bar{U}}(t)\}, \{\dot{\bar{\bar{U}}}(t)\}, \{\ddot{\bar{\bar{U}}}(t)\}$	Coefficients related to reduced model and their first and second time derivatives
$\{\bar{\Omega}\}$	Angular velocity represented with respect to the body frame
$\{\bar{F}(x,t)\}$	Internal force acting on the beam
$\{\bar{r}_b\}$	Position vector of any point of a body relative to the body frame and represented with respect to it
$\{\bar{T}(x,t)\}$	Internal torque acting on the beam
$\{\bar{v}\}_i, w_i$	i^{th} Eigenvector and eigenvalue
$\{\check{q}\}$	Overall generalized coordinates vector
$\{\dot{\Lambda}_{nh}\}$	Overall vector of Lagrange multipliers for non-holonomic constraints
$\{\dot{\lambda}_{nh}\}$	Lagrange multiplier vector for non-holonomic constraints
$\{\dot{\tilde{\Lambda}}_{nh}\}$	Approximated overall Lagrange multiplier for non-holonomic constraints
$\{\dot{q}_0\}$	Initial velocity vector of the generalized coordinates
$\{\Lambda_h\}$	Overall vector of Lagrange multipliers for holonomic constraints
$\{\lambda_h\}$	Lagrange multiplier vector for holonomic constraints
$\{\mathbb{G}_h\}$	Overall vector for holonomic constraints
$\{\mathbb{G}_{nh}\}$	Overall vector for non-holonomic constraints

$\{\mathbb{Q}\}$ Overall generalized forces vector

$\{\mathbb{Q}_d\}$ Overall generalized damping forces vector

$\{\mathbb{Q}_e\}$ Overall generalized external forces vector

$\{\mathbb{Q}_k\}$ Overall generalized elastic forces vector

$\{\mathbb{Q}_v\}$ Overall force vector due to the quadratic velocities

$\{\Omega\}$ Angular velocity represented with respect to the inertial frame

$\{\Omega_{op}\}$ Rotor operational angular speed

$\{\theta\}, \{\dot{\theta}\}, \{\ddot{\theta}\}$ Beam cross sections rotation, ang. velocity and ang. acceleration vectors

$\{\tilde{\tilde{q}}\}$ Overall approximated vector of generalized coordinates

$\{\tilde{\Lambda}_h\}$ Approximated Lagrange multiplier for holonomic constraints

$\{\tilde{\mathbb{Q}}_{d_{red}}\}$ Approximated generalized forces vector due to the damping forces for reduced model

$\{\tilde{\mathbb{Q}}_{e_{red}}\}$ Approximated generalized forces vector due to the external forces for reduced model

$\{\tilde{\mathbb{Q}}_{k_{red}}\}$ Approximated generalized forces vector due to the flexibility for reduced model

$\{\tilde{\mathbb{Q}}_{v_{red}}\}$ Approximated generalized forces vector due to the quadratic velocities for reduced model

$\{\tilde{q}_\Lambda\}$ Approximation for the overall vector of generalized coordinates including Lagrange multipliers

$\{\tilde{q}_{red}\}$ Approximated vector for reduced model

$\{F(x,t)\}$ External concentrated force vector in cross section

$\{F(x,t)\}$ External concentrated force vector in the beam cross section

$\{f(x,t)\}$ Total external distributed load vector

$\{F^e\}$ External force in element

$\{F_t\}$ External nodal forces acting in the tower

$\{f_f(x,t)\}$ Distributed load vector due to the fluid interaction

$\{f_o(x,t)\}$ Other distributed load vector

$\{N_t\}]$ Nonlinear forces due to the fluid

$\{q(t_0)\}, \{\dot{q}(t_0)\}$ Initial conditions in generalized coordinates

$\{q\}$ Vector of generalized coordinates

$\{q_0\}$ Initial displacements vector of the generalized coordinates

$\{q_\Lambda\}$ Overall vector of generalized coordinates including Lagrange multipliers

$\{Q_d\}$ Generalized damping force vector

$\{Q_e\}$ Generalized external force vector

$\{Q_k\}$ Generalized elastic force vector

$\{Q_v\}$ Generalized force vector due to the quadratic velocities

$\{Q_{c_h}\}$ Initial reaction vector due to the holonomic constraints

$\{Q_{c_{nh}}\}$ Initial reaction vector due to the non-holonomic constraints

$\{Q_R^T, Q_\Theta^T, Q_U^T\}^T$ Generalized force

$\{r\}$ Position vector of any point of a body

$\{r^*\}$ Residue vector

$\{r_{red}^*\}$ Residue vector for reduced model

$\{R_b\}$ Position vector of the origin of body frame

$\{T(x,t)\}$ External concentrated torque acting in the beam cross section

$\{U(t)\}, \{\dot{U}(t)\}, \{\ddot{U}(t)\}$ Nodal displacement, velocity and acceleration vectors

$\{U^e\}$ Element displacement vector

$\{u_a, v_a, w_a\}^T$ Components of the local wind velocity

$\{U_{\theta_L}\}(t)$ Vector of the (small) rotations of the section at the tip of the tower

$\{U_{u_L}(t)\}$ Displacement vector of the node at the tip of the tower

$\{w(x)\}, \{\dot{w}(x)\}, \{\ddot{w}(x)\}$ Tower central line displacements, velocity and acceleration vectors

A Tower cross section area (tube)

a Axial induction factor

a' Angular induction factor

$A_c(x)$ Full cross section area

A_{sw} Swept area

$c(r)$ Blade chord at r position

C_P Power factor

C_{D_b} Drag coefficient for the blade

C_{D_t} Drag coefficient for the tower

C_{L_b} Lift coefficient for the blade

C_{L_t} Lift coefficient for tower

C_l Added mass coefficient

C_{M_b} Torque coefficient for the blade

C_{Th} Thrust coefficient

c_{we} Weibull scale parameter

$C_y(r)$ Normalized distributed normal force at r position

$C_z(r)$ Normalized distributed tangential force at r position

D Diameter of the tower

E Tower Young's modulus

f Frequency

$F_l(r)$ Prandtl tip loss correction factor

$F_{b_y}(r), F_{b_z}(r)$ Forces acting in the blades (blade frame)

f_{we} Weibull probability density function

G Tower Shear modulus

g_h Holonomic constraint equations

g_{nh} Non-holonomic constraint equations

h_w Height of the water level

$I_{\omega y}$, $I_{\omega z}$ Parameters for the warping shape

$I_{xx}(x)$ Moment of inertia of area with respect to x axis

$I_{yy}(x)$ Moment of inertia of area with respect to y axis

$I_{zz}(x)$ Moment of inertia of area with respect to z axis

K_{sv} St. Venant torsion parameter

k_{we} Weibull form parameter

L Length of the tower

L^* Maximum height of the water level

L_e Length of the finite element

m_{b1}, m_{b2}, m_{b3} Blades masses

m_n Nacelle mass

m_s Shaft mass

m_{tip} Total mass at the tip of the tower

$m_x(x), m_y(x), m_z(x)$ External distributed torques

N_b Number of blades

n_c Number of constraint functions

n_{dof} Number of degrees of freedom for tower model

n_{eig} Number of eigenvectors used in approximation

n_{gc} Number of generalized coordinates

p_l Pressure at left of the plane of rotation

p_r Pressure at right of the plane of rotation

p_∞ Pressure far from the turbine

P_{av} Available power

P_{ex} Extracted power

$p_y(r)$ Normal distributed force at r position

$p_z(r)$ Tangential distributed force at r position

r Radial distance of a point at the plane of rotation with respect to the axis or rotation

S_f Power density function

$T_{b_y}(r), T_{b_z}(r)$ Torques acting in the blade (blade frame)

Th Thrust force

$u_x(x, y, z), u_y(x, y, z), u_z(x, y, z)$ Displacements in any point x, y and z of the tower

v_i Normal vector components

W_f Speed of the fluid

W_w Speed of the water

W_{a_∞} Wind speed far from the turbine

W_{a_l} Speed of the wind at left of the disk

W_{a_r} Speed of the wind at right of the disk

$W_{a_{t_s}}$ Wind speed for t_s minutes

W_a	Wind speed at the plane of rotation
x_0	Terrain roughness parameter
x_1	Height of wind speed measurements
$x_b \ y_b \ z_b$	Coordinates with respect to the body frame

...Yes, and how many times can a man turn his head
And pretend that he just doesn't see?
The answer, my friend, is blowin' in the wind
The answer is blowin' in the wind...

Bob Dylan, *Blowin' in the wind.*

1
Introduction

The proposal of this work is to study the dynamic behavior of a horizontal three-bladed wind turbine (HAWT), considering both deterministic and stochastic loading and to contribute with an algorithm for wind turbine evaluations using multi-body approximation. Two types of loading are possible: concentrated forces and torques (deterministic and stochastic), which, in a simplified way, simulates the wind and deterministic water loading. Although simplified, it is sufficiently comprehensive so that it can be a good basis for further studies and improvements aiming the understanding and development of such devices. Wind turbines are seemingly simple at a first glance, but are indeed challenging from the stand point of engineering. Considering the loading, for example, the action of the wind is far from being simple as it changes in intensity and direction at random. Considering the instantaneous variations of the wind (originated from the turbulence near the blades), it is known that its assessment is highly complex and crucial for predicting the life of various components of the system, especially the rotor and blades. So, in general, the action of the wind on the blades (and also on the tower and nacelle) is random and can be modeled as a set of stochastic processes. The action of wind on the blades causes twisting and bending. That loads are transmitted through the shaft to engine and to structure and also has a random nature. Besides, when the turbine is installed offshore the action of the tides, currents and waves load the tower and contribute to the complexity of the analysis. This is an ancient idea that still keeps challenging nowadays.

In order to achieve the purpose, in Chapter 2, some historical and general aspects on wind turbines are explored together with a bibliographic revision. The general dynamic formulation of rigid and flexible bodies is discussed in Chapter 3 as the base to formulate the whole turbine. The tower is considered a flexible tube, then, a general model for its structural analysis is obtained, using variational formulation and, then, the dynamics is approximated using the eigenvectors of the structure. Details of how the bodies are assembled imposing constraint functions are also discussed there, as well as the strategy for finding an approximating solution. Chapter 4 presents the models for deterministic and random wind and water forces that act on the turbine. Some aerodynamics related to the interaction between wind and blade are discusses in detail.

In Chapter 5, the results for some simulations are presented and discussed. In Chapter 6, the conclusions about the work are presented.

2
Wind energy

2.1
General aspects

Energy and momentum are contained in the wind and in the case of using wind turbines for generating electricity, the energy recovery occurs by transferring them to the blades that move a horizontal (or vertical) shaft which turns an electric generator. Attempts to transform wind energy (mechanical energy) into electrical energy begun at the end of the nineteenth century and was intensified during the 1970s, with the advent of the oil crisis. At that time, there was an impulse to develop equipment for wind turbines in a commercial scale, which happened also to other forms of energy generation, such as solar. Since the first commercial wind turbine (connected to the public grid), installed in 1976 in Denmark, the number of installed equipment is growing exponentially. In 1991, the European Wind Energy Association - EWEA had set a goal of installing 4 GW of wind power in Europe by the year 2000 and 11.5 GW by the year 2005. The forecasts were surmounted in years 1996 and 2001, respectively. Then, it was established the target of 40 GW in Europe by the year 2010. Data from the year 2011 showed that the installed capacity in Europe was about 97 GW keeping the rhythm of growing. The countries that showed the best results were Germany and Spain, with about 29 GW and 22 GW, respectively. From that time to now, the development in this area had an astonishing impulse. Wind energy capacity in Europe has been increasing of about 10% a year since 2013, so that the amount of installed power is of about 128.8 GW in European Union nowadays. The countries that keep still leading are Germany, Spain, UK and France with about 39 GW, 23 GW, 12 GW and 9.2 GW, respectively (data from the end of 2014,[1]). In the early 1990s, the United States had an installed power of about 4.6 GW and an annual growth of about 10%. In 2011, USA, Canada and Mexico had together a total installed capacity of about 53 GW (46.9 GW in the USA, 3.3 GW in Canada and 569 MW in Mexico). Data from 2014 presented larger values with a total capacity of about 78.1 GW (about 65.9 GW, 9.7 GW and 2.5 GW in USA, Canada and Mexico, respectively), showing a good advance in this period. Africa and Middle East took part on the race with an installed power of 1.1 GW, with Egypt being the most active on the African continent in early 1990's. Today, the panorama changed

[1] http://www.gwec.net/wp-content/uploads/2015/03/GWEC_Global_Wind_2014_Report_LR.pdf

a little and Morocco and South Africa are the leaders (785 MW and 570 MW, respectively). Asia continues under the leadership of China, which had in 2011, about 82 MW installed. In that year, China increased its production capacity in more than 17 GW, what was about ten times the installed capacity in Brazil at that time. Nowadays, China is from far still the leader. Its installed power is 114.6 GW which is only about 14% less than the total installed power in the whole Europe. India follows China but just with 22.5 MW installed, in the end of 2014. In Brazil, the real interest in using the wind as a source of energy came a little later. In $1976-77$, the Space Activities Institute from the Aerospace Technical Center, IAE/CTA, established a specific procedure for wind data (from anemometers) measured in Brazilian airports. It was verified that the annual mean of 4 m/s at 10 m high already pointed the coast of the Northeast and Fernando de Noronha island as good places to start pilot projects for generating of electricity [4].

In 1987, CHESF - São Francisco Hydro-Electric Company elaborated the study for the wind potential for Northeast [4] using data from anemographic results for a period of 5 years ($1977-1981$) from 81 stations at 10 m high, from Northeast Meteorological Net. Federal University of Paraíba was responsible for the analysis. The largest annual mean velocities found for the height of 10 m were 5.5 m/s and 4.3 m/s, for Macau, RN, and Caetité, BA, respectively. Other regional studies were carried out for mapping the energetic capacity in other Brazilian estates like Minas Gerais, Rio Grande do Sul and Rio de Janeiro [4].

In 1979, it was started the first National Atlas of Survey of the Preliminary Potential Wind by Eletrobrás-CONSULPUC. In 1980s, Eletrobrás and Padre Leonel Franca Foundation continued this work, realizing an extensive meteorological study that included data processing for 389 anemometer stations of 10m high, installed throughout the Brazilian territory and elaborating the first National Wind Potential Atlas [4]. The higher wind speeds happened next the shore and also in some spots with low roughness. Some places with wind speed and 5 m/s and 6 m/s were detected. In the 1990s, measurements in higher towers installed in specific spots for several regions in Brazil were carried out: states of Ceará, Bahia, Minas Gerais and Paraná. In 1998, the Brazilian Wind Energy Center - CBEE, the Federal University of Pernambuco - UFPE, with the support of ANEEL - National Electrical Energy Agency and the Ministry of Science and Technology - MCT, published the first version of the Wind Atlas of the Northeast. This resulted in the publication of the "Wind Potential Panorama" in Brazil. Unfortunately, nowadays the contribution of wind energy in electricity generation is still small compared to the installed capacity

for hydro and fossil fuels. Nevertheless, Brazil is the leader in Latin America followed by Chile with 836 MW. Recent data from Brazilian Association for Wind Energy-ABEEólica [2], Brazil has now 322 wind farms with a capacity of 8.12 GW already producing or in installation. Two of the largest are located in Água Doce, Santa Catarina and in Osorio, Rio Grande do Sul. The region that stands out is the Northeast. Wind maps developed by the Brazilian Wind Energy Center has shown that the area has one of the best resources in the world, having good wind speed, low turbulence and good uniformity [3]. The total potential is estimated in 30 GW [4] and Ceará holds 40% of the country's capacity with 17 farms.

Aiming to enlarge the exploration of new sources of energy, Brazilian government has gradually given incentives aiming to improve the sector. Proinfa (Incentive Program for Alternative Sources of Electric Energy) created by the Law 10.438/2002, implanted, by 2011, a total of 119 projects, among them, 41 related to wind energy (964 MW). This kind of incentive besides of contributing to diversify the Brazilian energetic alternatives, also fomented the generation of 150 thousand new jobs over the country and the industrial development. It is estimated that this investments will indirectly reduct the CO_2 emissions in about 2.5 millions tons eq/year. [5].

A known limitation of wind generation is its "inconsistency" in energy production, although it also occurs in other energy modes such as hydraulic. However, in Brazilian Northeast, wind generation has its peak concomitantly with the period of lower water availability. In this case, the wind power and hydraulic modal are perfectly complementary [6].

The biggest hindrance to the wind energy nowadays is economic. The cost of kW installed is higher than other types of power generation (hydraulic, thermoelectric, etc.) but has reduced significantly in recent decades. As happens with all economic activities, technological developments (advanced transmission systems, better aerodynamics and materials, control strategies in the operation of the turbine, etc.) improve together with the expansion of the production scale, provoking the reduction of costs and providing better performance and reliability for the equipments. This creates the conditions for the competitiveness.

Wind generation has advantaged and disadvantages. The main advantages are:

[2]http://www.portalabeeolica.org.br/index.php/2012-11-23-19-20-59.html
[3]http://www.aneel.gov.br/aplicacoes/atlas/pdf/06-energia_eolica(3).pdf
[4]http://www.brasil.gov.br/sobre/economia/energia/matriz-energetica/energia-eolica
[5]http://www.eletrobras.com/elb/Proinfa
[6]http://www.aneel.gov.br/aplicacoes/atlas/pdf/06-energia_eolica(3).pdf

- It is inexhaustible;
- No residue is generated;
- Versatility;
- Low environmental costs;
- The farms can share the place with others activities;
- Reduces energy dependence on fossil fuels;
- It is in conformance with international protocols (Kioto, e.g.);
- It has the potential to compete with traditional energy sources;
- Free energy once payback period is expired.

The disadvantages are:

- Visual impact;
- Noise from blades;
- Danger to animals (e.g. birds and bats);
- Electro-magnetic interference;

Those disadvantages must be evaluated carefully in order to attenuate their importance in the whole turbine project. The visual impact that one or a set of wind turbines causes to an observer is difficult to quantify due to its subjectivity. Nowadays, the towers are getting bigger and the speed of the rotors getting smaller. Low speeds together with better blade design brought down the noise to reasonable levels, although noise in turbines is not a big problem in offshore installations. Reduction of the blade speed tends to reduce the danger to migratory birds because they can see the blades and avoid them somehow. Anyway, the tendency is to install towers where there is not any intensive animal migration. It must be mentioned that it is possible to quantify somehow the risk of collisions in a given region during the operation [41]. Concerning to electro-magnetic interference, it is a fact and it can be produced and suffered by the electric-electronic components of the turbine. The blade movement also may affects the performance of TV and FM broadcast reception and a variety of navigation systems by obstructing, reflecting or refracting the electromagnetic waves. Modern blades are typically made of synthetic materials which have a minimal impact on the transmission of electromagnetic radiation. Nacelle insulation attenuates the turbine electrical system interference so it is not usually a potential problem on telecommunications. Interferences to mobile radio services are usually negligible. Anyway, preventive and corrective solutions to attenuate those effects are already available or under study [34][7].

2.2 Wind

2.2.1 Origin of the wind

The atmosphere is constituted of air, that is, a mixture of nitrogen, oxygen, and argon mainly as well as water vapor and other gases in smaller quantities. It can be divided into five main layers (troposphere, stratosphere, mesosphere, thermosphere and exosphere). The troposphere contains the water vapor and is the denser part of the atmosphere. The temperature in this layer declines with altitude although phenomena like inversion (when a sublayer of higher temperature can superpose another with lower temperature) may take place. The air movement in troposphere happens due to the difference between the radiation intensity over the planet surface and also due to its rotation. This is a complex movement of mass and energy and processes from the magnitude of thousands of kilometers in which huge masses of air move throughout the globe in periods of several days to local weather systems, whose magnitude range from one to hundreds of kilometers and very short turbulent movements (with a range of few meters and a lifetime of few minutes). At the equator, a low pressure region is created when the air is heated and blows up. Then it is deviated to east due to Coriolis acceleration. When in high altitudes and far from equator, the air masses go down and is deviated to the west due to the Coriolis acceleration and keep moving this way. Same phenomenon happens in other regions, near the poles and in temperate zones, as well. From the north pole, the cold air goes to south in low altitudes bending to the west. On the other hand, warm winds coming from the temperate subtropical high pressure zone make the opposite movement. In south hemisphere, similar phenomena occur. A deeper understanding on this subject can be obtained in [54] and [19].

The sub-layer from ground level to a height of approximately 1 km is called atmospheric boundary layer. Above it, the wind is considered not turbulent and in areas far from the high-pressure and low-pressure zones, the wind is considered only dependent on the horizontal pressure gradient and Coriolis acceleration [19]. Those winds are called geostrophic. On the other hand, the presence of low- or high-pressure regions, make wind to rotate. Those are called gradient wind. In the atmospheric boundary layer, the wind speed increases and turbulence decreases with height. Turbulence is generated in the presence of obstacles like buildings, vegetation and relief. The wind direction also is affected suffering a deviation from horizontal of typically 20^o downwards. Nevertheless, this variation is only noticeable for a height of about 200m from

the ground [19].

2.2.2 Local wind evaluation

The wind speed and direction change all time and its observation is made by using anemometers for quite long period of time (some years). This equipment is positioned at a given hight (x_1= 20m, x_1=50m) collecting data from wind speed and azimuthal direction. Those data may be analyzed in both time and frequency domain. Using the later, a power spectral density function is obtained which can be represented graphically as shown in Figure 2.1. The form of such a curve is typical, all having three zones [19][16]:

- A zone of low frequencies (periods of some days);
- A zone of high frequencies (periods of some seconds to some minutes related to turbulence);
- A zone of little spectral energy (periods between 10 minutes and 1 hour).

The graph depicted in Figure 2.1 shows that there is a very high density for frequencies of about 0.01 $cycle/h$ which correspond to a periods of several days. About 0.1 $cicle/h$, other maximum value happens, that may correspond to daily variations in wind velocity. A noticeable large density is present for lager frequencies (about 60 $cycle/h$ or 1 $cycle/min$). Nevertheless, as mentioned above, there is a region of very low spectral density in the interval of 1 $cycle/h$ to 6 $cycle/h$. This interval, the spectral gap, means that for sampling periods shorter than 1 h low frequencies are not detected and also that for those intervals, the mean of the process does not change in time and the variance is that associated to the turbulence. Also, low and high frequencies signals (long and short terms) are uncorrelated due to this low energy interval. This permits to model the wind speed as a quasi-stationary process defined as sum of a constant value, which represents the mean value of the wind speed in a given period of time plus a random signal representing the turbulence, that is

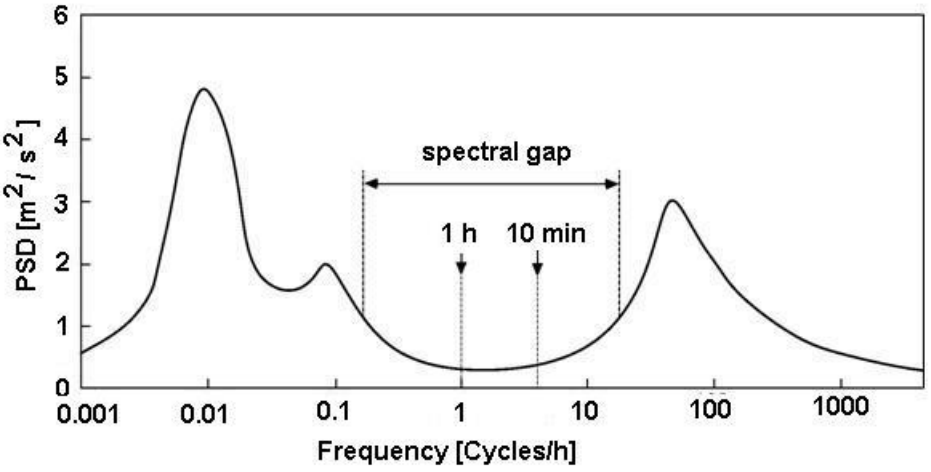

Figure 2.1: Typical power spectrum for horizontal wind component [16]

$$\begin{aligned}
\mathbf{W}_{a_x}(x_1,0,0,t) &= W_{a_x}(x_1) + \mathbf{W}_{a\sigma_x}(x_1,0,0,t) \\
\mathbf{W}_{a_y}(x_1,0,0,t) &= W_{a_y}(x_1) + \mathbf{W}_{a\sigma_y}(x_1,0,0,t) \\
\mathbf{W}_{a_z}(x_1,0,0,t) &= W_{a_z}(x_1) + \mathbf{W}_{a\sigma_z}(x_1,0,0,t)
\end{aligned} \tag{2.1}$$

where $\mathbf{W}_{a_x}(x_1,0,0,t)$, $\mathbf{W}_{a_y}(x_1,0,0,t)$ and $\mathbf{W}_{a_z}(x_1,0,0,t)$ are the total components of the wind velocity vector. $W_{a_x}(x_1)$, $W_{a_y}(x_1)$ and $W_{a_z}(x_1)$ are the horizontal mean wind speed in the interval of time considered at the acquisition height (x_1). $\mathbf{W}_{a\sigma_x}(x_1,0,0,t)$, $\mathbf{W}_{a\sigma_y}(x_1,0,0,t)$ and $\mathbf{W}_{a\sigma_z}(x_1,0,0,t)$ are Gaussian random processes with null mean standard deviation σ_a, modeling the turbulent speeds in three directions. Each period of 10 min to 1 h, depending on the analysis (or any standard recommendation), the turbulence is used for generating $3D$ velocity stochastic vector.

As the wind speeds are sampled at an specific height, two hypothesis are made in order to know the wind behavior in a larger area. First, the mean wind varies only with the height (coordinate x). This is known as the logarithmic wind profile function. Wind velocity vector component $W_a(x)$ is a function of the height from the ground (x) and is given by the following equation [71]:

$$W_a(x) = W_a(x_1)\frac{ln(x/x_0)}{ln(x_1/x_0)} \tag{2.2}$$

where x_1 is the height where the wind speed values were taken (sampled) and x_0 is the parameter relative to the roughness of the terrain and it is considered as size of the characteristic hight where the mean wind speed is null. [19][71]. Figure 2.2 depicts schematically the horizontal wind speed profile $W_a(x)$ and the random component $\mathbf{W}_{\sigma_a}(x,0,0,t)$.

Second, the wind has its own power spectral density and coherence functions. Some are available like von Karman, Davenport or Kaimal. For instance,

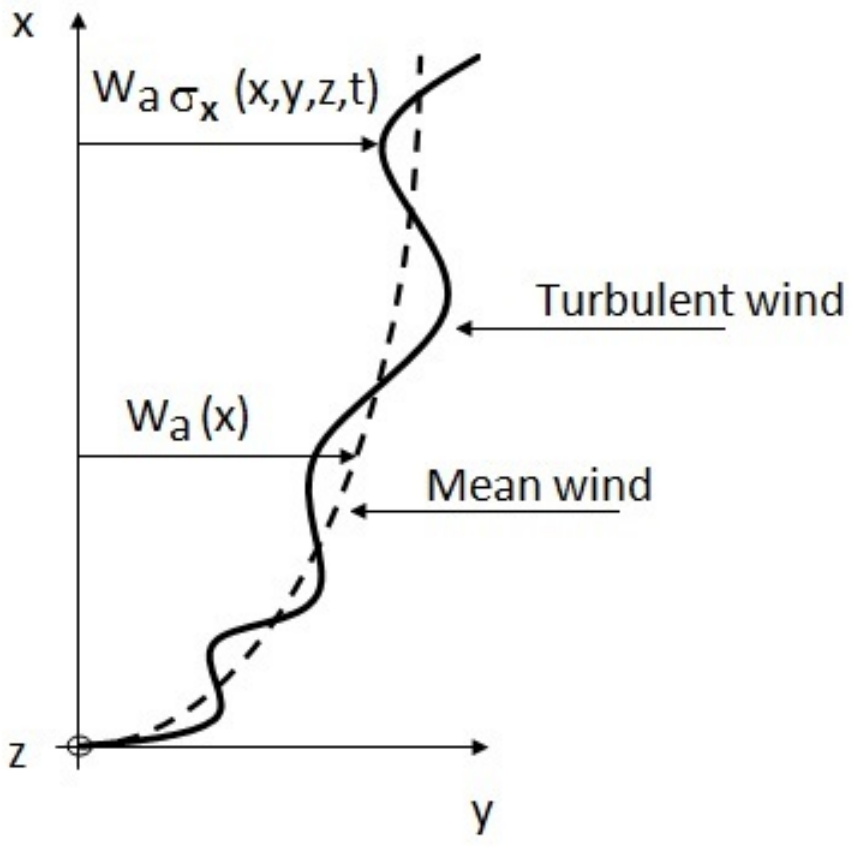

Figure 2.2: Wind speed profile and turbulent wind direction

the Kaimal spectrum [32] [31] is recommended by standard $IEC61400-1$ [71]. In Chapter 4, this approach will be used in order to generate the random processes acting in the rotor swept area.

Collecting the wind speed for a large period of time, mean wind speeds may be calculated for periods of time specified (10 min to 1 h, depending on the standard adopted). The number of those intervals of time, say Δt_w, must be representative of the whole turbine life time. Those values may be organized in a histogram where the mean speeds are plotted against the relative frequency of occurrence. The width of the data interval is in general 1 m/s. Figure 2.3 shows such a typical histogram which gives the relative frequency of any of those intervals Δt_w to have a given speed.

Several distribution were suggested to describe the wind regime given by histograms like that depicted in Figure 2.3, but the Weibull distribution is considered the adequate [16], [23], [71]. This distribution is given by

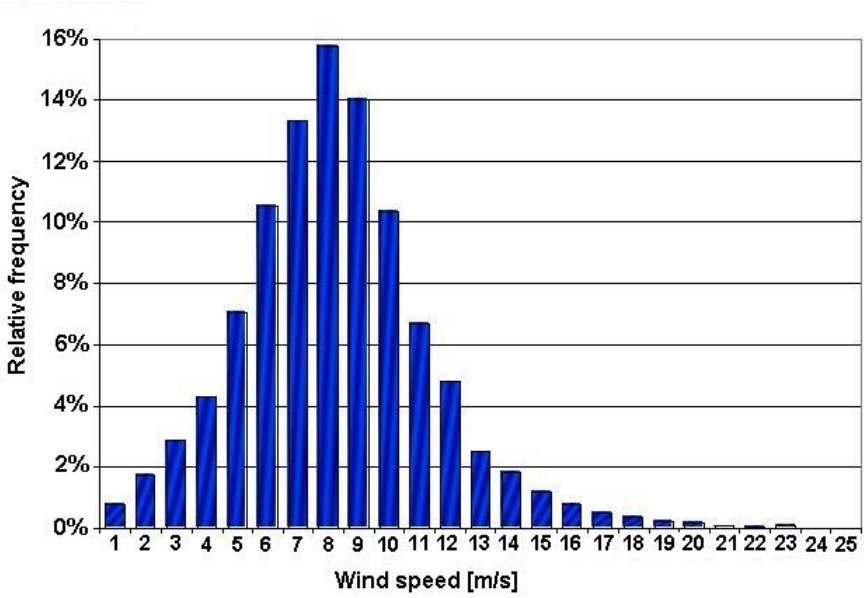

Figure 2.3: Histogram for the wind speed [16]

$$\begin{cases} f_{we\mathbf{W}_a}(W_a) = 1 - e^{-(\frac{W_a}{c_{we}})^{k_{we}}} \\ c_{we} = \frac{\bar{W}_a}{\Gamma(1+1/k_{we})} \\ 0 \leq W_a < \infty \end{cases} \tag{2.3}$$

where W_a is the wind speed, $\bar{W}_a$ is the total averaged wind speed, c_{we} is a scale parameter and k_{we} is a non-dimensional form parameter.

For $k_{we} = 2$, the Weibull distribution becomes a Rayleigh distribution and dependent on a single parameter, the mean value.

2.3 Wind evaluation

The companies interested in the exploration of a specific site need, at first, to get as complete as possible technical information about the intensity and regularity of the wind. This is done by collecting and analyzing wind data of the wind regime for a certain period of time (maybe for some years) before starting a project. Observing the documentation available from 1980s to now related to the wind distribution all over the country, it is noticed a clear improvement in the quality of the information. This is, in part, due to the competitiveness and more strict regulations established by the government which make investors and engineers be more careful with the investment and decisions about technical solutions. More region-specific studies were made in order to get more precise information on specific spots to give to the investors and engineers more comfort to decide. Nowadays, several states in Brazil have already elaborated their own wind map where a very detailed information

about the distribution of the wind can be found.

In order to know the state of the wind in a given place, to begin with, data from several spots over the region is obtained and then, maps as that depicted in Figure 2.4 are elaborated, showing the distribution of annual wind power flux taken all over the region at a specific height (that one is for 50 m height but other distribution can be obtained for other levels, for smaller regions or even for shorter periods [5] [4].

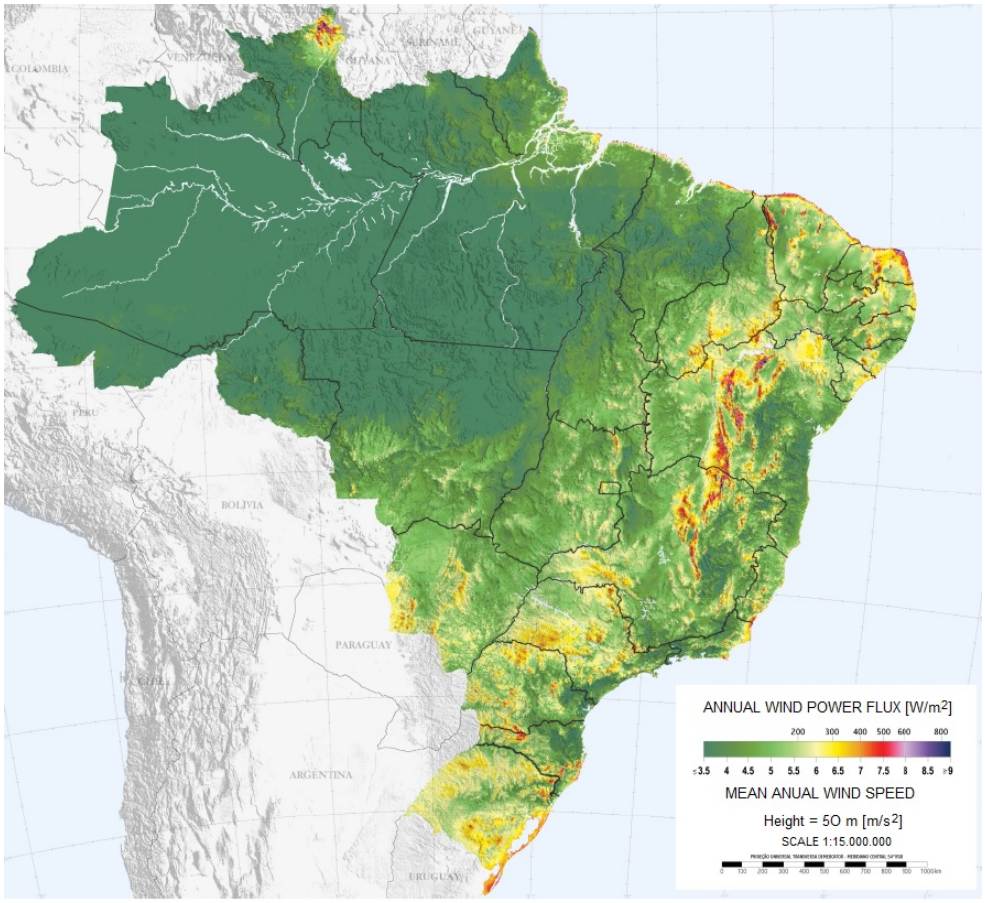

Figure 2.4: Distribution of Wind Potential in Brazil (Adapted from [4])

Other maps and tables containing the main information about the wind characteristics and details about its distribution must be also available like those containing the Weibull parameters. Graphics are also of good use and one of the most common are the wind rose containing the typical distribution for both, direction and speed of the wind in a region. An example is shown in Figure 2.5[7]. It shows that the prevailing wind is South-North direction and just roughly 0.5% of the time, the wind speed is situated between 8.23 m/s and 10.8 m/s and about 5% of the time the speed is situated between 3.09 m/s and 8.23 m/s, in that direction. It is also observed that the wind rarely

[7]https://en.wikipedia.org/wiki/Wind_rose

blows from South-East and that stronger winds (above 10.8 m/s) blows from Northwest-East and West directions but they are relatively rare. Finally, 3.6% of the time, there is no wind. [5][4].

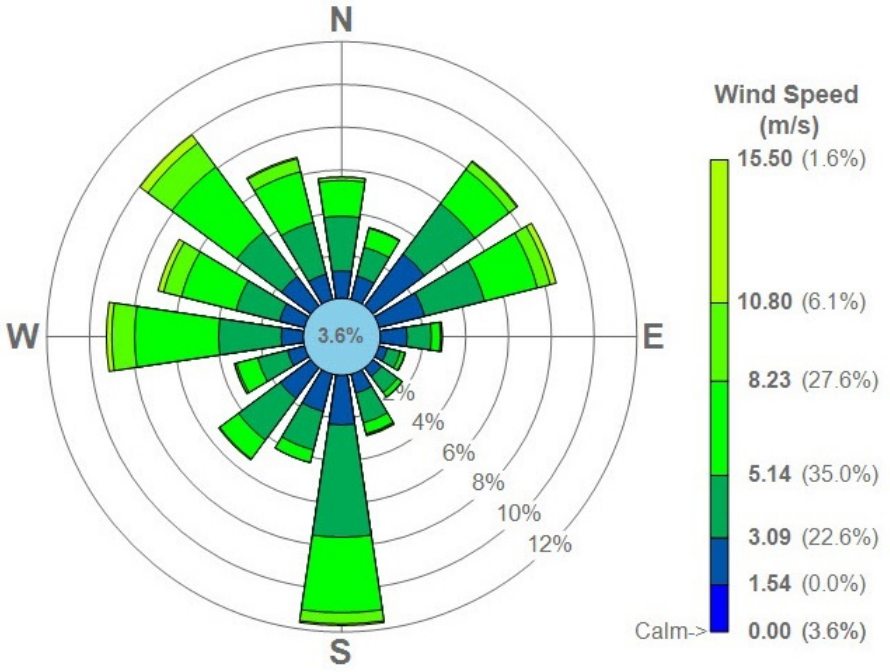

Figure 2.5: Wind regime in a given region

Selecting a place is critical and details are important. It is known from theory (see, for instance, [35]) that the power available from the wind is related to the cube of the wind speed. So a 25% increase in wind speed, almost double the power output.

2.4 Extracting energy from wind

There are basically two principles for extracting energy from wind:

- Using lift forces;
- Using drag forces.

The aerodynamic forces acting in a body are due to only two basic sources, namely, the pressure and the shear distribution over the body surface.

Figure 2.6 shows schematically the action of the wind in an airfoil (first drawing) in which the lift force is predominant. This kind of profile is used in airplanes and also in wind turbines blades. Depending on the relative position between the airfoil and the flow (depending of the angle of attack), the force configuration changes. In case of airfoils used in airplane wings, the goal is the increasing of the lift force and the reduction of the drag force. For wind

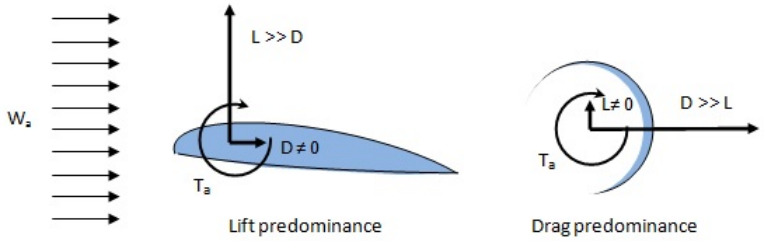

Figure 2.6: Lift and drag forces in solids

turbines, the maximization is focused in the force component in the plane of rotation. Some turbines make use of drag force and the "blade" profile must change in order to maximize this force. Lift force can be present, but marginally. This profile is shown in the right draw in Figure 2.6. Drag devices seem to be the first attempt to extract energy from wind and there is evidence of their usage in ancient mills, some still working, as those in the town of Nashtifan, located in the southern parts of Khorasan Razavi province in Iran (Figure 2.7)[8].

Figure 2.7: Ancient windmills in Iraq

Those windmills have vertical shafts and the wind panels rotate horizontally. In 14th century, the traditional windmill was created. Initially, built with wood but later rock and brick were used. The blades permitted to the air to pass trough and drag forces were important but the concept changed: the blades now moved in a plane perpendicular to the wind direction and its speed became no more limited as happened to drag devices, whose tangential speed is limited to the speed of the wind.

[8]http://www.amusingplanet.com/2014/07/the-ancient-windmills-of-nashtifan.htm2

2.4.1
Vertical and horizontal wind turbines

Vertical axis wind turbines are those whose axis of rotation is vertical. They are closer to the ground and seems to be the ideal for catching lower-speed wind in residential and urban areas. The rotor spins around a vertical axis and the blades can catch wind blowing from any direction. They typically require less maintenance than a horizontal axis wind turbine. There are currently two types of vertical axis wind turbines in production: Darrieus and Savonius. Darrieus wind turbines were designed and patented by Georges Jean Marie Darrieus, a French aeronautical engineer in 1931. They use basically lift forces and originally are formed by two big and slim arched blades as shown in Figure 2.8(a)[9]. In the Figure 2.9(a)[10], in a simplified way, it is explained its principle. Some have wires to stabilization from the tip to the soil, due their flexibility. Those turbines need a small external torque to be put in movement and for this purpose, a low-powered motor is used.

2.8(a): Darrieus turbine 2.8(b): Savonius turbine

Figure 2.8: Darrieus and Savonius turbines

[9]http://energythic.com/view.php?node=201
[10]http://datab.us/i/Darrieus%20wind%20turbine

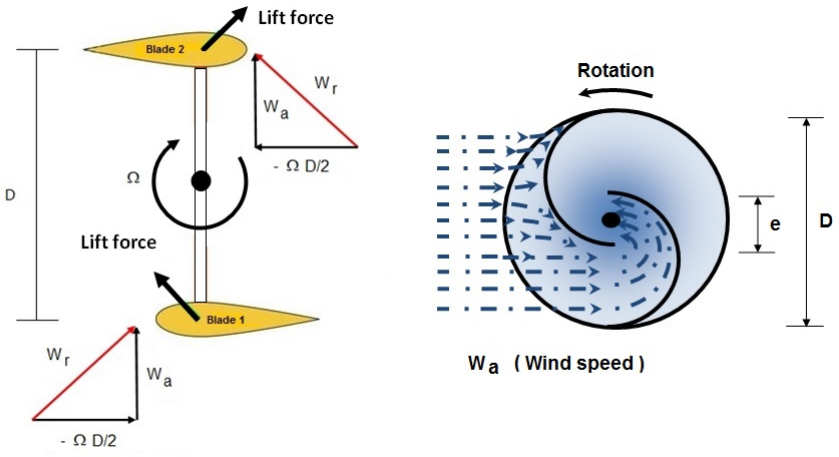

2.9(a): Darrieus principle 2.9(b): Savonius Principle

Figure 2.9: Darrieus and Savonius principles

Figure 2.10: Conjugation Darrieus/Savonius

The Figure 2.8(b) shows a real Savonius turbine. They explore drag forces mainly. It was invented by Sigurd Johannes Savonius in 1924 and the Figure 2.9(b) shows its principle. The idea is that the difference between the curvature, convex when moving against the wind (less drag) and concave when moving with the wind (more drag), causes the Savonius turbine to spin around the

vertical shaft. The relations between parameters e and d are important. Values of $\frac{e}{d}$ of $\frac{1}{3}$ were originally used. Now is known that its better performance is for a value of $\frac{1}{6}$ for an optimized rotor reaching C_P (power coefficient) of 0.3. That means that the internal flow is important for the performance. Savonius rotor is characterized as having big starting torques and start up with low intensity winds (2 m/s to 3 m/s) and it is one of the reasons for sometimes conjugating Darreus and Savonius turbines [73]. The Figure 2.10 shows this possibility.

They are drag-type devices, then extract much less of the wind's power than other similarly-sized lift-type turbines [44]. Besides having the velocity of the blade tip limited by the velocity of the wind, some power is consumed when part of the turbine is moving against the wind. In both types of turbines, the electrical items responsible to obtaining, treating and transmitting energy and the gearbox are located close to the ground, making the maintenance easier.

Drag principle was used to build the first vertical turbine which was used to product electrical energy from wind in 1887 by James Blyth in Scotland, as shown in Figure 2.11 [62].

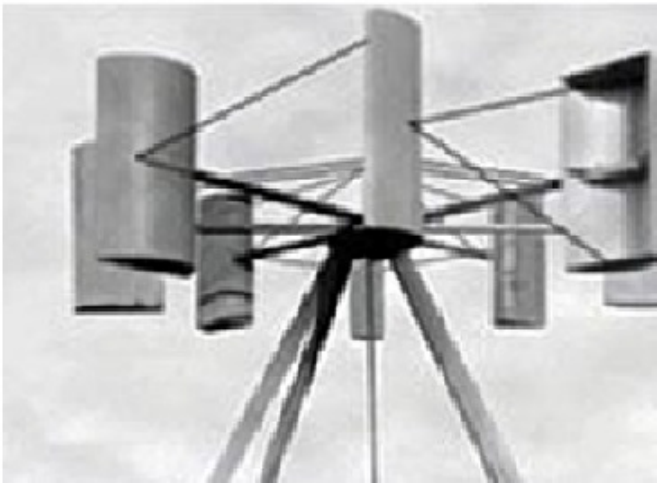

Figure 2.11: James Blyth Rotor

Horizontal turbines (HAWT) have the shaft of the rotor in the horizontal position. Currently, the experience accumulated over decades of development of horizontal turbines leaded to turbines with three blades, pitch and yaw control using induction generators [11], as illustrated in Figure 2.12(c). A simpler configuration is a rotor with two blades, Figure 2.12(b). This kind of turbine has its own particularities concerning stability, which is more critical than in other turbines with more blades. Generally rotating at higher angular velocity, they have the advantage of being cheaper and simpler to assemble. Besides, its

[11] http://www.aneel.gov.br/aplicacoes/atlas/pdf/06-Energy_Eolica (3).pdf

performance approaches those achieved by three bladed turbines. The simplest configuration is that with one single blade as can be seen in Figure 2.12(a).

The first wind turbines developed in a commercial scale had power between 10 kW and 50 kW. In the early 1990s, the power of the engines increased from the range of 100 kW - 300 kW to 300 kW - 750 kW. In 1999 the first wind turbines of 2MW was put in operation and today there are some from 3.6MW to 4.5MW [12] and even higher as that built by Siemens which is the largest in the world, located in the field Osterild, Denmark. Each one of the 3 blades is 75 meters long with a total diameter of 154 meters. The turbine is designed to generate a power of 6 MW.

2.12(a): One-bladed turbine

2.12(b): Two-bladed turbine

2.12(c): Three-bladed turbine

Figure 2.12: Horizontal turbines - one, two and three blades

2.5 Components of a horizontal turbine

2.5.1 Nacelle and internal components

In the nacelle, all the components for mechanical and electro-electronic system for transforming and treating the energy are installed (shaft, gear-box, generator and all circuits to treat the electric signal). The turbines can also work using direct drive system, not requiring gearboxes. This is possible by means of induction generators with several poles and control systems that allow their operation in any variable speed. In Figure 2.13 [13] is shown a nacelle with the components. In Figure 2.14 is shown a turbine with a direct drive system.

[12] ttp://www.aneel.gov.br/aplicacoes/atlas/pdf/06-Energia_Eolica(3).pdf
[13] http://www2.aneel.gov.br/aplicacoes/atlas/pdf/06-energia_eolica(3).pdf

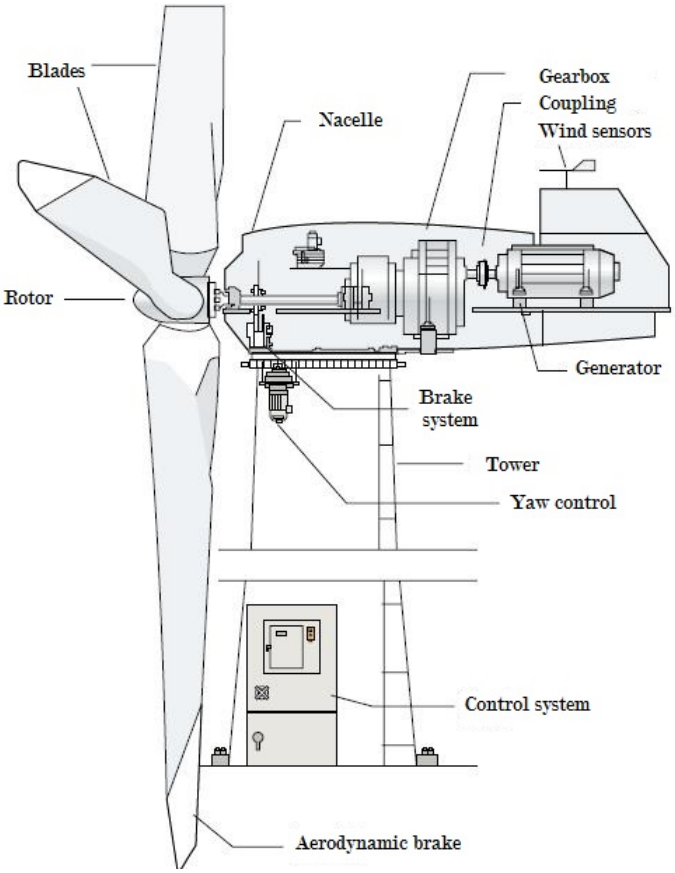

Figure 2.13: Nacelle with its elements

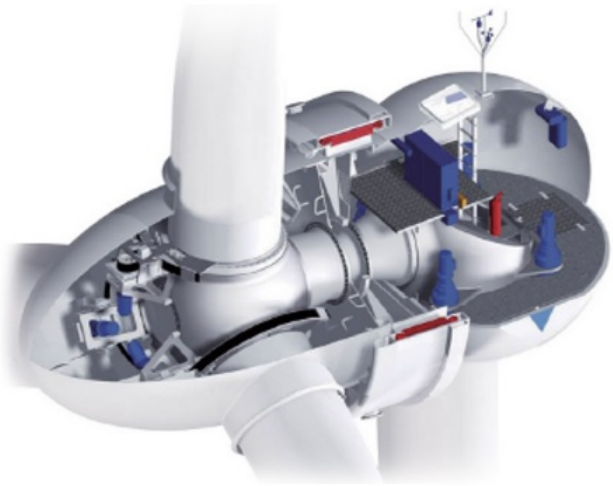

Figure 2.14: Direct drive turbine

2.5.2 Blades

The blades are made of composite material, fiberglass, in general but internally, in order to give resistance to structure, wood and aluminum are used. More recently carbon-fiber has been used in some components and there is a tendency

of making big blades completely of that material which permits to increase the blade length. There are some two-bladed wind turbines but three blades are the consolidated number and widely used. The blades transmit the loads caused by the wind to the structure through the shaft. They, together with the hub (which is coupled to the rotor shaft) comprises the rotary systems that generate mechanical energy. In Figure 2.15 is shown schematically the internal structure of a blade. As can be seen, they are like airplane wings, hollow and reinforced internally with structural parts. In the base, where they are fixed by bolts in the hub, they are made more rigid and resistant to support the moments and to permit its fixation. The profile changes from certain point aiming an optimized aerodynamic performance. Then externally, they are finished with plastic and fiberglass or even with carbon-fiber.

Turbines are getting bigger and so the blades. It is said that larger sizes will increase the competitiveness of the wind generation simply because larger blades can absorb more energy. The challenge is then to built larger blades with low weight. Carbon fiber is a good solution and maybe in the future, the complete blade will be built from carbon fiber which can improve the overall economics of wind turbines in several ways [14],[15]:

- They will have more precise aerodynamic;
- The weight will be considerably smaller;
- Smaller weighted nacelle, then less expensive tower and foundations;
- Longer blades, more wind energy at lower wind speeds;
- The costs will reduce as smaller masses will be manipulated.

2.5.3 Base

The base is the structure that supports the entire weight and variable load. Turbine bases are generally made of concrete and steel, like that shown in Figure 2.16, and holds the tower which is fixed by mean of screws. Figure 2.17 shows schematic drawings for various types of offshore foundations. From the left to the right, a mono-pile type foundation, a suction caisson type, multi-pod (tripod or tetra-pod) and gravity based foundation. Several other possibilities can be explored as shown in Figure 2.18, but some of them are not still a proved technology and need more time to consolidate [30]. The first is a "spar buoy" and the last is a kind of barge, both anchored and stabilized by mooring systems. The second type is a platform with legs to permit the stabilization

[14]http://www.gizmag.com/worlds-longest-wind-turbine-blade/25750/

[15]http://www.technologyreview.com/news/510031/the-quest-for-the-monster-wind-turbine-blade/

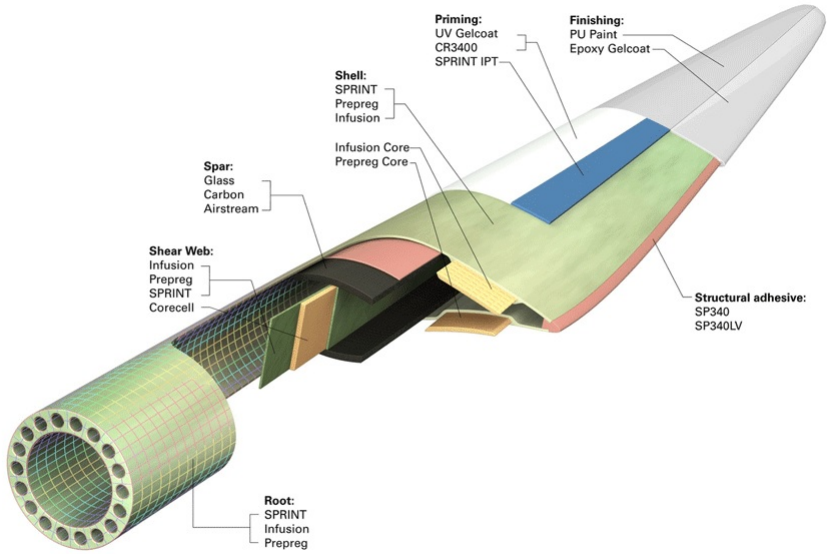

Figure 2.15: Blade structure

by a tensioned mooring system. Those turbines are in general relatively more expensive due to the structure needed to hold the tower and mooring systems. They must be stable enough to face the tides, currents and sea waves, keeping controlled oscillation. Some countries like Denmark, Germany, Portugal, USA and Japan have been investing on off-shore floating turbines. According to EWEA - European Wind Energy Association [16], the structure for holding the turbines (base) in- and offshore (on line) in 2009 were 65% single pillar; gravity, jacket, and tripod types, 25%. Floating turbines, less than 1%. This is consistent with the fact that floating turbines are more complicated to simulate and built, but it is a matter of time to those structures become a profitable way of obtaining energy. Figures 2.19(a) and 2.19(b) depicts two offshore types of turbines. The first is a floating turbine and the second is fixed in the bottom of the sea by mean of jackets and partially built with a truss.

[16] www.ewea.org

Figure 2.16: Base made with concrete and steel

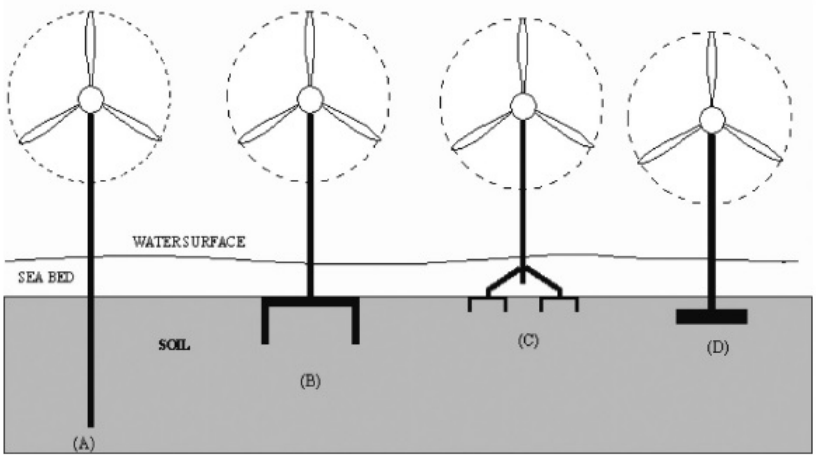

Figure 2.17: Foundations for off-shore turbines [1]

2.19(a): Floating turbine

2.19(b): Fixed turbine (jacket)

Figure 2.19: Real types of offshore turbines [30]

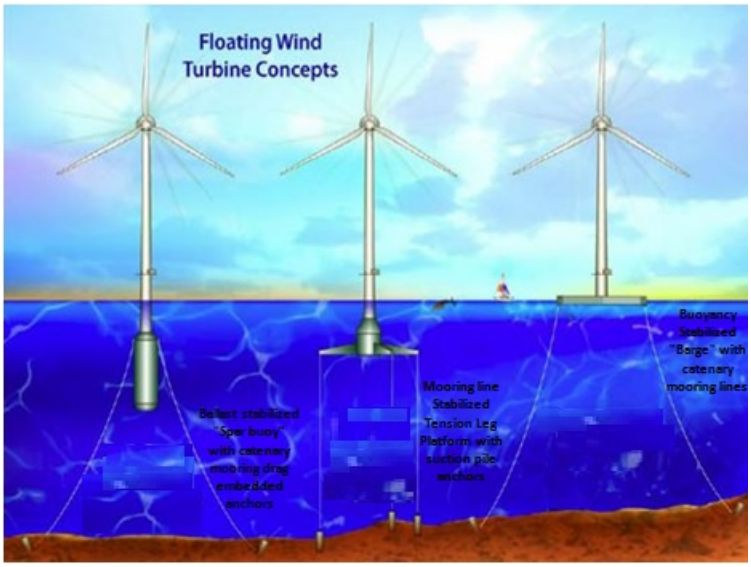

Figure 2.18: Concepts for floating off-shore turbines [30]

2.5.4 Tower

The tower is generally tubular in shape and has dimensions which depend on the required power, wind conditions and are constructed from welded steel plates mainly. They are built in segments and assembled by mean of screws. The cross-section is variable along the length of the tube, in general. Trusses are also used. The Figure 2.20 shows a typical tower segment.

Figure 2.20: Segments of a wind tower

2.5.5
Conditions for generation

Economically speaking, only wind speeds larger than 2.5 m/s (cut-in speed) are useful, so the region I in the graph depicted in Figure 2.21 must be avoided. From 2.5 m/s to 12.0 m/s, region II, the power available at the generator shaft performs useful electromechanical conversion and the wind power generation is proportional to the cube of wind speed. For wind speeds above 12.0 m/s and slower than 25.0 m/s, region III, the turbine is generating steadily and, in order to keep power limited, some kind of automatic power limiting system is activated (controlling of the pitch angle of the blades or using aerodynamic stall). If the wind speed exceeds 25.0 m/s, region IV, a protection procedure reduces the rotation of the blades and the electric generator is disconnected from the power grid. So, good places to be explored are those with high probability of having wind speeds in the region IV.

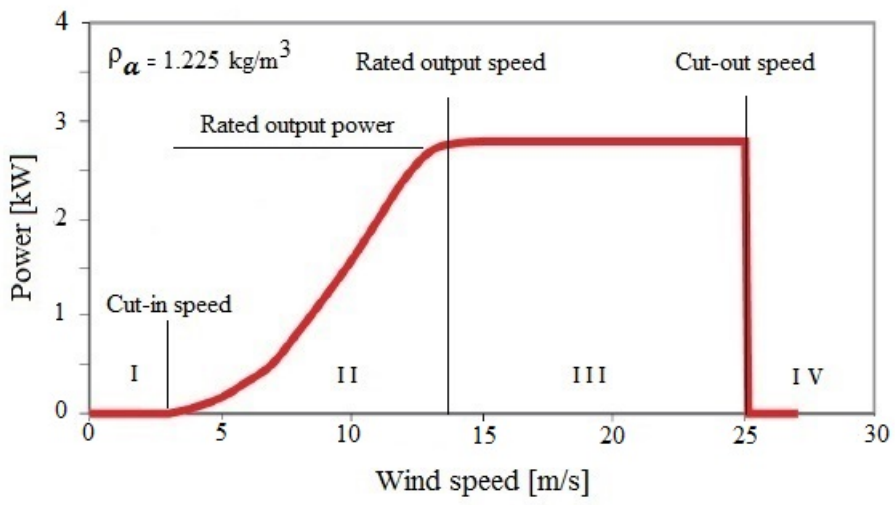

Figure 2.21: Wind turbine power curve [16]

2.6
Generators

Wind turbines, due to the variable speed of the wind, can not transform wind energy maintaining constant the rotation of the shaft, so the generator and electric installation must be capable of generating and delivering electricity to the network with constant frequency by using special electric circuits that treat the signal generated.

There are basically two types of generators used in wind generation: Asynchronous and synchronous generators. Asynchronous generators are three-phased and can be with cage rotor or wound rotor. As the asynchronous generators work in a higher operating speed than that of the turbine, they require gear-box to be coupled to the shaft in order to amplify the speed. Those generators rotate with some fraction of the frequency of line which is inversely proportional to the number of the poles of the generator. If a torque is applied, increasing or decreasing the shaft speed, a counter-torque appears and active power is absorbed or delivered to the line. This torque made by the generator is proportional to the slip (difference between the generator and line frequencies). They can start alone without any external action.

Synchronous generators work in a three-phased configuration, with independent excitation or permanent magnets in the rotor. In this technology, for lower power (less than 1 MW), the synchronous generator has a speed well above the turbine speed operation, requiring a gear-box coupled between the rotor shaft and the generator. But, for power greater than 1 MW, synchronous generators are typically manufactured with a large number of poles so that their speeds are in the same order, requiring only a planetary coupling [17]. Those generators do not start alone and must be somehow put in synchronization with the line. When synchronized, the generator keeps the speed very stable. When external torque is applied in the shaft, a counter-torque is developed so that the synchronization is kept.

2.6.1 Literature review

Nowadays, wind generation is intensively studied by groups pertaining to Universities and Companies. As a complex system, wind towers must be analyzed using different tools and approaches. It is invested time and money aiming the fast development of this challenging way to obtain clean energy so that it can be made competitive with other forms of energy. A fast look on the literature available in the usual sources, shows an astonishing quantity of researches and investigations in several fields that uses quite different approaches to solve specific problems. The researches are developed roughly in the following areas:

- Wind farm layout optimization;
- Sea and wind;
- Aero-elasticity and interaction fluid structure;

[17] http://catalogo.weg.com.br/files/wegnet/WEG-geracao-de-energia-eolica-tecnologias-atuais-e-futuras-artigo-tecnico-portugues-br.pdf

- Foundations;
- Control;
- Dynamics and Structure;
- Electric(Generation, signal processing, distribution);
- Law and environment;

Farm layout optimization

In the farm layout optimization, the focus is kept on the arrange of a set of turbines in the place chosen to be explored so that the obtained configuration is optimized following some criteria, in general, economic. Recently, in [75], it was discusses the optimization of a farm layout as a way to decrease wind power losses caused by the wake interaction between wind turbines aiming to figure out the best cost model for the layout optimization using two cost models (Mosetti's model and Chen's model). In [53], it was developed a novel evolutionary algorithm for optimal positioning of wind turbines in wind farms is proposed considering a realistic model for the wind farm considering orography, shape of the wind farm, simulation of the wind speed and direction, and costs of installation, connection and road construction among wind turbines. In [49], some current uncertainties in the offshore wind market were analyzed, identifying some uncertainties compromising offshore wind farm structural design, as examples, the design of the transition piece and the difficulties for the soil properties characterization. Evaluation of standardization in this field was made indicating that there is room to improvements in several points among them, those related to the lifetime and return period. In [51] it was identified that hurricanes are potential risk to shallow offshore turbines.

Aero-elasticity and interaction fluid-structure

The work presented in [11] studied the mooring system for tri-floater floating offshore wind turbines. Both ultimate (ULS) and accidental (ALS) limit states are examined for environmental loads for power production and parked wind turbine conditions. Also present a probabilistic model to estimate the number of turbines that would be destroyed by hurricanes in an offshore wind farm estimate the risk to offshore wind farms in four representative locations in the Atlantic and Gulf Coastal waters of the United States. Applying this approach it was shown that in the most vulnerable areas now being actively considered by developers, nearly half the turbines in a farm are likely to be destroyed in a 20-years period. In the work [14], it was investigated the technical and economic feasibility of ten commercial small wind turbines with rated power from 2.5 kW to 200 kW for five of the main European Union countries (France, Germany, Italy, Spain and The Netherlands) considering

their installation and operative conditions, evaluating some parameters that affect wind turbine performances estimating the annual cash flow during the expected plant life-time. In [20], it was elaborated a design method for combined aerodynamic and structural (aero-elastic) design of large wind turbine blades using the blade element momentum theory. The chord and twist distributions are determined with respect to the airfoil characteristics and the design tip speed ratio to yield optimal glide number and induction factors in a realistic and manufacturable design. A complete analysis of the blade is carried out including several structural blade components and the final structural design is found through an iterative process. Both ultimate loads and fatigue loads have been investigated. The design of several spars types to approximate the Sandia $SNL100-00$ blade ("monoplane spar") and the biplane blade ("biplane spar"), using analytical and computational models was presented in [52]. The analytical model used the method of minimum total potential energy; the computational model used beam finite elements with cross-sectional analysis. Simple load cases were applied to each spar and their deflections, bending moments, axial forces, and stresses were compared. Similar performance trends are identified with both the analytical and computational models. Buckling was carried out and a parametric analysis shows biplane spar configurations have 25 % - 35 % smaller tip deflections and 75 % smaller maximum root bending moments than monoplane spars of the same length and mass per unit span indicating that this configuration are attractive design for large (100 m) blades. A mathematical model for fluid dynamics wind turbine design(based on the blade element momentum theory) was developed, implemented and improved in [37]. The mathematical simulations have been compared with experimental data found in the literature.

Foundations

Tower foundations and their interactions with the soil is a field itself. In general and mainly in offshore installations this is a very expensive step and it is wiser to spend the all necessary time to explore the possible loading configurations to avoid surprises concerning to the operation. This is object of constant attention by the researchers. Still in 2015, [15] studied the fixation of large turbines in deeper waters when it is necessary to use multi-footing structures such as tripods or jackets to fix the turbine in the bottom. To improve that fixation, it was presented a concept of using helical pile foundations. This type of structure has been routinely applied onshore where large tension capacities are required.

Sea and wind

The behavior of a specific site concerning to extreme values was investigated in [72] for wave and wind. It was used real data Peaks Over Threshold (POT) extreme value estimation technique to analyze and to estimate the wind shear coefficients and gust factors. Seven to thirty-two years of buoy data at five locations near areas of possible commercial interest in gulf of Maine (USA) were examined and the results could be compared with the wind cast predictions.

Control

It was presented in [36] an intelligent wind turbine control system based on models integrating the following three approaches: data mining, model predictive control, and evolutionary computation. The model involves five different objectives with different weights controlling the wind turbine performance. These weights are adjusted in response to the variable wind conditions and operational requirements. In [8] it is made an study on a methodology for multidisciplinary design optimization of offshore wind turbines at system level using a formulation to integrate aerodynamic and structural design of the rotor and tower simultaneously, whose objective is to minimize the cost of energy, using several, geometric, dynamic and constitutive parameters. The model was tested in a real case. A model was developed in [58] on the strategy for performing maintenance aiming to minimize costs of a wind turbine with the maintenance, following multilevel opportunistic preventive maintenance strategy. In this strategy, opportunity for performing preventive actions on components is taken while a failed component is replaced. A numerical study is used to illustrate the model.

Legal and Environmental

Environmental laws are getting more important and strict. Situations where the turbine may cause damage to the environment, for instance, when it is responsible for a great number of animal fatalities, must be detected a priori to avoid extra costs due to the frequent shutdowns. Nowadays, neglecting environmental aspects may create important limitations to the viability of the project in the future. The contribution of [42] was a proposal for a general design platform for control system of wind turbines. Different models of wind turbine systems are summarized and a novel control strategy for wind turbine control is proposed as a general platform for control system design. In the work [9], observations of audio noise in frequency range from 20 Hz to 20000 Hz from wind turbines were made. The observations were performed about the

theoretically calculated 40 dB noise perimeter around the wind turbine farm at Oxhult, Sweden. This paper describes a newly designed and constructed a field qualified data acquisition system to measure spectra and total noise level of sound from wind turbines. In [41] it is proposed and studied a new methodological approach to reduce potential conflicts in the planning as well as during the operation phase of a wind energy project by quantifying the risk of the collision of migratory animals. The model permits to define areas with different collision risks so that the system is stopped when peak migration happen. In the work [18] the reasons why wind tower attracts bats causing a large number fatalities were analyzed. This study aims to determine the conditions to avoid this problem. Electro-magnetic interference has been studied as the presence of wind turbines or wind farms may cause troubles in telecommunication services. In [34] it was provided a general overview on Electro-magnetic interference with respect to big (some MW) wind turbines showing all types of electromagnetic interferences fields resulting from a GSM transmitter mounted on a big wind turbine. The fields were analyzed and described analytically the electro-magnetic fields. A comprehensive review on the impact of wind turbines on the telecommunication services (weather, air traffic control and marine radars, radio navigation systems, terrestrial television and fixed radio links) is presented in [7]. The description of the potential affections, the methodology to evaluate this impact and mitigation measures to be taken in case of potential degradation, both preventive and corrective are made. Anyway, preventive and corrective solutions to attenuate those effects are already available or under study.

Dynamics and structure

In a more accurate evaluation of this area, several subareas can be detected: modeling of blades, tower and their mutual interaction, evaluation of fatigue and life prediction, optimization and reliability. The development of wind turbines as a serious possibility of compete with other sources of energy started to become reality in the 1970s. In [50], it is made an analysis of the state of the art by 1989. He attests that from 1974 to 1989 the development of WTGs has progressed more than in the preceding 60 years. This happened due to the efforts of the governments, especially Canada, Denmark, Germany, Sweden, the U.K. and the U.S.A. Those countries put money to research development, installation, testing and gaining operating experience with large prototype wind turbine generators (TGW). By 1984, the technical problems were surmounted but the implementation of WTGs was not economical viable at that time and could not compete with conventional plants using nonrenew-

able fuels. The work discusses the main definitions related to wind turbines and attests that just for a little bit more than a decade of work on prototype units aimed at making the machines cheaper, more durable and demonstrating the reliability and availability of the units. The economics of WTGs can only improve with increased production showing a good agreement with the reality nowadays. The simpler way to model a wind turbine is consider it a column with concentrated mass with or without rotational inertia. The movement of the blades are considered concentrated loads (forces and torques) acting at the tip of the tower. The model is based on an Euler-Bernoulli beam. Several works have been published on the determination of natural modes for towers or piles surrounded or not by water, usually modeled in analyses as cantilevers with a tip mass. In the work [64], it was studied the eigenvalue problem of a beam with lumped mass and transversal spring at the tip subjected to an axial force which simulated a pier of a highway bridge. Hollow beams with variable cross-section with concentrated tip inertias immersed in fluid were studied in [48]. Since then, the problem has been studied mainly using strong formulation for obtaining exact responses (for exact is meant that the solutions are those in which the governing equation and boundary conditions are fulfilled exactly). Concerning numerical approach, [39] developed an algorithm using classical Rayleigh-Ritz method combined with Schmidt's procedure to analyze elastic restrained cantilever beams with tip mass and varying cross section. In [17], the authors based their studies in experimental and theoretical works to perform a modal analysis on an immersed beam with rotational and translational springs at its base. A review on this subject can be found in [69] for the state of the art by 1998. From that time on, some researchers have been still working on the subject considering the tower submersed or not, under several boundary conditions. It can also be mentioned [76] and [77], who formulated an immersed beam and compared the results to numerical ones. In [1], it was also developed an experimental methodology to obtain the soil structure interaction parameters, but without considering the presence of fluid, and compared the results to those from theoretical formulation. It is a fact that facing the problem using strong formulation, when the modal analysis is performed by direct solution of the differential equation of equilibrium by method of separation of variables, requires a big amount of work, mainly when complicated boundary conditions are imposed. Numerical approach, that means, variational formulation in conjunction with finite element discretization, seems to be the adequate method to reach, although not exact, an acceptable approximation for the solution. In [3], it was focused the study of the dynamic behavior of a two bladed wind turbine, considering random wind loading. The aerodynamic forces acting on

the blades were calculated using a simple approach, assuming that both, the fluctuation of the wind speed incident on the airfoil and pitch angle have a linear relation with the resultant loadings meaning that variations in lift and drag forces can be approximated by an affine transformation at a given point of operation. The nacelle and rotor blades were also considered rigid bodies mounted in a flexible tower. All movements, except for the in-plane rotation of the rotor, were considered small so that a linear approach could be applied. Based on this model, the calculation of stochastic stresses in critical spots over the structure was performed. In [65], it was investigated the characterization of the dynamic behavior of a specific type of turbine, considering the free vibration analysis (modal analysis), incorporating lumped mass and foundation effects. The analysis was made using both variational and strong formulations. In both approaches, some specific properties were chosen as random. Monte Carlo and collocation methods were used as the base to check out the effectiveness of the Finite Element algorithm. In the work [2], it was analyzed the dynamic behavior of a specific configuration of a wind turbine. A tower was attached to a flexible base which was permitted to move laterally and rotate in the bending plane. The analysis incorporated effects due to lumped mass, interactions between fluid and structure (the tower is considered partially immersed) as well as the foundation conditions. The analysis was made using variational formulation in a 2D approach. Some loading configurations were applied to the structure and the responses were analyzed.

In [12], it is presented a new method, so called constrained stochastic simulation, developed in order to generate extreme gust time series, to be used to calculate the extreme loading of wind turbines. The method produces stochastic gusts, denoted NewGust, which are, in a statistical sense, not distinguishable from gusts selected from a (very long) stochastic time series, with the same amplitude. This new probabilistic method enables wind turbine manufacturers to build more reliable and optimized wind turbines. Also the theoretical mean gust shape, as well as the probability of occurrence of gusts, has been verified by measurements and compared to real measured results. In [38], it was studied, among other subjects, the nonlinear equations of motion of a rotating wing are derived using the Bernoulli-Euler beam theory within a blade fixed rotating coordinate system. Instead of using a full model tower/blade, it is applied a forced support point motion, so that the tower-nacelle system is decoupled from the wing. A reduced modal model is derived for the blade permitting obtaining characteristic frequencies. An analysis of stability of the nonlinear wing is carried out by the use of Lyapunov exponents. It is shown that wind turbine wings (blades) experience significant changes in both flow

velocity and direction due to tower passage, rotation in a shear wind field, turbulence components, active control of the wing and elastic deformations. In the work presented in [79], a simplified but accurate dynamic wind turbine fatigue design is studied, resulting in an extensive discussion about the almost all aspects (economic , maintenance, fatigue and standardization) related to wind turbines. In [43], it was elaborated a design optimization model for placing frequencies of a wind turbine tower/nacelle/rotor structure in free yawing motion where the large amplitude caused by the yawing-induced vibrations in the case of horizontal-axis wind turbines or rotational motion of the blades about the tower axis in case of vertical-axis wind turbines. It is said that it can be a major cause of fatigue failure and might severely damage the whole tower/nacelle/rotor structure. Multi-body formulation was used in [25] to develop a new different updating algorithms of the moving frame of reference parameters for flexible structures based on the motion of one or two beam element nodes in the structure. The work [33] aimed to develop a mathematical model of a horizontal axis wind turbine with flexible tower and blades able to describe the flapping flexure of the tower and blades taking into account pitch angle and structural damping. The approximated solution is obtained by using eigenvalue approximation of the problem and compared to analytical solutions. Among other results it was observed small vibrations of the tower induce important blade deflections, and thus, the dynamic tower-blade coupling cannot be considered insignificant. In [68] it was studied a full probabilistic design of wind turbines. It was possible to assess the optimal reliability level by cost-benefit optimization is an offshore wind turbine example. The uncertainty modeling is illustrated by an example where physical, statistical and model uncertainties are estimated. In [74], the authors worked in a mixed flexible-rigid multi-body mathematical model and applied it to predict the dynamic performance of a wind turbine system. It is considered the rotor and the tower as flexible thin-walled structures. The wind turbine systems governing equations of each flexible and rigid body are derived using Lagrange approach. Using this model, the influence of the tower stiffness on the blade tip deformation is studied. It is made a simplified model considering a single pole tower configuration having thin-walled circular cross section with constant taper along the tower height where the modeling and the solution are obtained analytically. The fatigue is also a very important issue, as the turbines must be designed for a prescribed life when it must work profitably. Several works were developed in this area. In [45], it is determined the calibration of the appropriate partial safety Fatigue Design Factors (FDF) for steel substructures for OWTs (off shore wind turbines) in a reliability basis. The strength and load uncertainties

are described by stochastic variables leading to acceptable reliability level for fatigue failure of OWTs and the results are presented for calibrated optimal fatigue design factors, considering the influence of inspections order to extend and maintain a given target safety level. The interaction of foundation and the underlying soil is studied in [24]. A complete three bladed turbine is modeled using Euler-Lagrange approach. The foundation of the structure is modeled as a rigid gravity based foundation with two degrees of freedom whose movement is related to the surrounding soil by means of complex impedance functions generated using cone model. Simulations are carried out for different soil stiffness conditions for steady state and turbulent wind loading, developed using blade element momentum theory and the Kaimal spectrum. Comparison is made with standards. It is shown that soil-structure interaction affects the response of the wind turbine. An interesting work made by [59] looks to a different concept using Magnus effect to produce lift from rotating cylinders which works as blades. Determination of the power performance and characteristics of such generators are made. In this study, the importance of research carried out for determining lift and drag forces of rotating circular cylinders is highlighted and reviewed. The formulation for the potential flow around the "Magnus blades" is obtained and the blade element momentum (BEM) theory is formulated for this kind of blade. Two works, [40] and [78], used the reliability-based design optimization (RBDO). The former studied the mono-pile transition piece for offshore wind turbine system investigating two design approaches for the cost-effective and reliable design: deterministic optimization (DO) and RBDO. The later author, studied the tripod sub-structure of offshore wind turbines considering dynamic response requirements using a RBDO approach. The former attests that the costs of supporting structure of offshore wind turbines is so high that optimization in the design stage is a basic requirement and also that manufacturing tolerances, material properties, as well as environmental loads should be treated always as uncertainties since their variability has a strong effect on dynamic responses. Thats why RBDO must be used. The work [46] is dedicated to study of floating turbines focusing on designing of economic systems able to compete with fixed turbines. The preliminary platform design was obtained and the application on an experimental test showing good agreement for relevant platform properties. Finally, the work made in [29] demonstrated that fully flexible multi-body dynamic model can better reflect the operating condition of the wind turbine. As the calculation with the needed precision or the fully flexible multi-body dynamic model consumes much time, an artificial neural network method is proposed for the prediction of wind turbine dynamic behaviors. It is demonstrated that combination of the multi-body method and

the artificial neural network can reduce the simulation runtime, guaranteeing the accuracy meantime.

As can be noticed, wind turbines multidisciplinary subject and the state of art is now very advanced and very specialized. Therefore, in the author's opinion the model for a wind turbine must be obtained considering the complete set. This means to model, at least, the soil, the tower as a flexible component and the blades (flexible or not). In this work, the blades are considered rigid. It is a considerable simplification as there are couplings between flexibility, displacement and rotation degrees of freedom. The tower is a flexible cylindric tower installed over springs. As small angles and displacements are considered concerning to the tower, the only the flexibility is modeled which simplifies enormously the analysis. The nacelle is considered a rigid mass containing a shaft and a set of rigid blades. Water and wind can load the structure as well as concentrated forces and torques. Under those assumptions, a model is constructed using finite element to approximate the dynamics of the tower in a reduced model basis. The attitude of the body is parametrized using Euler parameters. This parameters introduce some inconveniences in the model but the matrices and partial derivatives are calculated in a more straightforward way. The evaluation of the dynamic response of these structures to wind and sometimes sea currents excitation requires calculation of natural frequencies and modes. This may be done at least for two reasons. First, the modal evaluation of the structure furnishes more understanding on its natural behavior. Second, the resulting dynamics can be obtained by approximating the response of the structure by a combination of the natural modes. This permits to model the problem in successive approximations, meaning that the more modes are used, the more precise is the approximation to the solution.

3
Dynamic formulation

The turbine will be analyzed as a multi-body system composed by 6 bodies: tower, nacelle, shaft and three blades and may be a semi-immersed in water. As depicted in Figure 3.1, springs are the support for the whole structure. The blades are fixed rigidly to the shaft configuring a rotor which can spin relatively to the nacelle. The top of the tower and the base of the nacelle are joined and in this section there is not any relative movement between the nacelle and the tower. Yaw is not modeled. The base of the tower can displace and rotate due to the flexibility of the springs. It will be made an analysis using Lagrangian approach, Newton-Euler equation is obtained for the system of bodies and, as they are linked somehow, it will be imposed the appropriate constraint equations. The basis for this development is given in section 7.2 in Appendix and was based in the work developed in [60], where a full model is presented for the general dynamics of a rigid and flexible multi-body. First, it is necessary to begin with the expression which represents the velocity of a body with respect to a inertial frame as the kinetic energy is used to obtain the equation of motion using Lagrangian formulation. As can be seen in Equation 7.68, repeated here, the total velocity vector of any point if a body b is given by

$$\dot{r}_b = \begin{bmatrix} [I] & [B_b] & [A_b][\bar{H}_b] \end{bmatrix} \begin{Bmatrix} \{\dot{R}_b\}^T \{\dot{\Theta}_b\}^T \{\dot{\bar{U}}_b\}^T \end{Bmatrix}^T \tag{3.1}$$

where $\{\dot{R}_b\}$, is the velocity of the origin of the body frame, and $\{\Theta_b\}$ is the vector containing the Euler parameters to model the attitude of the body. $[A_b]$ is the transformation matrix and $[\bar{H}_b]$ is the interpolating matrix. In this work the flexible component is the tower and will be modeled as an Euler-Bernoulli beam under a variational approach aiming to use Finite Element Method. Then, $\{\dot{\bar{U}}_b\}$ is the nodal velocity vector of any point of the body, relative to the body frame and $[\bar{H}_b]$, the interpolation matrix. $[B_b]\{\dot{\Theta}_b\} = \frac{d}{dt}\{[A_b]\{\bar{r}_b\}\}$. For rigid bodies, the third part of Equation 3.1 is null and the equation for the rigid components of the turbine is

$$\dot{r}_b = \begin{bmatrix} [I] & [B_b] \end{bmatrix} \begin{bmatrix} \{\dot{R}_b\}^T & \{\dot{\Theta}_b\}^T \end{bmatrix}^T \tag{3.2}$$

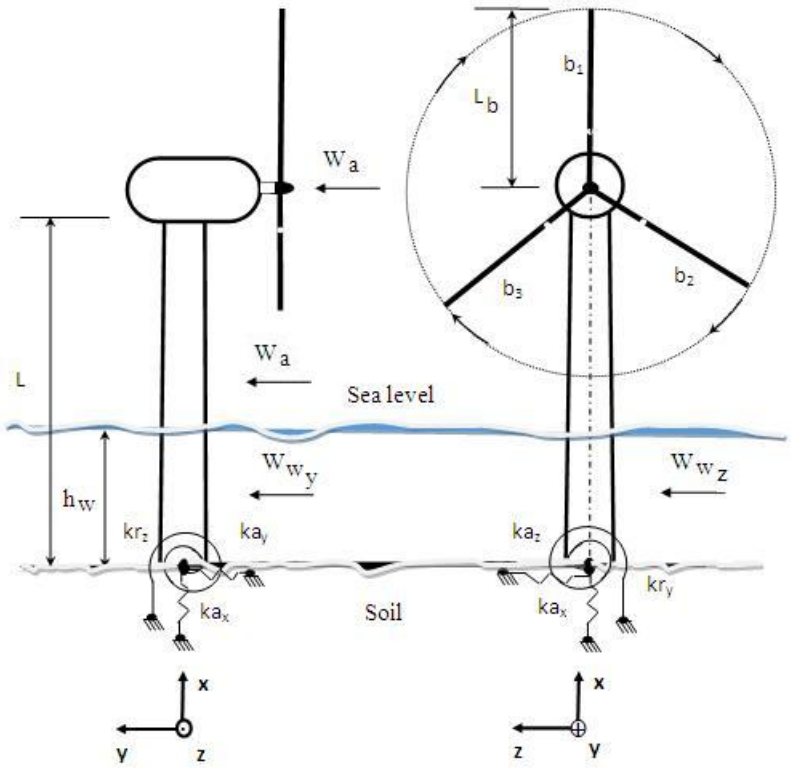

Figure 3.1: Model of the turbine in water

Nevertheless, if only the flexibility is considered, that is, neither the rotation nor the displacement of the body frame are important, then, the first and the second parts of that equation are null. The velocity for any point of the tower is given by

$$\dot{r}_b = \dot{\bar{r}}_b = [\bar{H}_b]\{\dot{\bar{U}}_b\}, \tag{3.3}$$

considering that $[A_b] = [I]$ (I is the identity matrix). As the body frame does not move, in this case, $\{\dot{\bar{U}}_b\} \equiv \{\dot{U}_b\}$. Then,

$$\dot{r}_b = \dot{\bar{r}}_b = [H_b]\{\dot{U}_b\}. \tag{3.4}$$

This second notation will be used. So, for nacelle, shaft and blades, the Equation 3.2 is used. Equation 3.4 is used for the tower dynamic formulation. Lagrange equation is used together with the appropriated constraints equations to assembly all the bodies adequately. A single coupled system of equations is obtained whose coupling is due to the presence of the constraint equations. The elements of the turbine will be analyzed separately, first, nacelle, shaft and blades, and then, the tower. This will be made as if they were not linked. The links will be discussed later, constraint equations will be deduced and incorporated to the equations of motion.

3.1
Dynamic formulation of the nacelle, shaft and blades

The Lagrangian equation for a system of constrained bodies is given by Equation 7.111, repeated here

$$\left\{\frac{d}{dt}\left\{\frac{\partial E_c}{\partial\{\dot{\breve{q}}\}}\right\}-\left\{\frac{\partial E_c}{\partial\{\breve{q}\}}\right\}-\{Q\}+\left\{\frac{\partial[\mathbb{G}_h]}{\partial\{\breve{q}\}}\right\}+\left\{\frac{\partial[\mathbb{G}_{nh}]}{\partial\{\dot{\breve{q}}\}}\right\}\right\}=\{0\} \tag{3.5}$$

where $[\bar{\mathbb{G}}_h]$ is the vector containing the augmented holonomic constraints and $[\bar{\mathbb{G}}_{nh}]$ is the vector containing the non-holonomic dissipation functions for the set of bodies [21]. E_c is the kinetic energy of the system which is a sum of the kinetic energies of all bodies and $\{\breve{q}\}$ is the vector containing all generalized coordinates. For a number i of bodies,

$$\{\breve{q}\}=\{\{R_1\}^T\ \{\Theta_1\}^T\ \{U_1\}^T\ \{R_2\}^T\ \{\Theta_2\}^T\ \{U_2\}^T...\{R_i\}^T\ \{\Theta_i\}^T\ \{\bar{U}_i\}^T\}^T. \tag{3.6}$$

For this work, the vector $\{\breve{q}\}$ was organized in the following way

$$\{\breve{q}\}=\{\{U\}^T\ \{R_n\}^T\ \{\Theta_n\}^T\ \{R_s\}^T\ \{\Theta_s\}^T\ \{R_{b1}\}^T\ \{\Theta_{b1}\}^T\ ...\ \{R_{b3}\}^T\ \{\Theta_{b3}\}^T\}^T \tag{3.7}$$

where the indexes $n, s, b1, b2$ and $b3$ mean nacelle, shaft and blades 1, 2 and 3. As the tower is the only flexible component the index "t" is not used. Related to the constraints, they can involve just the body itself. It may happen when the body has a fixed point or even a point with a prescribed trajectory. In the present work, for instance, it must be imposed that $(\{\Theta_b\}^T\{\Theta_b\}=1)$, index b meaning "body". This means that the Euler parameters used to define the attitude of the body are dependent. If the bodies do not have any link among them, the system of equations of motion for each body contains only the generalized coordinate associated to the body itself. So, the assembled system of equations for all bodies will have the following aspect

$$\begin{pmatrix} [M_1] & 0 & \cdots & 0 \\ 0 & [M_2] & \cdots & 0 \\ \vdots & \vdots & \vdots & \vdots \\ 0 & 0 & \cdots & [M_i] \end{pmatrix} \begin{pmatrix} \{\ddot{q}_1\} \\ \{\ddot{q}_2\} \\ \vdots \\ \{\ddot{q}_i\} \end{pmatrix} +$$
$$\begin{pmatrix} [J_{h_1}]^T & 0 & \cdots & 0 \\ 0 & [J_{h_2}]^T & \cdots & 0 \\ \vdots & \vdots & \vdots & \vdots \\ 0 & 0 & \cdots & [J_{h_i}]^T \end{pmatrix} \left([p_h] \begin{Bmatrix} \{g_{h_1}\} \\ \{g_{h_2}\} \\ \vdots \\ \{g_{h_i}\} \end{Bmatrix} + [k_h] \begin{Bmatrix} \{\lambda_1\} \\ \{\lambda_2\} \\ \vdots \\ \{\lambda_i\} \end{Bmatrix} \right)$$
$$\begin{pmatrix} [J_{nh_1}]^T & 0 & \cdots & 0 \\ 0 & [J_{nh_2}]^T & \cdots & 0 \\ \vdots & \vdots & \vdots & \vdots \\ 0 & 0 & \cdots & [J_{nh_i}]^T \end{pmatrix} \left([p_{nh}] \begin{Bmatrix} \{g_{nh_1}\} \\ \{g_{nh_2}\} \\ \vdots \\ \{g_{nh_i}\} \end{Bmatrix} + [k_{nh}] \begin{Bmatrix} \{\dot{\lambda}_1\} \\ \{\dot{\lambda}_2\} \\ \vdots \\ \{\dot{\lambda}_i\} \end{Bmatrix} \right) =$$
$$\begin{Bmatrix} \{Q_{v_1}\} \\ \{Q_{v_2}\} \\ \vdots \\ \{Q_{v_i}\} \end{Bmatrix} + \begin{Bmatrix} \{Q_{e_1}\} \\ \{Q_{e_2}\} \\ \vdots \\ \{Q_{e_i}\} \end{Bmatrix} + \begin{Bmatrix} \{Q_{d_1}\} \\ \{Q_{d_2}\} \\ \vdots \\ \{Q_{d_i}\} \end{Bmatrix} + \begin{Bmatrix} \{Q_{k_1}\} \\ \{Q_{k_2}\} \\ \vdots \\ \{Q_{k_i}\} \end{Bmatrix} \tag{3.8}$$

which has i independent sub-systems and i is associated to each body. $[k_{h_i}]$ and $[k_{nh_i}]$ are diagonal matrices containing the scale factors for Lagrange multipliers. $[p_{h_i}]$ and $[p_{nh_i}]$ are diagonal matrices containing the penalty coefficients. $\{Q_{v_i}\}$, $\{Q_{d_i}\}$, $\{Q_{k_i}\}$ and $\{Q_{e_i}\}$are the quadratic velocity, damping, flexibility and external loading vectors, respectively. It may also happen that the constraints involve generalized coordinates of two or more bodies, that is, they are linked somehow. In this case, the equations of motion of the body are no more independent, the constraints will depend on generalized coordinates associated to several bodies. As discussed in 7.7.1, in the Appendix, the equations for a rigid body i without constraints can be formulated as

$$\begin{bmatrix} m_i[I] & 0 \\ 0 & [\bar{G}_i]^T[\bar{\mathrm{J}}_i]\bar{G}_i] \end{bmatrix} \left\{ \ddot{q}_i \right\} = \begin{Bmatrix} \{0\} \\ \{-2[\dot{\bar{G}}_i]^T[\bar{\mathrm{J}}_n]\{\bar{\Omega}_i\}\} \end{Bmatrix} + \begin{Bmatrix} \{F_i\} \\ \{[B_i]^T\{F_i\}\} \end{Bmatrix}. \tag{3.9}$$

where m_i is the body mass, $[\bar{G}_i] = 2[\bar{E}_i]$ and $[E_i][\bar{E}_i^T] = [A_i]$. The matrix $[B_i]$ is the derivative of $[A_i]\{r_{b_i}\}$ with respect to vector of the generalized coordinates

$$\left\{ q_i \right\} = \left\{ R_{x_i} \quad R_{y_i} \quad R_{z_i} \quad \Theta_{0_i} \quad \Theta_{1_i} \quad \Theta_{2_i} \quad \Theta_{3_i} \right\}^T. \tag{3.10}$$

Equation 3.9 can be used to model all the rigid elements of the turbine.

The last element to be modeled is the tower. It is flexible, so, for large displacement and rotations, it is quite difficult to model due to the coupling of the generalized coordinates. Nevertheless, for linear approach when the displacements and rotations are small, only the flexibility is taken in consideration, that is, $\{R_t\}$ and $\{\Theta_t\}$ are null. So, the strategy used is to model the tower as an Euler-Bernoulli beam and as the nacelle is installed at the top of it ($x = L$), the tower and nacelle has the same rotations and the same displacement in the surface of contact, as mentioned. The tower analysis will be made next and then all the elements of the turbine will be assembled considering the links imposed by means of appropriated constraint equations.

3.2 Variational formulation of the tower

The tower is loaded axially by the nacelle and blades weights. So, it must be designed to support static as well as dynamic axial loads in order to avoid buckling. Axial loads (its own weights and those of the other components) also affect the lateral motion of the column, changing its natural frequency and this must be considered. In a complete analysis it will be modeled to consider axial and transversal loads as well as torsion. Simplifications will be made due to the symmetry of the cross section which permits to uncouple the kinematic of the tower into three independent structural elements:

- Bar, axially loaded;
- Beams axially and transversally loaded in two longitudinal orthogonal planes;
- Shaft, submitted to torsion.

The tower is the most complicated component in this work and is discussed in more detail in the Section 7.1 of the Appendix, where a set of differential equations is obtained together with conditions related to the state of the system at the beginning of the analysis, the initial and boundary conditions. As the purpose here is to use finite elements to get to an approximation of the solution in an iteratively way, it would be convenient to take that set of differential equations associating each equation to a space of admissible functions. This will result in a set of variational equations incorporating the natural boundary conditions. The space of the admissible functions defines the regularity of the problem and incorporate part of the essential conditions [57]. In variational formulation, the differential equations are projected in a space generated by some chosen base functions $\bar{\psi}(x)$, test functions, and integrated over the domain. Those functions have at least one restrictions and the resulting restricted set of functions is the admissible set

$$Adm = \left\{ \ \bar{\psi}(x) : (0, L) \rightarrow \Re \ : / \ \int_0^L \bar{\psi}^2(x) < \infty \right\}. \tag{3.11}$$

The choice of the base for Adm is crucial to approximate de solution for the problem. Some Variational Approximation Methods are: Rayleigh-Ritz, Galerkin, Petrov-Galerkin and Least Squares [57]. In the Galerkin method, the same base used to approximate the solution is used to project the dynamics. The space of admissible functions is linear with infinite dimension. So, any element of Adm, $\bar{\psi}_x$, can be expressed as a linear combination of the elements of the base, $\bar{\psi}$, so that, for arbitrary constants a_j,

$$\bar{\psi}_x = \sum_{j=1}^{\infty} a_j \bar{\psi}_j. \tag{3.12}$$

The next important point related to Galerkin method, consists in finding an approximation for the solution of the problem in a sub-set of Adm of finite dimension. From 3.12, using a subset of dimension N,

$$\bar{\psi}_x = \sum_{j=1}^{N} a_j \bar{\psi}_j + \sum_{k=N+1}^{\infty} a_k \bar{\psi}_k = \bar{\psi}^N + \bar{\epsilon}^N, \tag{3.13}$$

where $\bar{\psi^N} \in Adm^N$, a finite subset of Adm. Neglecting $\bar{\epsilon}^N$ means introducing an error in the solution. The variational problem is formulated with integral operators $\mathcal{I}(.)$ and $\mathcal{F}(.)$ as follows

$$\mathcal{I}(\bar{\psi}_x, \bar{\psi}) = \mathcal{F}(\bar{\psi}). \tag{3.14}$$

Substituting Equation 3.13 into Equation 3.14 one obtains

$$\mathcal{I}(\bar{\psi}^N + \bar{\epsilon}_x^N, \bar{\psi}) = \mathcal{F}(\bar{\psi}), \tag{3.15}$$

which can be rewritten as

$$\mathcal{I}(\bar{\psi}^N, \bar{\psi}) - \mathcal{F}(\bar{\psi}) = \mathcal{I}(\bar{\epsilon}^N, \bar{\psi}), \tag{3.16}$$

where $\mathcal{I}(\bar{\epsilon}^N, \bar{\psi})$ is the error of the approximation. Finally, Galerkin method imposes this projection error on the base of Adm to be null, meaning that the error is orthogonal to the space Adm^N.

$$\mathcal{I}(\bar{\psi}^N, \bar{\psi}) - \mathcal{F}(\bar{\psi}) = 0. \tag{3.17}$$

The base of eigenvectors associated to the mechanical problem can be used to approximate its dynamics [47]. This base has the advantage of containing informations on the structure behavior and one can chose the elements to use. The determination of the eigenvectors can be performed numerically by using finite element discretization of the structure. Then, the dynamic can be approximated as precise as needed. Next, the variational formulation will be applied using Galerkin method, that is, the equations

of motion are multiplied by weight functions that are the same used to approximate the solution. Then, the equations are integrated over the domain.

3.2.1 Bar formulation

For bar formulation, the first equation of 7.25 in Appendix applies. Multiplying it in both sides by the test function $\phi_{x_j} = \phi_{x_j}(x)$ one obtains

$$\int_0^L \frac{\partial}{\partial x}\left(EA\frac{\partial w_x}{\partial x}\right)\phi_{x_j}dx + \int_0^L f_x\phi_{x_j}dx = \int_0^L \rho A\ddot{w}_x\phi_{x_j}dx. \tag{3.18}$$

Integrating by parts,

$$\begin{aligned}&\phi_{x_j}EA\frac{\partial}{\partial x}w_x\Big|_L - \phi_{x_j}EA\frac{\partial}{\partial x}w_x\Big|_0 - \int_0^L \frac{\partial}{\partial x}\left(EA\frac{\partial}{\partial x}w_x\right)\frac{\partial}{\partial x}\phi_{x_j}dx \\ &- \int_0^L \rho A\ddot{w}_x\phi_{x_j}dx = -\int_0^L f_x\phi_{x_j}dx\end{aligned} \quad . \tag{3.19}$$

Recalling Equations 7.34 to 7.35 (Appendix), it follows that

$$\begin{aligned}&- m_{tip}\phi_{x_j}(L)\ddot{w}_x(L) - ka_x\phi_x w_x(0) + F(L,t)\phi_{x_j}(L) - \int_0^L EA\frac{\partial w_x}{\partial x}\frac{d}{dx}\phi_{x_j}dx \\ &- \int_0^L \rho A\ddot{w}_x\phi_{x_j}dx = -\int_0^L f_x\phi_{x_j}dx\end{aligned} \tag{3.20}$$

and now, one considers that the field $w(x,t)$ is approximated by a combination of functions, composed by a product of a spatial and a time dependent function $w(x,t) = \sum_1^N \phi_x(x)_i a_{xi}(t)$, that permits to obtain the following operators

$$\left[\mathcal{M}_x(\phi_{x_i},\phi_{x_j})\right]\ddot{a}_{x_i} + \left[\mathcal{K}_x(\phi_{x_i},\phi_{x_j})\right]a_{x_i} = \left[\mathcal{F}_x(\phi_{x_j})\right] \tag{3.21}$$

where

$$\begin{aligned}\mathcal{M}_x &= \left(\int_0^L \rho A\phi_{x_i}\phi_{x_j}dx + m_{tip}\phi_{x_i}(L)\phi_{x_j}(L)\right) \\ \mathcal{K}_x &= \left(\int_0^L EA\frac{d\phi_{x_i}}{dx}\frac{d\phi_{x_j}}{dx}dx + ka_x\phi_{x_i}\phi_{x_j}dx\right) \\ \mathcal{F}_x &= \left(\int_0^L f_x\phi_{x_j}dx + F_x(L,t)\phi_{x_j}(L)\right)\end{aligned} \quad . \tag{3.22}$$

3.2.2 Shaft formulation

The same is made for shaft model. Multiplying the second Equation of 7.25 in Appendix by the appropriate test functions ϕ_{θ_j},

$$\int_0^L \frac{\partial}{\partial x}\left(GI_{xx}\frac{\partial \theta_i}{\partial x}\right)\phi_{\theta_j}dx + \int_0^L m_x\phi_{\theta_j}dx = \int_0^L \rho I_{xx}\ddot{\theta}_x\phi_{\theta_j}dx \tag{3.23}$$

Integrating by parts

$$\begin{aligned}&\phi_{\theta_j}GI_{xx}\frac{\partial}{\partial x}\theta_x\Big|_L - \phi_{\theta_j}GI_{xx}\frac{\partial}{\partial x}\theta_x\Big|_0 - \int_0^L \frac{\partial}{\partial x}\left(GI_{xx}\frac{\partial}{\partial x}\theta_x\right)\frac{\partial}{\partial x}\phi_{\theta_j}dx + \\ &\int_0^L \phi_{\theta_j}m_x dx = \int_0^L \rho I_{xx}\ddot{\theta}_x\phi_{\theta_j}dx\end{aligned} \tag{3.24}$$

Recalling the boundary conditions given by Equations 7.46 and 7.47 (Appendix) it follows that

$$\begin{aligned}&-\phi_{\theta_j}J_{xx}\ddot{\theta}_x - \phi_{\theta_j}kr_x\theta_x + T_x(L,t)\phi_{\theta_j} - \int_0^L \frac{\partial}{\partial x}\left(GI_{xx}\frac{\partial}{\partial x}\theta_x\right)\frac{\partial}{\partial x}\phi_{\theta_j}dx + \\ &\int_0^L \phi_{\theta_j}m_x dx = \int_0^L \rho I_{xx}\ddot{\theta}_x\phi_{\theta_j}dx\end{aligned} \tag{3.25}$$

If $\theta_x(x,t) = \sum_1^N \phi_{\theta_j}(x)a_{\theta_j}(t)$ it becomes that

$$\left[\mathcal{M}_\theta(\phi_{\theta_i},\phi_{\theta_j})\right]\ddot{a}_{\theta_i} + \left[\mathcal{K}_\theta(\phi_{\theta_i},\phi_{\theta_j})\right]a_{\theta_i} = \left[\mathcal{F}_\theta(\phi_{\theta_j})\right] \tag{3.26}$$

where

$$\begin{aligned}\mathcal{M}_\theta &= \left(\int_0^L \rho I_{xx}\phi_{\theta_i}\phi_{\theta_j}dx + \mathtt{J}_{xx}\phi_{\theta_i}(L)\phi_{\theta_j}(L)\right)\\ \mathcal{F}_\theta &= \left(\int_0^L m_x\phi_{\theta_j} + T_x(L)\phi_{\theta_i}dx\right)\\ \mathcal{K}_\theta &= \left(\int_0^L GI_{xx}\frac{d\phi_{\theta_i}}{dx}\frac{d\phi_{\theta_j}}{dx}dx + kr_x\phi_{\theta_i}\phi_{\theta_j}\right)\end{aligned} \tag{3.27}$$

3.2.3 Beam formulation

Again, multiplying third equation of 7.25 by the test function $\psi_y(x) = \psi_y$ in Appendix and integrating over the domain one obtains

$$\int_0^L \frac{\partial^2}{\partial x^2}(EI_{zz}\frac{\partial^2}{\partial x^2}w_y)\psi_y dx + \int_0^L \frac{\partial}{\partial x}(P\frac{\partial}{\partial x}w_y)\psi_y dx + \int_0^L \frac{\partial}{\partial x}m_z\psi_y dx$$
$$+ \int_0^L \frac{\partial}{\partial x}(\rho I_{zz}\frac{\partial}{\partial x}\ddot{w}_y)\psi_y dx + \int_0^L (\rho A + C_l\rho_f A_c)\ddot{w}_y\psi_y dx +$$
$$\int_0^L sign\left(W_y - \dot{w}_y\right)\left(\rho_f DC_D W_y\dot{w}_y\right)\psi_y dx -$$
$$\int_0^L sign\left(W_y - \dot{w}_y\right)\left(\frac{1}{2}\rho_f DC_D\dot{w}_y^2\right)\psi_y dx = \int_0^L f_{o_y}\psi_y dx +$$
$$\int_0^L (1 + C_l)\rho_f A_c W_y\psi_y dx + \int_0^L sign\left(W_y - \dot{w}_y\right)\left(\frac{1}{2}C_l D(x)W_y^2\right)\psi_y dx +$$
$$\int_0^L \rho C_l A\dot{W}_y\psi_y dx. \tag{3.28}$$

Integrating by parts,

$$\psi_y\frac{\partial\psi_y}{\partial x}(EI_{zz}\frac{\partial^2}{\partial x^2}w_y)\mid_L - \psi_y\frac{\partial}{\partial x}\left(EI_{zz}\frac{\partial^2}{\partial x^2}w_y\right)\mid_0 - EI_{zz}\frac{\partial^2 w_y}{\partial x^2}\frac{d\psi_y}{dx}\mid_L +$$
$$EI_{zz}\frac{\partial^2 w_y}{\partial x^2}\frac{d\psi_y}{dx}\mid_0 + \int_0^L EI_{zz}\frac{\partial^2 w_y}{\partial x^2}\frac{d^2\psi_y}{dx^2}dx + P(x)\frac{\partial w_y}{\partial x}\psi_y\mid_L - P\frac{\partial w_y}{\partial x}\psi_y\mid_0 -$$
$$\int_0^L P(x)\frac{\partial w_y}{\partial x}\frac{\partial\psi_y}{\partial x}dx + \rho I_{zz}\frac{\partial\ddot{w}_y}{\partial x}\psi_y\mid_L - \rho I_{zz}\frac{\partial\ddot{w}_y}{\partial x}\psi_y\mid_0 - \int_0^L \rho I_{xx}\frac{\partial\ddot{w}_y}{\partial x}\frac{\partial\psi_y}{\partial x}dx +$$
$$m_z\psi_y\mid_L - m_z\psi_y\mid_0 - \int_0^L m_z\frac{\partial\psi_y}{\partial x}dx + \int_0^L \left(\rho A + C_l\rho_f A_c\right)\ddot{w}_y\psi_y dx +$$
$$\int_0^L sign\left(W_y - \dot{w}_y\right)\left(\rho_f DC_D W_y\dot{w}_y\right)\psi_y dx -$$
$$\int_0^L sign\left(W_y - \dot{w}_y\right)\left(\frac{1}{2}\rho_f DC_D\dot{w}_y^2\right)\psi_y dx = \int_0^L f_{o_y}(x,t)\psi_y dx +$$
$$\int_0^L \left(1 + C_l\right)\rho_f A_c W_y\phi_y dx + \int_0^L sign\left(W_y - \dot{w}_y\right)\left(\frac{1}{2}C_l DW_y^2\right)\psi_y dx +$$
$$\int_0^L \rho C_l A\dot{W}_y\psi_y dx. \tag{3.29}$$

Again, using conditions from Equations 7.30 to 7.33,

$$
\begin{aligned}
&m_{tip}\ddot{w}_y(L,t)\psi_y(L) + ka_y w_y(0,t)\psi_y(0) + \int_0^L \frac{\partial}{\partial x}\left[(EI_{zz}\frac{\partial}{\partial x}w_y\frac{\partial}{\partial x}\right]dx- \\
&\int_0^L (P(x)\frac{\partial}{\partial x}w_y)\psi_y dx - \int_0^L \frac{\partial}{\partial x}(\rho I_{zz}\frac{\partial}{\partial x})\psi_y dx + \int_0^L \frac{\partial}{\partial x}m_z\psi_y dx+ \\
&\int_0^L (\rho A + C_l\rho_f A_c)\ddot{w}_y\psi_y dx + \int_0^L sign\left(W_y - \dot{w}_y\right)\left(\rho_f DC_D W_y\dot{w}_y\right)\psi_y dx- \\
&\int_0^L sign\left[W_y - \dot{w}_y\right]\left[\frac{1}{2}\rho_f DC_D\dot{w}_y^2\right]\psi_y dx = \int_0^L f_{o_y}(x,t)\psi_y dx+ \\
&\int_0^L (1+C_l)\rho_f A_c W_y\psi_y dx + \int_0^L (sign(W_y - \dot{w}_y)\left[\frac{1}{2}C_l DW_y^2\right]\psi_y dx+ \\
&\int_0^L \rho C_l A\dot{W}_y\psi_y dx - T_z(L,t)\frac{\partial\psi_y}{\partial x}(L,t) - F_y(L,t)\psi_y.
\end{aligned}
\tag{3.30}
$$

If $\theta(x,t) = \sum_1^N \psi_{\theta_i}(x)a_{\theta_i}(t)$ it becomes that

$$
\begin{aligned}
&\mathcal{K}_y(\psi_{y_i},\psi_{y_j}) + \mathcal{P}_y(\psi_{z_i},\psi_{z_j}) - \mathcal{I}_z(\psi_{z_i},\psi_{y_j}) + \mathcal{M}_y(\psi_{y_i},\psi_{y_j})+ \\
&\mathcal{C}_y(w,\psi) + \mathcal{N}_y(\psi_{z_i},\psi_{y_j}) - \mathcal{F}_y(\psi_{y_j}) = 0
\end{aligned}
\tag{3.31}
$$

where the operators above are

$$
\begin{aligned}
&\mathcal{M}_y = -\int_0^L \rho I_{xx}\frac{\partial\ddot{w}_y}{\partial x}\frac{\partial\psi_y}{\partial x}dx + \int_0^L \left(\rho A + C_l\rho_f A_c\right)\ddot{w}_y\psi_y dx+ \\
&m_{tip}\ddot{w}_y(L,t)\psi_y(L) + ka_y w_y(0,t)\psi_y(0) \\
&\mathcal{K}_y = \int_0^L EI_{zz}\frac{\partial^2 w_y}{\partial x^2}\frac{\partial^2\psi_y}{\partial x^2}dx + ka_y w_y(0,t)\psi_y(0) \\
&\mathcal{P}_y = -\int_0^L P\frac{\partial w_y}{\partial x}\frac{\partial\psi_y}{\partial x}dx \\
&\mathcal{C}_y = sign\left(W_y(x,t) - \dot{w}_y(x,t)\right)\int_0^L D(x)\,C_D(x)\rho_f\dot{w}_y(x,t)\phi(x)dx \\
&\mathcal{N}_y = sign\left(W_y(x,t) - \dot{w}_y(x,t)\right)\int_0^L \frac{1}{2}D(x)\,C_D(x)\rho_f\dot{w}_y(x,t)^2\phi(x)dx \\
&\mathcal{I}_y = -\int_0^L \rho I_{xx}\frac{\partial\ddot{w}_y}{\partial x}\frac{\partial\psi_y}{\partial x}dx + \int_0^L \frac{\partial}{\partial x}m_z\psi_y dx \\
&\mathcal{F}_y = \int_0^L f_{o_y}(x,t)\psi_y dx + \int_0^L (1+C_l)\rho_f A_c W_y\psi_y dx+ \\
&\int_0^L sign\left(W_y - \dot{w}_y\right)\left[\frac{1}{2}C_l DW_y^2\right]\psi_y dx+ \\
&\int_0^L m_z\frac{\partial\psi_y}{\partial x}dx + \int_0^L \rho C_l A\dot{W}_y\psi_y dx + T_z(L,t)\frac{\partial\phi_y}{\partial x}(L,t) + F_y(L,t)\psi_y.
\end{aligned}
\tag{3.32}
$$

$\mathcal{M}_y$, $\mathcal{K}_y$, $\mathcal{P}_y$, $\mathcal{C}_y$, $\mathcal{N}_y$, and $\mathcal{F}_y$ are mass, stiffness, damping, non-linear

force and force operators for transversal displacements in plane xy. The same can be made for bending in the plane xz. Given a set of initial conditions, $w_x(x,t), w_y(x,t), w_z(x,t), \theta_x(x,t)$, they must be transformed to be given as functions of the nodal quantities. For the displacements

$$\begin{aligned} w_{0x}(x) &= \sum_{i=1}^{\infty} a_{x_i}(0)\phi_i(x); \qquad & w_{0y}(x) &= \sum_{i=1}^{\infty} a_{y_i}(0)\psi_i(x) \\ w_{0z}(x) &= \sum_{i=1}^{\infty} a_{z_i}(0)\psi_i(x); \qquad & \theta_{0x}(x) &= \sum_{i=1}^{\infty} a_{\theta_i}(0)\phi_i(x). \end{aligned} \tag{3.33}$$

For velocities,

$$\begin{aligned} \dot{w}_{0x}(x) &= \sum_{i=1}^{\infty} \dot{a}_{x_i}(0)\phi_i(x); \qquad & \dot{w}_{0y}(x) &= \sum_{i=1}^{\infty} \dot{a}_{y_i}(0)\psi_i(x) \\ \dot{w}_{0z}(x) &= \sum_{i=1}^{\infty} \dot{a}_{z_i}(0)\psi_i(x); \qquad & \theta_{0x}(x) &= \sum_{i=1}^{\infty} \dot{a}_{\theta_i}(0)\phi_i(x). \end{aligned} \tag{3.34}$$

Multiplying both sides of the equations above by the appropriated function ψ or ϕ and integrating in the domain $[0 \quad L]$, results in

$$\begin{aligned} a_{0_{x_i}} &= \frac{\int_0^L w_{0_x}\phi_i dx}{\bar{m}_{x_{ij}}}; \qquad & a_{0_{y_i}} &= \frac{\int_0^L w_{0_y}\psi_i dx}{\bar{m}_{y_{ij}}} \\ a_{0_{z_i}} &= \frac{\int_0^L w_{0_z}\psi_i dx}{\bar{m}_{z_{ij}}}; \qquad & a_{0_{\theta_i}} &= \frac{\int_0^L \theta_{0_x}\phi_i dx}{\bar{m}_{\theta ij}}. \end{aligned} \tag{3.35}$$

Using the same procedure, the initial nodal velocity vector can be obtained

$$\begin{aligned} \dot{a}_{0x_i} &= \frac{\int_0^L \dot{w}_{0_x}\phi_i dx}{\bar{m}_{x_{ij}}}; \qquad & \dot{a}_{0y_i} &= \frac{\int_0^L \dot{w}_{0_y}\psi_i dx}{\bar{m}_{y_{ij}}} \\ \dot{a}_{0z_i} &= \frac{\int_0^L \dot{w}_{0_z}\psi_i dx}{\bar{m}_{z_{ij}}}; \qquad & \dot{a}_{0_{\theta i}} &= \frac{\int_0^L \dot{\theta}_{0_x}\phi_i dx}{\bar{m}_{\theta_{ij}}} \end{aligned} \tag{3.36}$$

In equations above,

$$\begin{aligned} \bar{m}_{x_{ij}} &= \int_0^L \phi_i\phi_j dx; \qquad & \bar{m}_{y_{ij}} &= \int_0^L \psi_i\psi_j dx \\ \bar{m}_{z_{ij}} &= \int_0^L \psi_i\psi_j dx; \qquad & \bar{m}_{\theta_{ij}} &= \int_0^L \phi_i\phi_j dx. \end{aligned} \tag{3.37}$$

3.2.4 Finite element discretization

In finite element context, the domain is discretized in small sub-domains and the deformed geometry is interpolated using a set of interpolating functions. For beam element, it is quite usual to use two nodes Hermite interpolating functions and, for bar and shaft elements, linear Lagrangian polynomials for

interpolating the axial displacements and torsional angles [26]. The element is presented in Figure 3.2.4 and corresponds to twelve degrees of freedom. The Hermite polynomials are

$$\begin{aligned}
\psi^{(1)} = \psi^{(1)}(x_e) &= 1 + 2\frac{x_e^3}{L_e^3} - 3\frac{x_e^2}{L_e^2} \\
\psi^{(2)} = \psi^{(2)}(x_e) &= x_e + \frac{x_e^3}{L_e^2} - 2\frac{x_e^2}{L_e} \\
\psi^{(3)} = \psi^{(3)}(x_e) &= 3\frac{x_e^2}{L_e^2} - 2\frac{x_e^3}{L_e^3} \\
\psi^{(4)} = \psi^{(4)}(x_e) &= \frac{x_e^3}{L_e^2} - \frac{x_e^2}{L_e}
\end{aligned} \tag{3.38}$$

and Lagrange polynomials are

$$\begin{aligned}
\phi^{(1)} = \phi^{(1)}(x_e) &= \frac{1}{L_e}(L_e - x_e) \\
\phi^{(2)} = \phi^{(2)}(x_e) &= \frac{1}{L_e}x_e
\end{aligned} \tag{3.39}$$

where L_e is the length of the element and $0 \leq x_e \leq L_e$.

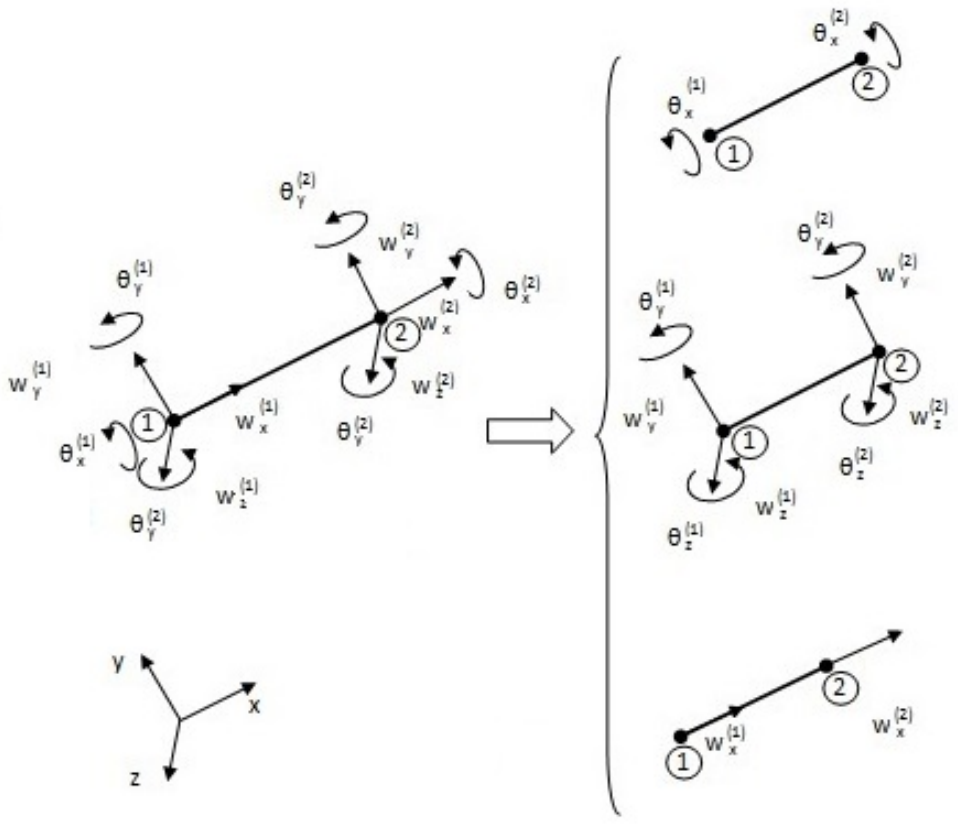

3.2(a): **Element with twelve d.o.f.**

So, the axial displacement element function is, using Lagrange polyno-

mials

$$w_{e_x} = \phi^{(1)} U_x^{e(1)} + \phi^{(2)} U_x^{e(2)} \tag{3.40}$$

and, using the same linear Lagrangian function to interpolate the angular displacements,

$$\theta_{e_x} = \phi^{(1)} U_{\theta_x}^{e(1)} + \phi^{(2)} U_{\theta_x}^{e(2)} \tag{3.41}$$

For transversal (y and z directions) displacements, one uses Hermite polynomials $\psi(x_e)$, so

$$w_{e_y} = \psi^{(1)} U_y^{e(1)} + \psi^{(1)} U_{\theta_z}^{e(1)} + \psi^{(2)} U_y^{e(2)} + \psi^{(2)} U_{\theta_z}^{e(2)} \tag{3.42}$$

$$w_{e_z} = \psi^{(1)} U_z^{e(1)} + \psi^{(1)} U_{\theta_y}^{e(1)} + \psi^{(2)} U_z^{e(2)} + \psi^{(2)} U_{\theta_y}^{e(2)} \tag{3.43}$$

The upper right indexes (1) and (2) mean node numbers. The Equations 3.40 to 3.43 can be gathered in a single 4×12 matrix so that,

$$\{U^e(x_e, t)\} = [H^e(x_e)]\{U^e(t)\} \tag{3.44}$$

where $\{U^e(x_e, t)\}$ is a vector containing the displacement functions, $[H^e(x_e)]$ is a matrix with the interpolating functions and the vector $U^e(t)$ is the nodal displacement vector for one finite element. This matrix equation is calculated for each element integrating the Equations 3.21,3.26,3.31 and 3.32 in element domain, resulting in the following expression, for each finite element

$$\begin{aligned} &[M_t^e]\{\ddot{U}^e(t)\} + [C_t^e]\{\dot{U}^e(t)\} + \{N_t^e(\dot{U}^e(t))\} + [K_t^e]\{U^e(t)\} = \{F_t^e(t)\}; \\ &\quad \{U^e(0)\} = \{U_0^e\} \quad \text{and} \quad \{\dot{U}^e(0)\} = \{\dot{U}_0^e\}, \end{aligned} \tag{3.45}$$

Using Equations 3.21, 3.26 and 3.31 one obtains all individual element matrices, which are assembled in a single global matrix, resulting in the following system:

$$\begin{aligned} &[M_t]\{\ddot{U}(t)\} + [C_t]\{\dot{U}(t)\} + \{N_t(\dot{U}(t))\} + [K_t]\{U(t)\} = \{F_t(t)\}; \\ &\quad \{U(0)\} = \{U_0\} \quad \text{and} \quad \{\dot{U}(0)\} = \{\dot{U}_0\}. \end{aligned} \tag{3.46}$$

The system represented in Equation 3.46 is formed by a set of differential equations which, together with the initial conditions, represents a time dependent and nonlinear problem, whose solution can be approximated using Newmark method. The nonlinearity is in the force $\{N_t(\dot{U})(t)\}$ which takes in consideration the interaction fluid-structure.

3.2.5 Construction of a reduced model

In general, the finite element formulation has a large number of degrees of freedom. Solving the problem in time can be expensive because of the large amount of computational operations. In order to diminish that number, more information about the structure must be obtained and a way to do so is to access its natural frequencies and modes. The natural modes and frequencies can be obtained by solving the eigenvalue problem

$$det\left[[K_t] - \varpi^2[M_t]\right] = 0. \tag{3.47}$$

Solving the Equation 3.47, a set of pairs of eigenvalues and its respective eigenvectors (ϖ_i^2,$\bar{v}_i$) is obtained. Then, the eigenvectors can be used to approximate the displacements of the structure and the more frequencies are considered, the better is the approximation of the solution. Nevertheless, to improve the approximation, the number of finite elements must be increased. It is expected that, as the number of finite elements tends to infinity, so do the eigenfunctions, and consequently, in the limit, the dynamics will be fully represented. Then it is must be possible to find a finite set of eigenfunctions and frequencies which approximate the dynamics within a certain precision [57]. This can be made iteratively by increasing the number of elements of the beam until the i_{th} mode converges for the required precision.

After obtaining a the set of n_{dof} eigenvalues ϖ_i^2 and their respective eigenvectors $\{\bar{v}\}_i$, they are organized in two matrices of dimension $n_{dof} \times n_{dof}$: one diagonal containing the eigenvalues and other, $[\bar{\bar{H}}]$, whose columns are composed by the eigenvectors. It is known that the eigenvectors form a base for the space $\Re^{n_{dof}}$ and the nodal displacement vector can be approximated by a linear combination of the eigenvectors as follows [27], [47]:

$$\{U(t)\} = [\bar{\bar{H}}]\{\bar{\bar{U}}(t)\}. \tag{3.48}$$

where $\{\bar{\bar{U}}(t)\}$ is a vector with time dependent components. The matrices and vectors after reduction will have the dimension $n_{eig} \times n_{eig}$ and $n_{eig} \times 1$. Although the Equation (3.46) is nonlinear, the non-linearities are not in the geometry. This means that a modal analysis can be performed using the undeformed configuration of the tower as the displacements and rotations are small. Due to the presence of the nonlinear force, the reduction of the degrees of freedom must be made on the incremental equation when applying the step by step method.

3.2.6
Incorporating the constraints

The turbine considered here is composed by six bodies. One of them, the tower, is flexible and the others are rigid. It is installed in the ground and small displacements and rotations are permitted at the base (x=0), due to the soil flexibility. The nacelle is fixed on top of tower and moves rigidly in connection with its top cross section. The shaft rotates keeping the axis of its proper rotation fixed with respect to the nacelle. It is also rigidly coupled to the blades. Each body was modeled separately in previous sections, but, due to the links they have, constraint equations must be introduced in order to impose the actual interaction between the bodies. Summarizing, the restriction imposed are:

- Tower tip cross section is rigidly coupled to the bottom surface of the nacelle;
- Shaft moves with the nacelle except for its proper rotation;
- Shaft and the blades are rigidly coupled.

As mentioned in section 3.1, the choice of the Euler parameters for defining the attitude of the rigid bodies imposed automatically five constraints, since those parameters are mutually dependent. They are:

$$\begin{aligned} g_{h_n} &= 1 - \{\Theta_n\}^T\{\Theta_n\} \\ g_{h_s} &= 1 - \{\Theta_s\}^T\{\Theta_s\} \\ g_{h_{b1}} &= 1 - \{\Theta_{b1}\}^T\{\Theta_{b1}\} \\ g_{h_{b2}} &= 1 - \{\Theta_{b2}\}^T\{\Theta_{b2}\} \\ g_{h_{b3}} &= 1 - \{\Theta_{b3}\}^T\{\Theta_{b3}\}. \end{aligned} \tag{3.49}$$

The tower is represented in Figure 3.2. The nacelle is installed on the tower and rotates rigidly with its top cross section. As the point (2) is common to both, nacelle and tower, then

$$\{g_{h_{t,n}}\} = \{U_{u_L}\} - [A_n]\{{}_n\bar{r}_t\} - \{R_n\}, \tag{3.50}$$

where $\{U_{u_L}\} = \{U_{u_L}(t)\}$ is the tower nodal displacement vector for $x = L$ (last node). The vector $\{{}_n\bar{r}_t\}$ is the position of the tower frame relative to nacelle frame and represented with respect to it (Figure 3.3).

The other holonomic constraints can be easily determined as

$$\begin{aligned} \{g_{h_{n,s}}\} &= \{R_n\} - [A_s]\{{}_s\bar{r}_n\} - \{R_s\} \\ \{g_{h_{s,b1}}\} &= \{R_s\} + [A_s]\{{}_s\bar{r}_h\} - [A_{b1}]\{{}_{b1}\bar{r}_h\} - R_{b_1} \\ \{g_{h_{s,b2}}\} &= \{R_s\} + [A_s]\{{}_s\bar{r}_h\} - [A_{b_2}]\{{}_{b2}\bar{r}_h\} - R_{b2} \\ \{g_{h_{s,b3}}\} &= \{R_s\} + [A_s]\{{}_s\bar{r}_h\} - [A_{b_3}]\{{}_{b3}\bar{r}_h\} - R_{b3} \quad , \end{aligned} \tag{3.51}$$

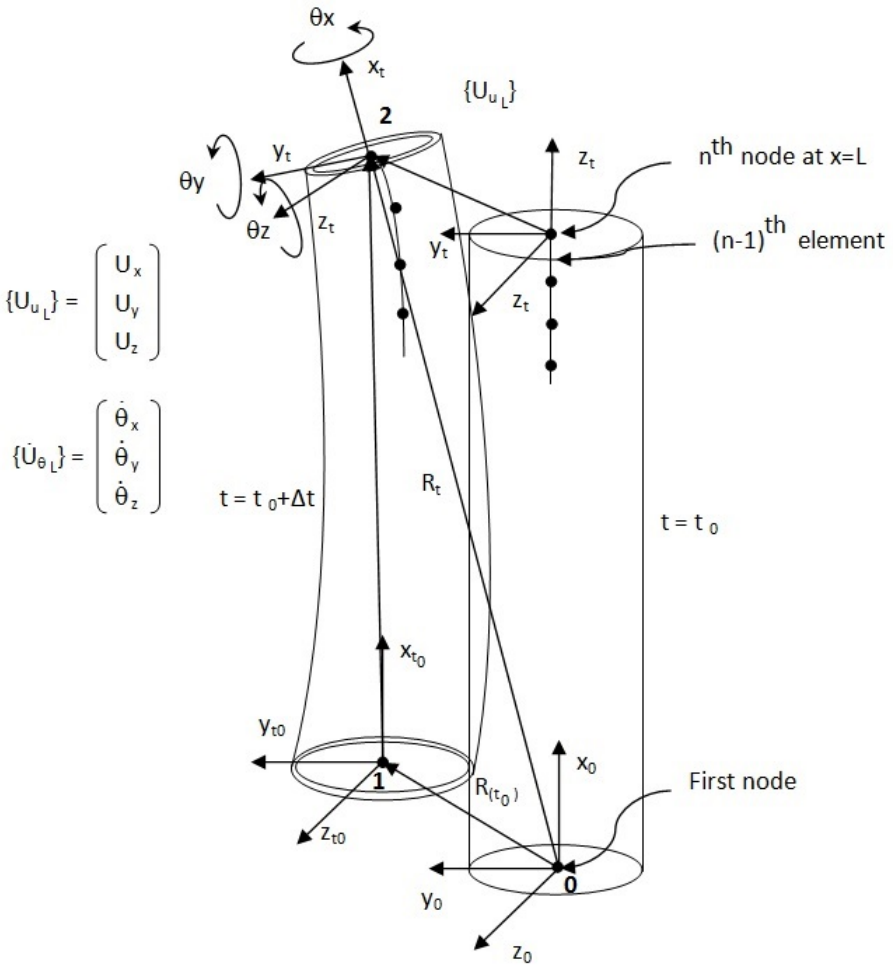

Figure 3.2: Tower

where $\{{}_s\bar{r}_n\}$, $\{{}_s\bar{r}_h\}$, $\{{}_{b1}\bar{r}_h\}$, $\{{}_{b2}\bar{r}_h\}$ and $\{{}_{b3}\bar{r}_h\}$ are represented in Figure 3.3.

For non-holonomic constraints, five sets of equations are obtained. Again, considering that the angular velocity of the top of the tower is the same as that experienced by the nacelle,

$$\{g_{nh_{t,n}}\} = \{\dot{U}_{\theta_L}\} - [G_n]\{\dot{\Theta}_n\} \tag{3.52}$$

where $\{\dot{U}_{\theta_L}\} = \{\dot{U}_{\theta_L}(t)\}$ is the vector with the angular velocities relative to the section containing the node at the tip of the tower ($x = L$). The matrix $[G]$ is defined in the section 7.2 of the Appendix. The shaft is carried by the nacelle but has a proper rotation. The nacelle and shaft angular velocities are the same except for the shaft spin. So, if the shaft angular velocity were the same as that of the nacelle, one would write

$$[\bar{G}_n]\{\dot{\Theta}_n\} = [A_n]^{-1}[G_s]\{\dot{\Theta}_s\}. \tag{3.53}$$

Now, one imposes that the first and the third components of 3.53 are the same and the third component is free, then

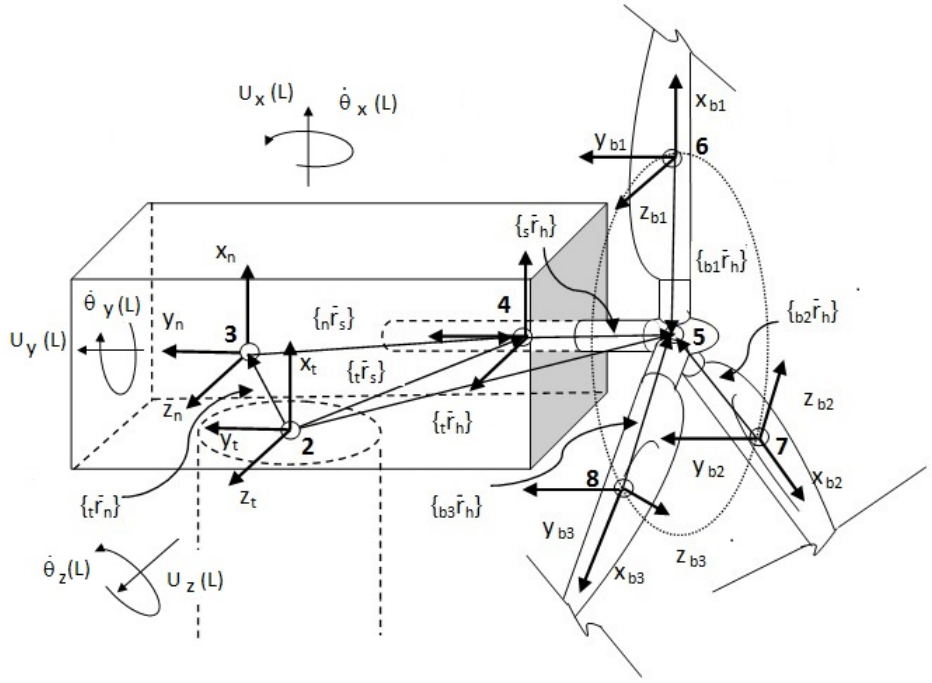

Figure 3.3: Nacelle, shaft and blades

$$\{g_{nh_{n,s}}\}_{1,3} = [\bar{G}_n]_{1,3}\{\dot{\Theta}_n\} - [\bar{G}_s^*]_{1,3}\{\dot{\Theta}_s\}, \tag{3.54}$$

where $[\bar{G}_s^*] = [A_n]^{-1}[G_s]$ and the index $1,3$ means that only the first and the third components are considered to be equal. The other component for shaft and nacelle are also in the same direction always but are different in magnitude. The difference between those two components gives the magnitude of the relative angular velocity between the shaft and the nacelle.

The other constraints result from the fact that the shaft and blades have the same angular velocity. Those assumptions are expressed as

$$\begin{aligned}
\{g_{nh_{s,b1}}\} &= [G_s]\{\dot{\Theta}_s\} - [G_{b1}]\{\dot{\Theta}_{b1}\} \\
\{g_{nh_{s,b2}}\} &= [G_s]\{\dot{\Theta}_s\} - [G_{b2}]\{\dot{\Theta}_{b2}\} \\
\{g_{nh_{s,b3}}\} &= [G_s]\{\dot{\Theta}_s\} - [G_{bl3}]\{\dot{\Theta}_{b3}\}.
\end{aligned} \tag{3.55}$$

One defines the following vectors of dimension 20×1 and 17×1:

$$[\mathbb{G}_h] = \{\{g_{h_{t,n}}\}^T \ \{g_{h_{n,s}}\}^T \ \{g_{h_{s,b1}}\}^T \ \{g_{h_{s,b2}}\}^T \ \{g_{h_{s,b3}}\}^T\}^T \tag{3.56}$$

$$[\mathbb{G}_{nh}] = \{\{g_{nh_{t,n}}\}^T \ \{g_{nh_{n,s}}\}^T \ \{g_{nh_{s,b1}}\}^T \ \{g_{nh_{s,b2}}\}^T \ \{g_{nh_{s,b3}}\}^T\} \tag{3.57}$$

The Jacobian matrix is then the derivatives of the holonomic set of equations with respect to all generalized coordinates, resulting in the following

20×38 matrix

$$\frac{\partial \mathbb{G}_h}{\partial \{q\}} = [\mathbb{J}_h] =$$

$$\begin{bmatrix}
[0_3] & [0_3] & -2\{\Theta_n\}^T & [0_3] & [0_4] & [0_3] & [0_4] & [0_3] & [0_4] & [0_3] & [0_4] \\
[0_3] & [0_3] & [0_4] & [0_3] & -2\{\Theta_s\}^T & [0_3] & [0_4] & [0_3] & [0_4] & [0_3] & [0_4] \\
[0_3] & [0_3] & [0_4] & [0_3] & [0_4] & [0_3] & -2\{\Theta_{b1}\}^T & [0_3] & [0_4] & [0_3] & [0_4] \\
[0_3] & [0_3] & [0_4] & [0_3] & [0_4] & [0_3] & [0_4] & [0_3] & -2\{\Theta_{b2}\}^T & [0_3] & [0_4] \\
[0_3] & [0_3] & [0_4] & [0_3] & [0_4] & [0_3] & [0_4] & [0_3] & [0_4] & [0_3] & -2\{\Theta_{b3}\}^T \\
[I_3] & -[I_3] & -[B_{n,t}] & [0_3] & [0_{34}] & [0_3] & [0_{34}] & [0_3] & [0_{34}] & [0_3] & [0_{34}] \\
[0_3] & [I_3] & [0_{34}] & -[I_3] & -[B_{s,n}] & [0_3] & [0_{34}] & [0_3] & [0_{34}] & [0_3] & [0_{34}] \\
[0_3] & [0_3] & [0_{34}] & [I_3] & [B_{hs}] & -[I_3] & -[B_{h,b1}] & [0_3] & [0_3] & [0_{34}] & [0_{34}] \\
[0_3] & [0_3] & [0_{34}] & [I_3] & [B_{h,s}] & [0_3] & [0_{34}] & -[I_3] & -[B_{h,b2}] & [0_{34}] & [0_{34}] \\
[0_3] & [0_3] & [0_{34}] & [I_3] & [B_{h,s}] & [0_3] & [0_{34}] & [0_3] & [0_3] & -[I_3] & -[B_{h,b3}]
\end{bmatrix},$$

where $[I_3]$ is the 3×3 identity matrix. $[0_3]$, $[0_{34}]$, $[0_{24}]$ and $[0_{23}]$ are 3×3, 3×4, 2×4 and 2×3, respectively. $[0_{13}]$ and $[0_{14}]$ are matrices with dimensions 1×3 and 1×4, respectively.

For non-holonomic constraints, the following 17×38 matrix is obtained (see, section 7.7 of the Annex).

$$\frac{\partial \mathbb{G}_{nh}}{\partial \{\dot{q}\}} = [\mathbb{J}_{nh}] =$$

$$\begin{bmatrix}
[I_3] & [0_3] & -[G_n] & [0_3] & [0_{34}] & [0_3] & [0_{34}] & [0_3] & [0_{34}] & [0_3] & [0_{34}] \\
[0_{23}] & [0_{23}] & [\bar{G}_n]_{1,3} & [0_{23}] & [G_s^*]_{1,3} & [0_3] & [0_{24}] & [0_{23}] & [0_{24}] & [0_{23}] & [0_{24}] \\
[0_3] & [0_3] & [0_{34}] & [0_3] & [G_s] & [0_3] & -[G_{b1}] & [0_3] & [0_{34}] & [0_3] & [0_{34}] \\
[0_3] & [0_3] & [0_{3x4}] & [0_3] & [G_s] & [0_3] & [0_{34}] & [0_3] & -[G_{b2}] & [0_3] & [0_{34}] \\
[0_3] & [0_3] & [0_{34}] & [0_3] & [G_s] & [0_3] & [0_{34}] & [0_3] & [0_{34}] & [0_3] & -[G_{b3}]
\end{bmatrix}$$

where $[G_s^*] = -[A]_n^{-1}[G_s]$, $[I_3]$ is the 3×3 identity matrix.

3.2.7
Assembling and solving the system of equations

It was obtained the equation for the motion of the rigid bodies, nacelle, shaft and blades (Equation 3.9). The formulation for the tower is given in Equation 3.46. In this section, the constraints were formulated resulting in Equations 3.58 and 3.58. It is now possible to assemble all equations and imposing the constrains so that the complete system shown in Equation 3.58 can be assembled:

$$\begin{cases} [\mathbb{M}]\{\ddot{\check{q}}\} + [\mathbb{J}_h]^T([\mathbb{P}_h]\{\mathbb{G}_h\} + [\mathbb{K}_h]\{\Lambda_h\}) + [\mathbb{J}_{nh}]^T([\mathbb{P}_{nh}]\{\mathbb{G}_{nh}\} + \\ [\mathbb{K}_{nh}]\{\dot{\Lambda}_{nh}\}) - \{\mathbb{Q}_d\} - \{\mathbb{Q}_k\} - \{\mathbb{Q}_v\} - \{\mathbb{Q}_e\} = \{0\} \\ [\mathbb{K}_h]\{\mathbb{G}_h\} = \{0\} \\ [\mathbb{K}_{nh}]\{\mathbb{G}_{nh}\} = \{0\} \\ \{\check{q}(t_0)\} = \{\check{q}_0\} \\ \{\dot{\check{q}}(t_0)\} = \{\dot{\check{q}}_0\} \\ \{\Lambda_h(t_0)\} = \{\Lambda_{0_{nh}}\} \\ \{\dot{\Lambda}_{nh}(t_0)\} = \{\dot{\Lambda}_{0_{nh}}\} \end{cases} \tag{3.58}$$

where $[\mathbb{M}]$ is the overall mass matrix (with the contribution of all bodies), $\{\mathbb{Q}_d\}$, $\{\mathbb{Q}_k\}$, $\{\mathbb{Q}_v\}$ and $\{\mathbb{Q}_e\}$, are vectors of the external generalized damping force, generalized force due to the flexibility of the body and other external elastic forces (springs, for instance), the quadratic velocity vector and the generalized external force, respectively. The calculation of those forces are presented in sections 7.6 and 7.8 of the Appendix. $\{\Lambda_h\}$ and $\{\dot{\Lambda}_{nh}\}$ are the Lagrange multipliers for holonomic and non-holonomic constrains, respectively. $\{\mathbb{G}_h\}$ and $\{\mathbb{G}_{nh}\}$ are the vector of the overall holonomic and non-holonomic functions respectively. All those vectors contain the contribution of all bodies that composes the system. The vector

$$\{\check{q}\} = \{\{U\}^T \quad \{q_n\}^T \quad \{q_s\}^T \quad \cdots \quad \{q_{b3}\}^T\}^T \tag{3.59}$$

is the vector of all the generalized coordinates. The matrices $\{\mathbb{J}_h\}$ and $\{\mathbb{J}_{nh}\}$ are presented in Equations 3.58 and 3.58. Finally, matrices $[\mathbb{K}_h]$, $[\mathbb{K}_{nh}]$, $[\mathbb{P}_h]$ and $[\mathbb{P}_{nh}]$ are diagonal overall matrices containing the scale factors and penalty factors holonomic and non-holonomic constraints.

Related to the initial conditions, it must be mentioned that they can not be applied independently, but the kinematic for all bodies must satisfy the constraints. If initial conditions are prescribed to the tower, then the angles and displacements at its tip must be the same as the base of the nacelle, and vice-versa. The angular velocity of the shaft must be the same as those of the rotation of the blades and so on. In this work, initial velocities and positions are null, except for the shaft and blades. For those components, it is possible to impose an initial speed. Next, it will be discussed the integration in time, but first, one must define the following augmented coordinate generalizes vector

$$\{q_\Lambda\} = \{\{U\}^T \quad \{q_n\}^T \quad \{q_s\}^T \quad \cdots \quad \{q_{b3}\}^T \quad \{\Lambda_h\} \quad \{\Lambda_{nh}\}\}^T, \tag{3.60}$$

in order to include the Lagrange multipliers. The problem presented in

Equation 3.58 is non-linear and, to be analyzed in a time interval $[0; t_{max}]$, it is usual to divide this interval into a certain number, say N, of sub-intervals of smaller uniform time steps of size Δt. Knowing the state in a time (for instance, in $t = 0$ (when the system given in Equation 3.58 is verified), one predicts the next values for accelerations, velocities and positions, by using the Newmark method, which defines the following integration scheme for the step $l + 1$

$$\begin{aligned} \{\dot{\tilde{q}}_\Lambda\}_{l+1} &= \{\dot{\tilde{q}}_\Lambda\}_l + (1-\gamma)\Delta t\{\ddot{\tilde{q}}_\Lambda\}_l + \gamma\Delta t\{\ddot{\tilde{q}}_\Lambda\}_{l+1} \\ \{\tilde{q}_\Lambda\}_{l+1} &= \{\tilde{q}_\Lambda\}_l + \Delta t\{\dot{\tilde{q}}_\Lambda\}_l + (\frac{1}{2}-\beta)(\Delta t)^2\{\ddot{\tilde{q}}_\Lambda\}_{l+1} \end{aligned} \tag{3.61}$$

where $\{\tilde{q}_\Lambda\}_l$, $\{\dot{\tilde{q}}_\Lambda\}_l$ and $\{\ddot{\tilde{q}}_\Lambda\}_l$ are approximations to $\{q_\Lambda\}$, $\{\dot{q}_\Lambda\}$ and $\{\ddot{q}_\Lambda\}$, respectively. The parameters γ and β are associated with the accuracy and stability of the scheme ([10],[26]). For dealing with the nonlinearities, the interactive Newton-Raphson method is used. At the end of each step the convergence is checked by measuring the error that must be below the level of precision required the approximate the solution. Newton-Raphson method defines the following iterative process for a k^{th} iteration

$$\begin{aligned} \{\ddot{\tilde{q}}_\Lambda\}_{l+1}^{k+1} &= \{\ddot{\tilde{q}}_\Lambda\}_{l+1}^{k} + \frac{1}{\beta\Delta t^2}\{\Delta\tilde{q}_\Lambda\} \\ \{\dot{\tilde{q}}_\Lambda\}_{l+1}^{k+1} &= \{\dot{\tilde{q}}_\Lambda\}_{l+1}^{k} + \frac{\gamma}{\beta\Delta t}\{\Delta\tilde{q}_\Lambda\} \\ \{\tilde{q}_\Lambda\}_{l+1}^{k+1} &= \{\tilde{q}_\Lambda\}_{l+1}^{k} + \{\Delta\tilde{q}_\Lambda\} \end{aligned} \tag{3.62}$$

where $\{\Delta\tilde{q}_\Lambda\}$ is the solution of the following linear system of algebraic equations

$$\left(\frac{1}{\beta\Delta t^2}\frac{\partial\{r^*\}}{\partial\{\ddot{q}_\Lambda\}} + \frac{1}{\beta\Delta t}\frac{\partial\{r^*\}}{\partial\{\dot{q}_\Lambda\}} + \frac{\partial\{r^*\}}{\partial\{q_\Lambda\}}\right)\{\Delta\tilde{q}_\Lambda\} = -\{r^*\}(\{\ddot{\tilde{q}}_\Lambda\},\{\dot{\tilde{q}}_\Lambda\},\{\tilde{q}_\Lambda\}). \tag{3.63}$$

The residue $\{r^*\}$ is defined as

$$\begin{aligned} \{r^*\} =& [\tilde{\mathbb{M}}]\{\ddot{\tilde{q}}\} + [\tilde{\mathbb{J}}_h]^T([\mathbb{P}_h]\{\tilde{\mathbb{G}}_h\} + [\mathbb{K}_h]\{\tilde{\Lambda}_h\}) + [\tilde{\mathbb{J}}_{nh}]^T([\mathbb{P}_{nh}]\{\tilde{\mathbb{G}}_{nh}\} + \\ & [\mathbb{K}_{nh}]\{\dot{\tilde{\Lambda}}_{nh}\}) - \{\tilde{\mathbb{Q}}_d\} - \{\tilde{\mathbb{Q}}_k\} - \{\tilde{\mathbb{Q}}_v\} - \{\tilde{\mathbb{Q}}_e\}, \end{aligned} \tag{3.64}$$

submitted to the same initial conditions presented in Equation 3.58. The constrained initial value problem of Equation 3.58 together with the Newmark scheme shown in Equation 3.61 define a nonlinear problem of algebraic equations with unknowns $\{q_\Lambda\}_l$, $\{\dot{q}_\Lambda\}_l$ and $\{\ddot{q}_\Lambda\}_l$. This is an approximation using Taylor expansion in step l and iteration k and imposing $\{r^*\}_l^{(k+1)} = \{0\}$. In order to solve the Equation 3.63 for $\{\Delta\tilde{q}_\Lambda\}$, the necessary derivatives of the residue with respect to $\{\tilde{q}_\Lambda\}$, $\{\dot{\tilde{q}}_\Lambda\}$ and $\{\ddot{\tilde{q}}_\Lambda\}$ must be calculated. They are

$$
\begin{aligned}
&\frac{\partial\{r^*\}}{\partial\{\ddot{q}_\Lambda\}} = [\tilde{\mathbb{M}}_\Lambda] \\
&\frac{\partial\{r^*\}}{\partial\{\dot{q}_\Lambda\}} = \frac{\partial}{\partial\{\dot{q}_\Lambda\}}\{[\tilde{\mathbb{M}}_\Lambda]\{\ddot{\tilde{q}}_\Lambda\}\} - \frac{\partial}{\partial\{\dot{q}_\Lambda\}}\{\tilde{\mathbb{Q}}_d\} - \frac{\partial}{\partial\{\dot{q}_\Lambda\}}\{\tilde{\mathbb{Q}}_k\} - \frac{\partial}{\partial\{\dot{q}_\Lambda\}}\{\tilde{\mathbb{Q}}_v\} \\
&- \frac{\partial}{\partial\{\dot{q}_\Lambda\}}\{\tilde{\mathbb{Q}}_f\} + \{[\tilde{\mathbb{J}}_{nh}]^T[\mathbb{P}_{nh}][\tilde{\mathbb{J}}_{nh}]\} + \{[\tilde{\mathbb{J}}_{nh}]^T[\mathbb{K}_{nh}]\} \\
&+ \frac{\partial[\tilde{\mathbb{J}}_{nh}]^T}{\partial\{\dot{q}_\Lambda\}}[\mathbb{P}_{nh}]\{\tilde{\mathbb{G}}_{nh}\} + \frac{\partial[\tilde{\mathbb{J}}_{nh}]^T}{\partial\{\dot{q}_\Lambda\}}[\mathbb{K}_{nh}]\{\dot{q}_\Lambda\} \\
&\frac{\partial\{r^*\}}{\partial\{q_\Lambda\}} = \frac{\partial}{\partial\{q_\Lambda\}}\{[\tilde{\mathbb{M}}_\Lambda]\{\ddot{\tilde{q}}_\Lambda\}\} - \frac{\partial}{\partial\{q_\Lambda\}}\{\tilde{\mathbb{Q}}_d\} - \frac{\partial}{\partial\{q_\Lambda\}}\{\tilde{\mathbb{Q}}_k\} - \frac{\partial}{\partial\{q_\Lambda\}}\{\tilde{\mathbb{Q}}_v\} \\
&- \frac{\partial}{\partial\{q_\Lambda\}}\{\tilde{\mathbb{Q}}_e\} + \{[\tilde{\mathbb{J}}_h]^T[\mathbb{P}_h][\tilde{\mathbb{J}}_h]\} + \{[\tilde{\mathbb{J}}_h]^T[\mathbb{K}_h]\} \\
&+ \frac{\partial[\tilde{\mathbb{J}}_h]^T}{\partial\{q_\Lambda\}}[\mathbb{P}_h]\{\tilde{\mathbb{G}}_h\} + \frac{\partial[\tilde{\mathbb{J}}_h]^T}{\partial\{q_\Lambda\}}[\mathbb{K}_h]\{q_\Lambda\}\}
\end{aligned}
\tag{3.65}
$$

where it was also considered that

$$
\frac{\partial}{\partial\{\dot{\tilde{q}}_\Lambda\}}([\tilde{\mathbb{J}}_h]^T[\mathbb{K}_h]\tilde{\Lambda}_h) = \frac{\partial}{\partial\{\dot{\tilde{q}}_\Lambda\}}([\mathbb{K}_{nh}]\dot{\tilde{\Lambda}}_{nh}) = 0. \tag{3.66}
$$

Concerning the constrains, it can be said that

$$
\begin{aligned}
-\{\tilde{\mathbb{G}}_h^*\} &= \frac{\partial}{\partial\{\tilde{\dot{q}}\}}\{\tilde{\mathbb{G}}_h\}\{\Delta\tilde{\dot{q}}\} = \tilde{\mathbb{J}}_h\{\Delta\tilde{\dot{q}}\} \\
-\{\tilde{\mathbb{G}}_{nh}^*\} &= \frac{\partial}{\partial\{\dot{\tilde{q}}\}}\{\tilde{\mathbb{G}}_{nh}\}\{\Delta\dot{\tilde{q}}\} = \tilde{\mathbb{J}}_{nh}\{\Delta\dot{\tilde{q}}\}
\end{aligned}
\tag{3.67}
$$

since, at the end of incremental step one imposes that $\{\tilde{\mathbb{G}}_h\}_l^{k+1} = 0$ and $\{\tilde{\mathbb{G}}_{nh}\}_l^{k+1} = 0$. The calculation of all derivatives is given in section 7.8 in Appendix.

In order to construct the reduced model with the eigenvectors of the structure, on has to define the following matrix $[\bar{\mathbb{H}}]$:

$$
[\bar{\bar{\mathbb{H}}}] = \begin{bmatrix}
\bar{\bar{H}}_{11} & \bar{\bar{H}}_{12} & \cdots & \bar{\bar{H}}_{1n_{eig}} & 0 & \cdots & 0 \\
\bar{\bar{H}}_{21} & \bar{\bar{H}}_{22} & \cdots & \bar{\bar{H}}_{2n_{eig}} & 0 & \cdots & 0 \\
\vdots & \vdots & \vdots & \vdots & \vdots & \vdots & \vdots \\
\bar{\bar{H}}_{n_{dof}1} & \bar{\bar{H}}_{n_{gc}2} & \cdots & \bar{\bar{H}}_{n_{dof}n_{eig}} & 0 & \cdots & 0 \\
1 & 0 & 0 & \cdots & 0 & \cdots & 0 \\
0 & 1 & 0 & \cdots & 0 & \cdots & 0 \\
0 & 0 & 1 & \cdots & 0 & \cdots & 0 \\
\vdots & \vdots & \vdots & \vdots & \vdots & \vdots & \vdots \\
\cdots & \cdots & \cdots & \cdots & 1 & 0 & 0 \\
0 & 0 & \cdots & \cdots & 0 & 1 & 0 \\
0 & 0 & \cdots & \cdots & 0 & 0 & 1
\end{bmatrix}
\tag{3.68}
$$

so that

$$[\bar{\bar{\mathbb{H}}}]\{\tilde{q}_{red}\} = \{\tilde{q}_\Lambda\} \tag{3.69}$$

and, now, the vector $\{\tilde{q}_{red}\}$ contains in first n_{eig} lines, the reduced beam d.o.f.

So, substituting Equation 3.69 into 3.63, it becomes

$$\left(\frac{1}{\beta\Delta t^2}\frac{\partial\{r^*\}}{\partial\{\ddot{q}_\Lambda\}} + \frac{1}{\beta\Delta t}\frac{\partial\{r^*\}}{\partial\{\dot{q}_\Lambda\}} + \frac{\partial\{r^*\}}{\partial\{q_\Lambda\}}\right)[\bar{\bar{\mathbb{H}}}]\{\Delta\tilde{q}_{red}\} = -\{r^*\}(\{\ddot{\tilde{q}}^*_\Lambda\},\{\dot{\tilde{q}}^*_\Lambda\},\{\tilde{q}^*_\Lambda\}). \tag{3.70}$$

Projecting the dynamics into the space generated by the eigenvectors,

$$[\bar{\bar{\mathbb{H}}}]^T\left(\frac{1}{\beta\Delta t^2}\frac{\partial\{r^*\}}{\partial\{\ddot{q}_\Lambda\}} + \frac{1}{\beta\Delta t}\frac{\partial\{r^*\}}{\partial\{\dot{q}_\Lambda\}} + \frac{\partial\{r^*\}}{\partial\{q_\Lambda\}}\right)[\bar{\bar{\mathbb{H}}}]\{\Delta\tilde{q}_{red}\} = -\{r^*_{red}\} \tag{3.71}$$

and

$$\{r^*_{red}\} = [\bar{\bar{\mathbb{H}}}]^T\{r^*\}(\{\ddot{\tilde{q}}^*_\Lambda\},\{\dot{\tilde{q}}^*_\Lambda\},\{\tilde{q}^*_\Lambda\}).\text{,} \tag{3.72}$$

Using the matrix $[\bar{\bar{\mathbb{H}}}]$, only the degrees of freedom related to the tower will be transformed. The matrices 3.58, 3.58 can be transformed in order to consider the reduced tower degrees of freedom. The transformation results, for $[\mathbb{J}_{nh_{red}}]$,

$$[\mathbb{J}_{h_{red}}] = \begin{bmatrix}
\{0_{n_{eig}}\} & \{0_3\} & -2\{\Theta_n\}^T & \{0_3\} & \{0_4\} & \{0_3\} & 2\{0_4\} & \{0_3\} & \{0_4\} & \{0_{nm}\} & \{0_4\} \\
\{0_{n_{eig}}\} & \{0_3\} & \{0_4\} & \{0_3\} & -2\{\Theta_s\}^T & \{0_3\} & \{0_4\} & \{0_3\} & [\{0_4\} & \{0_3\} & \{0_4\} \\
\{0_{n_{eig}}\} & \{0_3\} & \{0_4\} & \{0_3\} & \{0_4\} & \{0_3\} & -2\{\Theta_{b1}\}^T & \{0_3\} & \{0_4\} & \{0_3\} & \{0_4\} \\
\{0_{n_{eig}}\} & \{0_3\} & \{0_4\} & \{0_3\} & \{0_4\} & \{0_3\} & \{0_4\} & \{0_3\} & -2\{\Theta_{b2}\}^T & \{0_3\} & \{0_4\} \\
\{0_{n_{eig}}\} & \{0_3\} & [0_4] & \{0_3\} & \{0_4\} & \{0_3\} & \{0_4\} & \{0_3\} & \{0_4\} & \{0_3\} & -2\{\Theta_{b3}\}^T \\
[\bar{\bar{H}}_{u_L}] & -[I_3] & -[B_{n,t}] & [0_3] & [0_{34}] & [0_3] & [0_{34}] & [0_3] & [0_{34}] & [0_3] & [0_{34}] \\
[0_{3n_{eig}}] & [I_3] & [0_{34}] & -[I_3] & -[B_{s,n}] & [0_3] & [0_{34}] & [0_3] & [0_{34}] & [0_3] & [0_{3x4}] \\
[0_{3n_{eig}}] & [0_3] & [0_{34}] & [I_3] & [B_{hs}] & -[I_3] & -[B_{h,b1}] & [0_3] & [0_3] & [0_{34}] & [0_{34}] \\
[0_{3n_{eig}}] & [0_3] & [0_{34}] & [I_3] & [B_{h,s}] & [0_3] & [0_{34}] & -[I_3] & -[B_{h,b2}] & [0_{34}] & [0_{34}] \\
[0_{3n_{eig}}] & [0_3] & [0_{34}] & [I_3] & [B_{h,s}] & [0_3] & [0_{34}] & [0_3] & [0_3] & -[I_3] & -[B_{h,b3}]
\end{bmatrix}.$$

and for $[\mathbb{J}_{nh_{red}}]$,

$$[\mathbb{J}_{nh_{red}}] = \begin{bmatrix}
[\bar{\bar{H}}_{\theta_L}] & [0_3] & -[G_n] & [0_3] & [0_{34}] & [0_3] & [0_{34}] & [0_3] & [0_{34}] & [0_3] & [0_{34}] \\
[0_{3nm}] & [0_3] & [G_n] & [0_3] & [G^*_s] & [0_3] & [0_{34}] & [0_3] & [0_{34}] & [0_3] & [0_{34}] \\
[0_{3nm}] & [0_3] & [0_{34}] & [0_3] & [G^s] & [0_3] & [0_{34}] & [0_3] & [0_{34}] & [0_3] & [0_{34}] \\
[0_{3nm}] & [0_3] & [0_{34}] & [0_3] & [G_s] & [0_{33}] & -[G_{b1}] & [0_3] & [0_{34}] & [0_3] & [0_{34}] \\
[0_{3nm}] & [0_3] & [0_{3x4}] & [0_3] & [G_s] & [0_3] & [0_{34}] & [0_3] & -[G_{b2}] & [0_3] & [0_{34}] \\
[0_{3nm}] & [0_3] & [0_{34}] & [0_3] & [G_s] & [0_3] & [0_{34}] & [0_3] & [0_{34}] & [0_3] & -[G_{b3}]
\end{bmatrix}$$

and the constraint $g_{h_{t,n}}$ can be rewritten as

$$\{g_{h_{t,n}}\} = [\bar{\bar{H}}_{u_L}]\{\bar{\bar{U}}_{u_L}(t)\} - [A_n](_n r_t) - \{R_n\}. \tag{3.73}$$

and $g_{nh_{t,n}}$, as

$$\{g_{nh_{t,n}}\} = [\bar{\bar{H}}_{\theta_L}]\{\dot{\bar{\bar{U}}}_{\theta_L}(t)\} - [G_n]\{\dot{\Theta}_n\} \tag{3.74}$$

The matrices $[\bar{\bar{H}}_{u_L}]$ and $\bar{\bar{H}}_{\theta_L}]$ are sub-matrices of the eigenvectors matrix $[\bar{\bar{H}}]$ associated to the system, and defined as below

$$[\bar{\bar{H}}_{u_L}] = \begin{pmatrix} \bar{\bar{H}}_{u_{n_{dof}-5,1}} & ... & \bar{\bar{H}}_{n_{dof}-5,2} & \cdots & \bar{\bar{H}}_{n_{dof}-5,n_{eig}} \\ \bar{\bar{H}}_{n_{dof}-4,1} & ... & \bar{\bar{H}}_{n_{dof}-4,2} & \cdots & \bar{\bar{H}}_{n_{dof}-4,n_{eig}} \\ \bar{\bar{H}}_{n_{dof}-3,1} & ... & \bar{\bar{H}}_{n_{dof}-3,2} & \cdots & \bar{\bar{H}}_{n_{dof}-3,n_{eig}} \end{pmatrix} \tag{3.75}$$

$$[\bar{\bar{H}}_{\theta_L}] = \begin{pmatrix} \bar{\bar{H}}_{n_{dof}-2,1} & ... & \bar{\bar{H}}_{n_{dof}-2,2} & \cdots & \bar{\bar{H}}_{n_{dof}-2,n_{eig}} \\ \bar{\bar{H}}_{n_{dof}-1,1} & ... & \bar{\bar{H}}_{n_{dof}-1,2} & \cdots & \bar{\bar{H}}_{n_{dof}-1,n_{eig}} \\ \bar{\bar{H}}_{n_{dof},1} & ... & \bar{\bar{H}}_{n_{dof},2} & \cdots & \bar{\bar{H}}_{ndof,n_{eig}} \end{pmatrix} \tag{3.76}$$

where the components $\bar{\bar{H}}_{u_{ij}}$ and $\bar{\bar{H}}_{\theta_{ij}}$ are obtained for $x = L$ and are associated to the degrees of freedom of displacement and rotation, respectively, at the node of the beam at the interface with the nacelle.

Taking in consideration Equations 3.67, the problem is finally formulated as

$$\begin{aligned} &[\mathfrak{K}_{red}]\{\Delta\tilde{q}_{red}\} = -\{r^*_{red}\} \\ &[\tilde{\mathbb{J}}_{h_{red}}]\{\Delta\tilde{\dot{q}}_{red}\} = -\{\tilde{\mathbb{G}}^*_{nh_{red}}\} \\ &[\tilde{\mathbb{J}}_{nh_{red}}]\{\Delta\tilde{\ddot{q}}_{red}\} = -\{\tilde{\mathbb{G}}^*_{nh_{red}}\}, \end{aligned} \tag{3.77}$$

with the initial conditions

$$\begin{aligned} &\{\check{q}(t_0)\} = \{q_0\} \\ &\{\dot{\check{q}}(t_0)\} = \{\dot{q}_0\} \\ &\{\Lambda_h(t_0)\} = \{\Lambda_0\} \\ &\{\dot{\Lambda}_{nh}(t_0)\} = \{\dot{\Lambda}_0\}, \end{aligned} \tag{3.78}$$

where, $\{r^*_{red}\}$ is given by the Equation 3.72.The vectors $\{q_{red}\}$ and $\{\check{q}_{red}\}$ are, respectively:

$$\{q_{red}\} = \{\{\bar{\bar{U}}\}^T \quad \{q_n\}^T \quad \{q_s\}^T \quad \cdots \quad \{q_{b3}\}^T \quad \{\Lambda_h\} \quad \{\Lambda_{nh}\}\}^T \tag{3.79}$$

and

$$\{\check{q}_{red}\} = \{\{\bar{\bar{U}}\} \quad \{q_s\}^T \quad \cdots \quad \{q_{b3}\}^T\}^T. \tag{3.80}$$

The matrix $\mathfrak{K}_{red}$ is

$$\mathfrak{K}_{red} = \bar{\bar{\mathbb{H}}}^T \left(\frac{1}{\beta\Delta t^2}\frac{\partial\{r^*\}}{\partial\{\ddot{q}_\Lambda\}} + \frac{1}{\beta\Delta t}\frac{\partial\{r^*\}}{\partial\{\dot{q}_\Lambda\}} + \frac{\partial\{r^*\}}{\partial\{q_\Lambda\}} \right) \bar{\bar{\mathbb{H}}}. \tag{3.81}$$

The incremental scheme is given by Equations 3.61 and 3.62. Operationally, the appropriated derivatives are performed in Equation 7.8. So, the matrix at the left of the system given in 3.77 is obtained. Then, the second and third matrices are obtained and assembled. The initial conditions must be introduced (considering the they are compatible with the constraints) and

the system is solved for the Lagrange multipliers and accelerations. With the initial state determined, the Newmark and Newton-Raphson schemes are used to integrate in time.

Related to the convergence criteria, two measures are used in this work to check the level of precision. One controls the evolution of the residue and the other the constraints. In practical terms, this procedure of founding the approximation for the solution continues until the L^2 norm of the residual vector and the residual constraints vector becomes smaller than a specified tolerance, that is

$$\begin{aligned} \|r^*_{red}\| &\leq \epsilon_{r^*} \\ \|\mathbb{G}^*_{red}\| &\leq \epsilon_{\mathbb{G}^*}, \end{aligned} \tag{3.82}$$

where ϵ_{r^*} and $\epsilon_{\mathbb{G}^*}$ are imposed tolerances.

4
Loading

4.1
Wind and water loads acting on the tower

The wind passes through the plane of rotation causing torques and forces that are felt by the tower through the shaft. The tower is affected by the wind directly when the it flows around. Also, mainly in case of upwind turbines, complex effects take place when the blades pass in front of the tower causing perturbation in the flow. Terrain roughness and other turbines installed nearby also causes the flow to be perturbed and affects the behavior of the tower. In some offshore structures, the tower is partially immersed, so that the movement of the water loads the tower. The loads will vary with the direction of the currents and surface waves. On the other hand, the presence of the water damps the structure and reduces its natural frequencies due to the "added mass" effect, whenever there is a relative acceleration between the fluid and the tower. In this work, only the current effect will be considered without any wave effects.

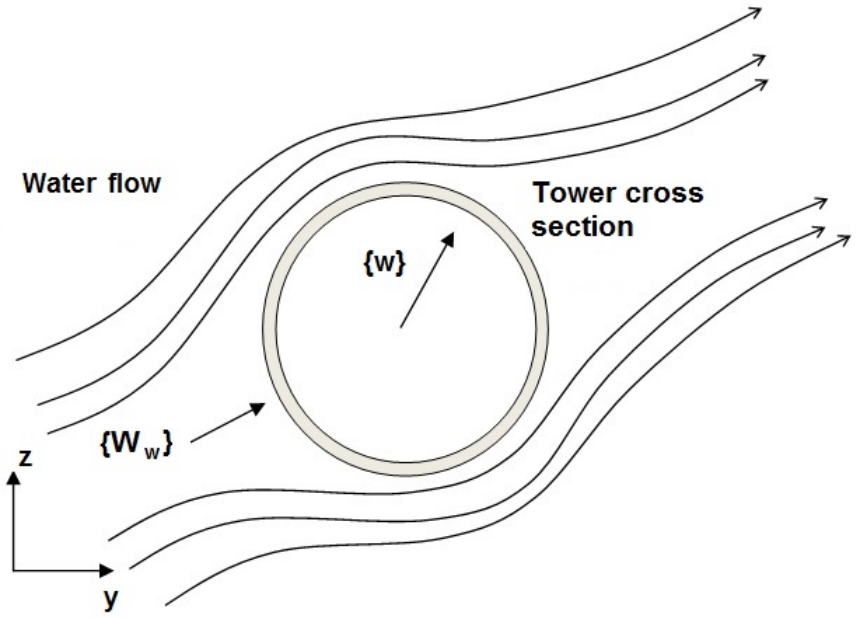

Figure 4.1: Fluid interaction with the tower (cross section)

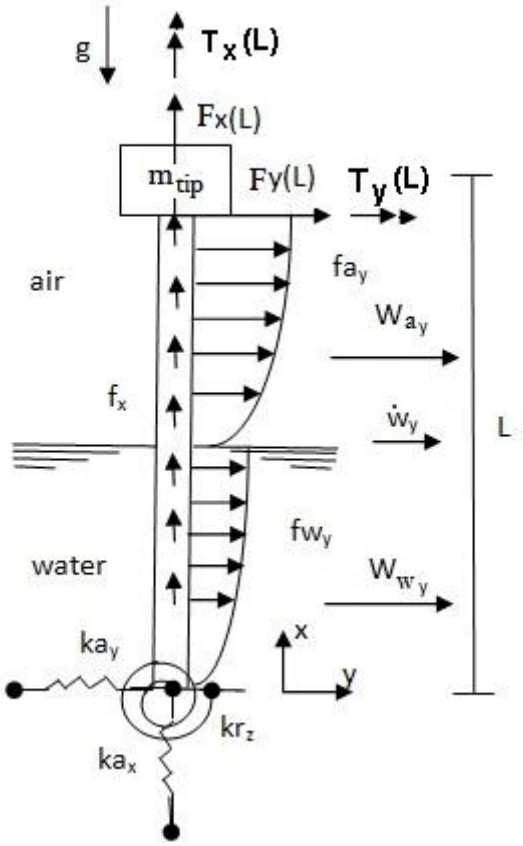

4.2(a): **Model (plane xy)**

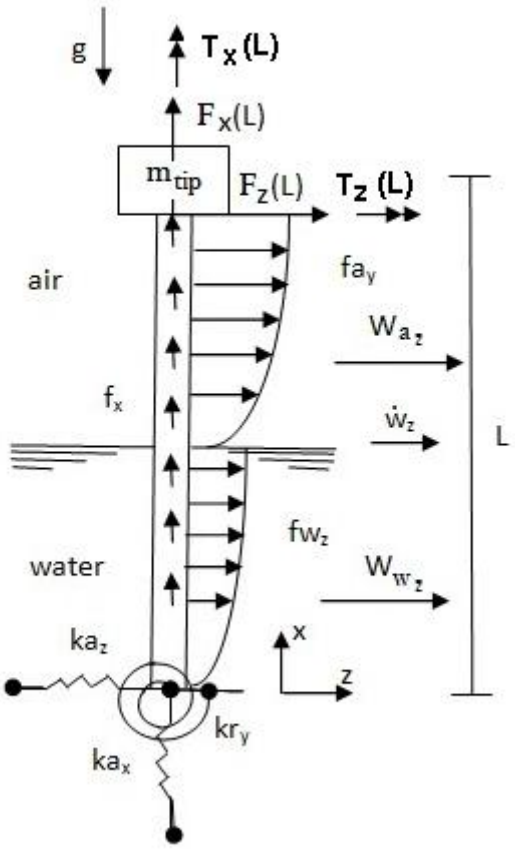

4.2(b): **Model (plane xz)**

The wind deterministic speed can be modeled by a logarithmic equation given in Equation 2.2, which describes the mean profile of the wind as the height varies and, for the case of immersed tower,

$$W_a(x) = \bar{W}_a(x_1)(log((x - h_w)/x_0)/log(x_1/x_0)), \quad [h_w < x \leq L^*], \quad (4.1)$$

where, h_w is the height of level of the water surface and L^* is the maximum height of the water level.

The water deterministic speed in this work is modeled as

$$W_w(x,t) = \bar{W}_w(x) + \Delta\bar{W}_w(x)cos(\varpi_w t + \theta_w), \quad [0 \leq x \leq h_w], \quad (4.2)$$

with

$$W_w(x,t) = \|\{W_w(x,t)\}\| \quad (4.3)$$

and $\bar{W}_w(x)$ and $\Delta\bar{W}_w(x)$ are constant functions of x.

$$\{W_w(x,t)\} = \begin{Bmatrix} 0 \\ W_{w_y}(x,t) \\ W_{w_z}(x,t) \end{Bmatrix}. \quad (4.4)$$

4.2 Wind loads in the blades

As discussed previously, the focus of this thesis is kept in horizontal axis wind turbine (HAWT) what means that the wind blows perpendicularly to the plane of the rotor. When wind approaches the plane of the rotor it is influenced by the rotor itself, slows down and the pressure increases. When passing through the blades it transfers kinetic energy so that the pressure drops, causing a force over the blades (thrust). The process can be explained using simplified models without using any specific turbine design, but only energy concepts [35]. The simpler idea is to consider the turbine as a permeable actuator disc and assume that the interaction fluid/disc is ideal. This is known as 1-D momentum theory for ideal turbines [23]. It can be found in those two previous references all the details about the interaction between blades and wind. Nevertheless, those ideas and concepts will be again shown here just because they are the key for understanding the subject. First it is considered that a front of wind with diameter equal to that of the rotor contains the available power of

$$P_{av} = \frac{1}{2}\rho_a A_{sw} W_{a\infty}^3. \tag{4.5}$$

However, this power is not entirely transmitted to the blades because not all mass will pass through the blades as shown in Figure 4.2. Besides, the wind after passing the turbine may still has kinetic energy. This means that there must be a limit in the transmission of energy from the wind mass to the blades. This is known as the Betz limit(after Albert Betz (1885-1968)). Then, the power factor, the relation between the extracted and available power is

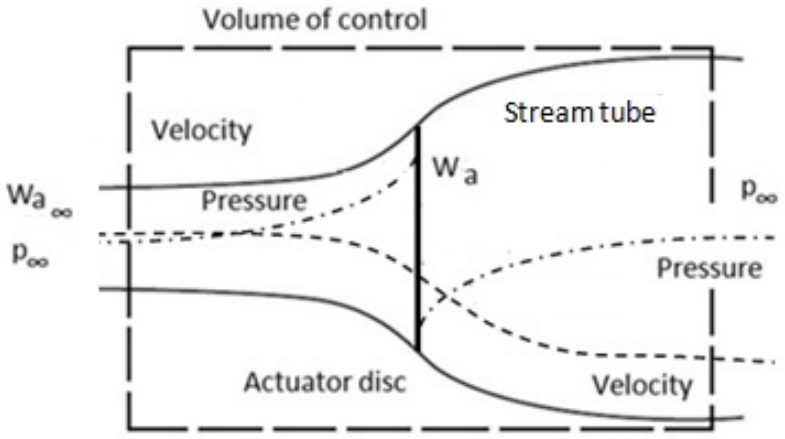

Figure 4.2: Conservative flow in an actuator [23]

$$C_P = P_{ex}/P_{av} \tag{4.6}$$

4.2.1 1-D Momentum theory for ideal turbine

As already mentioned, this theory idealizes a permeable disc positioned perpendicularly to the ideal flow. The assumptions are [23]:

- The disc is permeable and considered a drag device;
- Mach number is small and density of the air is constant;
- The flow is stationary, incompressible and frictionless;
- It is considered an infinite number of blades;
- The wake does not rotate downstream;
- Far from the disk, the static pressure upstream and downstream are equal to the undisturbed static pressure.

Under those conditions, Bernoulli equation can be applied just at left and at right of the disc, considering that

$$\Delta p = p_l - p_r \tag{4.7}$$

and using continuity considerations

$$W_{a_l} = W_{a_r} = W_a. \tag{4.8}$$

Then, applying Bernoulli equation,

$$p_\infty + \frac{1}{2}\rho_a W_{a_\infty}^2 = p + \frac{1}{2}\rho_a W_a^2 \tag{4.9}$$

and

$$(p_l - \Delta p) + \frac{1}{2}\rho_a W_{a_l}^2 = p_r + \frac{1}{2}\rho_a W_{a_r}^2 \tag{4.10}$$

Combining two previous equations

$$\Delta p = \frac{1}{2}\rho_a (W_{a_\infty}^2 - W_{a_r}^2) \tag{4.11}$$

The thrust force is resultant of the drop of the pressure in the rotor plane and is

$$Th = \Delta p A_{sw} = \frac{1}{2}\rho_a (W_{a_\infty}^2 - W_{a_r}^2) A_{sw} \tag{4.12}$$

Applying the integral equation (momentum equation) in the volume of Figure 4.2 to calculate the variation of the momentum in axial direction, it becomes that:

$$Th = -(\rho_a W_{a_r}^2 A_r + \rho_a W_{a_\infty}^2 (A_{cv} - A_r) + \dot{m}_{out} W_{a_\infty} - \rho_a W_{a_\infty}^2 A_{cv}) \tag{4.13}$$

The mass that crosses the control volume per unit of time, using conservation of mass, is

$$\dot{m}_{out} = \rho_a A_r (W_{a_\infty} - W_{a_r}) \tag{4.14}$$

and,

$$\dot{m} = \rho_a W_a A_{sw} = \rho_a W_{a_r} A_r \tag{4.15}$$

Combining 4.13, 4.14 and 4.15, results that

$$Th = \rho_a W_a A_{sw} (W_{a_\infty} - W_{a_r}) \tag{4.16}$$

It is possible to demonstrate that [23]

$$W_a = \frac{1}{2}(W_{a_\infty} + W_{a_r}) \tag{4.17}$$

Using this, the power equation becomes

$$P_{ex} = \frac{1}{2}\rho_a W_{a_\infty} A_{sw} (W_{a_\infty}^2 - W_{a_r}^2) \tag{4.18}$$

The axial induction factor a is defined as

$$a = \frac{W_{a_\infty} - W_a}{W_{a_\infty}} \tag{4.19}$$

then

$$W_a = (1-a) W_{a_\infty}. \tag{4.20}$$

Considering that the power transmitted to the device is the same as that lost by the wind

$$P_{ex} = \frac{1}{2}\rho_a W_{a_\infty}^3 a(1-a)^2 A_{sw}. \tag{4.21}$$

The thrust is then

$$Th = \frac{1}{2}\rho_a W_{a_\infty}^2 a(1-a) A_{sw}. \tag{4.22}$$

The power coefficient was defined in Equation 4.6. Substituting the equation 4.21 into 4.6 it results in

$$C_P = 4a(1-a)^2 \tag{4.23}$$

and in the same way for the thrust,

$$C_{Th} = 4a(1-a). \tag{4.24}$$

Derivatives of C_P and C_T with respect to a equated to zero gives the maximum coefficient $C_P = 16/27$ for $a = 1/3$. For thrust coefficient, the maximum is $C_T = 1$ and occurs for $a = 0.5$. The value of $C_P = 16/27$ is the Betz limit. This theory is limited to values for induction factor $a <\approx 0.4$ [23]. Due to the mechanical and electrical efficiency, the amount of power obtained

is even smaller. Then, useful electric power P_{out} is affected by the overall power coefficient

$$\eta_{tot} = \frac{P_{out}}{\frac{1}{2}\rho_a A_{sw} W_{a_\infty}^3}, \tag{4.25}$$

$$\eta_{tot} = \eta_{ele}\eta_{mec}C_P, \tag{4.26}$$

so that, the useful electric power is

$$P_{out} = \eta_{tot}(\frac{1}{2}\rho_a A_{sw} W_{a_\infty}^3). \tag{4.27}$$

4.2.2 Rotation in wake

Only one direction was used and necessary to understand the mechanism of transmission of energy from wind to the turbine, although radial components are present in this kind of flow too. Two important quantities, the thrust over the disk and power transfered could be calculated without any reference to the blades. Nevertheless, in real turbines, after exiting the rotor the flow rotates due the interaction with the blades and this has to be also considered. This interaction produces the torque which makes the blades rotate in the opposite direction of that of the wind. The problem must be analyzed in each position r of the blade as the tangential velocity of each point of the blade changes linearly from the hub to the tip of the blade. Than, the properties of flow are dependent on r. The Figure 4.3 shows the flow at upwind with two components of velocity u_a, axial and v_a, radial. One starts, assuming that the magnitudes of those speed components do not change when passing through the plane of rotation, but the presence of the blade results in an angular component w_a. As the flow is considered radially symmetric, it can be said that the variation in time of an infinitesimal angular momentum of any chosen infinitesimal ring like that shown in Figure 4.2 is equal to the infinitesimal torque over the ring. So,

$$dTa = 2\rho_a W_a \omega_a r^2 \pi r dr. \tag{4.28}$$

The Bernoulli constants can be calculated for points 1 and 2, so that it can be obtained [35]

$$b_1 - b_2 = \Delta p - \frac{1}{2}\omega_a^2 r^2 \tag{4.29}$$

where b_1 and b_2 are the Bernoulli constants at point $1-3$ and $2-4$ respectively. This means that the infinitesimal torque in the blades decreases the kinetic energy of the fluid of an amount $-\frac{1}{2}\omega_a^2 r^2$. This also means that when the fluid

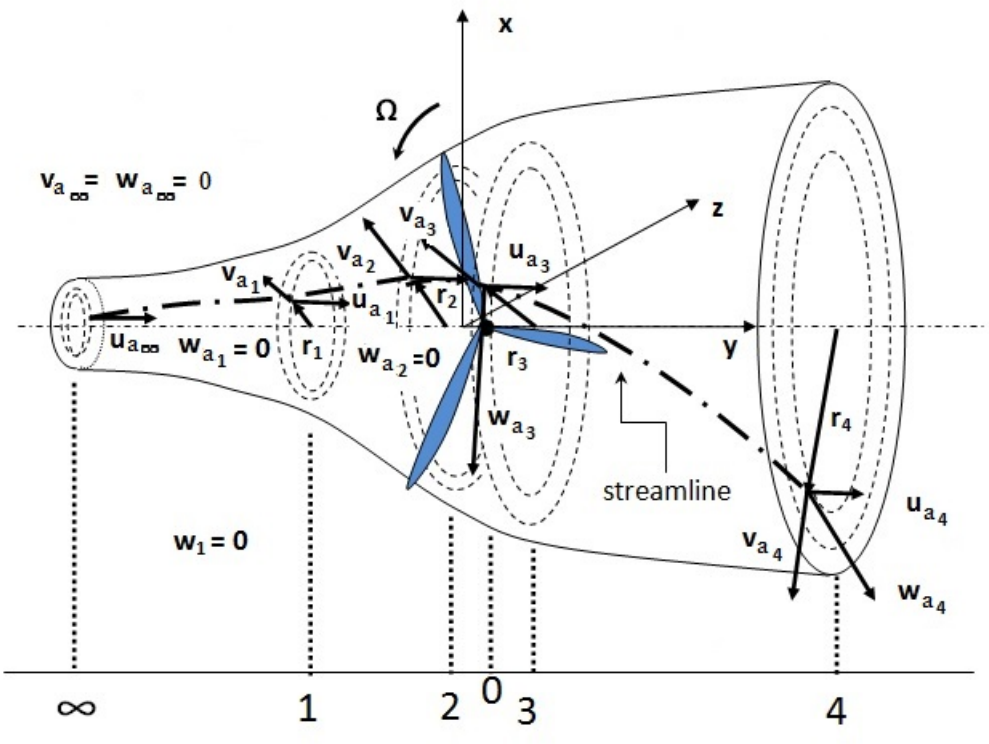

Figure 4.3: Flow with rotation in wake

rotates, the term Δp must decrease to keep the total energy constant since the axial velocity is constant when passing through the plane of rotation. So,

$$\begin{aligned} p_\infty - p_r &= \frac{1}{2}\rho_a(W_{a_2}^2 - W_{a_1}^2) + \frac{1}{2}\rho_a\omega_{a_2}^2 r_2^2 \frac{1}{2}\rho_a\omega^2 r^2 + \\ (h_0 - h_1) &= \frac{1}{2}\rho_a(W_{a_2}^2 - W_{a_1}^2) + \frac{1}{2}\rho_a(\omega_{a_2}^2 r_2^2 - \omega_a^2 r^2) + \Delta p \quad .. \end{aligned} \tag{4.30}$$

Also, applying Bernoulli equation between plane 3 and 4 it is found that

$$\Delta p = \frac{1}{2}\rho_a(-\Omega_b^2 + (\Omega_b - \omega_a)^2 r^2 = \rho_a(\Omega_b + \omega_a)\omega_a r^2. \tag{4.31}$$

Substituting 4.31 into 4.30 results in

$$p_1 - p_2 = \frac{1}{2}\rho_a(W_{a_2}^2 - W_{a_1}^2) + \rho_a(\Omega_b + \omega_a)r^2. \tag{4.32}$$

Using the variation of the axial momentum in control volume as made in previous section,

$$dTh = \rho_a u_2(W_{a_1} - W_{a_2})dA_2 = (\Omega_b + \omega_{a_2}) + (p_1 - p_2)dA_{sw_2}. \tag{4.33}$$

But,

$$dTh_w = \rho_a(\Omega_b + \omega_a)\Omega_b r^2 dA_{sw}, \tag{4.34}$$

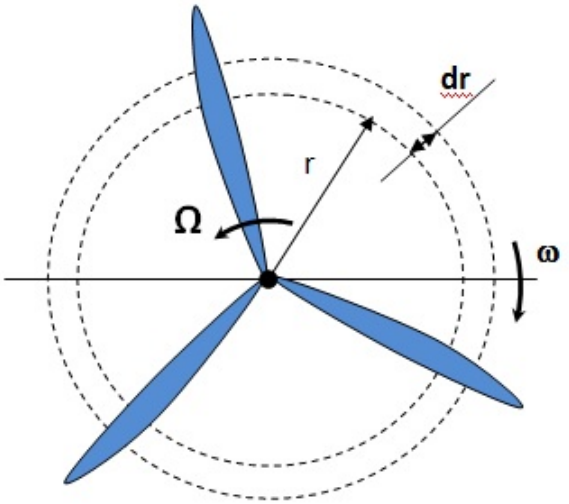

Figure 4.4: Infinitesimal rotating wind volume - view from downwind

then, combining equations 4.30, 4.33 and 4.34 it results that,

$$\frac{1}{2}(W_{a_\infty} - W_{a_2})^2 = \left(\frac{\Omega_b + \frac{\omega_{a_2}}{2}}{W_{a_2}} - \frac{\Omega_b + \frac{\omega_{a_2}}{2}}{W_{a_\infty}}\right) W_{a_2} r_2^2 \omega_{a_2}. \tag{4.35}$$

Now, defining the tangential induction factor $a' = \frac{W_a}{2\Omega_b}$,

$$dTh_w = \Delta p dA = 4\rho_a \pi \Omega_b^2 a'(1+a')r^3 dr. \tag{4.36}$$

It was already shown that (Equation 4.22)

$$dTh_w = 2\rho_a \pi W_a (W_a - W_{a_1}) dA = 4\pi\rho_a W_{a_1}^2 a(1-a) r dr \tag{4.37}$$

and, as the two previous equations represents the same quantity, they can be equated to permit to obtain the relation between the two induction factors a and a'. The following equality is obtained

$$\frac{a(1+a)}{a'(1+a')} = \frac{\Omega_b^2 r^2}{W_{a_1}^2} = \lambda_b(r)^2, \tag{4.38}$$

where $\lambda_b(r)$ is the speed ratio at a radial position r in the blade. The torque acting on the infinitesimal ring element is, then

$$dTo = 4\rho_a \pi W_{a_1} \Omega_b a'(1-a) r^3 dr. \tag{4.39}$$

The power can be obtained as

$$dP = \frac{1}{2}\rho_a A_{sw} W_{a_1}^3 \left(\frac{8}{\lambda_b^2} a'(1-a)\lambda_b^3(r) d\lambda_b\right). \tag{4.40}$$

The power coefficient is obtained by the integration over the transversal swept area A_{sw} for all local infinitesimal power coefficient, resulting in

$$C_P = \frac{8}{\lambda_b^2}\int_0^R a'(1-a)\lambda_b^3(r)d\lambda_b. \tag{4.41}$$

For a given available power P_{av}, the coefficient C_P changes as a function of a. If the angles of attack are small enough to avoid stall, a and a' are not independent and the Equation 4.38 is valid ([35], [23]). Then, the Equation 4.38 can be written in the following way

$$a' = -\frac{1}{2} + \frac{1}{2}\sqrt{1 + \frac{4}{\lambda_b^2(r)}a(1-a)}. \tag{4.42}$$

Solving both Equation 4.42 and Equation 4.41 for maximizing the power coefficient, one obtains

$$\lambda^2(r) = \frac{(1-a)(4a-1)^2}{(1-3a)}; \qquad \text{and} \qquad a' = \frac{1-3a}{4a-1}. \tag{4.43}$$

The maximum power coefficient is then calculated substituting the Equation 4.43 into Equation 4.41 and performing the integration in relation to the induction factor a. That is,

$$C_{P_{opt}} = \frac{24}{\lambda_b^2}\int_{a_1}^{a_2} \frac{(1-a)(1-2a)(1-4a)}{(1-3a)}. \tag{4.44}$$

In Equation 4.44, $\lambda_b = 0$ happens for $a_1 = 0.25$ and $\lambda_b = \infty$ when $a_2 = \frac{1}{3}$. The final expression for the power coefficient is then ([35])

$$C_{P_{opt}} = \frac{8}{729\lambda_b^2}\left[\frac{64}{5}x^5 + 72x^4 + 124x^3 + 38x^2 - 63x - 12ln(x) - 4x^{-}1\right]_{x=(1-3a_2)}^{x=0.25}. \tag{4.45}$$

The analysis made in this section completes the simpler model discussed in previous section (1D model), in which it was not considered the rotation of the wind when leaving the turbine. So, it is expected that in the limit, both models tends to give the same results. In fact, this happens when λ_b tends to large values, what means a and $C_{P_{opt}}$ approaching $\frac{1}{3}$ and $\frac{16}{27}$ (Betz limit), respectively [35].

4.2.3 Blade element theory

In the simple one-dimensional model, details of the rotor geometry, number blades, chord length distribution as well as the kind of airfoils are not considered. Blade element theory, developed by Herman Glauert (1892-1934), permits the calculation of loads, thrust and power for different set ups of wind speed rotations and pitch angles. The wind-cylinder presented previously is

discretized into N_b annular elements of length dr. The sides are stream-lines, so the mass in each volume is constant in time. Concerning to the flow, some hypothesis are assumed [23]:

- The volumes are independent each other;
- Forces from the blades on the flow are constant in each annular element;
- Rotor assumed with infinite number of blades;
- Pressure along the curve stream lines enclosing the wake does not give any axial force component.

Under those conditions it can be used the formulation developed in previous section [23]. The Figure 4.5 shows a cut in a position r of the blade determining a shape of an airfoil. The angle $\theta_b(r)$ is the sum of the pitch angle , θ_{b_0}, and the twist of the blade $\beta_b(r)$. The Figure 4.6 shows the forces acting in a particular section of the blade. Basically two forces act: the thrust in the direction of the wind and the torque, orthogonal to the thrust. The drag is the force acting in the direction of the relative wind and is caused by the viscosity of the fluid. The lift force acts orthogonally to the relative direction of the wind.

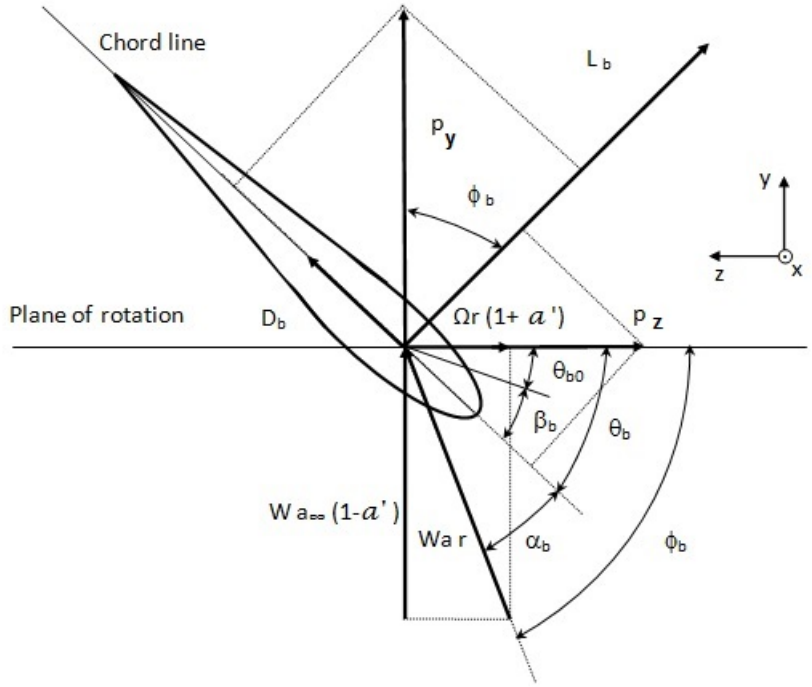

Figure 4.5: Flow with rotation in wake

It can be seen in the Figure 4.5 that the following equation can be derived:

$$tan(\phi_b) = \frac{(1 - a(r))W_{a_\infty}}{(1 - a(r)')\Omega_b r} \tag{4.46}$$

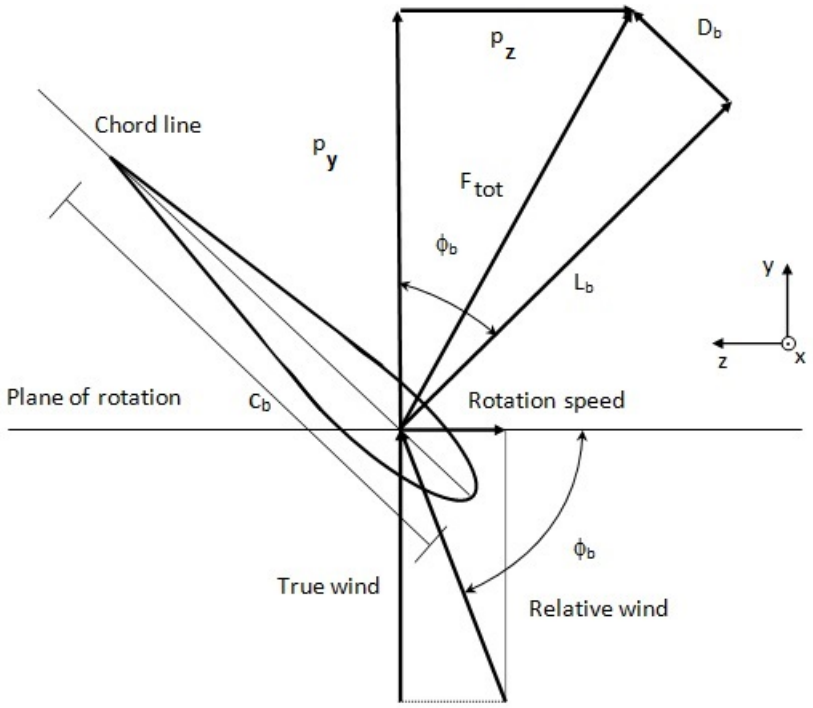

Figure 4.6: Forces in a section of a blade

and

$$\alpha_b(r) = \phi_b(r) - \theta_b(r) \tag{4.47}$$

and also,

$$\theta_b(r) = \theta_0 + \beta_b(r). \tag{4.48}$$

Lift and drag forces can be calculated as

$$L_b(r) = \frac{1}{2}\rho_a W_a^2 c_b(r) C_{L_b}(r) \tag{4.49}$$

$$D_b(r) = \frac{1}{2}\rho_a W_a^2 c_b(r) C_{D_b}(r). \tag{4.50}$$

Projecting the two forces in rotor plane and perpendicular directions,

$$p_y(r) = L_b cos(\phi_b(r)) + D_b(r) sin(\phi_b(r)) \tag{4.51}$$

$$p_z(r) = L_b sin(\phi_b(r)) - D_b(r) cos(\phi_b(r)). \tag{4.52}$$

Normalizing with $\frac{1}{2}\rho_a W_a^2 c_b(r)$

$$C_y(r) = C_{L_b} cos(\phi_b(r)) + C_{D_b}(r) sin(\phi_b(r)) \tag{4.53}$$

$$C_z(r) = C_{L_b}(r)sin(\phi_b(r)) - C_{D_b}(r)cos(\phi_b(r)) \tag{4.54}$$

where

$$C_y(r) = \frac{P_y}{\frac{1}{2}\rho_a W_a^2 c_b(r)} \tag{4.55}$$

and

$$C_z(r) = \frac{P_z}{\frac{1}{2}\rho_a W_a^2 c_b(r)}. \tag{4.56}$$

From figure 4.5,

$$W_a sin(\phi_b(r)) = \Omega_b(1 - a(r)) \tag{4.57}$$

$$W_a cos(\phi_b(r)) = \Omega_b r(1 + a'(r)). \tag{4.58}$$

Defining the solidity ($\sigma_b(r)$) as a fraction occupied buy the blades in the circumference of radius r it comes that

$$\sigma_b(r) = \frac{c_b(r)N_b}{2\pi r}. \tag{4.59}$$

Then,

$$dT_y(r) = N_b p_y(r)dr \tag{4.60}$$

$$dT_z(r) = rN_b p_z(r)dr \tag{4.61}$$

resulting that

$$dT_y(r) = \frac{1}{2}\rho_a N_b W_{a_\infty}^2(1-a)^2(1/sin^2(\phi_b))c_b(r)C_L(r)dr \tag{4.62}$$

$$dT_z(r) = \frac{1}{2}\rho_a N_b W_{a_\infty}(1-a(r))\Omega_b r(1+a'(r))(1/sin(\phi_b(r))cos(\phi_b(r)))C_L(r)c_b(r)rdr \tag{4.63}$$

It is obtained the following equations

$$a(r) = \frac{1}{(\frac{4sin^2(\phi_b(r))}{\sigma_b(r)C_y(r)} + 1)} \quad \text{and} \quad a'(r) = \frac{1}{(\frac{4cos(\phi_b(r))sin(\phi(r))}{\sigma_b(r)C_z(r)} - 1)}. \tag{4.64}$$

Up to this point all the parameters were determined to make possible to use the BEM theory. To make it operational, a set of steps must be performed so that in a iterative way, the loads an moments can be calculated. Below, a flowchart showing the steps to achieve this [23].

- Step 1 $\Longrightarrow$ initialize $a(r)$ and $a'(r)$ $(a(r) = 0; a'(r) = 0)$;
- Step 2 $\Longrightarrow$ Compute $\phi(r)$ using eq 4.46
- Step 3 $\Longrightarrow$ Compute the local angle of attack using equation 4.47;
- Step 4 $\Longrightarrow$ Read off $C_L(\alpha_b(r))$ and $C_D(\alpha_b)$ from table for r;
- Step 5 $\Longrightarrow$ Compute $C_y(r)$ and $C_z(r)$ from eq 4.53 and 4.54;
- Step 6 $\Longrightarrow$ Compute $a(r)$ and $a'(r)$ from Equations 4.64
- Step 7 $\Longrightarrow$ If $a(r)$ and $a'(r)$ gets stable and changes within certain tolerance;
- Step 8 $\Longrightarrow$ Compute the loads on the segment of the blades.

4.2.4
Numerical evaluation for the moments and forces

The equations obtained above must be integrated along the blade in order to obtain the forces and torques acting on the blades. Experimentally, three loads per unity length are obtained, when testing the airfoil: lift force, drag force and torque. The Figure 4.7 shows a blade with sections and the corresponding graphs for forces p_y and p_z. Usually [23], the intervals are integrated from r_i to r_{i+1} assuming a linear function between that two points and are calculated as follows. First assume that

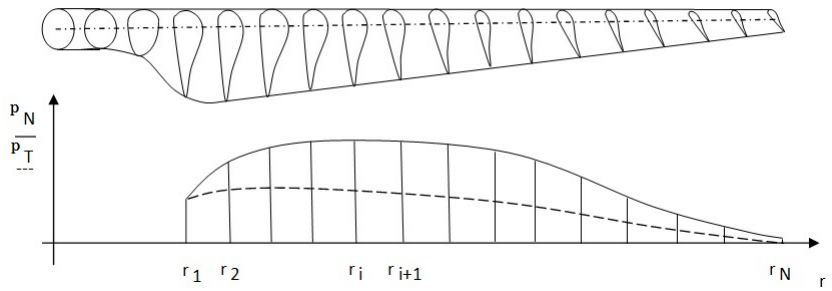

Figure 4.7: Division of the blade in N sections

$$p_{z_i} = a_{z_i} r + b_{z_i} \tag{4.65}$$

so,

$$a_{z_i} = \frac{(p_{z_{i+1}} - p_{z_i})}{(r_{i+1} - r_i)} \quad \text{and} \quad b_{z_i} = \frac{(p_{z_i} r_{i+1} i - p_{z_{i+1}} r_i)}{(r_{i+1} - r_i)} \tag{4.66}$$

$$dT_z = \int_{r_i}^{r_{i+1}} r p_{z_i} dr = \int_{r_i}^{r_{i+1}} (a_{z_i} r^2 + b_i r) dr \tag{4.67}$$

$$\Delta T_{z_{i,i+1}} = (\frac{1}{3} a_{z_i} r^3 + \frac{1}{2} b_{z_i} r^2) \mid_{r_i}^{r_{i+1}} = \frac{1}{3} a_{z_i} (r_{i+1}^3 - r_i^3) + \frac{1}{2} b_{z_i} (r_{i+1}^2 - r_i^2) \tag{4.68}$$

$$T_z = N_b (\sum_{1}^{N-1} T_{z_{i,i+1}}) \tag{4.69}$$

The same idea can be used to calculate the other forces and torques components.

4.2.5
Prandtl tip loss factor

When deducing the aerodynamics about the blade, some hypothesis were made including the one imposing that the number of the blades were infinite. The problem is that, in practice, the number of blades are small and this affects the turbine performance. This problem was solved by Prandtl who proposed

the following relation for the correction factor related to the finite number of blades [23]:

$$F_l = \frac{2}{\pi} cos^{-1}(e^{-f_l}) \tag{4.70}$$

and

$$f_l(r) = \frac{N_b}{2} \frac{L_b - r}{r sin(\phi r)} \tag{4.71}$$

This correction is applied in the induction factors [23]

$$a(r) = \frac{1}{\frac{4F_l(r)sin^2(\phi(r))}{\sigma_b(r)C_y(r)} + 1} \quad \text{and} \quad a'(r) = \frac{1}{\frac{4F_l(r)cos(\phi(r))sin(\phi)}{\sigma_(r)C_z(r)} - 1}. \tag{4.72}$$

4.2.6 Corrections for a larger than 0.4

If the value of $a(r)$ approaches 0.4, momentum theory is not valid anymore. The solution for the flow is obtained empirically a relation between the trust coefficient $C_z(r)$ and $a(r)$.

As an example on may has [23]

$$\begin{aligned} C_{Th_z}(r) &= 4a(r)(1 - a(r))F_l(r), \quad \text{if} a(r) \leq 1/3 \\ C_{Th_z}(r) &= 4a(r)(1 - \frac{1}{4}(5 - 3a(r))a(r))F_l(r) \quad \text{if } a(r) \geq \frac{1}{3} \end{aligned} \tag{4.73}$$

Other relations can be obtained in other authors [23]. From the local aerodynamics, the infinitesimal thrust dTh on an annular element is given by Equation 4.63 . For an annular control volume C_T is, by definition

$$C_z(r) = \frac{dT}{\frac{1}{2}\rho_a W_{a_\infty}^2 2\pi r dr} \tag{4.74}$$

Using the equation 4.62 to substitute dT,

$$C_z = \frac{(1 - a(r))^2 \sigma C_y}{sin^2(\phi)} \tag{4.75}$$

Equating the two equations, 4.74 and 4.75, it comes that, for $a(r) < a_c$,

$$4a(r)(1 - a(r))F = \frac{(1 - a(r))^2 \sigma_b(r) C_y(r)}{sin^2(\phi(r))} \tag{4.76}$$

$$a = \frac{1}{(\frac{4F_l(r)sin^2(\phi(r))}{\sigma_b(r)C_y(r)}) + 1}. \tag{4.77}$$

If $a > a_c$

$$4(a_c^2 + (1 - 2a_c)a(r))F_l(r) = \frac{(1 - a(r))^2 \sigma_b(r) C_y}{sin^2(\phi(r))}, \tag{4.78}$$

giving [23]

$$a(r) = \frac{1}{2}[2 + K_l(r)(1 - 2a_c) - \sqrt{((K_l(r)(1 - 2a_c) + 2)^2 + 4(K_l(r)a_c^2 - 1))}] \tag{4.79}$$

$$K_l(r) = \frac{4F_l(r)sin^2(\phi(r))}{\sigma_b(r)C_y(r)}. \tag{4.80}$$

4.2.7 Wind simulations

The real wind is variable in time and space, that means that in the plane of rotation, in a position (x, z), the wind speed is a function of time and it is random as shown in Figure 4.8. The problems is now how to find this function considering information from the local wind. This is made by using the power spectral density for the local wind.

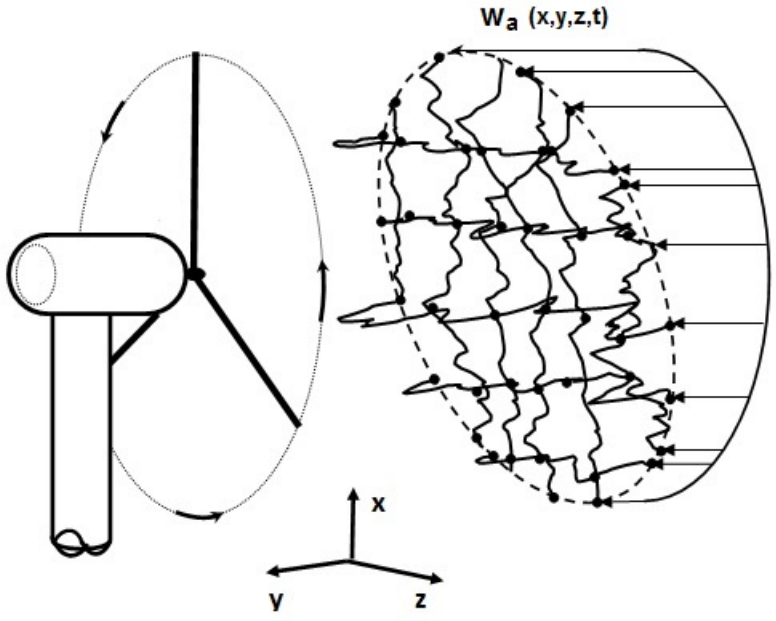

Figure 4.8: Stochastic wind

Given a power spectral density, it is possible to determine the correspondent time series [57]. Nevertheless, this is just a realization of the random process and only makes sense for ergodic processes. Then, a more elaborated theory must be applied to deal with more general processes. When analyzing the wind behavior, each point in the plane of rotation may be considered a random process and to each process is associated a power spectral density function. The mutual influence among process are modeled by a coherence function. Using this two functions, a set of harmonic functions are created and superposed, weighted by coefficients that account for the relative importance that each frequency value has in the time response, considering the density and spatial correlation. As already discussed in Chapter 2, the wind spectral density function and coherence functions where already studied, for the atmospheric boundary layer and different analytical expressions to approximate S_f

functions exist, (such as the Kaimal, Frost or von Karman) [70]. For example, the Kaimal spectrum as given in [23]:

$$S_f(f) = \frac{I_w^2 W_{t_s} l}{\left(1 + 1.5\frac{fl}{W_{a_{t_s}}}\right)^{\frac{5}{3}}} \tag{4.81}$$

$I_w = \frac{\sigma_w}{W_{a_{t_s}}}$ is the turbulence intensity, f is the frequency (in Hz), $W_{a_{t_s}}$ is the t_s min averaged wind speed (maybe from standards), and l is a length scale, $l = 20h$ for $h < 30m$ and $l = 600m$ for $h > 30m$, where h is the height above ground level. The coherence function is dependent on the relative positions between two individual processes and also on the frequency considered. The coherence function is

$$Coh_{jk}(\bar{l}_{jk}, f) = exp\left(-12\left(\frac{f\bar{l}_{jk}}{W_{a_{t_s}}}\right)\right) \tag{4.82}$$

where j and k indexes represent two single process in two different positions in the plane of rotation. $\bar{l}_{jk}$ are the distances between the two point in analysis. The spectral representation method starts by considering n Gaussian stationary random processes $f_j^0(t), j = 1, 2, ...n$ with zero mean and with a cross spectral density matrix $S^0(\omega_s)$ given by

$$[S^0(\omega)] = \begin{bmatrix} S_{11}^0 & S_{12}^0 & ... & S_{1n}^0 \\ S_{21}^0 & S_{22}^0 & ... & S_{2n}^0 \\ \vdots & \vdots & \ddots & \vdots \\ S_{n1}^0 & S_{n2}^0 & ... & S_{nn}^0. \end{bmatrix} (0 \leq \omega \geq \infty) \tag{4.83}$$

By definition, $S^0(\omega)_{jk} = \mathfrak{F}\left(R_{jk}^0\right)$ where $\mathfrak{F}(\cdot)$ means the Fourier transform operator and R_{jk}^0 is the cross-correlation. As the process is stationary, $S_{jk}^0 = \bar{S}_{jk}^0$, $R_{jk}^0(\tau) = R_{kj}^0(\tau)$ and S_{jk}^0 is Hermitian and positive definite [57]. One defines $[\mathfrak{H}]$ as a triangular matrix for which the Fourier transform exists and also satisfies the relation

$$[S^0(\omega)] = [\mathfrak{H}(\omega)][\mathfrak{H}(\omega)]^T \tag{4.84}$$

$[\mathfrak{H}]^T$ is the transpose complex conjugate. The matrix $[\mathfrak{H}(\omega)]$ can be obtained by the Spectral Representation Method [56] and a methodology to do will be discussed next. Considering the equation, the process can be simulated by the series

$$W_{a_j}(t) = \sum_{k=1}^{m}\sum_{n=1}^{N} |\mathfrak{H}| \sqrt{2\Delta\omega} cos[\hat{\omega}_n t + \theta_{jk}(\omega_n) + \Phi_{kn}]. \tag{4.85}$$

where $\Delta\omega$ is the interval of the discretization and $\hat{\omega}_n = \omega_n + \psi_{kn}\Delta\omega$, where NP is the number of points, ψ_{kn} are random values uniformly distributed between 0 and 1, Φ_{kn} is the random independent phase angles uniformly distributed

between 0 and 2π and

$$\theta_{jk}(\omega_n) = tan^{-1}\left(\frac{\Im\left(\mathfrak{H}_{jk}(\omega_n)\right)}{\Re\left(\mathfrak{H}_{jk}(\omega_n)\right)}\right). \tag{4.86}$$

If the matrix $[\mathfrak{H}_{jk}(\omega_n)]$ is real, then, $\theta_{jk}(\omega_n)]$=0. It can be proved that [56] the processes $W_{a_j}(t)$, simulated by Equation 4.85 can produces the cross correlation $R^0_{jk}(\tau)$ and the spectral density $S^0_{jk}(\omega_s)$, with respect to the group mean. With the formulation presented is possible to derive the time dependent wind velocity field. The path to do so will be presented next.

First, a matrix, S_{jk}, is mounted, containing the elements

$$S_{jk} = Coh_{jk}\sqrt{S_{jj}S_{kk}} \tag{4.87}$$

where S_{jj} and S_{kk} are the psd functions of points j and k respectively. The off diagonal terms S_{jk} are the magnitudes of the cross-spectra. If the number of points in space is NP, then, the matrix S_{jk} has the dimension $NP \times NP$. Then, a lower triangular $\mathfrak{H}$ matrix is computed through following recursive formulation:

$$\mathfrak{H}_{jk} = \frac{S_{jk} - \sum_{l=1}^{k-1} H_{jl}\mathfrak{H}_{kl}}{\mathfrak{H}_{kk}} \tag{4.88}$$

$$\mathfrak{H}_{kk} = \sqrt{(S_{kk} - \sum_{l=1}^{k-1}\mathfrak{H}^2_{kl})} \tag{4.89}$$

For each point indexed by k and for each discrete frequency, $f_n = n/T$, a random number, Φ_{kn}, between 0 and 2π, is sorted to represent the phase as in equation. n varies between 1 and $N/2$, where N is the number of discrete points in the time histories ($t = i\Delta t, \quad i = 1, \cdots, N$). Then, one determines the vector of complex velocities components $\{W_a(f_n)\}$, calculated as:

$$\Re(W_{a_j}(f_n)) = \sum_{l=1}^{j}\mathfrak{H}^2_{jk}cos(\phi_{kn}); \quad \text{and} \quad \Im(W_{a_j}(f_n)) = \sum_{l=1}^{j}\mathfrak{H}^2_{jk}sin(\phi_{km}) \tag{4.90}$$

Then, the amplitude and the phase are

$$\begin{aligned} A_j(f_n) &= \sqrt{\Re(W_a(f_n))^2 + \Im(W_a(f_n))^2} \\ \Phi_j(f_n) &= \frac{\Im(W_a(f_n))}{\Re(W_a(f_n))} \end{aligned} \tag{4.91}$$

and all time histories at the points $j = 1, NP$ can be computed as:

$$\begin{aligned} W_{aj}(t) &= \bar{W_a} + \sum_{n=1}^{N/2} 2A_j(f_n)cos(2\pi f_n t - \Phi_j(f_n)) \\ t &= i\ \Delta t, \quad \text{for} \quad i = 1, ..., N \end{aligned} \tag{4.92}$$

Time series of two points apart are of course different but this difference grows with the distance. The coherence depends on the frequency and the

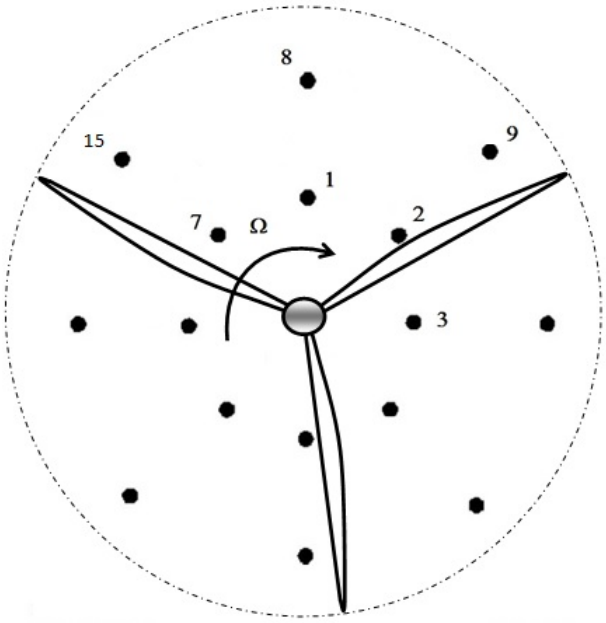

Figure 4.9: Points to simulate the velocity (view from upwind)

lower the frequency, the better is the correlation [23].

The natural choice of points for calculation of the punctual wind speeds is that shown in Figure 4.9 [23] because the points are aligned with the blade. The field determined by methodology above gives the velocities for fixed points but the blades sweep through the grid. So, interpolation must be made to obtain the value for the wind speed between to radial set of points. Those velocities in space do not represent the true action over the blade [23]. It means that it should be determined the time history of the wind seen by a point on the blade. A time history for a point on the rotating blade is called rotational sampling and it was shown in [70] that it can be directly calculated for a blade with a constant rotational speed.

5
Evaluation of a turbine

A turbine, schematically represented in the Figure 3.1 whose parameters are given in the Table 5.1 and Table 5.2, was loaded and simulated in time. It is supposed to be installed in the ground whose dynamic behavior is represented by the springs as indicated. It can be also partially immersed and subjected forces due to the water and wind flows but the wind is considered to act only in the blades. The wind will be considered as being equivalent to random forces and torques acting at the top of the structure. The displacements are measured with respect to inertial frames situated at the center of the mass of the bodies at $t = t_0$. The Table 5.2 gives details about the nacelle, shaft and blades configurations. Same of turbine data were taken from [1], but some were adopted. In the same way, blade data were adopted and based on data taken from [23]. They are shown in graphics depicted in Figure 5.2 for chord length and twist angles, ($\beta_b(r)$, $c(r)$ and $\theta_T(r)$), as well as, for the drag, lift and torque coefficients ($C_D(r)$, $C_L(r)$ and $C_M(r)$). They are all as a function of angle of attack α.

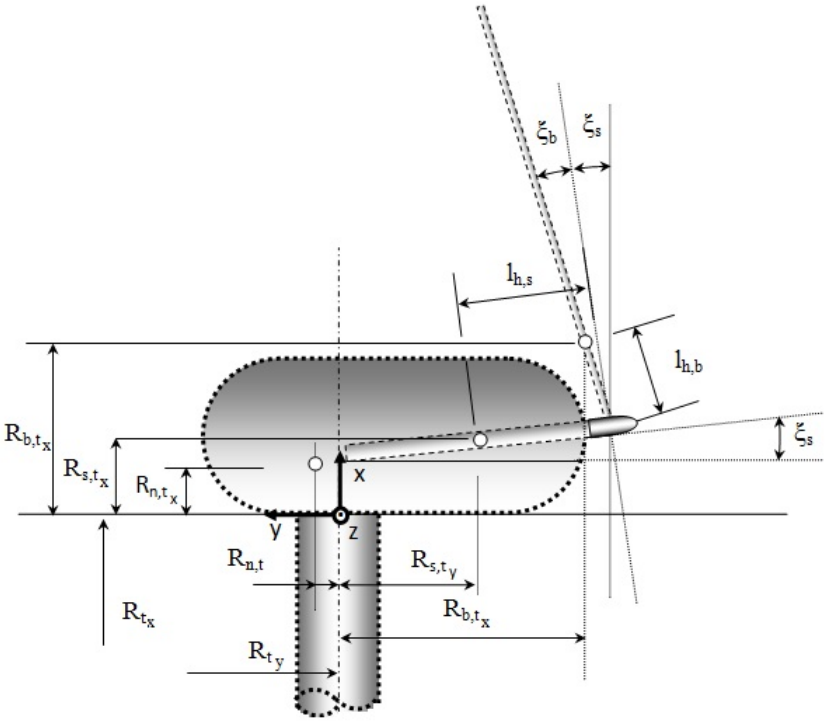

Figure 5.1: Nacelle details (Table 5.2)

Table 5.1: Parameters used in all simulations

Tower	**Values**	**Nacelle**	**Values**
L	55 m	m_n	35700 kg
D	3.37 m	$J_{n_{xx}}$	666600 kgm^2
th_t	0.0068 mm	$J_{n_{yy}}$	33330 kgm^2
E	210 GPa	$J_{n_{zz}}$	666600 kgm^2
G	85 GPa	$J_{n_{xy}}$	0 kgm^2
ν	0.3	$J_{n_{xz}}$	0 kgm^2
ρ	7860 kg/m^3	$J_{n_{yz}}$	0 kgm^2
Blade	**Values**	**Shaft**	**Values**
m_b	2000 kgm^2	D_s	0.4 m
L_b	25 m	th_s	0.01 m
$J_{b_{xx}}$	333 kgm^2	L_s	3 m
$J_{b_{yy}}$	33330 kgm^2	ρ_s	7860 kg/m^3
$J_{b_{zz}}$	33330 kgm^2	–	–
$J_{b_{xz}}$	0 kgm^2	–	–
$J_{b_{xy}}$	0 kgm^2	–	–
$J_{b_{yz}}$	0 kgm^2	–	–
Soil	**Values**	**Wind**	**Values**
ka_x	∞	x_0	0.1 m
ka_y	7.5×10^8 N/m	x_1	50 m
ka_z	7.5×10^8 N/m	W_{a_1}	10 m/s
kr_x	∞	–	–
kr_y	1.55×10^{10} Nm/rad	–	–
kr_z	1.55×10^{10} Nm/rad	–	–
Water	**Values**	**Flow**	**Values**
ρ_w	1000 kg/m^3	C_l	1
ν_w	1.72×10^{-5} kg/m^3	C_{D_a}	0.8
–	–	C_{D_w}	1.0

Table 5.2: Dimensions used in calculation

Parameters	**Values**	**Parameters**	**Values**
R_{n,t_x}	0.5 m	$l_{h,b}$	7 m
R_{n,t_y}	1.0056 m	$l_{h,s}$	1.5 m
R_{n,t_z}	0 m	m_{tip}	39.7e3 kg
R_{s,t_x}	0.5 m	J_{tip_x}	1.0843e6 kgm^2
R_{s,t_y}	-4 m	J_{tip_y}	4.2733e5 kgm^2
R_{s,t_z}	0 m	J_{tip_z}	1.0843e6 kgm^2
R_{h,t_x}	0.5 m	ξ_s	0^o
R_{h,t_y}	-5.5 m	ξ_b	0^o
R_{h,t_z}	0 m	-	-

The turbine has its parameters given the Table 5.1 and the airfoil data are shown in graphs of Figure 5.2.

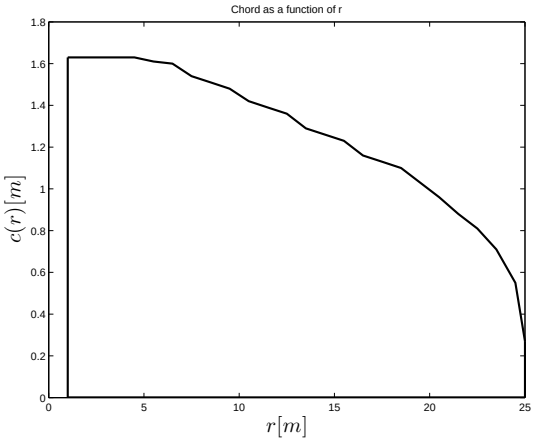

5.2(a): Chord length (c(r))

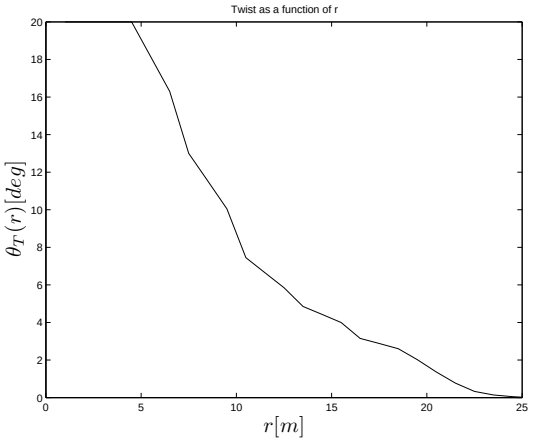

5.2(b): Twist ($\beta_b(r)$)

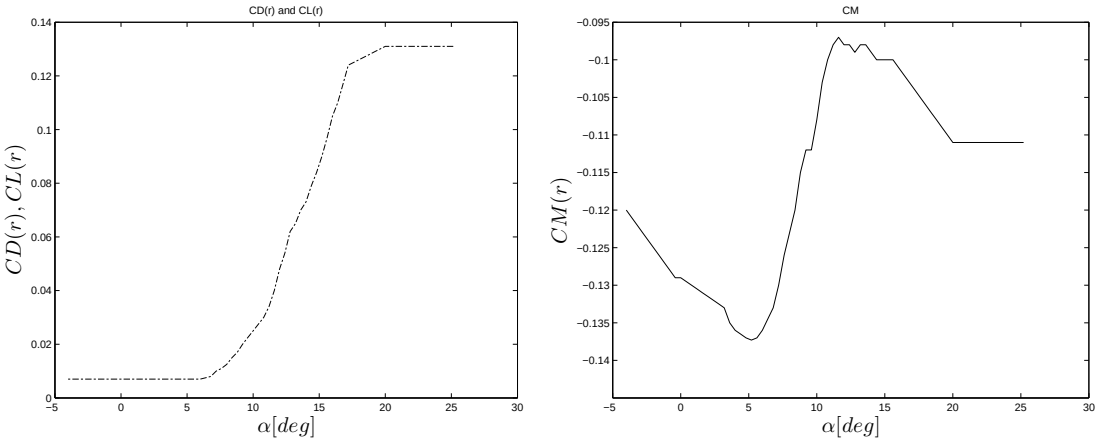

5.2(c): C_{D_b} and C_{L_b} 5.2(d): C_{M_b}

Figure 5.2: Blade details

In order to simulate energy generation, a generator used here and it has a very simplified model. It is supposed that if it is working at the operational speed $\bar{\Omega}_{op}$ no torque is generated. If its speed is smaller than the operational speed, for instance when the wind is very weak, then the generator acts like a motor and generate a positive torque, consuming energy. On the contrary, for instance when the wind is strong enough, the rotor tends to increase its speed and then, the generator acts to stabilize the speed close to, but a bit higher, than the operational one. In this case, electric energy is generated. The counter torque produced is proportional to the difference $\bar{\Omega}_{op} - \bar{\Omega}_{s_y}$. Then on has

$$\bar{T}_g = k_g(\bar{\Omega}_{op} - \bar{\Omega}_{s_y}) \tag{5.1}$$

where k_g is a constant associated to the generator. $\bar{\Omega}_{op}$ and $\bar{\Omega}_{s_y}$ are the operational and actual speeds of the shaft/blades in y_s axis direction. $\bar{\Omega}_{s_y}$ is the components of the shaft angular velocity in the direction y_s represented in the shaft coordinate frame.

The turbine evaluation will be made in two steps in order to approximate the dynamics in a more efficient way. First, a number of eigenfunction must be chosen so that the tower dynamics is approximated properly and the simulations can be carried out. After that, the number of elements of the set (of the eigenvectors) is increased and a new dynamic analysis is performed. Both results are compared and a decision must be made, based on a prescribed precision, if the results converged to a good approximation of the solution. The codification of all presented by now was made in MathLab®and simulated for an specific turbine. This is discussed next.

5.1 Modal analysis

The determination of eigenfunctions and eigenvalues is performed in order to get more information about the structure and then construct the reduced model. $2D$ analysis can be made in order to evaluate the dynamics of the structure and the mutual influence of the components of the system in a simpler way with low computational costs [2]. Nevertheless, real wind turbine moves in $3D$ space and this code was made in order to make possible a more realistic dynamic analysis. The geometric and constitutive data were introduced in the program and the eigenvalues were obtained. The modal results can be obtained for immersed and non-immersed tower. To simulate this, a concentrated mass in the tip of the tower (m_{tip}) is considered, whose magnitude is the sum of the individual masses of the nacelle, shaft and blades. Also, the matrix of inertia [$\mathtt{J}_{tip}$] represents the composition of all individual inertia matrices (nacelle, shaft and blades). It is considered, for tower modal calculations, that the center of the mass m_{tip} is in the axis of the tower and its distance from the top of the tower is not relevant (just concerning to the modal evaluation). In this case, the resultant matrix of inertia for the mass m_{tip} is diagonal. Two modal analysis will be made for two situations. For a turbine installed inland and another, offshore, semi-immersed. In the latter case, the presence of the water affects the natural behavior of the tower, as already was discussed in the work. The case of inland installation, it is considered that the air has little influence in the natural motion of tower.

5.1.1 Tower installed inland

This simulation was made imposing at first a precision of a value equal or less than 0.1%. The program initiates with a minimum number of 20 elements and doubles the value at each iteration. For the prescribed precision an approximation for the eigenvalues and eigenvectors were obtained with a calculated precision of 0.072 % after three interactions. The number of necessary finite elements for that precision was 80 elements. Imposing the precision of 0.01 %, the results were obtained after 5 iterations and 320 elements were necessary to give a precision of 0.0045 %. It took approximately 1.3 s for obtaining the first set of results and 260 s for the second. The graphic results for precision of 0.01% are presented in Figures 5.1.1 to 5.1.1. In the Table 5.3, the natural frequency values for the two imposed precisions (0.1% and 0.01%) are presented. Also, the difference between those two results is shown in the 4^{th} column of that table. It can be observed that the maximum absolute value

for the error was 0.02.

Table 5.3: First 20 natural frequencies for inland turbine in Hz

Mode	Precis. 0.1 %	Precis. 0.01%	Differ.	Mode	Precis. 0.1%	Precis. 0.01 %	Differ.
1^{th}	0.458	0.458	-1.0^{-7}	11^{th}	30.140	30.138	-1.8^{-3}
2^{th}	0.460	0.460	-1.0^{-7}	12^{th}	38.799	38.797	-2.0^{-3}
3^{th}	2.670	2.670	-1.0^{-7}	13^{th}	39.599	39.597	-2.1^{-3}
4^{th}	4.144	4.144	-6.4^{-6}	14^{th}	50.404	50.401	-3.1^{-3}
5^{th}	4.736	4.736	-1.3^{-5}	15^{th}	59.928	59.914	-1.4^{-2}
6^{th}	9.985	9.984	-4.1^{-5}	16^{th}	61.983	61.975	-7.2^{-3}
7^{th}	11.727	11.727	-9.7^{-6}	17^{th}	62.439	62.432	-7.3^{-3}
8^{th}	12.356	12.356	-8.6^{-5}	18^{th}	89.744	89.724	-2.0^{-2}
9^{th}	21.047	21.047	-3.8^{-4}	19^{th}	89.819	89.771	-4.9^{-2}
10^{th}	22.699	22.698	-4.3^{-4}	20^{th}	90.039	90.019	-2.0^{-2}

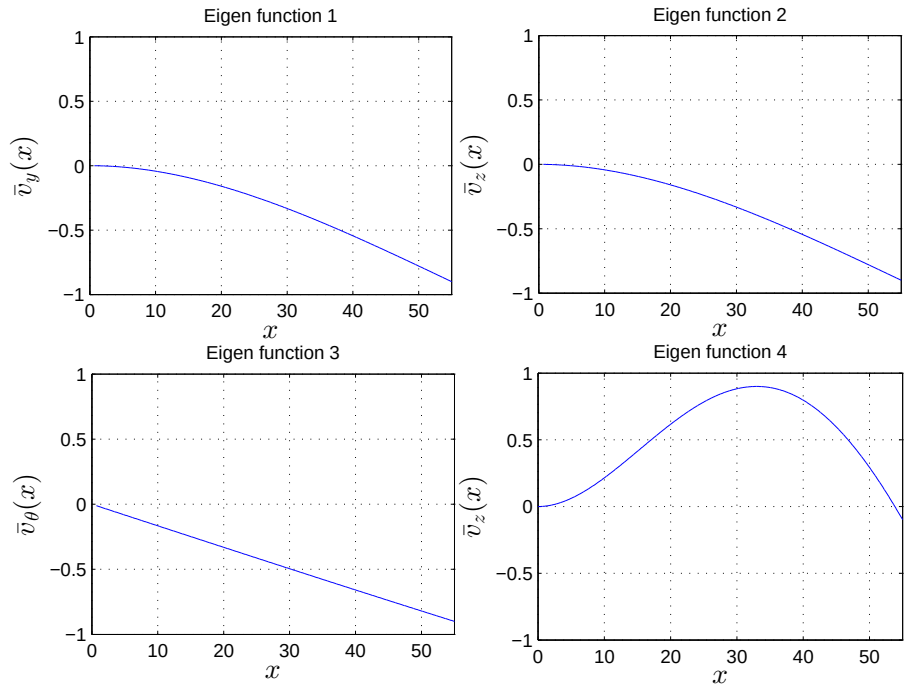

Figure 5.3: 1^{st} to 4^{th} eigenvectors - precision: 0.01%

The eigenvalues and the respective eigenvectors were organized in a sequence of ascending magnitude in order to give an idea of the components of the spectrum. This helps to select the components to be used in the reduced model, that may be chosen in a sequential manner or not. It can be sometimes

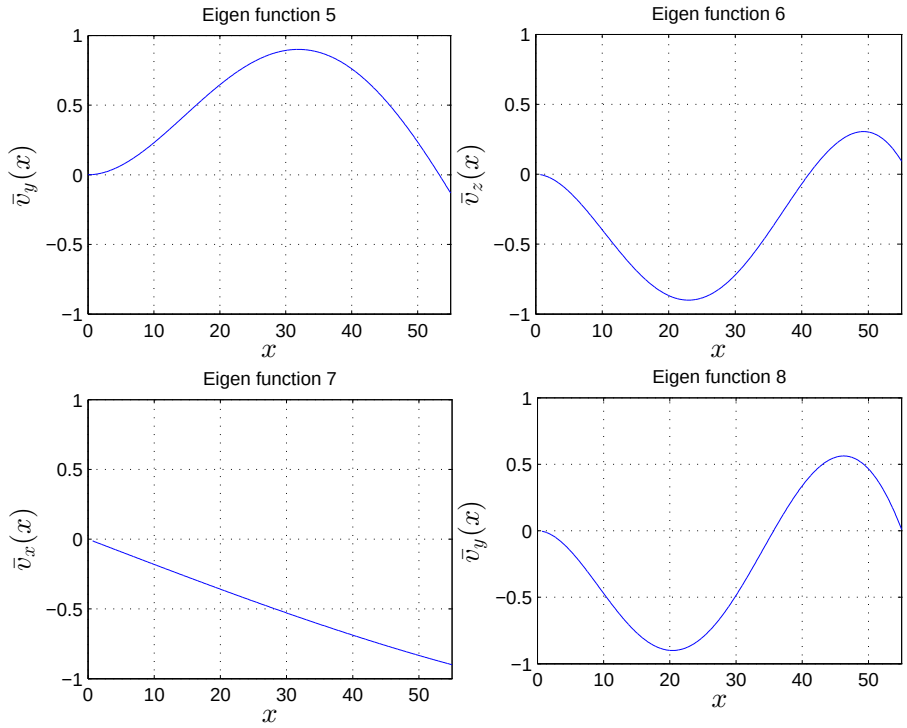

Figure 5.4: 5^{th} to 8^{th} eigenvectors - precision: 0.01%

interesting to chose the eigenfunctions in a more convenient way. In present work the motion of the tower in axial, torsional, and transversal planes are independent. That means that the eigenvectors have null in all d.o.f except for in one. Looking at the Table 5.3 and Figures 5.1.1 to 5.1.1, it can be taken, for instance, three eigenfunctions for each movement of the tower, that is, for axial displacement, 7^{th} and 14^{th} eigenfunctions. For motion in plane xy and xz, 1^{st}, 5^{th}, 8^{th} and 2^{nd}, 4^{th}, 6^{th} eigenfunction. Finally for twist displacement, 3^{st}, 11^{th} and 15^{th}. In the present case, each kind of movement of the tower will be formed by a linear combination of those chosen eigenfunction. As mentioned above, the natural behavior of the tower is dependent, among other properties, on the mass and moment of inertia of the set installed at its tip, as well as, on its own distributed weight. The Table 5.5 shows the natural frequencies for some tip loads and moments of inertia and their relative deviation from those results presented in Table 5.3. It is clear that as the mass or the moments of inertia of the set formed by nacelle and blades increases, the frequencies drop, that is, the natural tower motion gets slower.

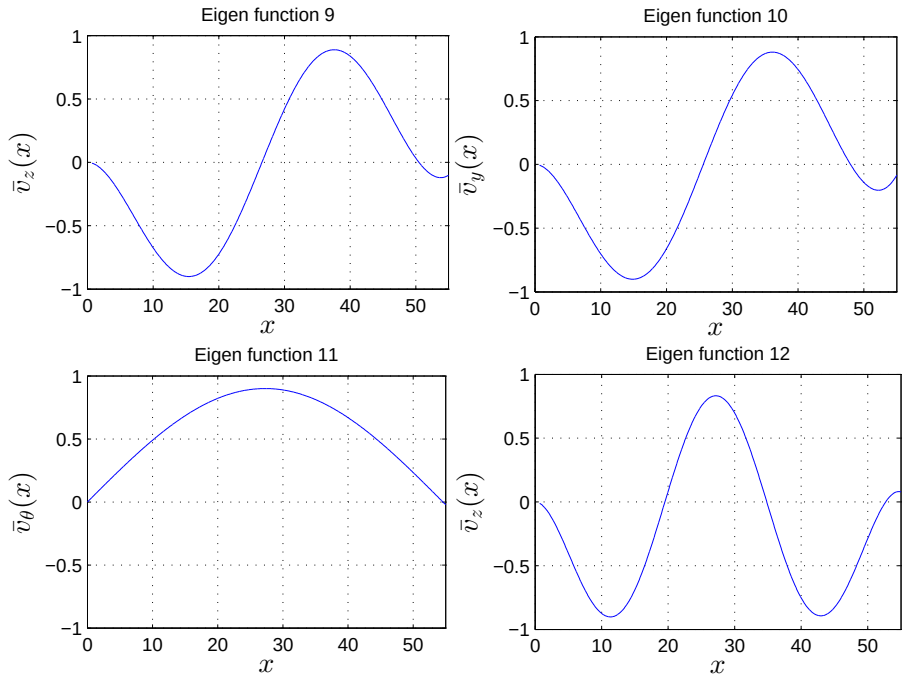

Figure 5.5: 9^{th} to 12^{th} eigenvectors - precision: 0.01%

Table 5.4: First 20 natural frequencies in air and immersed (20m) in Hz

Mode	Nat. freq. In air	Nat. freq. In water	Mode	Nat. freq. In water	Nat. freq. In air
1^{th}	0.458	0.459	11^{th}	30.140	31.204
2^{th}	0.460	0.459	12^{th}	38.799	38.786
3^{th}	2.670	2.644	13^{th}	39.599	49.880
4^{th}	4.144	4.121	14^{th}	50.404	50.404
5^{th}	4.736	5.140	15^{th}	59.928	59.926
6^{th}	9.985	9.927	16^{th}	61.983	61.975
7^{th}	11.727	11.727	17^{th}	62.439	70.957
8^{th}	12.356	15.764	18^{th}	89.744	89.739
9^{th}	21.047	21.019	19^{th}	89.819	89.818
10^{th}	22.699	30.135	20^{th}	90.039	95.821

5.1.2 Semi-immersed tower

As the tower is 55m high and the blades have 25m, it is necessary to ensure some distance between the tip of the blades and the surface of the water. It will be considered a distance of 10m between the water surface and the tip of the blades as a safe distance. Under this assumption, the highest possible level reached by the water surface is 20m. The simulations were carried out, the

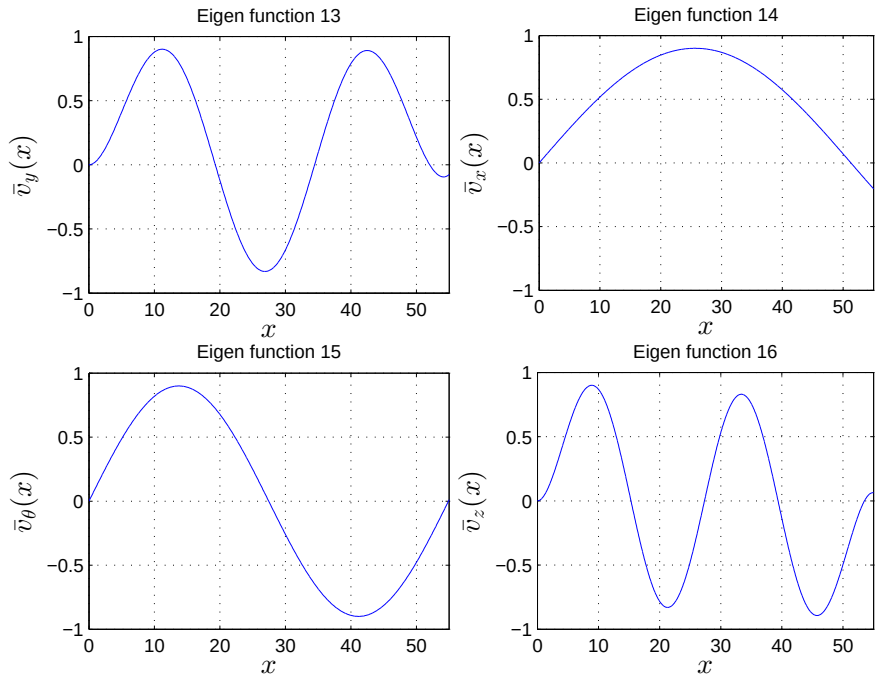

Figure 5.6: 13^{th} to 16^{th} eigenvectors - precision: 0.01%

natural frequencies were obtained and given in Table 5.4, together with the values for inland turbine. Not all the frequencies are affected by the presence of the fluid but those related to the lateral displacement of the tower (planes xy and xz). It can be seen at the graphs presented in the Figure 5.1.2 for some modes that they happen at lower frequencies if compared to the case of in which any fluid is present.

As expected, the results corroborate what was previously discussed. A comparison between the two data, those for the tower in the air, Table 5.3, and those for the tower semi-immersed, is presented in Table 5.4. The values show the differences are quite significant specially for higher frequencies. Also must be noticed that the values in plane xy and xz are different because the moments of inertia in y and z directions are also different.

5.2 Deterministic turbine Dynamics

The algorithm developed to integrate the system of equation of motion is based on Newmark method and parameters (β and γ) must be set in order to the convergence to happen. In the simulations carried out here, the following Newmark parameters were used: $\beta = 0.25$ and $\gamma = 0.5$. The increment of time was set to be 1/10 of the smallest tower period. It will be presented only

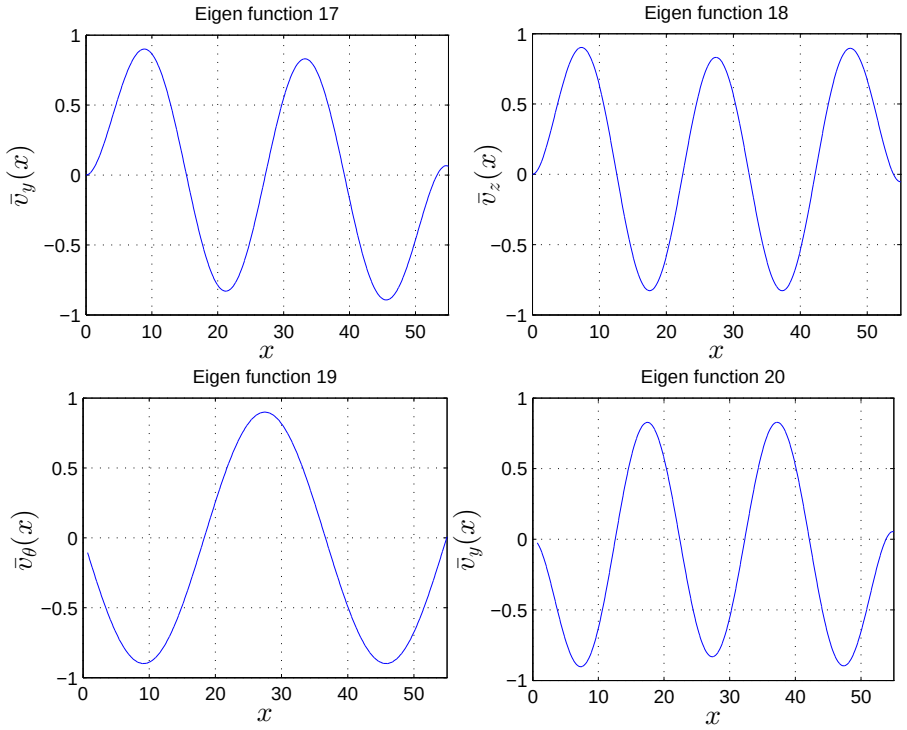

Figure 5.7: 17^{th} to 20^{th} eigenvectors - precision: 0.01%

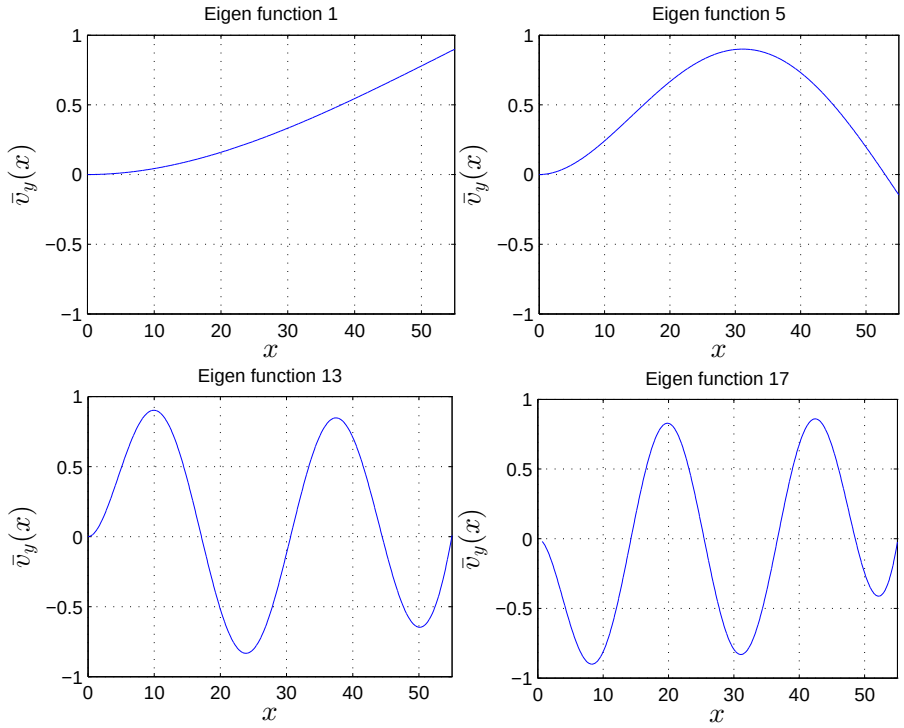

Figure 5.8: Some affected beam modes for the semi-submersed tower (plane xy) - precision: 0.01%

Table 5.5: First 20 natural frequencies for several mass and moments of inertia

Nat. Freq.	$3 \times Jyy$	$3 \times Jzz$	$3 \times Jxx$	$3 \times m_{tip}$
1^{st}	0.455	0.452	0.458	0.286
2^{nd}	0.460	0.458	0.460	0.293
3^{rd}	2.670	2.670	1.556	2.670
4^{th}	3.990	3.022	4.145	4.134
5^{th}	4.144	4.736	4.736	4.665
6^{th}	9.645	8.421	9.985	7.320
7^{th}	9.985	11.728	11.728	9.919
8^{th}	11.728	12.356	12.356	12.365
9^{th}	20.889	20.394	21.048	20.822
10^{th}	21.047	22.699	22.699	22.548
11^{th}	30.139	30.140	29.979	30.139
12^{th}	38.716	38.479	38.799	38.5478
13^{th}	38.798	39.600	39.600	39.357
14^{th}	50.402	50.404	50.404	48.198
15^{th}	59.917	59.929	59.847	59.917
16^{th}	61.927	62.439	61.983	61.729
17^{th}	61.977	89.618	89.744	62.180
18^{th}	89.693	89.618	89.744	62.180
19^{th}	89.729	89.766	89.490	89.776
20^{th}	89.781	90.040	90.040	89.781
Nbr elem	160	80	80	160
Time	1.4s	1.3s	1.4s	1.46s
Erro(Hz)	0.0434 %	0.0721 %	0.0721 %	0.0434 %

displacements in x, z plane because the other are much smaller and will be omitted.

5.2.1 Turbine with constant rotor speed

In this simulation, the turbine is assumed to have a constant rotor angular speed of 0.2 rad/s. Any load is applied, except for its own weight. So, the analysis considers that the turbine started from a static equilibrium. It is considered that structure is under its own weight and already in equilibrium under that load. The results for the displacements of the center of mass of the blades are depicted in Figures 5.9, 5.10 and 5.11. The rotation of the rotor does not affects the tower because it is balanced. Then, theoretically, the tower does not move with the simple rotation of the rotor, then, its dynamics was approximated using 4 eigenvectors. It can be seen also the graph in the Figure 5.12 the harmonic nature of the loads on the blades due to the centripetal force. At the beginning of the analysis, blade 1 is in the vertical position (pointing up). The time of simulation was 60 s.

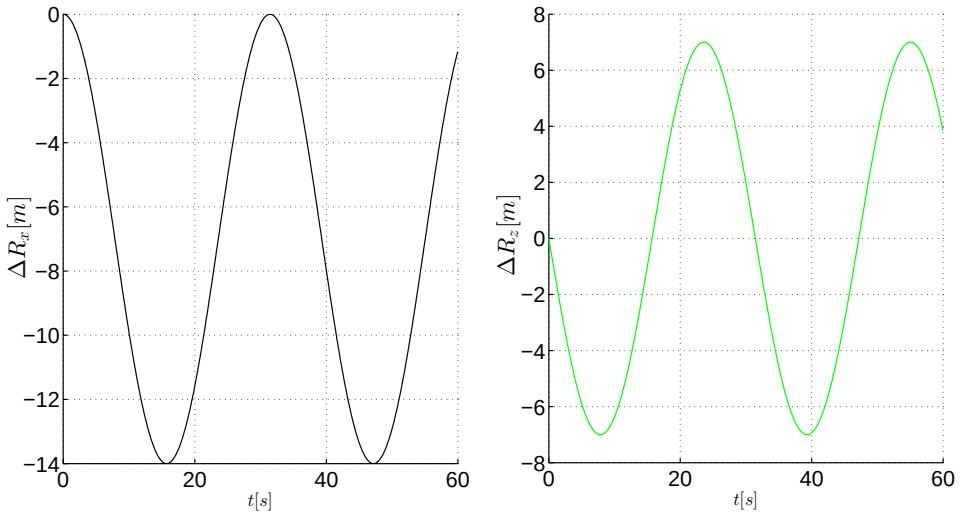

Figure 5.9: Blade 1 - Displacement of the center of mass - constant speed

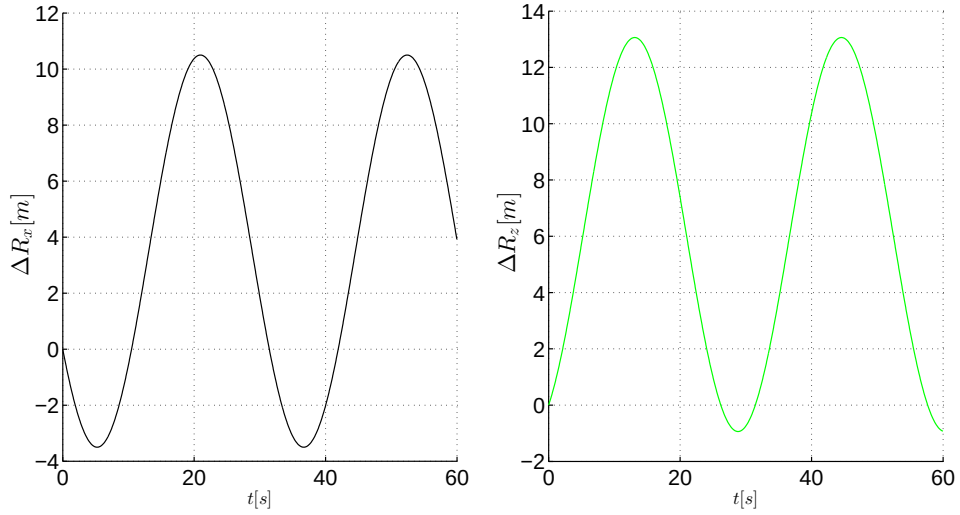

Figure 5.10: Blade 2 - Displacement of the center of mass - constant speed

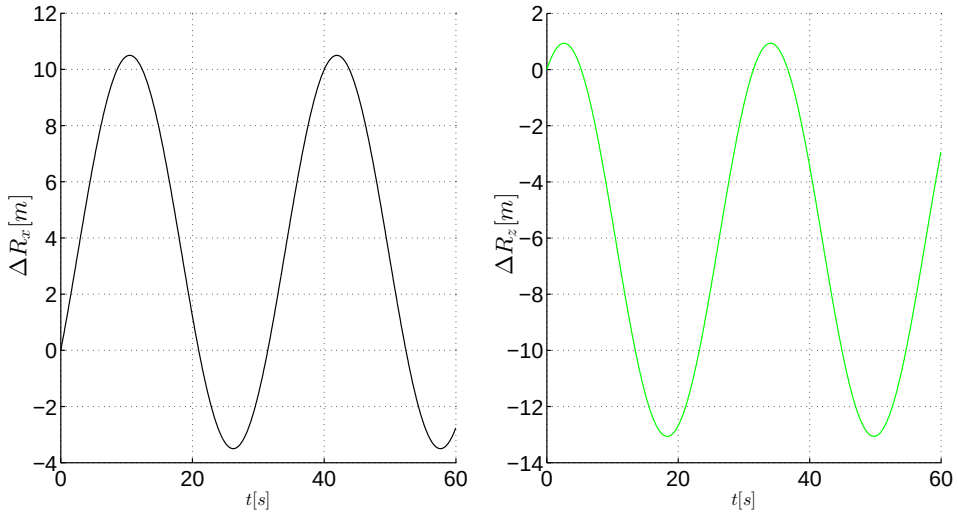

Figure 5.11: Blade 3 - Displacement of the center of mass - constant speed

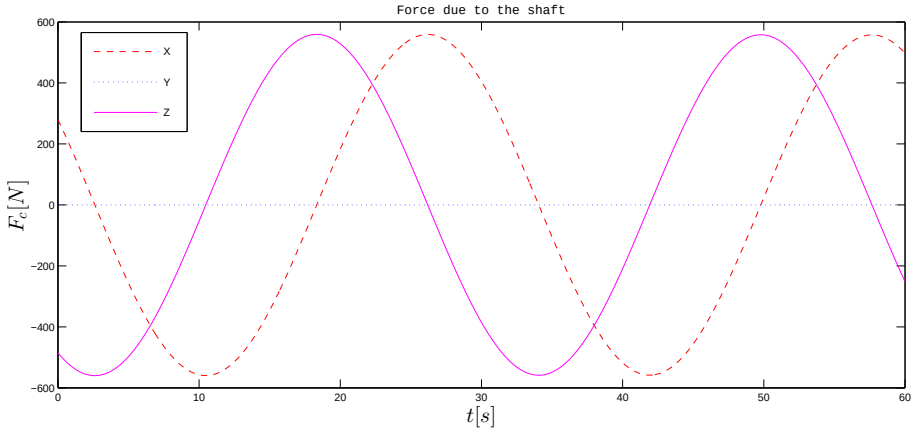

Figure 5.12: Centripetal force acting on the blade 2 - constant speed

5.2.2 Turbine loaded by an external torque

This simulation is made to see the behavior of the rotor when submitted to a constant torque without any limitations in the rotor speed. It is expected that the rotor in this circumstances will accelerate constantly since there is not any dissipative forces acting in the model. In this simulation, the turbine is also assumed to be at rest in time $t = 0$. Then, an external torque is imposed in the rotor by applying forces in the blades in the plane of rotation. Those forces follow the blades, always keeping their direction parallel to z direction considering the local frames. They have the magnitude of 1000 N and as they are applied in the center of the mass of the blades, the total positive torque acting in the shaft is 21000Nm, since the distance of the center of mass from

the axis of the shaft is 7 m.In fact, the graphs in Figure 5.13 shows that. In Figure 5.14 it is shown the position of the blades center of masses near the plane of rotation with time.

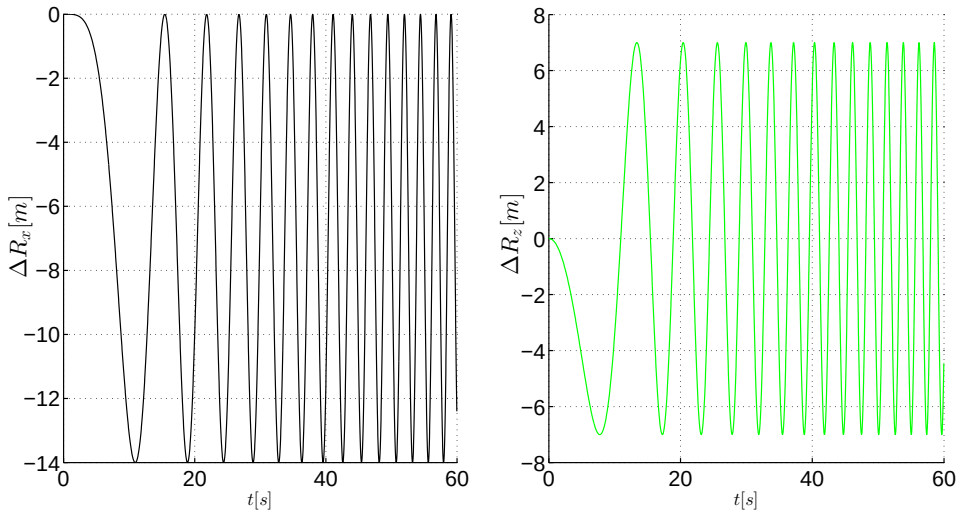

Figure 5.13: Blade 1 - Displacement of the center of mass - external torque

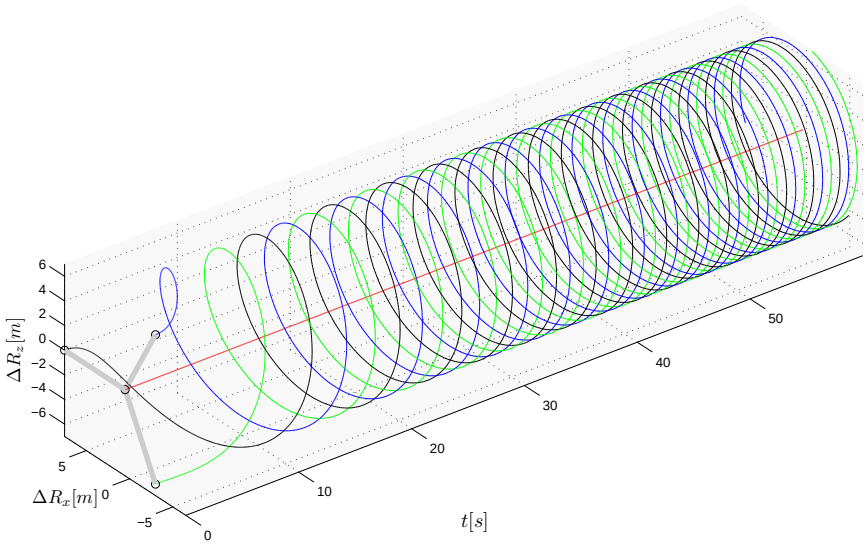

Figure 5.14: Positions of blades center of mass with time - external torque

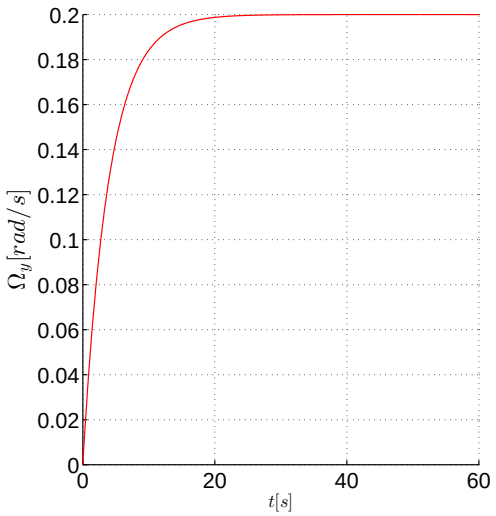

Figure 5.15: Angular velocity - turbine with a generator

5.2.3 Turbine with a generator

If the turbine is not generating it can be accelerated beyond the safe limit as happened in the previous simulation. But if it is producing energy, safety systems ensure its operation at a minimum risk. In this simulation, the turbine is put to operate assuming that it is initially at rest by means of an electric motor which is connected to the rotor. This will generate a torque that will turn the shaft (Equation 5.1). The graph shown in Figure 5.16 depicts the displacement of center of mass for blade 1 while that in Figure 5.17, the positions of the center of mass of the three blades in time. The Figure 5.15 depicts the evolution of the proper rotation of the shaft. Again, as in the previous simulation, it is considered that structure is under its own weight and already in equilibrium under that load. As the rotation of the rotor does not affects the tower, this motion has no importance so that only some numerical noise in a very small scale is obtained. As in the previous simulation, only 4 eigenvectors were use for modeling the tower dynamics. Again, at the beginning of the analysis, the blade 1 is in the vertical position (pointing up) and the simulation took 60 s.

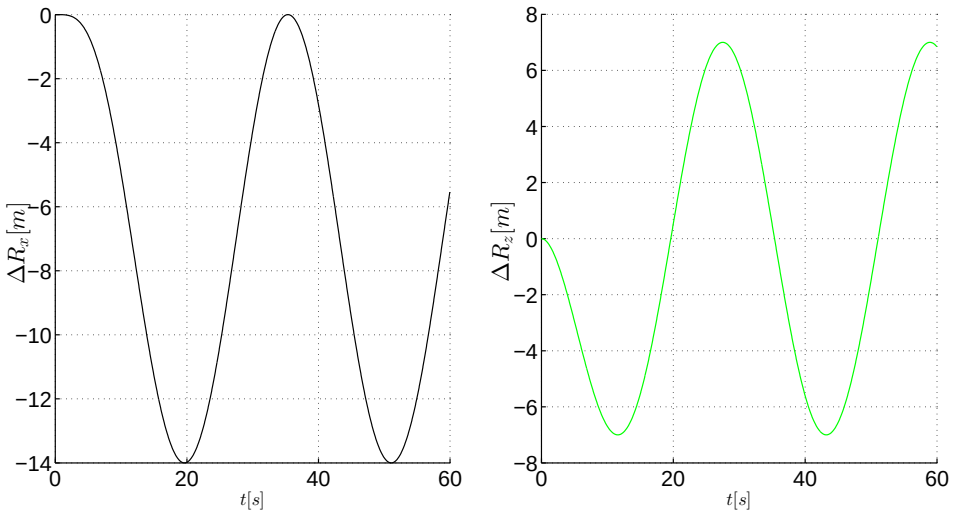

Figure 5.16: Blade 1 - Displacement of the center of mass - turbine with a generator

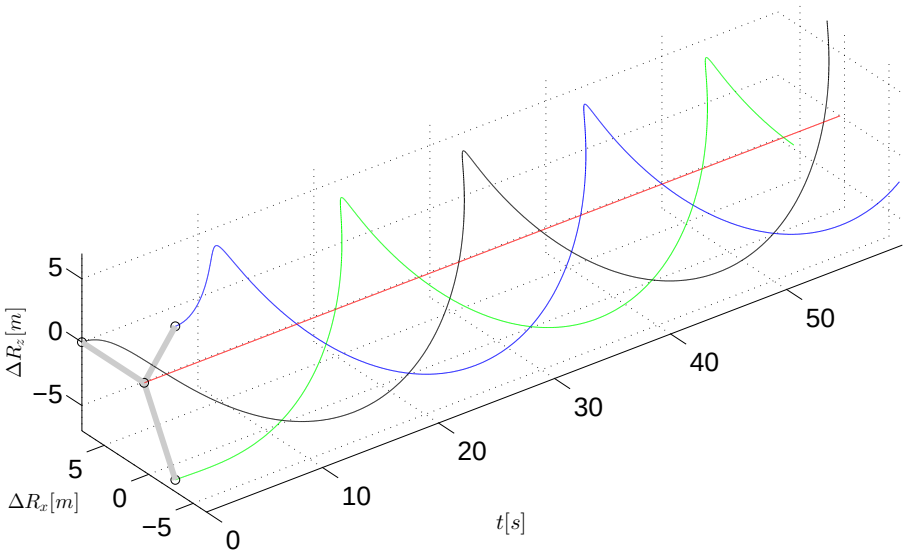

Figure 5.17: Positions of blades center of mass with time - turbine with generator

5.2.4
Turbine loaded by an external torque, with a generator

If the motor/generator is on, the torque made by the forces will act together with that torque made by the motor to put the rotor in the operation rotation.

Then the axial component of the acceleration of the shaft is, approximately

$$\dot{\Omega}_y = \frac{T_{b_y}}{J_{b_y}} = (21000 + 500000 \times 0.2)/(3 \times (2000 \times 7^2 + 33330)) \approx 0.31 \frac{rad}{s^2}. \quad (5.2)$$

This same result was obtained in the simulation which can be observed in the graph of the Figure 5.18. This graph shows the angular acceleration of the rotor in its axis or rotation from a value of approximately 0.31 rad/s to zero. If no resistance is found by the external torque, the blades will rotate in an ascending angular velocity as can be seen in graphs presented in Figure 5.13. If a generator is present, a counter-torque given by the Equation 5.1 will tend to stabilize the rotor speed. Two situations were explored: in the first the magnitude of the generator constant is $k_g = 100000$Nms/rad and in the second, the generator is able to apply a larger counter-torque ($k_g = 500000$Nms/rad). The results for the displacements in blades center of mass are shown in Figures 5.19 for the first case and in Figure 5.22, for the second. It can be noticed the differences between the two graphs for the angular speed due to the proper rotation of the shaft. As expected, in the second case, Figure 5.23, the stabilization is faster. As in the previous simulation, it is considered that structure is under its own weight, in equilibrium before starting the motion. Only 4 eigenvectors were use for modeling the tower. Again, at the beginning of the analysis, the blade 1 is in the vertical position (pointing up).

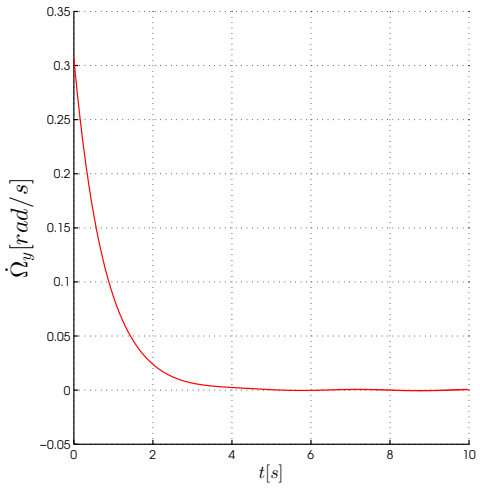

Figure 5.18: Shaft axial angular acceleration - turbine with generator and external torque

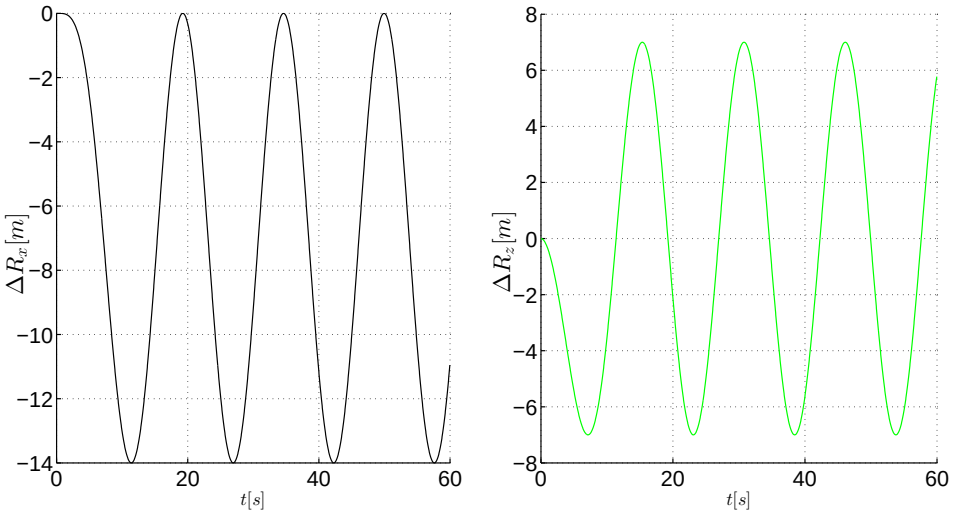

Figure 5.19: Blade 1 - Displacement of the center of mass

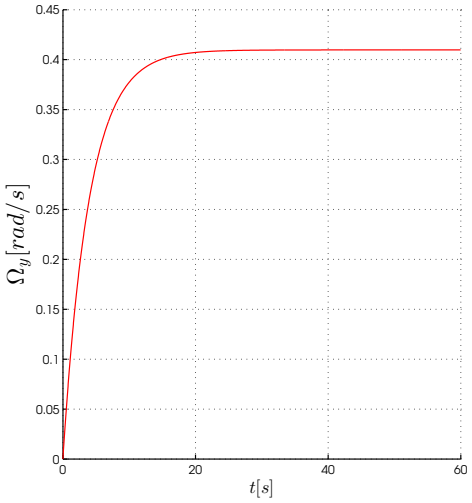

Figure 5.20: 1 - Angular velocities

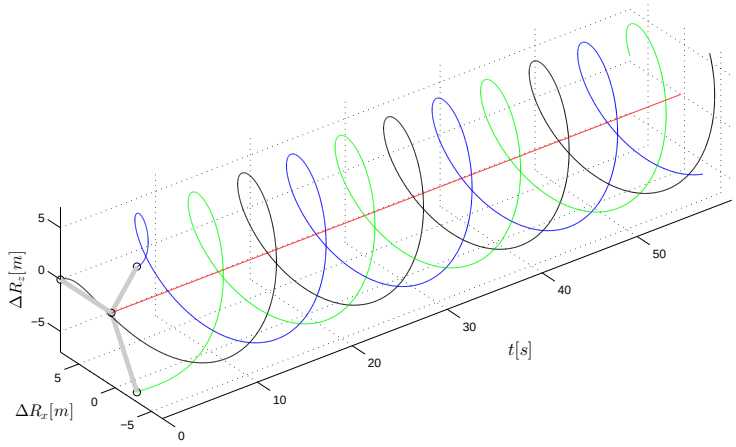

Figure 5.21: Positions of blades center of mass with time - turbine with generator and torque

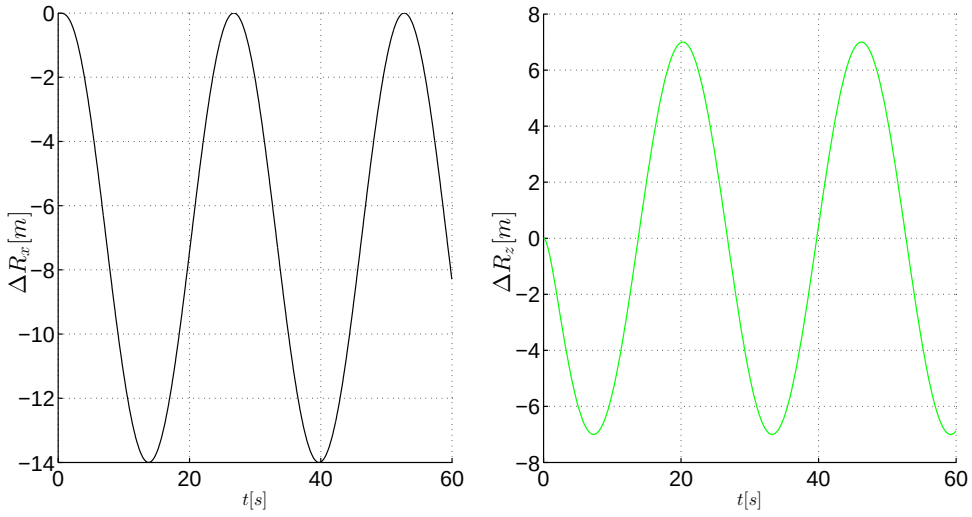

Figure 5.22: Blade 1 - Displacement of the center of mass - turbine with generator and torque

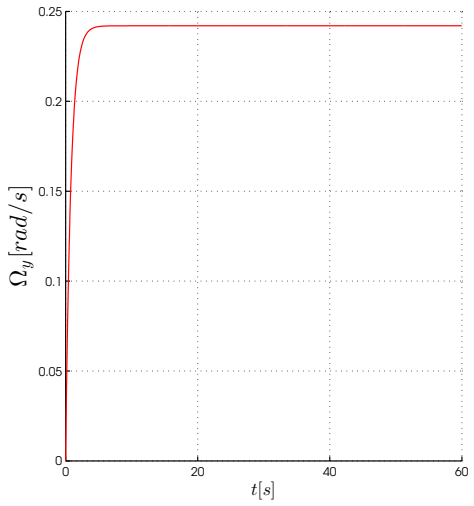

Figure 5.23: Blade 1 - Angular velocity

5.2.5 Deterministic water loads

In this case, the turbine is semi-immersed in water. Loads are present due to the water current. For water, one uses the Equation 4.2. The parameters related to the water motion are:

$h_w = L^* = 20\ m$; $x_1 = 50\ m$; $x_0 = 0.1\ m$; $\bar{W}_w(x) = \bar{W}_w = 0\ m/s$; $\Delta\bar{W}_w(x) = \Delta\bar{W}_w = 1\ m/s$; $\varpi_w = 0.2\ Hz$; $\iota_w = 0\ rad$

giving the following equation for the water velocity expression:

$$W_w(x,t) = cos(0.4\pi t),\ [0 \leq x \leq h_w]. \tag{5.3}$$

It will be assumed that the flow is in the z direction, so, the vector velocity of the water is

$$\{W_w(x,t)\} = \begin{Bmatrix} 0 \\ 0 \\ cos(0.4\pi t) \end{Bmatrix} \tag{5.4}$$

in m/s. The Figure 5.24 presented below depicts the results for this simulation. The nonlinearities due to the interaction fluid-structure make this simulation to be slow. The integration is made in element level. In the element domain the fluid velocity in the two lateral motion of the beam must be known so that the forces can be calculated properly.

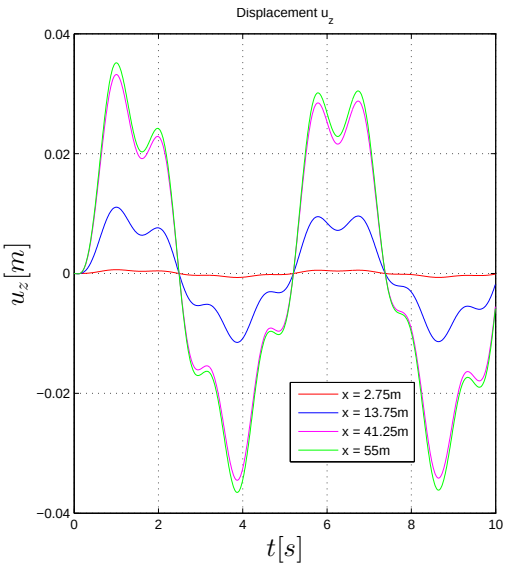

Figure 5.24: Z tower displacement at x=2.75 m, 13.7 5m, 41.25m and 55m

5.3 Turbine under random forces and torques at the tip

Concentrated force and torque $\{F(L,t)\}$ and $\{T(L,t)\}$ are applied at the tip of the turbine ($x = L$, in the tower). This can somehow simulate the action of the wind over the structure. The rotor is free but at rest and the loads are considered random.

It was mentioned previously that, due to the symmetry considerations, each eigenvector can be associated to a single structural component, namely, a bar (axis x), two beams (moving in xy and xz planes) and a shaft (torsion). This means that it is possible to increase the number of eigenvectors, improving the dynamics of one specific structural component. For instance, one begins the analysis, chosen 11 modes to be used in the approximation of the tower dynamics: they are chosen to be from the 1^{st} to the 9^{th}, the 11^{th} and the 14^{th}, meaning four eigenvectors for each beam motion, two for axial motion and one for rotation. Using this in the simulation, the displacements obtained for the tower in the four heights are depicted in Figure 5.26. Then, the 14^{th} eigenvalue was removed from the set and the results are given in the Figure 5.27, where it is observed that the graph for x displacement got smoother. Finally, the set was reduced in order to contain the 1^{st} to the 6^{th} eigenvectors. This means that all components are considered and each beam motion is represented using two functions. The results for this possibility is in Figure 5.28. This will be considered a good approximation in this work and the further simulations will be performed using this set.

Concerning to the loads, it was supposed that no complete information is available. It is know, however, that the force acts in y direction and the torque in z direction. Besides, their magnitude will be always in the intervals $[F_{y_l} \;\; F_{y_u}]$, for the force, and $[T_{z_l} \;\; T_{z_u}]$, for the torque, whose values are, respectively, 7000 N, 13000 N, 70000 Nm and 130000 Nm. With that information, as discussed in Section 7.10 of the Appendix, the PDF associated to this information that maximizes the uncertainty is, via Principle of Maximum Entropy [61], the uniform distribution. Taking in consideration the limits imposed in loading it can be said that,

$$\begin{array}{l} f_{\mathbf{F}}(f|F_{y_l}, F_{y_u}) = \dfrac{1}{F_{y_l} - F_{y_u}}; \;\; F_{y_l} \leq F_y \leq F_{y_u}. \\ 0; \;\; \text{otherwise.} \end{array} \quad , \tag{5.5}$$

and

$$\begin{array}{l} f_{\mathbf{T}}(f|T_{z_l}, T_{z_u}) = \dfrac{1}{T_{z_l} - T_{z_u}}; \;\; T_{z_l} \leq T_z \leq T_{z_u}. \\ 0; \;\; \text{otherwise.} \end{array} \tag{5.6}$$

All the other variables and parameters are considered deterministic and can be obtained in the Table 5.1 and Table 5.2. Under those assumptions, Monte Carlo simulation was performed in order to find out the structure response when submitted to this loading.

The time for simulation was 10 s and the processes were obtained for a number of 100 realizations. Incorporating the last set of eigenvalues as discussed above in the turbine kinematics and simulating using the random loads discussed above, the results for stresses can be obtained, as shown in graphs of the Figures presented next. The Figure 5.29, shows the graphs with the distribution of the axial stresses for the four points located at $5\%L = 2.75$m, $25\%L = 13.75$m, $75\%L = 41.25$m and $1\%L = 55$m located as depicted in Figure 5.25. The Figures 5.31 and 5.32 show the stresses as a set of realizations of random processes, considering that the force and the torque are both random. In the Figure 5.3 is shown a zoom in a part of the graph of the first graph of the Figure 5.31, showing random stresses in more detail. The graphs show a clear superposition of two axial stress components. One due to the bending motion, with lower frequency and other with higher frequency caused by pure axial loads (due to the weight of the structure itself). This happens because at $t = 0$, the turbine is considered instantaneously loaded, causing those oscillations in x (axial) direction.

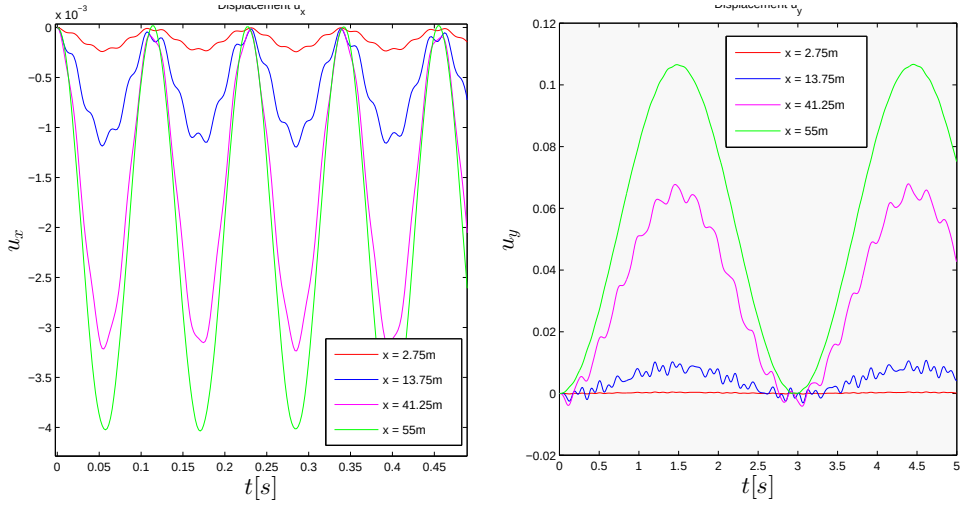

Figure 5.26: Results using the first set of eigenvectors

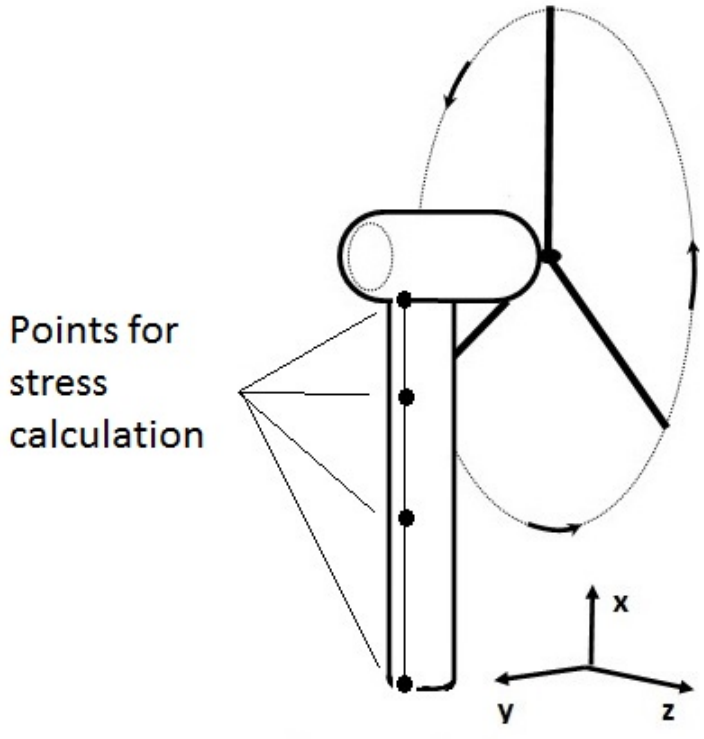

Figure 5.25: Points for stress calculation

5.3.1 Wind loads

In this work, the random wind can be modeled as forces and torques at the tip of the tower. But, in order to improve the algorithm to make it possible the full random wind implementation, the approach presented in Chapter 4, the BEM method, was implemented so that forces and torques acting in the blades

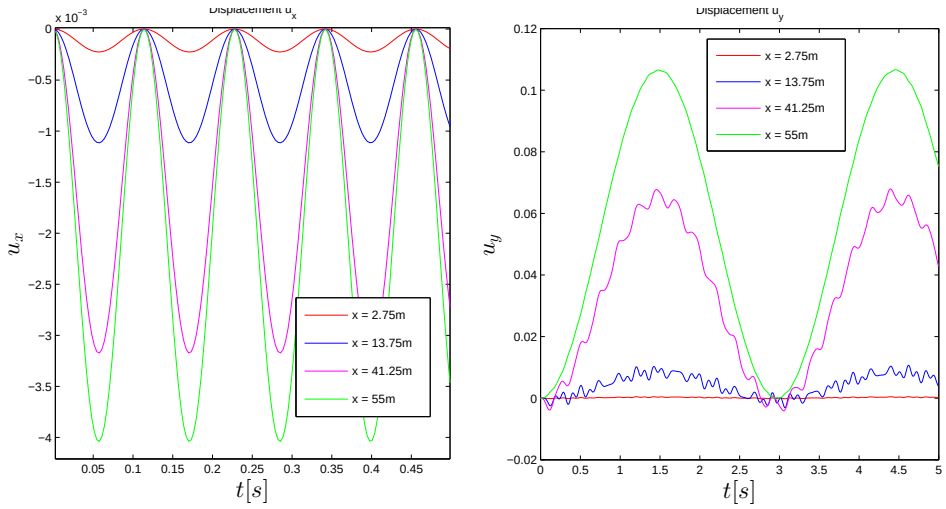

Figure 5.27: Results using the second set of eigenvectors

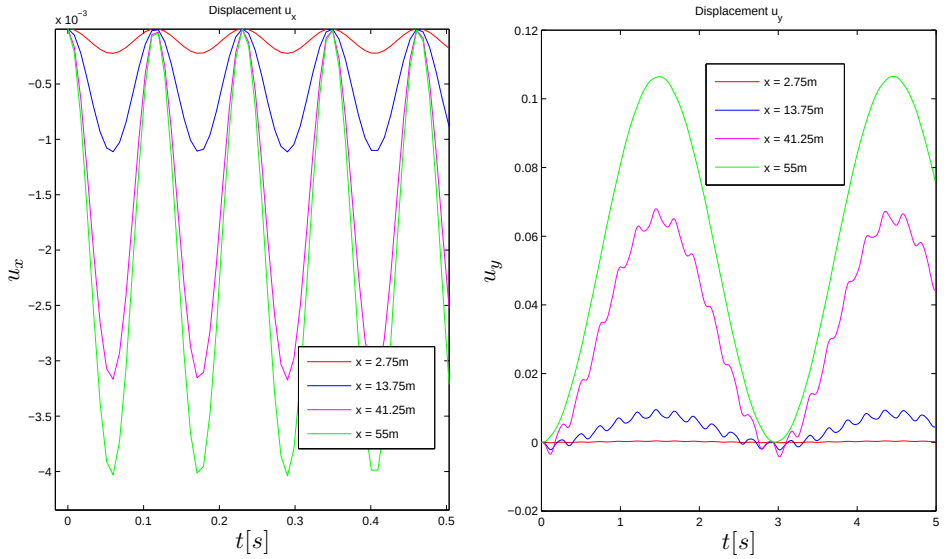

Figure 5.28: Results using the third set of eigenvalues

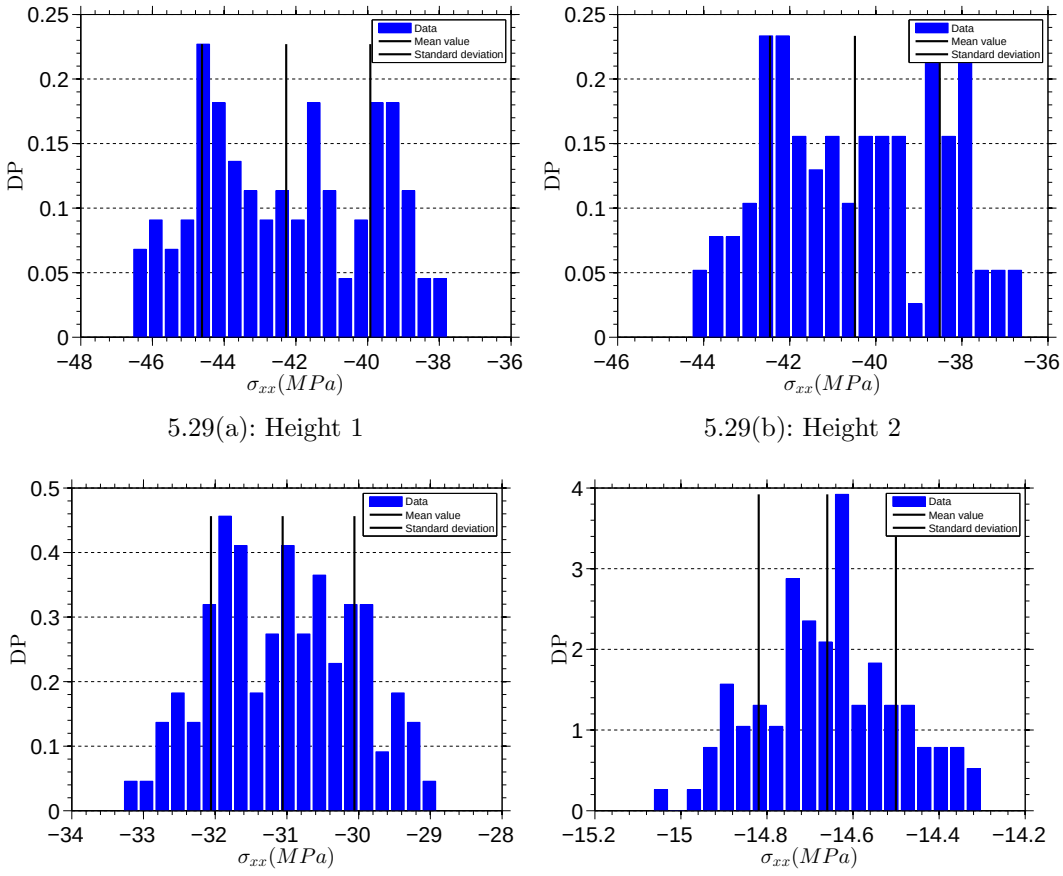

5.29(a): Height 1

5.29(b): Height 2

5.29(c): Height 3

5.29(d): Height 4

Figure 5.29: Axial stress distribution in four points in the tower

for one dimension wind can be calculated. The following data are considered in calculation:

- The velocity for t_s interval was $W_{a_{t_s}} = 5.5$m/s;
- Hub height $(H_h) = 55m$;
- Length of the blade $(L_b) = 25m$;
- Wind speed at reference height (x_1) was of =5.5;
- Roughness of the terrain $(x_0) = 0.1$ m;

The wind speed at the hub height is found to be 5.5 m/s. The speed of the blades (the same of the shaft) is considered to be 0.2 rad/s. The calculated parameters for this velocity as well as the ones of the blade adopted here are presented in Figures 5.33 to 5.36. Those from Figure 5.33 show the axial and angular induction factors as a function of the radial position r along the blade length. The Figures 5.34 depicts graphs for the local relative wind speeds and the pith angle for each radial position of the blades. Figure 5.35 depicts the distributed normal (perpendicular to the plane of the rotation) and tangential (responsible for the rotation of the blades) forces. Figure 5.36 shows the torques acting in the blades. Notice that, in the first graph is shown the

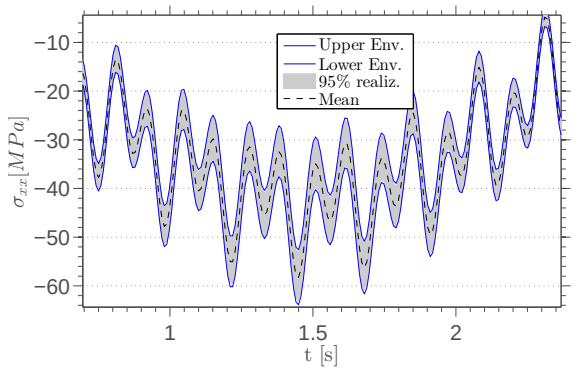

Figure 5.30: Zoom in the first graph of Figure 5.31

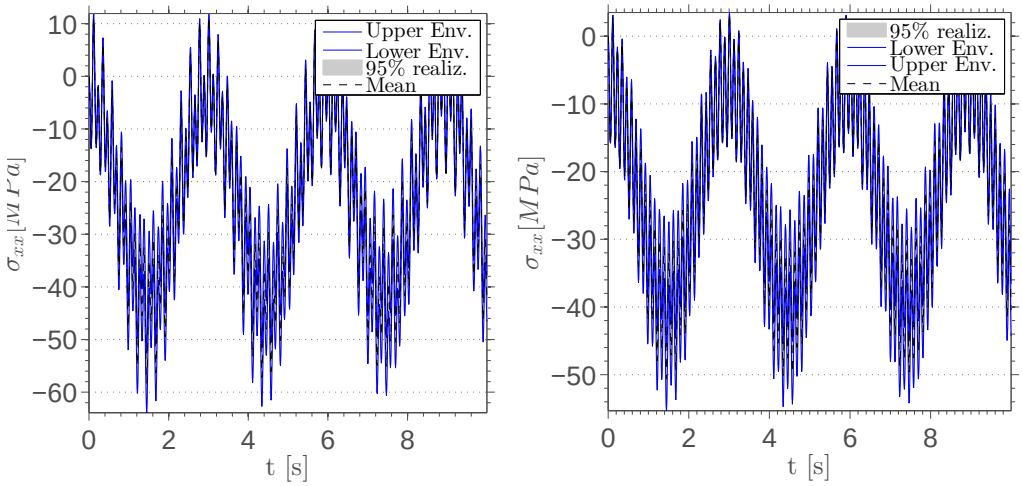

Figure 5.31: Axial stresses at point of heights 1 and 2

torque component orthogonal to the blade, responsible for the rotation of the shaft. In the second graph, the in-plane component of the torque that bends the blade in the direction of the wind. It must be said that in thee present work there is no any control of the pitch angle. Consequently, the data available for the airfoil do not permit a large variation in the air speed.

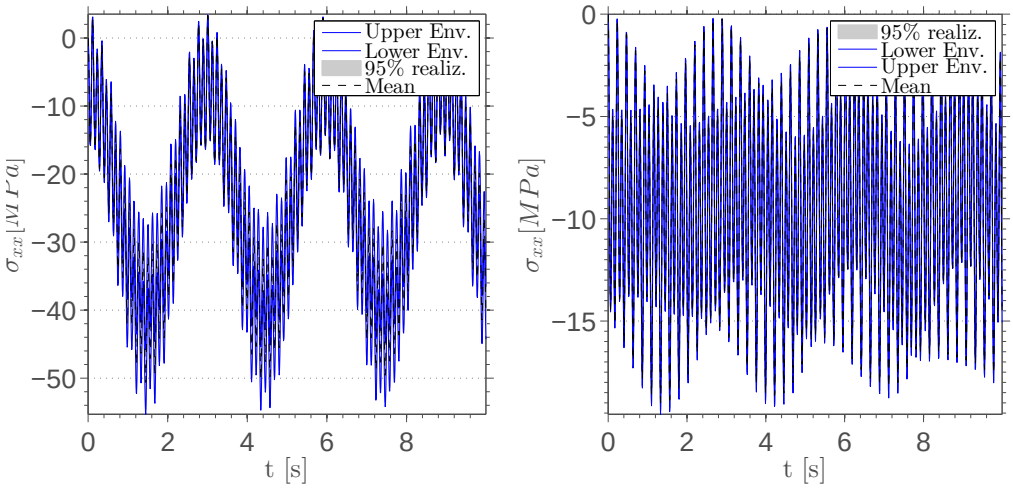

Figure 5.32: Axial stresses at point of heights 3 and 4

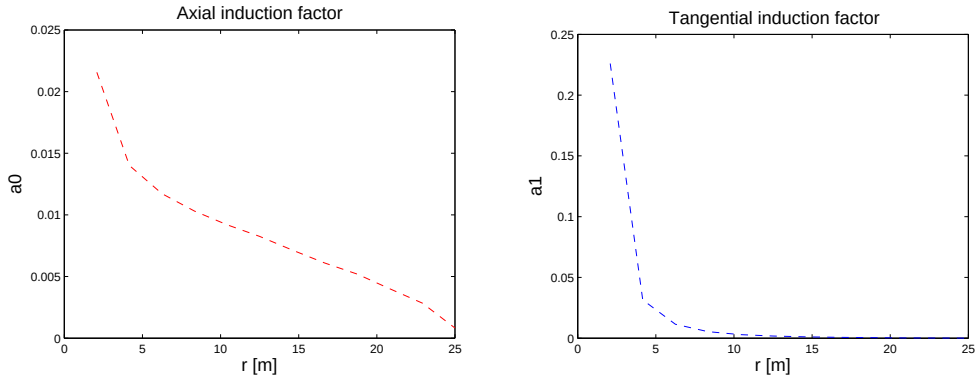

5.33(a): Axial

5.33(b): Tangential

Figure 5.33: Induction factors

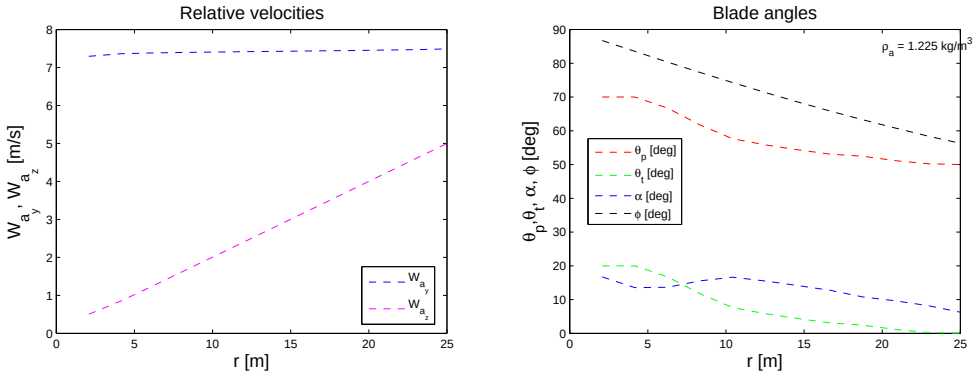

5.34(a): Wind speeds

5.34(b): Blade angles

Figure 5.34: Wind speed and blade angle

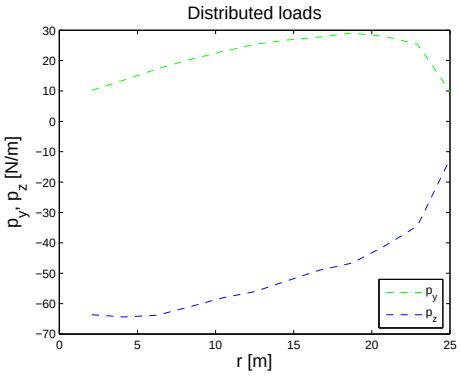

5.35(a): Distributed forces

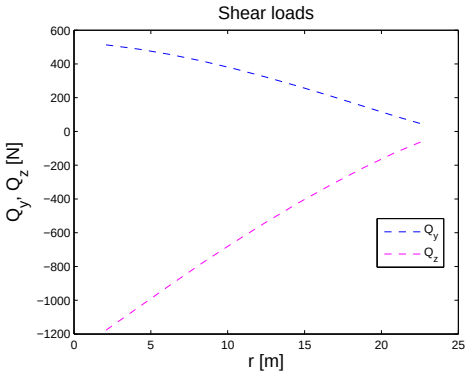

5.35(b): Shear forces

Figure 5.35: Forces

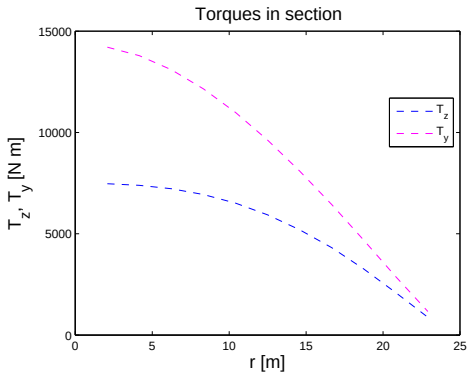

5.36(a): Torques in blade

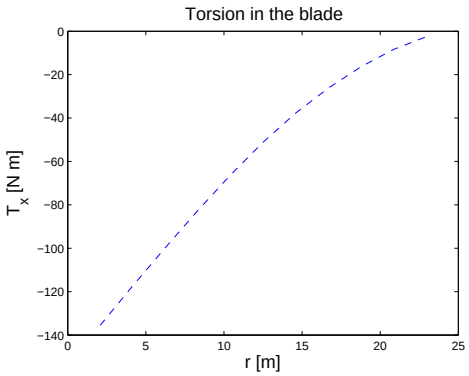

5.36(b): Torsion of the blade

Figure 5.36: BEM calculations - $W_a = 5.5$ m/s and $\Omega_y = 0.2$ rad/s

6
Conclusions

In order to obtain a basic platform for developing and studying the several dynamics of a HAWT a complete structure formed by base, tower, nacelle, shaft and three blades was modeled and analyzed. The soil flexibility was modeled by axial and torsional springs. The tower is a tube of constant cross section and considered to be the only flexible component. The shaft, also a tube, and the three blades form a rigid rotor. In the case of real design of turbines it is necessary to adjust the geometry of the blades to maximize the power coefficient. In this work, the wind actions were modeled as random forces an torques at the tip of the tower. However, Blade Element Momentum was incorporated to the model as well as the random wind generation.

The forces due to the water action as well as the concentrated ones can be constant or harmonic. In order to simulate the energetic production it was coupled an induction motor which reacts depending on the signal of the difference between the actual angular velocity of the rotor and a prescribed operational angular velocity.

The dynamics is represented by a system of nonlinear differential equations such that each rigid body is represented by seven generalized coordinates, namely, three displacements of the center of mass and four Euler parameters for modeling the attitude. The tower is modeled using finite elements of two nodes. Due to symmetries involved it was possible to uncouple the tower dynamics into three different elements: a beam for bending, a bar and a shaft for axial and torsional movements, respectively. Hermite polynomials were used for beam approximation and Lagrange polynomials for the others. To deal with the large number of degrees of freedom resulting from the finite element discretization of the tower, a reduction of the model is performed. Then, the approximation of the solution is obtained step by step using the reduced model. A code for integrating the equations was developed based in the Newmark method and the convergence at the end of each step is reached using Newton-Raphson method, under a imposed a tolerance.

The model was codified in Matlab®and permits:

- The calculation of desired modes of the tower for a given precision for a further reduction of d.o.f.;
- The calculation of the external loads (wind, water or others);
- Reduction of the number of tower d.o.f and free chosen of the modes to be used;

- The integration in time using an integrator based on Newmark method;
- To perform a random simulation, if it is the case;
- The calculation of the kinematic and dynamic quantities:
  - Position, velocities and accelerations of the center of mass for all the rigid bodies;
  - Angular velocity and acceleration of the rigid bodies;
  - Forces and torques in four sections of the tower;
  - Stresses (von Mises, axial and shear) in any four sections of the tower in any chosen point;
  - Forces and torques in shaft and blades at the hub connection.

The time spent in obtaining the approximation for the solution depends on the number of the eigenvalues used to approximate the solution. It increases considerably for large number of eigenvalues. This happens for two reasons: the matrices get larger and the time step gets smaller because the integrator uses, as increment, 1/10 of the smaller period. For instance, for obtaining the results for the problem of the Section 5.2.4 it took on average 35 s using 6 eigenvectors. Using 3 eigenvectors, only 6s are spent. If the analysis with deterministic movement of the water is performed, the time spent is quite high. For the problem of the section 5.2.5, 1h:5min was spent, for instance and this happens due to the nonlinearities caused by the interaction fluid structure, due to the Morison equation.

This work aims to be a comprehensive (although not profound) modeling of the dynamics of a HAWT as it has almost all steps for the wind turbine analysis, as can be noticed. Wind turbines are complex structures and are still nowadays under intense study. So, this work may be improved in several ways, in short, medium and long terms. In short term it can be mentioned:

- Implementation of a more realistic wind model,
  - Using a realistic set of blades;
  - Modeling pitch control.
- Evaluations must be made using other time integrators. As mentioned the integrator used was developed by the author based in Newmark method, in order to save time;
- Coupling of a more realistic electric generation system;
- Implementation of variable cross sections. Improvement in graphic interface (animation for instance).

In medium term:

- Implementation of random water loading;
- Implementation of the flexibility for shaft and blades;
- Implementation of Reliability analysis;

In long therm:

- Implementation of a control system (pitch and yaw);
- Extend the analysis to floating bases;

The simulations show that the program can deal with initial angular velocities and several kinds of loads including random ones. In this case, a distribution of stresses are determined so that calculating probabilities can be easily calculated. The formulation using Euler parameters showed to be effective. The matrices and vectors involved are simple functions of Euler parameters. Derivatives involving those structures, needed in the Newmark method, are either linear with respect to those parameters or constant. It saves time in the analysis.

7
Appendix

7.1
Formulation for the tower

7.1.1
Beam kinematics

Beams are important structural elements and the interest in its behavior is very old. In 17th century Jacob Bernoulli (1654−1705) discovered that the curvature of an elastic beam under pure bending is proportional to the moment applied and Daniel Bernoulli (1700 − 1782), formulated the differential equation of motion of a vibrating beam. Leonhard Euler (1707−1783) studied the problem later and contributed to the theory studying several loading configurations and their responses [22]. The Euler-Bernoulli beam theory was developed under the hypothesis that the cross-sections remain orthogonal to the neutral line (passes through the centroid of the cross section), as represented in Figure 7.1−a, for the plane xy, and the shear strain is null. Then, this beam theory is the simplest, whose limitations leads to errors, depending on the case. The absence of shear strains makes the beam more rigid and as a consequence, in dynamical problems, it overestimates the natural frequencies specially for those of higher modes [22]. It is good for slender beams and those cases where the shear can be neglected. The Rayleigh (1842 − 1919) beam theory (1877) included the effect of the rotation of the cross-section in inertia of the beam and was an improvement on Euler-Bernoulli theory. It corrected partially the overestimation of natural frequencies in Euler-Bernoulli model, but just marginally [22]. Both formulations lead to differential equations whose unknown variable is the deflection of the neutral line. Timoshenko (1878-1972) proposed a beam theory which associates the effects of shear distortion to the Euler-Bernoulli model [66][67]. This model is suitable to non-slender beams and for high-frequency responses where shear or rotary effects are not negligible. Two independent variables are considered for characterizing the behavior of the beam: the deflection of its neutral line and the angle between the tangent to this line and the plane of the cross-sections after deformation, as shown in Figure 7.2. The difference between those two angles are the shear angles, $\{\Psi_i(x,t)\}$, $(i = z, y)$ and are caused by shear forces. Consequently, two differential equation are obtained for beam formulation in each plane xy and xz. In Euler-Bernoulli model, $\{\Psi(x,t)\} = \{0\}$, then $\{\theta_z(x,t)\} = -\{\frac{\partial}{\partial x} w_y(x,t)\}$

and $\{\theta_y(x,t)\} = \{\frac{\partial}{\partial x}w_z(x,t)\}$, as can be seen in Figure 7.1. If the sections remain plane the shear strains must be constant, but, at the edge of the cross sections surface, the strain are null. This discrepancy is overcome by using the shape factors (also called the shear coefficient or area reduction factor) which give the ratio of the average strain on a section to the shear strain at the centroid. Those coefficients contain information on the material of the beam as it is a function of Poisson's ratio, on the shape of the cross-section, as well as, on the frequency of vibration. Some researchers suggested methods to calculate the shape factor as a function of the shape of the cross-section and Poisson's ratio and [63] demonstrated the variation in the shape factor with frequency.

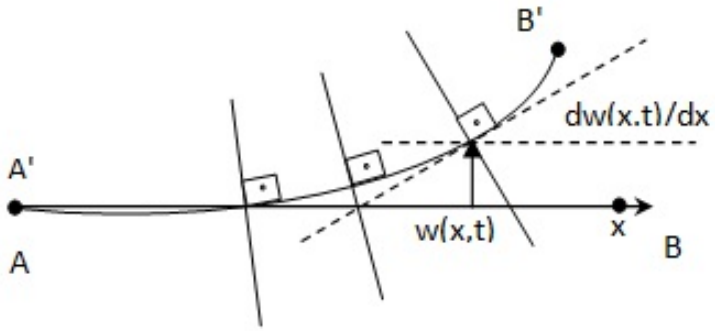

Figure 7.1: Euler-Bernoulli hypothesis

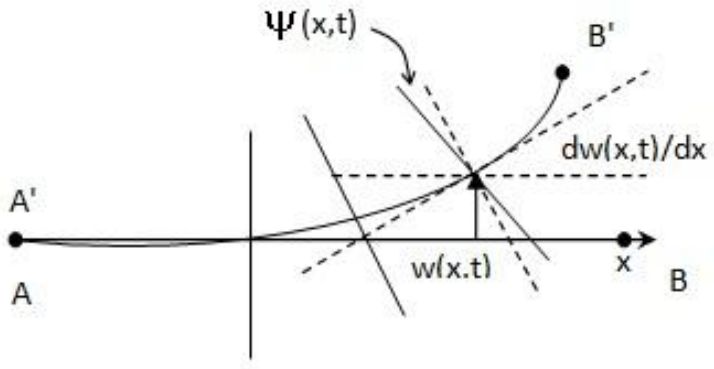

Figure 7.2: Timoshenko hypothesis

Theory of Elasticity was used to model beams and, under the hypothesis imposed in each approach, the results showed compatibility under the hypotheses for Timoshenko and Euler-Bernoulli models. Despite their limitations, the Euler-Bernoulli and Timoshenko beam theories are still widely used [22].

Next, it will be discussed a model for beam analysis, that can be simplified into Timoshenko, Rayleigh and Euler-Bernoulli. For sake of completeness, in

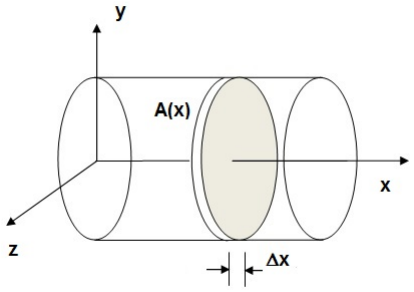

7.3(a): Loaded beam

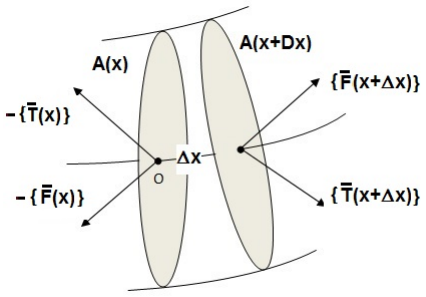

7.3(b): Deformed sections

Figure 7.3: Deformation process

this discussion it will be included the beam twist resulting in a coupled system with bending in two directions, axial traction/compression and warping of the cross sections, as well as, the influence of the axial forces in lateral motion. What follows concerning to the determination of the equations of motion of the tower was based in [6].

7.1.2 Beam Dynamics

A cylinder with length L, area of the cross-section $A = A(x)$ at an axial position x, $0 \leq \times \leq L$, moments of inertia of area $I_{xx} = I_{xx}(x)$, $I_{yy} = I_{yy}(x)$ and $I_{zz} = I_{zz}(x)$, density $\rho = \rho(x)$ is represented in Figure 7.3. The movement of the beam after being loaded can be completely described by its displacements $\{w\} = \{w(x,t)\}$ and rotations of the cross section, $\{\theta\} = \{\theta(x,t)\}$. The cylinder is loaded by a distributed force per unit length $\{f\} = \{f(x,t)\}$ and by a distributed moment $\{m\} = \{m(x,t)\}$. There is a total mass m_{tip} (which is the sum of the mass of the nacelle and blades) fixed at its tip, and springs at its base, simulating the behavior of the soil. Those rotational springs have spring constants kr_x, kr_y, kr_z and the translational ones have constants ka_x, ka_y, ka_y, respectively. The model is simplified and one considers that rotations and displacements are small. So, the undeformed and deformed state can both be described in a fixed inertial frame with base unit vectors $\{\hat{x}_0\}$, $\{\hat{y}_0\}$ and $\{\hat{z}_0\}$. As the external loads are applied the beam is deformed and the that loads are balanced by an internal section force vector $\{\bar{F}\} = \{\bar{F}(x,t)\}$ and an internal section torque $\{\bar{T}\} = \{\bar{T}(x,t)\}$ whose components are

$$\{\bar{F}\} = (\bar{F}_x, \bar{F}_y, \bar{F}_z)^T \quad \text{and} \quad \{\bar{T}\} = (\bar{T}_x, \bar{T}_y, \bar{T}_z)^T \tag{7.1}$$

$\bar{F}_x = \bar{F}_x(x,t)$ is the axial force, whereas the components $\bar{F}_y = \bar{F}_y(x,t)$ and $\bar{F}_z = \bar{F}_z(x,t)$ are the shear forces components in the y- and z -directions.

The axial component $\bar{F}_x = \bar{F}_x(x,t)$ is the torque in x direction, due to the twist the cylinder. The components $\bar{F}_y = \bar{F}_y(x,t)$ and $\bar{T}_z = \bar{T}_z(x,t)$ in the y- and z-directions are torques due to the bending of the cylinder. It is assumed that the displacements remain small the equation of motion can be established in the referential state. Referring to the small segment of the cylinder in Figure 7.3 at the coordinate x, the load in the section is supposed to be applied in the centroid of the area. At the right end-section, these vectors are changed into $\{\bar{F} + d\bar{F}\}$ and $\{\bar{T} + d\bar{T}\}$, respectively. The following equation of equilibrium can be formulated

$$\begin{aligned} &\{\bar{F}\} + \{d\bar{F}\} - \{\bar{F}\} + \{f\}dx = \rho A dx\{\ddot{w}\} \\ &\{d\bar{F}\} + \{f\}dx = \rho A\{\ddot{w}\}dx \end{aligned} \tag{7.2}$$

Taking the moment of the forces with respect to the point 0,

$$\begin{aligned} &\{\bar{T}\} + \{d\bar{T}\} - \{\bar{T}\} + \{\hat{x}\} \times \{\bar{F} + d\bar{F}\}dx + \{m\}dx + \{f\}\frac{dx^2}{2} = \\ &\{d\bar{T}\} + \{\hat{x}\} \times \{\bar{F} + d\bar{F}\}dx + \{m\}dx + \{f\}\frac{dx^2}{2} = \\ &\int_A \rho(y^2 + z^2)dAdx\{\ddot{\theta}\}. \end{aligned} \tag{7.3}$$

Developing the term $\{d\bar{T}\} + \{\hat{x}\} \times \{\bar{F} + d\bar{F}\}$ of equations 7.3,

$$\{\hat{x}_0\} \times \{\bar{F}\} = \{\hat{x}_0\} \times (\bar{F}_x\{\hat{x}_0\} + \bar{F}_y\{\hat{y}_0\} + \bar{F}_z\{\hat{z}_0\}) = -\bar{F}_z\{\hat{y}_0\} + \bar{F}_y\{\hat{z}_0\}). \tag{7.4}$$

If it is considered that the axial force affects the transversal movement due to the deflection of the cylinder, than

$$\{\hat{x}\} \times (\bar{F}_x\frac{\partial w_y}{\partial y}\{\hat{y}\} + \bar{F}_x\frac{\partial w_z}{\partial z}\{\hat{z}\}) = (\bar{F}_x\frac{\partial w_y}{\partial z})\{\hat{z}\} - (\bar{F}_x\frac{\partial w_z}{\partial z})\{\hat{y}\}. \tag{7.5}$$

The Equations 7.2 and 7.3 above, taking in consideration the Equations 7.4 and 7.5, can be written in its components in three directions

$$\begin{aligned} &\frac{\partial}{\partial x}\bar{F}_x + f_x = \rho A\ddot{w}_x \\ &\frac{\partial}{\partial x}\bar{F}_y + f_y = \rho A\ddot{w}_y \\ &\frac{\partial}{\partial x}\bar{F}_z + f_z = \rho A\ddot{w}_z \\ &\frac{\partial}{\partial x}\bar{T}_x + m_x = \rho I_{xx}\ddot{\theta}_x \\ &\frac{\partial}{\partial x}\bar{T}_y - \frac{\partial}{\partial x}(\bar{F}_x\frac{\partial w_z}{\partial x}) + \bar{F}_z + m_y = \rho I_{yy}\ddot{\theta}_y, \\ &\frac{\partial}{\partial x}\bar{T}_z + \frac{\partial}{\partial x}(\bar{F}_x\frac{\partial w_y}{\partial x}) + \bar{F}_y + m_z = \rho I_{zz}\ddot{\theta}_z \quad . \end{aligned} \tag{7.6}$$

The distribution of stress in the surfaces of cross sections permits one to write the following

$$\begin{aligned} \bar{F}_x &= \int_A \sigma_{xx} dA; \quad \bar{F}_y = \int_{A_t} \sigma_{xy} dA; \;\; \bar{F}_z = \int_A \sigma_{xz} dA \\ \bar{T}_x &= \int_A (\sigma_{xz} y - \sigma_{xy} z) dA; \;\; \bar{T}_y = \int_A \sigma_{xx} z dA; \;\; \bar{T}_z = \int_A \sigma_{xx} y dA \quad . \end{aligned} \tag{7.7}$$

Now, it will be discussed the deformation hypothesis.

7.1.3 Kinematics of deformation

As mentioned before, classical beam theory is based in the idea that the deformations take place, keeping all the cross sections plane. The movement to a deformed position is uniquely described by a vector of lateral displacements of the axial neutral line $\{w\} = \{w(x)\}$ and a vector (just for small rotations) of rotation $\{\theta\} = \{\theta(x,t)\}$. This angle can be considered as a sum of two components: One dependent on the deflection of the neutral line $\{w\} = \{w(x,t)\}$ and other due to de action of the shear forces, $\{\Psi\} = \{\Psi(x,t)\}$. So, $\{\theta\} = \frac{\partial}{\partial x}\{w\} + \{\Psi\}$. Then, any (x,y,z) pertaining to any undeformed cross-section can be related to a point in the deformed cross-section in the following way

$$\begin{aligned} u_x(x,y,z) &= w_x + z\theta_y - y\theta_z \\ u_y(x,y,z) &= w_y - z\theta_x \\ u_z(x,y,z) &= w_z + y\theta_x. \end{aligned} \tag{7.8}$$

Recalling the definition of strain (in case of small deformations), it becomes that,

$$\begin{aligned} \epsilon_{xx}(x,y,z) &= \frac{\partial u_x}{\partial x} = \frac{\partial w_x}{\partial x} + z\frac{\partial \theta_y}{\partial x} - y\frac{\partial \theta_z}{\partial x} \\ \gamma_{xy}(x,y,z) &= \frac{\partial u_x}{\partial y} + \frac{\partial u_y}{\partial x} = \frac{\partial w_y}{\partial x} - z\frac{\partial \theta_x}{\partial x} - \theta_z \\ \gamma_{xz}(x,y,z) &= \frac{\partial u_x}{\partial z} + \frac{\partial u_z}{\partial x} = \frac{\partial w_z}{\partial x} + y\frac{\partial \theta_x}{\partial x} + \theta_y. \end{aligned} \tag{7.9}$$

Equations 7.9 for γ_{xy} and γ_{xz} shows that they are neither dependent on y nor on z. This means that those strains are constant or null in the section. Under the Euler-Bernoulli model hypothesis, they are null.

On the other hand, for Timoshenko beam, shear deformation is included a priori in the model as a constitutive relation, as will be shown later. The model says that the strain is constant in section. This is not true and a way to remedy this inconsistency is to use shape factors.

The Equations 7.8 consider that the twist of the cylinder does not produce

any change in the cross-sections. This is true for beams whose section is circular. In any other case, the twist of the beam causes deformation in the cross-section and induce an additional non-planar displacement in the x-axis, say, $\omega = \omega(y, z)$. This affects only the axial component of the displacement and be generally written as $u_\omega(x, y, z) = \omega(y, z)\frac{\partial}{\partial x}\theta_x$. Under these considerations, the total displacement is, after the deformation, given by

$$u_x(x, y, z) = w_x + z\theta_y - y\theta_z + \omega\frac{\partial\theta_x}{\partial x}, \tag{7.10}$$

so, the components of Equation 7.9 for strains are completed as below

$$\begin{aligned}
\epsilon_{xx}(x, y, z) &= \frac{\partial u_x}{\partial x} = \frac{\partial w_x}{\partial x} + z\frac{\partial\theta_y}{\partial x} - y\frac{\partial\theta_z}{\partial x} + \omega\frac{\partial^2\theta_x}{\partial x^2} \\
\gamma_{xy}(x, y, z) &= \frac{\partial u_x}{\partial y} + \frac{\partial u_y}{\partial x} = \frac{\partial w_y}{\partial x} - \theta_z + (\frac{\partial\omega}{\partial y} - z)\frac{\partial\theta_x}{\partial x} \\
\gamma_{xz}(x, y, z) &= \frac{\partial u_x}{\partial z} + \frac{\partial u_z}{\partial x} = \frac{\partial w_z}{\partial x} + \theta_y + (\frac{\partial\omega}{\partial z} + y)\frac{\partial\theta_x}{\partial x}
\end{aligned} \tag{7.11}$$

7.1.4 Differential equations

Taking in consideration the constitutive relations,

$$\begin{aligned}
\sigma_{xx} &= E\epsilon_{xx} = E(\frac{\partial w_x}{\partial x} + z\frac{\partial\theta_y}{\partial x} - y\frac{\partial\theta_z}{\partial x} + \omega\frac{\partial^2\theta_x}{\partial x^2}) \\
\sigma_{xy} &= G\gamma_{xy} = G(\frac{\partial w_y}{\partial x} - \theta_z + (\frac{\partial\omega}{\partial y} - z)\frac{\partial\theta_x}{\partial x}) \\
\sigma_{xz} &= G\gamma_{xz} = G(\frac{\partial w_z}{\partial x} + \theta_y + (\frac{\partial\omega}{\partial z} + y)\frac{\partial\theta_x}{\partial x})
\end{aligned} \quad . \tag{7.12}$$

Equations 7.7 can be integrated over the cross-section using Equations 7.12, so that the following relation is obtained:

$$\begin{aligned}
\bar{F}_x &= E(A\frac{\partial w_x}{\partial x} + I_y\frac{\partial\theta_y}{\partial x} - I_z\frac{\partial\theta_z}{\partial x} + I_\omega\frac{\partial^2\theta_x}{\partial x^2}) \\
\bar{F}_y &= G(\kappa_y A(\frac{\partial w_y}{\partial x} - \theta_z) + I_{\omega_y}\frac{\partial\theta_x}{\partial x}) \\
\bar{F}_z &= G(\kappa_z A(\frac{\partial w_z}{\partial x} + \theta_y) + I_{\omega z}\frac{\partial\theta_x}{\partial x}) \\
\bar{T}_x &= G(I_z(\frac{\partial w_z}{\partial x} + \theta_y) - I_y(\frac{\partial w_y}{\partial x} - \theta_z) + K_{sv}\frac{\partial\theta_x}{\partial x}) \\
\bar{T}_y &= E(I_y\frac{\partial w_x}{\partial x} + I_{yy}\frac{\partial\theta_y}{\partial x} - I_{yz}\frac{\partial\theta_z}{\partial x} + I_{\omega z}\frac{\partial\theta_x}{\partial x}) \\
\bar{T}_z &= E(-I_z\frac{\partial w_x}{\partial x} - I_{yz}\frac{\partial\theta_y}{\partial x} + I_{zz}\frac{\partial\theta_z}{\partial x} - I_{\omega y}\frac{\partial\theta_x}{\partial x})
\end{aligned} \quad , \tag{7.13}$$

where the parameters $I_{\omega y}$, I_z, I_y, I_ω, K_{sv}, I_{yy}, I_{zz}, $I_{\omega y}$ and $I_{\omega z}$ are defined as below

$$
\begin{aligned}
&I_{wy} = \int_A (\frac{\partial \omega}{\partial y} - z) dA; \quad I_{wz} = \int_A (\frac{\partial \omega}{\partial z} + y) dA \\
&I_y = \int_A z dA; \quad I_z = \int_A y dA; \quad I_\omega = \int_A \omega dA; \quad I_{xx} = \int_A x^2 dA \\
&I_{zz} = \int_A z^2 dA; \quad I_{yz} = \int_A yz dA; \quad I_{\omega y} = \int_A \omega y dA; \\
&I_{\omega z} = \int_A \omega z dA; \quad K_{sv} = I_{xx} + \int_A (y\frac{\partial \omega}{\partial z} - z\frac{\partial \omega}{\partial y})
\end{aligned} \tag{7.14}
$$

The parameters listed above are the cross-sectional area, A, the shape factors κ_y and κ_z, for compensating the fact that the shear stresses are not constant in the section. $I_{\omega y}$ and $I_{\omega z}$ are dependent on the warping shape $\omega(y, z)$ and also on the geometric characteristics. I_y and I_z are denoted as the first order moment about y and z. I_ω is the first moment of the warping shape function. I_{yy}, I_{zz} and I_{yz} are the moment and product of inertia of area with respect to y and z. $I_{\omega y}$ and $I_{\omega z}$ are the moments of the warping shape function. Finally, K_{sv} is related to the St. Venant torsion.

Considering what was exposed by now, the following matrix equation can be written

$$
\begin{Bmatrix} \bar{F}_x \\ \bar{T}_x \\ \bar{T}_y \\ \bar{T}_z \\ \bar{F}_y \\ \bar{F}_z \end{Bmatrix} = [\mathbb{E}_1] \begin{Bmatrix} \frac{\partial w_x}{\partial x} \\ \frac{\partial w_y}{\partial x} \\ \frac{\partial w_z}{\partial x} \\ \frac{\partial \theta_x}{\partial x} \\ \frac{\partial \theta_y}{\partial x} \\ \frac{\partial \theta_z}{\partial x} \\ \theta_y \\ \theta_z \\ \frac{\partial^2 \theta_x}{\partial x^2} \end{Bmatrix}, \tag{7.15}
$$

where,

$$
[\mathbb{E}_1] = \begin{bmatrix}
EA & 0 & 0 & 0 & EI_y & -EI_z & 0 & 0 & EI_\omega \\
0 & -GI_y & GI_z & K_{sv} & 0 & 0 & GI_z & GI_y & 0 \\
EI_y & 0 & 0 & EI_{\omega z} & EI_{yy} & -EI_{yz} & 0 & 0 & 0 \\
-EI_z & 0 & 0 & -EI_{\omega y} & -EI_{yz} & EI_{zz} & 0 & 0 & 0 \\
0 & G\kappa_y A & 0 & GI_{\omega y} & 0 & 0 & 0 & -G\kappa_y A & 0 \\
0 & 0 & G\kappa_z A & GI_{\omega z} & 0 & 0 & G\kappa_z A & 0 & 0
\end{bmatrix} \tag{7.16}
$$

Recalling the Equations 7.6, it comes that

$$\begin{Bmatrix} \frac{\partial}{\partial x}\bar{F}_x \\ \frac{\partial}{\partial x}\bar{T}_x \\ \frac{\partial}{\partial x}\bar{T}_y \\ \frac{\partial}{\partial x}\bar{T}_z \\ \frac{\partial}{\partial x}\bar{F}_y \\ \frac{\partial\theta_y}{\partial x}\bar{F}_z \end{Bmatrix} + \begin{Bmatrix} 0 \\ 0 \\ \bar{F}_z \\ \bar{F}_y \\ 0 \\ 0 \end{Bmatrix} + \begin{Bmatrix} 0 \\ 0 \\ -\bar{F}_x\frac{\partial w_z}{\partial x} \\ \bar{F}_x\frac{\partial w_y}{\partial x} \\ 0 \\ 0 \end{Bmatrix} + \begin{Bmatrix} f_x \\ m_x \\ m_y \\ m_z \\ f_y \\ f_z \end{Bmatrix} = \begin{Bmatrix} \rho A\ddot{w}_x \\ \rho I_{xx}\ddot{\theta}_x \\ \rho I_{zz}\ddot{\theta}_y \\ \rho I_{yy}\ddot{\theta}_z \\ \rho_t A\ddot{w}_y \\ \rho A\ddot{w}_z \end{Bmatrix} \tag{7.17}$$

Working with Equations 7.15 and making appropriated substitutions in Equations 7.17, it results that

$$\frac{\partial}{\partial x}\left\{ [\mathbb{E}_1] \begin{Bmatrix} \frac{\partial w_x}{\partial x} \\ \frac{\partial w_y}{\partial x} \\ \frac{\partial w_z}{\partial x} \\ \frac{\partial\theta_x}{\partial x} \\ \frac{\partial\theta_y}{\partial x} \\ \frac{\partial\theta_z}{\partial x} \\ \theta_y \\ \theta_z \\ \frac{\partial^2\theta_x}{\partial x^2} \end{Bmatrix} \right\} + [\mathbb{E}_2] \begin{Bmatrix} \frac{\partial w_x}{\partial x} \\ \frac{\partial w_y}{\partial x} \\ \frac{\partial w_z}{\partial x} \\ \frac{\partial\theta_x}{\partial x} \\ \frac{\partial\theta_y}{\partial x} \\ \frac{\partial\theta_z}{\partial x} \\ \theta_y \\ \theta_z \\ \frac{\partial^2\theta_x}{\partial x^2} \end{Bmatrix} + \begin{Bmatrix} 0 \\ 0 \\ -\bar{F}_x\frac{\partial w_z}{\partial x} \\ \bar{F}_x\frac{\partial w_y}{\partial x} \\ 0 \\ 0 \end{Bmatrix} + \begin{Bmatrix} f_x \\ m_x \\ m_y \\ m_z \\ f_y \\ f_z \end{Bmatrix} = \begin{Bmatrix} \rho A\ddot{w}_x \\ \rho I_{xx}\ddot{\theta}_x \\ \rho I_{zz}\ddot{\theta}_y \\ \rho I_{yy}\ddot{\theta}_z \\ \rho A\ddot{w}_y \\ \rho A\ddot{w}_z \end{Bmatrix}, \tag{7.18}$$

where,

$$[\mathbb{E}_2] = \begin{pmatrix} 0 & 0 & 0 & 0 & 0 & 0 & 0 & 0 & 0 \\ 0 & 0 & 0 & 0 & 0 & 0 & 0 & 0 & 0 \\ 0 & 0 & 0 & 0 & 0 & 0 & 0 & 0 & 0 \\ 0 & 0 & -G\kappa_z A & -GI_{\omega z} & 0 & 0 & G\kappa_z A & 0 & 0 \\ 0 & 0 & G\kappa_z A & GI_{\omega z} & 0 & 0 & G\kappa_z A & 0 & 0 \\ 0 & 0 & 0 & 0 & 0 & 0 & 0 & 0 & 0 \\ 0 & 0 & 0 & 0 & 0 & 0 & 0 & 0 & 0 \end{pmatrix} \tag{7.19}$$

This system of differential equations needs the initial conditions to be prescribed

$$\{w(x,0)\} = \{w_0(x)\} \quad \{\dot{w}(x,0)\} = \{\dot{w}_0(x)\}. \tag{7.20}$$

For boundary conditions, if the essential ones are prescribed, one can use

$$\begin{aligned} \{w(0,t)\} = \{w_0(t)\}; \quad \{w(L,t)\} = \{w_L(t)\} \\ \{\dot{w}(L,t)\} = \{\dot{w}_L(t)\}; \quad \{\dot{w}(L,t)\} = \{\dot{w}_L(t)\} \end{aligned} \tag{7.21}$$

On the other hand, if the natural conditions are active, one can use

$$\begin{aligned} \{\bar{F}(0,t)\} = \{\bar{F}_0(t)\}; \quad \{\bar{T}(0,t)\} = \{\bar{T}_0(t)\} \\ \{\bar{F}(L,t)\} = \{\bar{F}_L(t)\}; \quad \{\bar{T}(L,t)\} = \{\bar{T}_L(t)\}. \end{aligned} \tag{7.22}$$

7.1.5 Model for this work

As already mentioned, wind turbines are columns which must resist to axial distributed (its own weight, for instance) and concentrated loads (it holds the mass of the nacelle and blades), in conjunction with loads transversally applied to its longitudinal axis resultant of the movement of the blades, action of the wind, and, in case of offshore turbines, sea waves, currents and tides. The Figure 7.4 represents a situation of using a wind turbine which is installed on the sea, whose soil has some elasticity (represented by springs), and can be partially submersed, that is, the level of the sea can reach part of the tubular structure. In this case, interaction between fluid and structure is present. The right drawing in Figure 7.4 shows scheme to model the turbine. The center of mass of the whole set, nacelle, shaft and blades is in the axis of the tower. Although conic tubes with large relations between the length and mean diameter are used in practice, in this work, the tower is a tube of constant cross section. For cases of circular cross sections, the warping is null, as well as the parameter cross product I_{yz}. Recalling the Equation 7.18, it is observed that the constitutive relation for shear stresses are already present in formulation. Nevertheless, in Euler-Bernoulli beam, no hypothesis is made with respect to shear stresses and one has to step back to equation 7.17. Differentiating the third and fourth lines with respect to x, results in

$$\begin{aligned}
&\frac{\partial}{\partial x}\left(\frac{\partial}{\partial x}\bar{T}_y\right)+\frac{\partial}{\partial x}\bar{F}_z-\frac{\partial}{\partial x}\left(\bar{F}_x\frac{\partial w_z}{\partial x}\right)+\frac{\partial}{\partial x}m_y=\frac{\partial}{\partial x}\left(\rho I_{zz}\ddot{\theta}_y\right)\\
&\frac{\partial}{\partial x}\left(\frac{\partial}{\partial x}\bar{T}_z\right)+\frac{\partial}{\partial x}\bar{F}_y+\frac{\partial}{\partial x}\left(\bar{F}_x\frac{\partial w_y}{\partial x}\right)+\frac{\partial}{\partial x}m_z=\frac{\partial}{\partial x}\left(\rho I_{yy}\ddot{\theta}_z\right).
\end{aligned} \tag{7.23}$$

Under those considerations, the system of equation given in Equations 7.23 above becomes uncoupled except for the terms $\frac{\partial}{\partial x}\left(\bar{F}_x\frac{\partial w_z}{\partial x}\right)$ and $\frac{\partial}{\partial x}\left(\bar{F}_x\frac{\partial w_y}{\partial x}\right)$. Those term are the two components resulting of the actions of the axial internal force in the two directions y and z. This terms couples the first and the last two equations. They are dependent on the axial force but affects the lateral motion of the tower by increasing its natural frequencies (and stability), if upwards, and reducing them, if downwards. In order to uncouple the equations, one assumes that the axial force that affects the lateral motion of the tower is the weight of the structure itself and any load applied axially at the top of the tower. Mathematically,

$$\bar{F}_x(x)\approx P_x(x)=-g(m_{tip}+\int_x^L\rho A(\eta)d\eta)+F_x(L,t) \tag{7.24}$$

where $F_x(L,t)$ is an arbitrary vertical concentrated load acting at point $x = L$. Finally, the set of uncoupled equations can be obtained. From Equations 7.13, it is clear that, $\bar{T}_y = -EI_{zz}\frac{\partial w_z}{\partial x}$ and $\bar{T}_z = EI_{yy}\frac{\partial w_y}{\partial x}$. Also, imposing the shear angle to be null, ($\theta_y = -\frac{\partial w_z}{\partial x}$ and $\theta_z = \frac{\partial w_y}{\partial x}$), following Euler-Bernoulli beam formulation, the second and third equations in 7.6 can be introduced in the fourth and fifth equations, also considering Equations 7.17, the system becomes

$$
\begin{aligned}
&-\frac{\partial}{\partial x}\left(EA\frac{\partial w_x}{\partial x}\right) + \rho A\ddot{w}_x = f_x \\
&-\frac{\partial}{\partial x}\left(GI_{xx}\frac{\partial \theta_x}{\partial x}\right) + \rho I_{xx}\ddot{\theta}_x = m_x \\
&-\frac{\partial}{\partial x}\left(\frac{\partial}{\partial x}EI_{zz}\frac{\partial^2 w_z}{\partial x^2}\right) - \frac{\partial}{\partial x}\left(\bar{F}_x\frac{\partial w_z}{\partial x}\right) + \frac{\partial}{\partial x}m_y + \frac{\partial}{\partial x}\left(\rho I_{zz}\frac{\partial \ddot{w}_z}{\partial x}\right) + \\
&\rho A\ddot{w}_z = f_z \\
&\frac{\partial}{\partial x}\left(\frac{\partial}{\partial x}EI_{yy}\frac{\partial^2 w_y}{\partial x^2}\right) + \frac{\partial}{\partial x}\left(\bar{F}_x\frac{\partial w_y}{\partial x}\right) + \frac{\partial}{\partial x}m_z - \frac{\partial}{\partial x}\left(\rho I_{yy}\frac{\partial \ddot{w}_y}{\partial x}\right) + \\
&\rho A\ddot{w}_y = f_y.
\end{aligned}
\tag{7.25}
$$

This means that the problem can be analyzed in four independent formulations:

- A beam/column moving only in x-y plane, submitted to bending and axial loading effect;
- A beam/column moving only in x-z plane, submitted to bending and axial loading effect;
- A bar, submitted to traction and compression;
- A shaft, submitted to torsion.

It is considered that the support is a pillar its base is permitted to rotate and move laterally as shown in Figure 7.4. Those conditions can be modeled by using translational and rotational springs at the base whose elastic constants are ka_x, kr_x, ka_y, kr_y, ka_z, kr_z [17] [1]. Those six springs simulates the soil characteristics as well as the specificities relative to the installation of the base (a pillar) in the ground. The tower has a mass of magnitude m_{tip} and matrix of inertia $[\mathrm{J}_{tip}]$ installed at its tip. The center of mass is at a height of h_m from the top of the beam (at $x = L$). The tower is submitted to wind and water loads.

If the tower is immersed in a fluid, in this case,water, the generalized Morison equation [13] can be used to model the force (per unity of length) acting at the lateral of the tower during the relative transversal movement

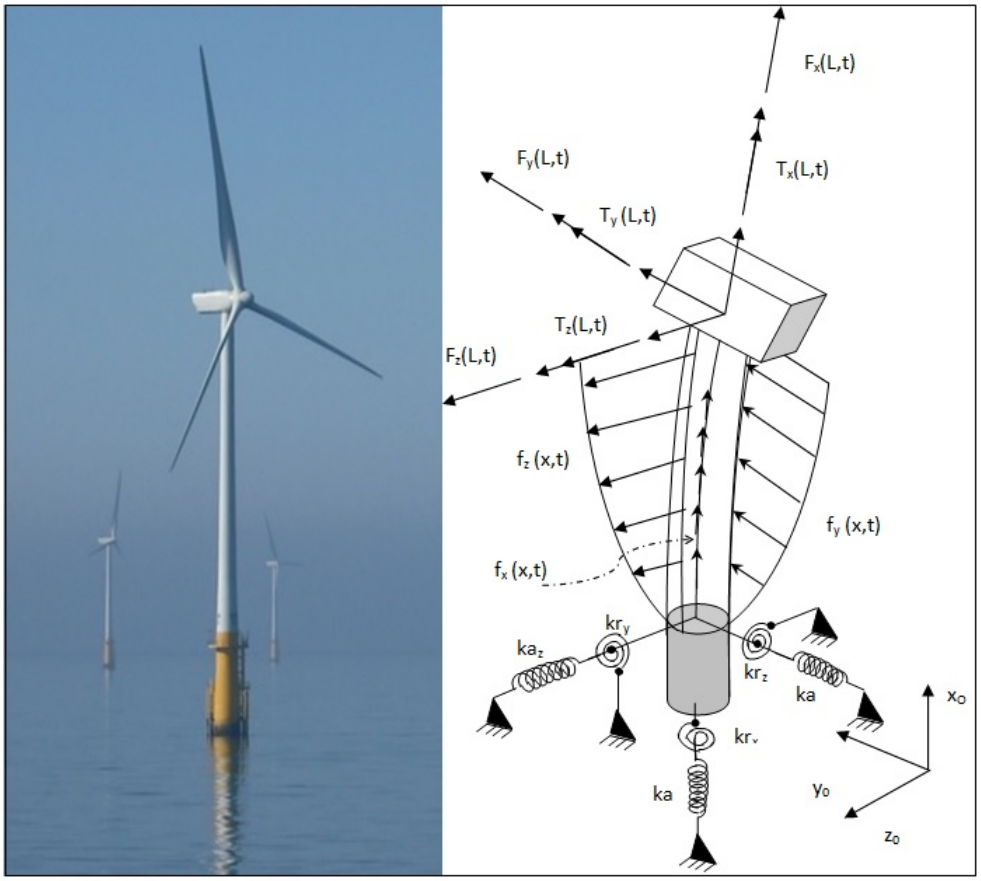

Figure 7.4: Wind tower and its model

between the tower itself and the fluid. It must be said that the present model does not include other more complex effects like von Karman vortexes nor the perturbation in the flow caused when the blades pass in front of the tower. This can be made for wind and water but it can be said that the effects due to the water is much more important. Considering an infinitesimal slice of the tower at any point x immersed in a fluid, the components of the force vector per unit of length acting in the direction of the flow [13]

$$f_{f_i}(x,t) = \rho_f A_c(x) W_{f_i}(x,t) + \rho_f C_l A_c(x)(\dot{W}_{f_i}(x,t) - \ddot{w}_i(x,t)) + \frac{1}{2}\rho_f D(x) C_D(x) \left|\dot{W}_{f_i}(x,t) - \dot{w}_i(x,t)\right| (\dot{W}_{f_i}(x,t) - \dot{w}_i(x,t)). \tag{7.26}$$

where the index i means any transversal displacement in y or z directions. W_{f_i} is the speed of the fluid transversally to the axis of the cylinder. This distributed load can only affect the lateral movement of the tower, so that its component x direction is null. So, concerning to beam formulation, one recall the Equation 7.25.

Combining them with with Equation 7.26, one obtains, for plane xy

$$
\begin{aligned}
&-\frac{\partial^2}{\partial x^2}\left(EI_{zz}\frac{\partial^2}{\partial x^2}w_y\right)-\frac{\partial}{\partial x}(P_x\frac{\partial}{\partial x}w_y)+\frac{\partial}{\partial x}\left(\rho I_{zz}\frac{\partial}{\partial x}\ddot{w}_y\right)+\\
&(\rho A+C_l\rho_f A_c)\ddot{w}_y+sign\left(W_{f_y}-\dot{w}_y\right)\left(\rho_f D(x)C_D(x)W_{f_y}\dot{w}_y\right)-\\
&sign\left(W_{f_y}-\dot{w}_y\right)\left(\frac{1}{2}\rho_f DC_D\dot{w}_y^2\right)+\frac{\partial}{\partial x}m_z=f_{o_y}+\\
&(1+C_l)\rho_f A_c(x)W_{f_y}+sign\left(W_{f_y}-\dot{w}_y\right)\left(\frac{1}{2}C_lDW_{f_y}^2\right)+\rho C_lA\dot{W}_{f_y}
\end{aligned}
\tag{7.27}
$$

and, for plane xz direction,

$$
\begin{aligned}
&\frac{\partial^2}{\partial x^2}(EI_{yy}\frac{\partial^2}{\partial x^2}w_z)+\frac{\partial}{\partial x}(P_x\frac{\partial}{\partial x}w_z)-\frac{\partial}{\partial x}(\rho I_{yy}\frac{\partial}{\partial x}\ddot{w}_z)+\\
&(\rho A+C_l\rho_f A_c)\ddot{w}_z+sign\left(W_{f_z}-\dot{w}_z\right)\left(\rho_f DC_DW_{f_z}\dot{w}_z\right)-\\
&sign\left(W_{f_z}-\dot{w}_z\right)\left(\frac{1}{2}\rho_f DC_D\dot{w}_z^2\right)+\frac{\partial}{\partial x}m_y=f_{o_z}+\\
&(1+C_l)\rho_f A_cW_{f_z}+sign\left(W_{f_z}-\dot{w}_z\right)\left(\frac{1}{2}C_lDW_{f_z}^2\right)+\rho C_lA\dot{W}_{f_z}.
\end{aligned}
\tag{7.28}
$$

In the Equations (7.26), $C_l = 1$ and C_D is the drag coefficient and D the diameter for a section of a cylinder. Consider that $f_i(x,t) = f_{f_i}(x,t)+f_{o_i}(x,t)$, $i = y, z$, and that $f_{o_i}(x,t)$ represents other distributed forces acting in the tower.

The Equations 7.27 and 7.28 are nonlinear in $\dot{w}$. In the case studied here, the tower is immersed in water from the bottom to some specific height, say $x = h_w,\ 0 \leq h_w \leq L^*$, where L^* is an admissible length, as it must be kept a safe distance between the surface of the fluid and the tip of the blades. The rest of the tower interacts with the air. As the presence of the fluid causes an apparent increasing of mass when transversal accelerations are present, the tower behaves as if it was made of two different materials with different densities. So, two differential equations must be obtained for each interval of the domain and for each longitudinal plane (xy and xz), concerning to transversal movement, what is quite easy when using finite element discretization. Next an analysis of the boundary conditions will be performed.

Boundary and initial conditions

Concerning to the boundary conditions at the base of the tower ($x = 0$) there are two possibilities: Springs are not active and the column is fixed into the ground. It is equivalent to set the spring constants to infinity. In this case, for the essential boundary conditions, both the vector displacement of the neutral line and the angular component associated to the torsion are null. Then,

$$\{w(0,t)\} = \{0\} \qquad \text{and} \qquad \theta_x(0,t) = 0. \tag{7.29}$$

On the other hand, if the springs are active, no essential boundary conditions is imposed so that the natural ones show up. Considering the Figures 7.1.5 to 7.1.5, the forces and torques at $x = 0$ and $x = L$ can be determined.

Boundary conditions for $(x = 0)$

$$\{\bar{F}(0,t)\} = \begin{pmatrix} ka_x & 0 & 0 \\ 0 & ka_y & 0 \\ 0 & 0 & ka_z \end{pmatrix} \begin{pmatrix} w_x(0,t) \\ w_y(0,t) \\ w_z(0,t) \end{pmatrix} \tag{7.30}$$

$$\{\bar{T}(0,t)\} = \begin{pmatrix} kr_x & 0 & 0 \\ 0 & 0 & -kr_y \\ 0 & kr_z & 0 \end{pmatrix} \begin{pmatrix} \theta_x(0,t) \\ \frac{\partial w_y(0,t)}{\partial x} \\ \frac{\partial w_z(0,t)}{\partial x} \end{pmatrix} \tag{7.31}$$

Boundary conditions for $(x = L)$

$$\{\bar{F}(L,t)\} = -m_{tip} \begin{pmatrix} \ddot{w}_x(L,t) \\ \ddot{w}_y(L,t) \\ \ddot{w}_z(L,t) \end{pmatrix} + \{F(L,t)\} \tag{7.32}$$

$$\{\bar{T}(L,t)\} = - \begin{pmatrix} J_{xx} & 0 & 0 \\ 0 & & J_{yy} \\ 0 & J_{zz} & 0 \end{pmatrix} \begin{pmatrix} \ddot{\theta}_x \\ \frac{\partial \ddot{w}_y(L,t)}{\partial x} \\ \frac{\partial \ddot{w}_z(L,t)}{\partial x} \end{pmatrix} + \{T(L,t)\} \tag{7.33}$$

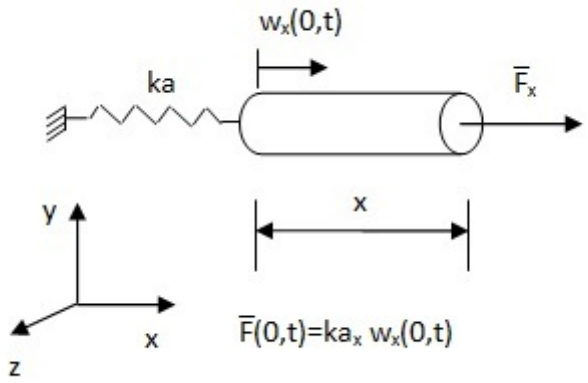

7.5(a): Bar model $(x = 0)$

Using the Equations 7.17 and the conditions given from Equation 7.30 to Equations 7.33.

Bar formulation

For $x = 0$,

$$AE\frac{\partial}{\partial x} w_x(0,t) = ka_x w_x(0,t) \tag{7.34}$$

For $x = L$,

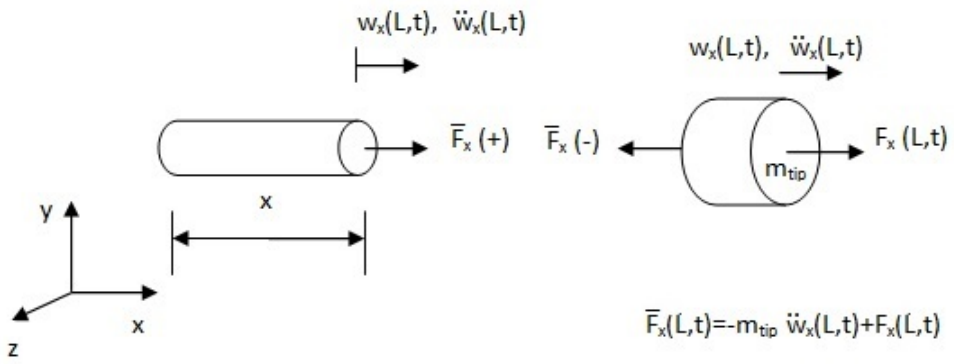

7.5(b): Bar model ($x = L$)

$$AE\frac{\partial w_x(0,t)}{\partial x} = -m_{tip}\ddot{w}_z(L,t) + F_x(L,t) \tag{7.35}$$

Beam formulation Considering that

$$T_y = -EI_{zz}\frac{\partial^2 w_z(x,t)}{\partial x^2} \tag{7.36}$$

and

$$T_z = EI_{yy}\frac{\partial^2 w_y(x,t)}{\partial x^2} \tag{7.37}$$

At $x = 0$,

$$\bar{F}_y(0,t) = -\frac{\partial}{\partial x}\left(EI_{zz}\frac{\partial^2 w_y(0,t)}{\partial x^2}\right) - m_z(0,t) - P(L)\frac{\partial w_y(L,t)}{\partial x} + \rho I_{zz}\frac{\partial \ddot{w}_y}{\partial x}(0,t) = ka_y w_y(0,t) \tag{7.38}$$

$$\bar{F}_z(0,t) = -\frac{\partial}{\partial x}\left(EI_{yy}\frac{\partial^2}{\partial x^2}w_z(0,t)\right) + m_y(0,t) - P(L)\frac{\partial w_z(0,t)}{\partial x} - \rho_t I_{yy}\ddot{w}_z(0,t) = ka_z\frac{\partial}{\partial x}w_z(0,t) \tag{7.39}$$

$$\bar{T}_y(0,t) = -EI_{zz}(x)\frac{\partial^2}{\partial x^2}w_z(0,t) = -kr_y\frac{\partial}{\partial x}w_z(0,t) \tag{7.40}$$

$$\bar{T}_z(0,t) = EI_{yy}(x)\frac{\partial^2}{\partial x^2}w_y(0,t) = kr_z\frac{\partial}{\partial x}w_y(0,t) \tag{7.41}$$

At $x = L$,

$$\bar{F}_y(L,t) = -\frac{\partial}{\partial x}\left(EI_{zz}\frac{\partial^2}{\partial x^2}w_y(L,t)\right) - m_z(L,t) - P_x(L)\frac{\partial w_y(L,t)}{\partial x} + \rho I_{zz}\ddot{w}_y(L,t) = -m_{tip}\ddot{w}_y(L,t) + F_y(L,t) \tag{7.42}$$

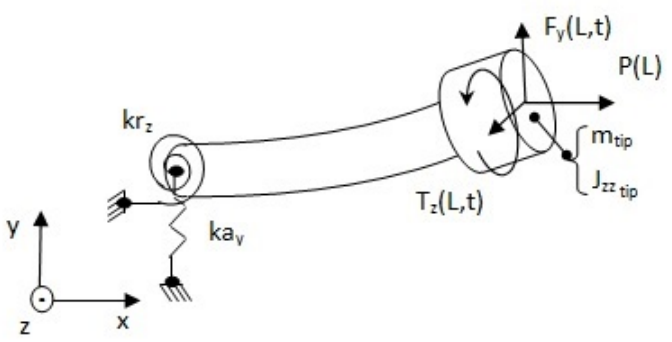

7.5(c): Beam model

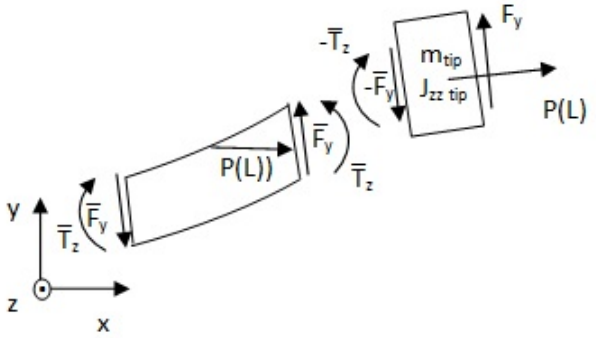

7.5(d): **Forces and torques**

Figure 7.5: Beam - Boundary conditions in plane xy

$$\bar{F}_z(L,t) = -\frac{\partial}{\partial x}\left(EI_{yy}\frac{\partial^2}{\partial x^2}w_z(L,t)\right) + m_z(L,t) - P_x(L)\frac{\partial w_z(L,t)}{\partial x} + \rho I_{yy}\ddot{w}_y(L,t) = -m_{tip}w_z(L,t) + F_z(L,t) \tag{7.43}$$

$$\bar{T}_y(L,t) = -EI_{yy}\frac{\partial^2}{\partial x^2}\left(w_z(L,t)\right) = -J_{yy}\frac{\partial}{\partial}\ddot{w}_z(L,t) + T_y(L,t) \tag{7.44}$$

$$\bar{T}_z(L,t) = EI_{zz}\frac{\partial^2}{\partial x^2}\left(w_y(L,t)\right) = -J_{zz}\frac{\partial\ddot{w}_y(L,t)}{\partial} + T_z(L,t) \tag{7.45}$$

Shaft formulation

At $x = 0$,

$$\bar{T}_x(0,t) = GI_{xx}\frac{\partial\theta(0,t)}{\partial x} = kr_x\theta_x(0,L) \tag{7.46}$$

For $x = L$,

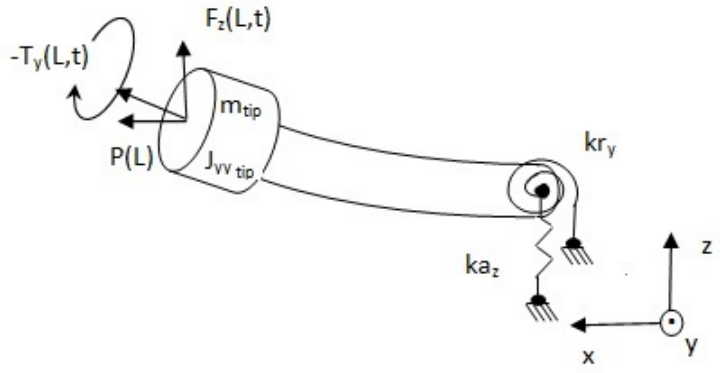

7.6(a): Beam model

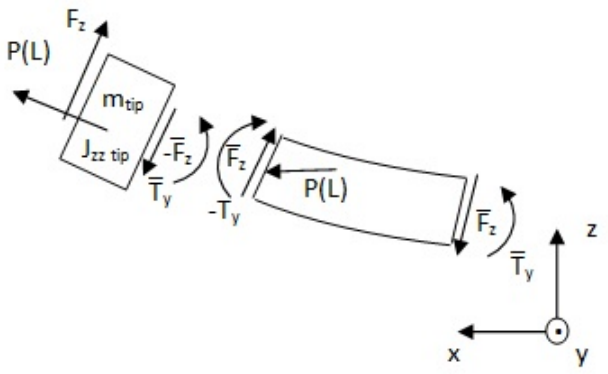

7.6(b): Forces and torques

Figure 7.6: Beam - Boundary conditions in plane xz

$$\bar{T_x}(L,t) = GI_{xx}\frac{\partial\theta(L,t)}{\partial x} = J_{xx}\ddot{\theta}_x(L,t) - T_x(L,t) \tag{7.47}$$

As initial conditions one has $\{w(x,0)\} = \{w_0\}$ and $\{\dot{w}(x,0)\} = \{\dot{w}_0\}$ and $\{\theta(x,0)\} = \{\theta_0\}$ and $\{\dot{\theta}(x,0)\} = \{\dot{\theta}_0\}$.

7.2 Kinematics of a rigid body

To describe a rigid body motion, it is necessary, first, to establish an inertial coordinate system (or an inertial frame) and then to chose a point of the body and make it the origin of another coordinate system (the body frame). If one makes this frame attached to the body, all coordinates of the points of the body, with respect to the body frame, remain the same throughout its motion. Two important theorems helped to understand the dynamic of rigid bodies. In the first, Euler proved that the motion of any rigid body (or of its frame) with a fixed point (with respect to the inertial frame) is a rotation about an axis

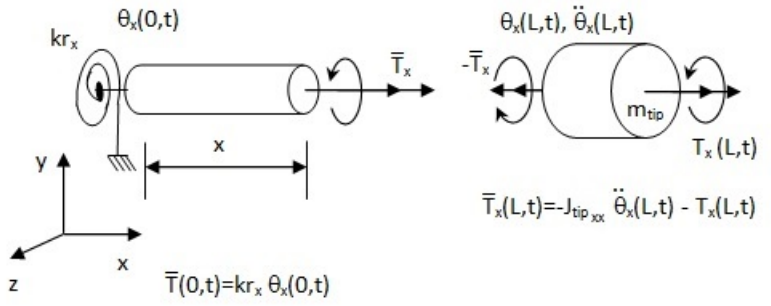

7.7(a): Shaft model

that passes trough this point. Later, Chasles demonstrated that the general motion of a body frame can be separated into two independent movements: a translation of the origin and a rotation about an axis whose direction is fixed with respect to a inertial frame.

Suppose two frames, (x_b y_b z_b), attached to the body and other, inertial, (x_0 y_0 z_0), fixed elsewhere. $\{\bar{r}_{b_B}\}$ is the representation of a vector indicating the position of a point B of the body with respect to the body frame (index "b") and measured relatively to it (indicated as a bar). If this vector initially coincides with the spatial point $P0$, after the movement, the point B goes to a new position in space, P. Then, its representation in the inertial coordinate system will be

$$\{r_{b_P}\} = \{R_b\} + [A_b]\{\bar{r}_{b_B}\} \tag{7.48}$$

where $\{r_P\}$ is the vector of final position represented with respect to the inertial frame, $\{R_b\}$ is the position of the origin of the body frame, represented with respect the inertial frame and $[A_b]$ is the rotation or transformation matrix. If one considers that this is valid for any point of the body, both indexes, "B" and "P", can be suppressed and the expression in Equation 7.48 can be re-written as

$$\{r_b\} = \{R_b\} + [A_b]\{\bar{r}_b\} \tag{7.49}$$

where $\{r_b\}$ and $\{\bar{r}_b\}$ are vectors indicating the position of any point of the body "b" relative to the inertial frame. $\{\bar{r}_b\}$ is relative also represented with respect to the body frame. There are some possible ways to define that matrix [60]. This means that there are also some possibilities to describe the attitude of the body in space. It may be done using Euler angles, Euler parameters, Rodrigues parameters or direction cosines. Taking in consideration Chasles theorem, one can separate the translation from rotations, and, just for sake of simplicity, forget for a wile about the former and concentrate in the latter.

Euler theorem says that a body goes from an attitude to another just by rotating about an axis whose direction is given by the unity vector $\{v_b\}$, fixed in relation to the inertial frame $(x_0 \;\; y_0 \;\; z_0)$. The angle of rotations is ϑ_b as shown in Figure 7.7. It can be demonstrated [60] that the position vector the new position of the vector $\{\bar{r}_b\}$ after rotation, is given by

$$\{\breve{r}_b\} = \left([I] + [\tilde{v}_b]sin(\vartheta_b) + 2[\tilde{v}_b]^2 sin^2(\frac{\vartheta_b}{2})\right)\{\bar{r}_b\}. \tag{7.50}$$

In Equation 7.50, $\{\bar{r}_b\}$ is measured relatively to the body system origin but written with respect to the inertial frame. In this transformation, four dependent parameters are involved: three components of the unity vector about which the body rotates and the angle of rotation. The dependency among those parameters is due to the fact that the three coordinates of the vector $\{v_b\}$ are dependent. From Equation 7.50 it is clear that

$$[A_b] = [I] + [\tilde{v}_b]sin(\vartheta_b) + 2[\tilde{v}_b]^2 sin^2(\frac{\vartheta_b}{2}). \tag{7.51}$$

The Euler parameters are

$$\Theta_{0_b} = cos(\frac{\vartheta_b}{2}); \quad \Theta_{1_b} = v_{1_b} sin(\frac{\vartheta_b}{2}); \quad \Theta_{2_b} = v_{2_b} sin(\frac{\vartheta_b}{2}); \quad \text{and} \quad \Theta_{3_b} = v_{3_b} sin(\frac{\vartheta_b}{2}). \tag{7.52}$$

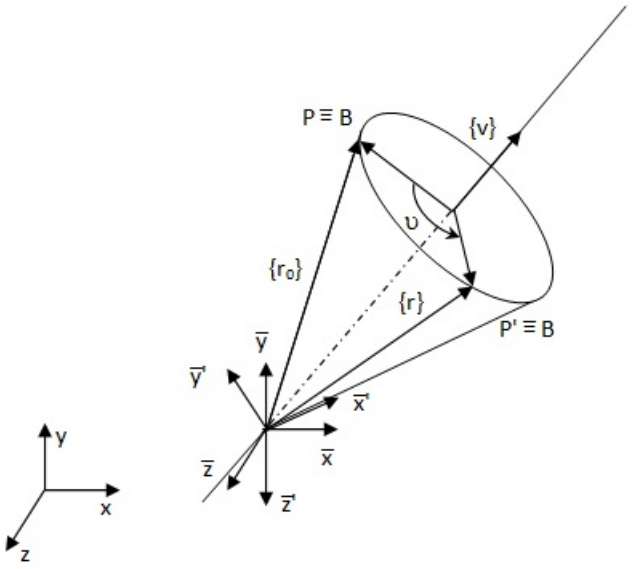

Figure 7.7: Rotation of a rigid body

The matrix $[A_b]$, in terms of Euler parameters is

$$[A_b] = \begin{pmatrix} 1 - 2\Theta_{2_b}^2 - 2\Theta_{3_b}^2 & 2(\Theta_{1_b}\Theta_{2_b} - \Theta_{0_b}\Theta_{3_b}) & 2(\Theta_{1_b}\Theta_{3_b} + \Theta_{0_b}\Theta_{2_b}) \\ 2(\Theta_{1_b}\Theta_{2_b} + \Theta_{0_b}\Theta_{3_b}) & 1 - 2\Theta_{1_b}^2 - \Theta_{3_b}^2 & 2(\Theta_{2_b}\Theta_{3_b} - \Theta_{0_b}\Theta_{1_b}) \\ 2(\Theta_{1_b}\Theta_{3_b} - \Theta_{0_b}\Theta_{2_b}) & 2(\Theta_{2_b}\Theta_{3_b} + \Theta_{0_b}\Theta_{1_b}) & 1 - 2\Theta_{1_b}^2 - \Theta_{2_b}^2 \end{pmatrix}. \tag{7.53}$$

The matrix transformation $[A_b]$ also can be written as a product of two matrices.

$$[A_b] = [E_b][\bar{E}_b]^T \tag{7.54}$$

where,

$$[E_b] = \begin{pmatrix} -\Theta_{1_b} & \Theta_{0_b} & -\Theta_{3_b} & \Theta_{2_b} \\ -\Theta_{2_b} & \Theta_{3_b} & \Theta_{0_b} & -\Theta_{1_b} \\ -\Theta_{3_b} & -\Theta_{2_b} & \Theta_{1_b} & \Theta_{0_b} \end{pmatrix}, [\bar{E}_b] = \begin{pmatrix} -\Theta_{1_b} & \Theta_{0_b} & \Theta_{3_b} & -\Theta_{2_b} \\ -\Theta_{2_b} & -\Theta_{3_b} & \Theta_{0_b} & \Theta_{1_b} \\ -\Theta_{3_b} & \Theta_{2_b} & -\Theta_{1_b} & \Theta_{0_b} \end{pmatrix}.$$

The matrices E_b and $\bar{E}_b$ are used to obtain the angular velocity as follows

$$[G_b] = 2[E_b] \qquad \text{and} \qquad [\bar{G}_b] = 2[\bar{E}_b]. \tag{7.55}$$

so that

$$\begin{aligned} \{\Omega\} &= [G_b]\{\dot{\Theta}\} \qquad \text{and} \qquad \{\bar{\Omega}\} = [\bar{G}_b]\{\dot{\Theta}_b\} \\ \{\dot{\Omega}\} &= [G_b][\ddot{\Theta}_b] \qquad \text{and} \qquad \{\dot{\bar{\Omega}}_b\} = [\bar{G}_b][\ddot{\Theta}_b] \end{aligned} \tag{7.56}$$

where $\{\Omega_b\}$, $\{\bar{\Omega}_b\}$ are the representation of the angular velocity of the body with respect to the inertial and body frames, respectively. In the same way, $\{\dot{\Omega}_b\}$ and $\{\dot{\bar{\Omega}}_b\}$ representation of the angular acceleration of the body with respect to the inertial and body frames, respectively.

The derivative of the matrix $[A_b]$ with respect to the Euler parameters are

$$\frac{\partial[A_b]}{\partial\Theta_{0_b}} = \begin{bmatrix} 0 & -2\Theta_{3_b} & 2\Theta_{2_b} \\ 2\Theta_{3_b} & 0 & -2\Theta_{1_b} \\ -2\Theta_{2_b} & 2\Theta_{1_b} & 0 \end{bmatrix} \qquad \frac{\partial[A_b]}{\partial\Theta_{2_b}} = \begin{bmatrix} 0 & 2\Theta_{2_b} & 2\Theta_{3_b} \\ 2\Theta_{2_b} & -4\Theta_{1_b} & -2\Theta_{1_b} \\ 2\Theta^j_{3_b} & 2\Theta_{0_b} & -4\Theta_{1_b} \end{bmatrix} \tag{7.57}$$

$$\frac{\partial[A_b]}{\partial\Theta_{2_b}} = \begin{bmatrix} -4\Theta_{2_b} & 2\Theta_{1_b} & 2\Theta_{1_b} \\ 2\Theta_{1_b} & 0 & 2\Theta_{3_b} \\ -2\Theta_{1_b} & 2\Theta_{2_b} & -4\Theta_{2_b} \end{bmatrix} \qquad \frac{\partial[A_b]}{\partial\Theta_{4_b}} = \begin{bmatrix} -4\Theta_{3_b} & -2\Theta_{0_b} & 2\Theta_{1_b} \\ 2\Theta_{0_b} & -4\Theta_{3_b} & 2\Theta_{2_b} \\ 2\Theta_{1_b} & 2\Theta_{2_b} & 0 \end{bmatrix}$$

The second derivative of the matrix A with respect to the generalized coordinates is constant matrix as well as the first derivatives of $[G_b]$ and $[\bar{G}_b]$. This information will be used when calculating the derivatives of the residue in step by step formulation. It is easily obtained from Equations 7.55 and 7.58.

The derivative of the matrix A_b with respect to time is

$$[\dot{A}_b]\{\bar{r}_b\} = [B_b]\{\dot{\Theta}_b\}, \tag{7.58}$$

where,

$$B_{b_{ik}} = \frac{\partial(A_{b_{ij}}\bar{r}_{b_j})}{\partial\Theta_b^k}, \tag{7.59}$$

that is, the differentiation of the product $[A_b]\{\bar{r}_b\}$ with respect to the generalized coordinates. Operationally, the scheme to obtain the matrix $B_{b_{ik}}$ is as follows:

$$[B] = \left[\left\{\left[\frac{\partial[A_b]}{\partial\Theta_{1_b}}\right]\{\bar{r}_b\}\right\}\left\{\left[\frac{\partial[A_b]}{\partial\Theta_{2_b}}\right]\{\bar{r}_b\}\right\}\left\{\left[\frac{\partial[A_b]}{\partial\Theta_{3_b}}\right]\{\bar{r}_b\}\right\}\left\{\left[\frac{\partial[A_b]}{\partial\Theta_{4_b}}\right]\{\bar{r}_b\}\right\}\right]. \tag{7.60}$$

In the approximation of the solution in a multi-body formulation, a step by step algorithm is used. In order to formulate the tangent matrix, it will be necessary to determine the derivatives of $[B_b]\{\dot{\Theta}_b\}$ and $[B_b]\{\ddot{\Theta}_b\}$. Multiplying both sides of the Equation 7.59 the vector $\{\dot{\Theta}_{b_k}\}$ and differentiating with respect to Θ_{b_m}, one obtains

$$\frac{\partial(B_{ik}\dot{\Theta}_{b_k\,k})}{\partial\Theta_{b_m}} = \frac{\partial^2(A_{b_{ij}}\bar{r}_j)}{\partial\Theta_{b_k}\partial\Theta_{b_m}}\dot{\Theta}_{b_k}. \tag{7.61}$$

In the same way;

$$\frac{\partial(B_{ik}\ddot{\Theta}_{b_k})}{\partial\Theta_{b_m}} = \frac{\partial^2(A_{b_{ij}}\bar{r}_{b_j})}{\partial\Theta_{b_k}\partial\Theta_{b_m}}\ddot{\Theta}_{b_k}. \tag{7.62}$$

7.3 Kinematics of a flexible body

If deformations are present when the body moves, than, Equation 7.49 changes to

$$\{r_b\} = \{R_b\} + [A_b]\{\bar{\bar{r}}_b\} \tag{7.63}$$

where now, the vector $\{\bar{\bar{r}}_b\}$ is composed by two parts, one relative to rotation of rigid body and other relative to the deformation, as shown in Figure 7.8

Then

$$\{\bar{\bar{r}}_b\} = \{\bar{r}_b\} + \{\bar{u}_b\} \tag{7.64}$$

were $\{\bar{u}_b\} = [\bar{H}_b(x_b, y_b, z_b)]\{\bar{U}_b\}$ is the a function representing the displacements of the body. The matrix $[\bar{H}_b(x_b, y_b, z_b)]$ is the shape matrix and it is dependent on the on the hypothesis of the body deformation. $\{\bar{U}_b\}$ is the time-dependent elastic generalized coordinates. The final coordinates of the body is, in the deformed state,

$$\{r_b\} = \{R_b\} + [A_b]\{\bar{r}_b\} + [A_b][\bar{H}_b]\{\bar{U}_b\}. \tag{7.65}$$

Velocity is obtained by differentiating the Equation 7.65 with respect to time, results in

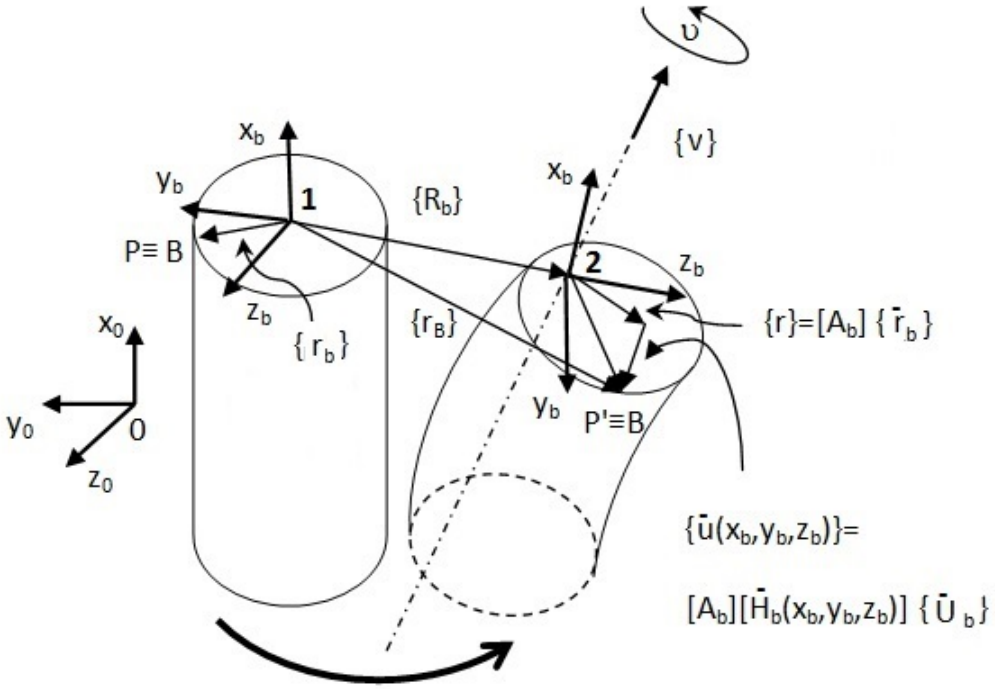

Figure 7.8: Rotation of a flexible body

$$\{\dot{r}_b\} = \{\dot{R}_b\} + [\dot{A}_b]\{\bar{r}_b\} + [A_b][\bar{H}_b]\{\dot{\bar{U}}_b\} \tag{7.66}$$

since $\{\dot{\bar{r}}_b\} = \{0\}$. Operating in the second term of the right side of Equation 7.66 it is possible to obtain the following relation

$$[\dot{A}_b]\{\bar{r}_b\} = [B_b]\{\dot{\Theta}_b\}. \tag{7.67}$$

The matrix $[B_b]$ is a matrix whose columns are formed by the products of the matrices resultant from the derivatives of the matrix $[A_b]$ with respect to each Euler parameter Θ_{b_i} multiplied by the vector $\{\bar{r}_b\}$. Then, the Equation 7.66 becomes

$$\{\dot{r}_b\} = \{\dot{R}_b\} + [B_b]\{\dot{\Theta}_b\} + [A_b][\bar{H}_b]\{\dot{\bar{U}}_b\} \tag{7.68}$$

The Equation 7.68 can be rewritten in the following way

$$\dot{r}_b = \begin{bmatrix}[I] & [B_b] & [A_b][\bar{H}_b]\end{bmatrix}\left[\{\dot{R}_b\}^T\ \{\dot{\Theta}_b\}^T\ \{\dot{\bar{U}}_b\}^T\right]^T, \tag{7.69}$$

or

$$\{\dot{r}_b\} = [L_b]\{\dot{q}_b\}. \tag{7.70}$$

In the same way, differentiating the vector $\{\dot{r}_b\}$ with respect to time again,

$$\{\ddot{r}_b\} = [L_b]\{\ddot{q}_b\} + \{\dot{L}_b\}\{\dot{q}_b\} \tag{7.71}$$

and the matrix $\{\dot{L}_b\}$ is

$$\{\dot{L}_b\} = \left[[0] \quad [\breve{L}_b] \quad [\breve{B}_b]\{\dot{\Theta}_b\}\right] \tag{7.72}$$

where, [0] is the 3×3 identity matrix. The matrix $[\breve{B}_b]$ is built so that each column is the product of the matrix resultant from the derivatives of the matrix $[A_b]$ with respect to each Euler parameter Θ_{b_i} multiplied by the vector $[\bar{H}_b]\{\dot{\bar{U}}_b\}$. The vector $\{\breve{L}_b\}$ is calculated as

$$\breve{L}_{b_i} = \frac{\partial}{\partial\Theta_{b_m}}\frac{\partial}{\partial\Theta_{b_k}} A_{b_{ij_b}} \bar{r}_{b_j} \dot{\Theta}_{b_m} \dot{\Theta}_{b_k}. \tag{7.73}$$

In previous equations, $\{R_b\}$, $\{\Theta_b\}$ and $\{\bar{U}_b\}$ are the generalized coordinates associated to the body b, for translation, rotation and deformation, respectively. For flexible bodies,

$$\{q_b\} = \begin{Bmatrix} \{R_b\} \\ \{\Theta_b\} \\ \{\bar{U}_b\} \end{Bmatrix}. \tag{7.74}$$

If the body is considered rigid, the generalized coordinates relative to the body b are

$$\{q_b\} = \begin{Bmatrix} \{R_b\} \\ \{\Theta_b\} \end{Bmatrix}. \tag{7.75}$$

7.4 Virtual work and generalized forces

Newton's second law says that the resultant of the forces acting on a particle i is equal to the rate of variation of its linear momentum, that is

$$\{F\}^i = m^i\{\dot{r}^i\} \tag{7.76}$$

or

$$\{F\}^i - m^i\{\dot{r}^i\} = 0. \tag{7.77}$$

where $\{F\}^i$ is the resultant force acting at the body which is composed by external forces $\{F_e\}^i$ and that forces due to the restriction of its motion (constraints), $\{F_c\}^i$. $\{\dot{r}^i\}$ and m^i are the velocity vector and mass of any particle i. Then,

$$\{F_e\}^i + \{F_c\}^i - m^i\{\dot{r}^i\} = 0. \tag{7.78}$$

Multiplying the Equation 7.78 by a vector of virtual displacements $\delta\{r\}^i$ one obtains

$$(\{F_e\}^i + \{F_c\}^i - m^i\{\dot{r}^i\})\delta\{r\}^i = 0. \tag{7.79}$$

For all particles,

$$\sum_{i=1}^{n_p}(\{F_e\}^i + \{F_c\}^i - m^i\{\dot{r}^i\}).\delta\{r\}^i = 0 \tag{7.80}$$

Developing, the equation 7.80,

$$\sum_{j=1}^{n}\sum_{i=1}^{n_p}(\{F_e\}^i + \{F_c\}^i - m^i\{\dot{r}^i\}).\frac{\partial\{r\}^i}{\partial q_j}\delta q_j = 0. \tag{7.81}$$

If the motion of the particle is constrained (for instance, they movement must be over a surface or line), only certain admissible virtual displacements are possible and they must be parallel to the constraint and the reaction must be perpendicular to it. In this case, the product $\{F_c\}^i.\frac{\partial\{r\}^i}{\partial q_j}\delta q_j = 0$. Then,

$$\sum_{i=1}^{n_p}(\{F_e\}^i - \{m^i\{\dot{r}^i\}).\frac{\partial\{r\}^i}{\partial q_j}\delta q_j = 0, \tag{7.82}$$

which is the d'Alembert principle for a particle i. The Equation 7.82 can be put in the form

$$\delta W_e + \delta W_i = \sum_{i=1}^{n_p}\{F_e\}^i.\frac{\partial\{r\}^i}{\partial q_j}\delta q_j - \sum_{i=1}^{n} m^i\{\dot{r}^i\}.\frac{\partial\{r\}^i}{\partial q_j}\delta q_j = Q_e^i\delta q_j - Q_i^i\delta q_j \tag{7.83}$$

where, Q_e^i and Q_i^i are defined as the virtual external forces and virtual inertial forces, respectively, associated to the virtual displacement δq_j.

7.5 Lagrangian equation

7.5.1 Unconstrained motion

If the position $\{r\}$ of a particle i is described by a set of generalized coordinates, q_j, $j = 1, 2, \cdots n$, and also by the time, that is,

$$\{r\}^i = \{r(q_1, q_2, \cdots, q_n, t)\}^i, \tag{7.84}$$

then, if one differentiate it with respect to time, it gives

$$\{\dot{r}\}^i = \sum_{j=1}^{n}\frac{\partial\{r\}^i}{\partial q_j}\dot{q}_j + \frac{\partial\{r\}^i}{\partial t} \tag{7.85}$$

and then, differentiating with respect to q_k it is obtained

$$\frac{d}{dt}(\frac{\partial\{r\}^i}{\partial q_k}) = \sum_{k=1}^{n}\frac{\partial^2\{r\}^i}{\partial q_j q_k}\dot{q}_k + \frac{\partial^2\{r\}^i}{\partial q_j \partial t} = \frac{\partial\{\dot{r}\}^i}{\partial q_j}. \tag{7.86}$$

The increment of virtual work associated to the inertia forces for all particles is

$$\delta W_i = \sum_{i=1}^{n_p}\sum_{j=1}^{n} m^i\{\ddot{r}\}^i \cdot \frac{\partial\{r\}^i}{\partial q_j}\delta q_j \tag{7.87}$$

Changing the order of the summation, the equation 7.87 can be re-written as

$$\delta W_i = \sum_{j=1}^{n} \left(\sum_{i=1}^{n_p} (m\{\ddot{r}\})^i \cdot \frac{\partial \{r\}^i}{\partial q_j} \right) \delta q_j \tag{7.88}$$

The following equality can be obtained:

$$\sum_{i=1}^{n_p} \frac{d}{dt} \left(m^i \{\dot{r}\}^i \cdot \frac{\partial \{r\}^i}{\partial q_j} \right) = \left(\sum_{i=1}^{n_p} m^i \{\ddot{r}\}^i \cdot \frac{\partial \{r\}^i}{\partial q_j} \right) + \sum_{i=1}^{n_p} m^i \{\dot{r}\}^i \cdot \frac{d}{dt} \left(\frac{\partial \{r\}^i}{\partial q_j} \right), \tag{7.89}$$

which can be put in the form

$$\sum_{i=1}^{n_p} m^i \{\ddot{r}\}^i \cdot \frac{\partial \{r\}^i}{\partial q_j} = \sum_{i=1}^{n_p} \frac{d}{dt} \left(m^i \{\dot{r}\}^i \cdot \frac{\partial \{r\}^i}{\partial q_j} \right) - \sum_{i=1}^{n_p} m^i \{\dot{r}\}^i \cdot \frac{d}{dt} \left(\frac{\partial \{r\}^i}{\partial q_j} \right). \tag{7.90}$$

Substituting the right side of Equation 7.90 knowing that $\frac{\partial \{\dot{r}\}^i}{\partial \dot{q}_j} = \frac{\partial \{r\}^i}{\partial q_j}$, it follows that

$$\begin{aligned} &\sum_{i=1}^{n_p} m^i \{\ddot{r}\}^i \cdot \frac{\partial \{r\}^i}{\partial q_j} = \\ &\sum_{i=1}^{n_p} \left\{ \frac{d}{dt} \left[\frac{\partial}{\partial \dot{q}_j} \left(\frac{1}{2} m^i \{\dot{r}\}^{i^T} \cdot \{\dot{r}\} \right) \right] - \frac{\partial}{\partial q_j} \left(\frac{1}{2} m^i \{\dot{r}\}^{i^T} \cdot \{\dot{r}\}^i \right) \right\} \end{aligned} \tag{7.91}$$

The term $\frac{1}{2} m^i \{\dot{r}\}^{i^T} \cdot \{\dot{r}\}^i$ is the kinetic energy associated to particle i. Recalling that the total kinetic energy is $E_c = \sum_{i=1}^{n_p} E_c^i$, the equation 7.91 becomes

$$\sum_{i=1}^{n_p} m^i \{\ddot{r}\}^i \cdot \frac{\partial \{r\}^i}{\partial q_j} = \sum_{i=1}^{n_p} \left(\frac{d}{dt} \left(\frac{\partial E_c}{\partial \dot{q}_j} \right)^i - \left(\frac{\partial E_c}{\partial q_j} \right)^i \right) \tag{7.92}$$

From equation 7.83, it can be said that

$$\sum_{j=1}^{n} \left[\frac{d}{dt} \left(\frac{\partial E_c}{\partial \dot{q}_j} \right) - \left(\frac{\partial E_c}{\partial q_j} \right) - Q_{e_j} \right] \delta q_j = 0. \tag{7.93}$$

where Q_{e_j} is the generalized force associated to the generalized coordinate q_j. In case of independence of the generalized coordinates the Equation 7.93 becomes the Lagrange equation

$$\frac{d}{dt} \left(\frac{\partial E_c}{\partial \dot{q}_j} \right) - \left(\frac{\partial E_c}{\partial q_j} \right) - Q_{e_j} = 0; \qquad j = 1, 2, \cdots, n. \tag{7.94}$$

7.5.2 Constrained motion

As already mentioned before, the analysis of multi-body systems includes somehow restrictions in the bodies movements, in general due to the interactions among the bodies themselves which are connected by mechanical links as universal, prismatic or re-volute joints. These restrictions in the movement of the bodies, the kinematic constraints, are introduced in the dynamic formulation of the system by a set o non-linear algebraic constraint equations, dependent of the system generalized coordinates and also on time, that is

$$\{g(\dot{q}, q, t)\} = \{0\} \tag{7.95}$$

where $\{g(\dot{q}, q, t)\} = (g_1(\{\dot{q}\}, \{q\}, t) \;\; g_2(\{\dot{q}\}, \{q\}, t) \cdots g_{n_c}(\{\dot{q}\}, \{q\}, t))$ is a vector with n_c independent constraints. If the constraint are not dependent on $\dot{q}$ it is defined as holonomic and Equation 7.95 becomes,

$$\{g_h(q, t)\} = \{0\}. \tag{7.96}$$

If in Equation 7.96 the time appear explicitly, then, the system is said to be scleronomic, otherwise it is called reonomic. There are at least two possibilities for dealing with constraints [60]. In the simpler, used for holonomic systems, some coordinates are chosen as independent and written as functions of the others

$$\{g_{h_d}(q_d)\} = \{g_{h_i}(q_i)\} \tag{7.97}$$

where $\{q_d\}$ and $\{g_{h_i}\}$ are the dependent and independent set of coordinates. Then,

$$\{J_{h_d}\}\{\delta q_d\} = \{J_{h_i}\}\{\delta q_i\} \tag{7.98}$$

where $[gh_d] = \frac{\partial g_{h_d}}{\partial q_d}$ and $[g_{h_i}] = \frac{\partial g_{h_i}}{\partial q_i}$ are the Jacobian matrices for dependent and independent coordinates, respectively. The matrix J_{h_d} is invertible and follows that

$$\{\delta q_d\} = -[J_{h_d}]^{-1}[J_{h_i}]\{q_i\}. \tag{7.99}$$

It can be written that

$$\{\delta q\} = \begin{bmatrix} \{\delta q_i\} \\ \{\delta q_d\} \end{bmatrix} = \begin{bmatrix} [I] \\ [\bar{B}_{di}] \end{bmatrix} \{\delta q_i\}, \tag{7.100}$$

The constraints are now function of only independent coordinates. Returning to D'Alembert equation,

$$\left[\frac{d}{dt}\{\frac{\partial E_c}{\partial\{\dot{q}\}}\}^T - \{\frac{\partial E_c}{\partial\{q\}}\}^T - \{Q\}^T\right][\bar{B}_{di}] = \{0\}^T. \tag{7.101}$$

The other possibility is to use the Lagrange undetermined multipliers. It can be used in any systems but it is mandatory in non-holonomic systems

because it is not possible, in such a systems, the separation of dependent from independent generalized coordinates (they are velocity-dependent an non-integrable). For application in this work, the later method is used. First, one separates the constraints into two groups:

$$\{g(\{q\},t)\} = \{0\} \tag{7.102}$$

and

$$\{g(\{\dot{q}\},t)\} = \{0\} \tag{7.103}$$

and associate to the constraints, Lagrange multipliers $\{\lambda\} = (\lambda_1 \ \lambda_2 \ \lambda_3 \cdots \lambda_{n_c})^T$ and $\{\dot{\lambda}\} = (\dot{\lambda}_1 \ \dot{\lambda}_2 \ \dot{\lambda}_3 \cdots \dot{\lambda}_{n_c})^T$ in the following way:

$$\breve{g}_h(\{q\},\{\lambda_h\}) = \frac{1}{2}[p_h]\{g_h\}^T\{g_h\} + [k_h]\{\lambda_h\}^T\{g_h\} = 0. \tag{7.104}$$

and analogously, for non-holonomic constraints,

$$\breve{g}_{nh}(\{\dot{q}\},\{\dot{\lambda}_{nh}\}) = \frac{1}{2}[p_{nh}]\{g_{nh}\}^T\{g_{nh}\} + [k_{nh}]\{\dot{\lambda}_{nh}\}^T\{g_{nh}\} = 0. \tag{7.105}$$

where the first part of the Equations 7.104 and 7.105 are equations of penalty and $[p_h]$ and $[p_{nh}]$ are diagonal matrices containing penalty factors [21]. The second part are the application of the Lagrange multipliers and the diagonal matrices $[k_h]$ and $[k_{nh}]$ are formed by scale factors associated to each multiplier. Differentiating Equations 7.104 and 7.105 with respect to $\{q\}$ and $\{\dot{q}\}$, respectively,

$$\left\{\frac{\partial\{\bar{g}_h\}}{\partial\{q\}}\right\} = [J_h]^T(p_h\{\bar{g}_h\} + k_h\{\lambda_h\}) \tag{7.106}$$

$$\left\{\frac{\partial\{\bar{g}_{nh}\}}{\partial\{q\}}\right\} = [J_{nh}]^T(p_{nh}\{\bar{g}_{nh}\} + k_{nh}\{\dot{\lambda}_{nh}\}) \tag{7.107}$$

Combining the previous equation with Equation 7.93 results that

$$\{\delta q\}^T\left[\frac{d}{dt}\left\{\frac{\partial E_c}{\partial\{\dot{q}\}}\right\} - \left\{\frac{\partial E_c}{\partial\{q\}}\right\} - \{Q\} + \left\{\frac{\partial\bar{g}_h}{\partial\{q\}}\right\} + \left\{\frac{\partial\bar{g}_{nh}}{\partial\{\dot{q}\}}\right\}\right] = 0 \tag{7.108}$$

The components of the vector $\{\delta q\}$, that is, the generalized coordinates, are dependent. In order to overcome this limitation, the vectors $\{\lambda_h\}$ and $\{\dot{\lambda}_{nh}\}$ can be selected so that [60]

$$\{\delta q_d\}^T\left[\frac{d}{dt}\left\{\frac{\partial E_c}{\partial\{\dot{q}\}_d}\right\} - \left\{\frac{\partial E_c}{\partial\{q\}_d}\right\} - \{Q\}_d + \left\{\frac{\partial\bar{g}_h}{\partial\{q\}_d}\right\} + \left\{\frac{\partial\bar{g}_{nh}}{\partial\{\dot{q}\}_d}\right\}\right] = 0 \tag{7.109}$$

For the independent variables it can be written that

$$\{\delta q_i\}^T \left[\frac{d}{dt} \left\{ \frac{\partial E_c}{\partial \{\dot{q}_i\}} \right\} - \left\{ \frac{\partial E_c}{\partial \{q\}_i} \right\} - \{Q\}_i + \left\{ \frac{\partial \bar{g}_h}{\partial \{q\}_i} \right\} + \left\{ \frac{\partial \bar{g}_{nh}}{\partial \{\dot{q}\}_i} \right\} \right] = 0 \tag{7.110}$$

As $\{\delta q_i\}^T$ is formed by independent generalized coordinates, Equation 7.110 reduces to

$$\frac{d}{dt} \left\{ \frac{\partial E_c}{\partial \{\dot{q}\}} \right\} - \left\{ \frac{\partial E_c}{\partial \{q\}} \right\} - \{Q\} + \left\{ \frac{\partial \bar{g}_h}{\partial \{q\}} \right\} + \left\{ \frac{\partial \bar{g}_{nh}}{\partial \{\dot{q}\}} \right\} = \{0\} \tag{7.111}$$

This equation is valid to a system of bodies having links among them.

7.6
Equation of motion of a body without constraints

Utilizing the Lagrange's equation one can write the system of equation of motion of a body or a set of bodies in the multi-body analysis. Here, the Equation 7.111 will be developed and the equation of motion will be found for a body b without links, that is, any constraint is imposed. Using the virtual work concept it can be said that

$$\delta W_b = \delta W_{b_f} + \delta W_{b_e} \tag{7.112}$$

where δW_b is the virtual work resulting from the action of all forces acting o body b, W_{b_s} and W_{b_e} is the virtual work due to elastic and external forces, respectively. The, for the elastic forces,

$$\delta W_{b_f} = -\{q_b\}^T [K_b] \{\delta q_b\} \tag{7.113}$$

where $[K_b]$ is the stiffness matrix for body b. For the external forces,

$$\delta W_e = \{Q_e\}^T \{\delta q_b\}. \tag{7.114}$$

Substituting Equations 7.113 and 7.114 in Equation 7.112 it results in

$$\delta W_b = -\{q_b\}^T [K_b] \{\delta q_b\} + \{Q_{b_e}\}^T \{\delta q_b\} \tag{7.115}$$

or

$$\{Q_b\} = -[K_b]\{q_b\} + \{Q_{b_e}\}. \tag{7.116}$$

Developing the two first terms of Lagrange's equation, one finds that

$$\frac{d}{dt}\{\frac{\partial E_{c_b}}{\partial \dot{q}_b}\} - \{\frac{\partial E_{c_b}}{\partial q_b}\} = [M_b]\{\ddot{q}_b\} + [\dot{M}_b]\{\dot{q}_b\} - \frac{1}{2}\left[\frac{\partial}{\partial \{q_b\}} \left(\{\dot{q}_b\}^T [M_b] \{\dot{q}_b\} \right) \right]^T. \tag{7.117}$$

one can define the following vector

$$\{Q_{b_v}\} = -[\dot{M}_b]\{\dot{q}_b\} - \frac{1}{2}\left[\frac{\partial}{\partial \{q_b\}} \left(\{\dot{q}_b\}^T [M_b] \{\dot{q}_b\} \right) \right\}^T. \tag{7.118}$$

Combining the equation 7.116, 7.117, 7.117 and 7.118, it is obtained the second order differential system of equations below

$$[M_b]\{\ddot{q}_b\} + [K_b]\{q_b\} = \{Q_{b_e}\} + \{Q_{b_v}\} \tag{7.119}$$

The vector $\{Q_{b_v}\}$ is called the quadratic velocity vector and can be written in the following way [60]

$$\{Q_{b_v}\} = \left\{\{Q_{b_v}\}_R^T \{Q_{b_v}\}_\Theta^T \{Q_{b_v}\}_U^T\right\}^T \tag{7.120}$$

where

$$\begin{aligned}
\{Q_{b_v}\}_R &= -[A_b]\left\{[\tilde{\bar{\Omega}}_b]^2\{\bar{I}_{\breve{r}_b}\} + 2[\tilde{\bar{\Omega}}_b][\bar{I}_{\bar{H}_b}]\{\bar{U}_b\}\right\} \\
\{Q_{b_v}\}_\Theta &= -2[\dot{\bar{G}}_b]^T[\bar{I}_{\Theta\Theta}]\{\bar{\Omega}_b\} - 2[\dot{\bar{G}}_b]^T[\bar{I}_{\Theta f}]\{\dot{\bar{U}}_b\} \\
\{Q_{b_v}\}_U &= -\int_{\bar{V}} \rho\left\{[\bar{H}_b]^T\{[\tilde{\bar{\Omega}}_b]^2\{\breve{r}_b\} + 2[\tilde{\bar{\Omega}}_b]\{\dot{\bar{u}}_b\}\}d\bar{V}\right\}
\end{aligned} \tag{7.121}$$

where $[\bar{I}_{\breve{r}_b}] = \int_{\bar{V}} \bar{\breve{r}}_b d\bar{V}$ and $[\bar{I}_{\bar{H}_b}] = \int_{\bar{V}} \bar{H}_b d\bar{V}$.

7.7
Constraints used in this work

Lets suppose that two bodies (b_1) and (b_2) represented in Figure 7.9 have a condition that the distance of two points $P1$ and $P2$ is a function of the generalized coordinates and of the time. This is a restriction to the movement of both bodies and can be modeled with the following constraint equation

$$\{R_{b_1}\} + [A_{b_1}]\{\bar{r}_{b_1 P_1}\} - \{R_{b_2}\} - [A_{b_2}]\{\bar{r}_{b_2 P_2}\} = \{r_{P_1,P_2}\} \tag{7.122}$$

In the present work this constraint is not dependent on the time (position of points $B1$ and $B2$ coincides all time), than

$$\{R_{b_1}\} + [A_{b_1}]\{\bar{r}_{b_1 P_1}\} - \{R_{b_2}\} - [A_{b_2}]\{\bar{r}_{b_2 P_2}\} = \{0\} \tag{7.123}$$

and P_2 coincide with P_1. When the bodies are imposed to have some restriction related to their angular velocity, the constraints equation are non-holonomic. Non-holonomic constraints may be given by [60]

$$[\mathtt{G}]\{\dot{q}\} + \{g_0\} = 0 \tag{7.124}$$

where $\{g_0\} = \{g_0(\{q\}, t)\}$ and $[\mathtt{G}] = [\mathtt{G}(\{q\}, t)]$ is a $n_c \times n$ matrix.

In this work the non-holonomic constraints used have simpler form where $\{g_0\} = \{0\}$ and $[\mathtt{G}] = [\mathtt{G}(\{q\})]$. It is imposed when the angular velocities between two orientations (or two bodies) are imposed to be the same. Then,

$$\{\Omega_{b_2}\} - \{\Omega_{b_1}\} = \{0\} = [\mathtt{G}(\{q_{b_2}\})]\{\dot{q}_{b_2}\} - [\mathtt{G}_{b_1}(\{q_{b_1}\})]\{\dot{q}_{b_1}\}. \tag{7.125}$$

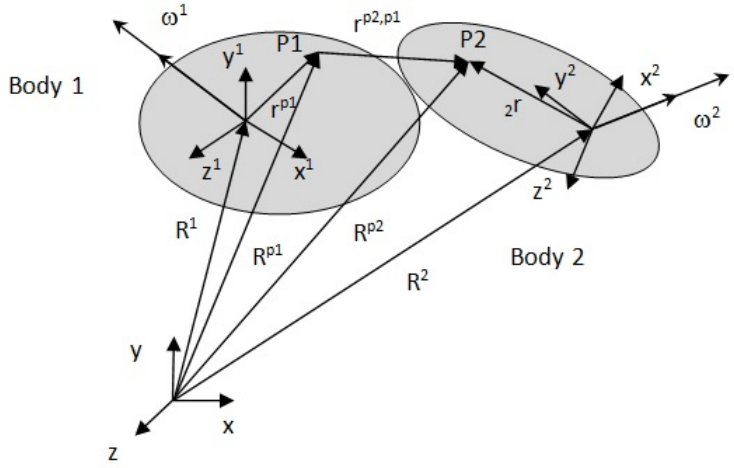

Figure 7.9: Link between two bodies

7.7.1 General formulation for a rigid body

In order to mount the system of equations for the solution of a multi-body system, one begins with the expression for the kinetic energy associated with one moving body as the nacelle, shaft and blades will be considered rigid bodies. The kinetic energy of a body in movement is

$$E_{c_b} = \frac{1}{2}\int_{\bar{V}} \rho_b \{\dot{r}_b\}^T \{\dot{r}_b\} d\bar{V}. \tag{7.126}$$

Using equation 7.70, one writes

$$E_{c_b} = \frac{1}{2}\{\dot{q}_b\}^T \left[\int_{\bar{V}} \rho_b [L_b]^T [L_b] d\bar{V}\right] \{\dot{q}_b\} \tag{7.127}$$

The term under integration is the mass matrix of the body.

$$E_{c_b} = \frac{1}{2}\{\dot{q}_b\}^T [M_b] \{\dot{q}_b\} \tag{7.128}$$

$$\begin{aligned} &[M_b] = \int_{\bar{V}} \rho_b \begin{bmatrix} [I] \\ [B_b]^T \end{bmatrix} \begin{bmatrix} [I] & [B_b] \end{bmatrix} d\bar{V} = \\ &\int_{\bar{V}} \rho \begin{bmatrix} [I] & [B_b] \\ symm. & [B_b]^T [B_b] \end{bmatrix} \bar{V} = \begin{bmatrix} [m_{RR}] & [m_{R\Theta}] \\ symm. & [m_{\Theta\Theta}] \end{bmatrix} \end{aligned} \tag{7.129}$$

where,

$$[m_{RR}] = \int_V \rho[I]d\bar{V}, \quad [m_{\Theta\Theta}] = \int_{\bar{V}} \rho[B_b]d\bar{V}, \text{ and } [m_{\Theta\Theta}] = \int_{\bar{V}} [B_b]^T[B_b]d\bar{V}. \tag{7.130}$$

The load due to the quadratic velocity is given by Equation 7.121 is

$$\{Q_{v_b}\} = \left[(\{Q_{v_b}\})_R^T (\{Q_{v_b}\})_\Theta^T (\{Q_v\})_U^T\right]^T \tag{7.131}$$

and, for a rigid body, whose frame is at the center of mass, are

$$\begin{aligned} \{Q_{v_b}\}_R &= [0] \\ \{Q_{v_b}\}_\Theta &= -2[\dot{\bar{G}}_b]^T[\bar{I}_{\Theta\Theta_b}]\{\bar{\Omega}_b\}. \end{aligned} \tag{7.132}$$

For external forces one has

$$\begin{aligned} \{Q_e\}_R &= \{F_b\} \\ \{Q_e\}_\Theta &= \{B_b\}^T\{F_b\} \quad , \end{aligned} \tag{7.133}$$

where the matrix $[B_b]$ is calculated at the point of application of the force $[F_b]$. Now, each sub-matrix can be calculated.

Sub-matrix $[m_{RR}]$

$$[m_{RR}] = \int_{\bar{V}} \rho_b d\bar{V} \begin{pmatrix} 1 & 0 & 0 \\ 0 & 1 & 0 \\ 0 & 0 & 1 \end{pmatrix} = m_b \begin{pmatrix} 1 & 0 & 0 \\ 0 & 1 & 0 \\ 0 & 0 & 1 \end{pmatrix} \tag{7.134}$$

where m_b is the mass of the body.

Sub-matrix $m_{R\Theta}$. This sub-matrix is null for rigid bodies if the first moment of mass in null, that is, the body coordinate system is set in the center of mass.

$$[m_{R\theta}] = -[A_b] \left[\int_{\bar{V}} \rho_b [\tilde{\bar{\bar{r}}}_b] d\bar{V}\right] [\bar{G}_b] \tag{7.135}$$

where

$$[\bar{I}_{\bar{\bar{r}}_b}] = \int_{\bar{V}} \begin{pmatrix} 0 & -\bar{\bar{r}}_3 & \bar{\bar{r}}_2 \\ \bar{\bar{r}}_3 & 0 & -\bar{\bar{r}}_1 \\ -\bar{\bar{r}}_2 & \bar{\bar{r}}_1 & 0 \end{pmatrix} d\bar{V} \quad \text{and} \quad [\bar{G}_b] = 2[\bar{E}_b] \tag{7.136}$$

It must be considered that $\{\bar{I}_{\bar{\bar{r}}_b}\} = \{\bar{I}_{\bar{r}_b}\} + \{\bar{I}_{\bar{u}_b}\}$, where and $\{\bar{I}_{\bar{\bar{r}}_b}\} = \int_{\bar{V}} \{\bar{\bar{r}}_b\} d\bar{V}$, $\{\bar{I}_{\bar{r}_b}\} = \int_{\bar{V}} \bar{r}_b d\bar{V}$ and $\{\bar{I}_{\bar{u}_b}\} = \int_{\bar{V}} \bar{u}_b d\bar{V}$.

For rigid bodies with the origin of the frame put in the center of mass, one has that $\{\bar{I}_{\bar{r}_b}\} = \{\bar{I}_{\bar{u}_b}\} = \{0\}$.

Sub-matrix $[m_{\theta\theta}]$

This matrix depends of the generalized coordinates of rotation and of deformation.

$$m_{\theta\theta} = \int_{\bar{V}} \rho_b [B_b]^T [B_b] dV = \int_{\bar{V}} \rho_b ([A_b][\tilde{\bar{r}}_b][\bar{G}_b])^T ([A_b][\tilde{\bar{r}}_b][\bar{G}_b]) d\bar{V} \tag{7.137}$$

$$[m_{\theta\theta}] = \int_{\bar{V}} \rho_b ([\bar{G}_b]^T [\tilde{\bar{r}}_b]^T [\tilde{\bar{r}}_b][\bar{G}_b] d\bar{V} = [\bar{G}_b]^T \left[\int_{\bar{V}} \rho_b [\tilde{\bar{r}}_b]^T [\tilde{\bar{r}}] \right] \bar{G}_b d d\bar{V} = [\bar{G}_b]^T [\bar{I}_{\theta\theta}][\bar{G}_b] \tag{7.138}$$

The tensor $[\bar{I}_{\theta\theta}]$ depends on the geometry of the body also its process of deformation. If the body ir rigid, this tensor is the tensor of inertia [J], then,

$$[m_{\theta\theta}] = [\bar{G}_b]^T [\bar{\mathrm{J}}_b][\bar{G}_b] \tag{7.139}$$

and, for the generalized load $\{Q_v\}$

$$\begin{aligned} \{Q_{v_R}\} &= [0] \\ \{Q_{v_\Theta}\} &= -2[\dot{\bar{G}}_b]^T [\bar{\mathrm{J}}_b]\{\bar{\Omega}_b\} \end{aligned} \tag{7.140}$$

All these elements of the turbine are considered rigid, and their equation of motion have the same form. As the form is the same the analysis will be made for a generic body b. The equation of motion of a rigid body with the frame located in its center, under a force $\{\bar{F}_b\}$, is

$$\begin{bmatrix} m_b[I] & 0 \\ 0 & [\bar{G}_b]^T [\bar{\mathrm{J}}_b][\bar{G}_b] \end{bmatrix} \left\{ \ddot{q}_b \right\} = \begin{Bmatrix} \{0\} \\ \{-2[\dot{\bar{G}}_b]^T [\bar{\mathrm{J}}_b]\{\bar{\Omega}_b\}\} \end{Bmatrix} + \begin{Bmatrix} \{F_b\} \\ \{[B_b]^T \{F_b\}\} \end{Bmatrix} \tag{7.141}$$

where,

$$[M_b] = \begin{bmatrix} m_b[I] & 0 \\ 0 & [\bar{G}_b]^T [\bar{\mathrm{J}}_b][\bar{G}_b] \end{bmatrix}, \qquad \{Q_v\} = \begin{Bmatrix} \{0\} \\ \{-2[\dot{\bar{G}}_b]^T [\bar{\mathrm{J}}_b]\{\bar{\Omega}_b\}\} \end{Bmatrix}$$

and

$$\{Q_e\} = \begin{Bmatrix} \{F_b\} \\ \{[B_b]^T \{F_b\}\} \end{Bmatrix} \tag{7.142}$$

7.8 Differentiating the residue

The expressions obtained in formulation of the turbine generate a vectors that need to be differentiated with respect to the generalized coordinates. This derivatives appear when the system of equation of motion are to be solved

using a step by step method performing an incremental approximation. They will be used to obtain the derivatives of the residue with respect to incremental displacement. The expressions to be determined are
The residue $\{r^*\}$ is defined as

$$\begin{aligned}\{r^*\} =&[\tilde{\mathbb{M}}]\{\tilde{\ddot{q}}\} + [\tilde{\mathbb{J}}_h]^T([\mathbb{P}_h]\{\tilde{\mathbb{G}}_h\} + [\mathbb{K}_h]\{\tilde{\Lambda}_h\}) + [\tilde{\mathbb{J}}_{nh}]^T([\mathbb{P}_{nh}]\{\tilde{\mathbb{G}}_{nh}\}+\\ &[\mathbb{K}_{nh}]\{\dot{\tilde{\Lambda}}_{nh}\}) - \{\tilde{\mathbb{Q}}_c\} - \{\tilde{\mathbb{Q}}_k\} - \{\tilde{\mathbb{Q}}_v\} - \{\tilde{\mathbb{Q}}_f\},\end{aligned} \tag{7.143}$$

submitted to the same initial conditions presented in Equation 3.58. The constrained initial value problem of Equation 3.58 together with the Newmark scheme shown in Equation 3.61 define a nonlinear problem of algebraic equations with unknowns $\{q_\Lambda\}_l$, $\{\dot{q}_\Lambda\}_l$ and $\{\ddot{q}_\Lambda\}_l$. This is an approximation using Taylor expansion in step l and iteration k and imposing $\{r^*\}_l^{(k+1)} = \{0\}$. In order to solve the Equation 3.63 for $\{\Delta\tilde{q}_\Lambda\}$, the necessary derivatives of the residue with respect to $\{\tilde{q}_\Lambda\}$, $\{\dot{\tilde{q}}_\Lambda\}$ and $\{\ddot{\tilde{q}}_\Lambda\}$ must be calculated. They are

$$\begin{aligned}&\frac{\partial\{r^*\}}{\partial\{\ddot{q}_\Lambda\}} = [\tilde{\mathbb{M}}_\Lambda]\\ &\frac{\partial\{r^*\}}{\partial\{\dot{q}_\Lambda\}} = \frac{\partial}{\partial\{\dot{q}_\Lambda\}}\{[\tilde{\mathbb{M}}_\Lambda]\{\ddot{\tilde{q}}_\Lambda\}\} - \frac{\partial}{\partial\{\dot{q}_\Lambda\}}\{\tilde{\mathbb{Q}}_c\} - \frac{\partial}{\partial\{\dot{q}_\Lambda\}}\{\tilde{\mathbb{Q}}_k\} - \frac{\partial}{\partial\{\dot{q}_\Lambda\}}\{\tilde{\mathbb{Q}}_v\}\\ &- \frac{\partial}{\partial\{\dot{q}_\Lambda\}}\{\tilde{\mathbb{Q}}_f\} + \{[\tilde{\mathbb{J}}_{nh}]^T[\mathbb{P}_{nh}][\tilde{\mathbb{J}}_{nh}]\} + \{[\tilde{\mathbb{J}}_{nh}]^T[\mathbb{K}_{nh}]\}\\ &+ \frac{\partial[\tilde{\mathbb{J}}_{nh}]^T}{\partial\{\dot{q}_\Lambda\}}[\mathbb{P}_{nh}]\{\tilde{\mathbb{G}}_{nh}\} + \frac{\partial[\tilde{\mathbb{J}}_{nh}]^T}{\partial\{\dot{q}_\Lambda\}}[\mathbb{K}_{nh}]\{\dot{q}_\Lambda\}\\ &\frac{\partial\{r^*\}}{\partial\{q_\Lambda\}} = \frac{\partial}{\partial\{q_\Lambda\}}\{[\tilde{\mathbb{M}}_\Lambda]\{\ddot{\tilde{q}}_\Lambda\}\} - \frac{\partial}{\partial\{q_\Lambda\}}\{\tilde{\mathbb{Q}}_c\} - \frac{\partial}{\partial\{q_\Lambda\}}\{\tilde{\mathbb{Q}}_k\} - \frac{\partial}{\partial\{q_\Lambda\}}\{\tilde{\mathbb{Q}}_v\}\\ &- \frac{\partial}{\partial\{q_\Lambda\}}\{\tilde{\mathbb{Q}}_f\} + \{[\tilde{\mathbb{J}}_h]^T[\mathbb{P}_h][\tilde{\mathbb{J}}_h]\} + \{[\tilde{\mathbb{J}}_h]^T[\mathbb{K}_h]\}\\ &+ \frac{\partial[\tilde{\mathbb{J}}_h]^T}{\partial\{q_\Lambda\}}[\mathbb{P}_h]\{\tilde{\mathbb{G}}_h\} + \frac{\partial[\tilde{\mathbb{J}}_h]^T}{\partial\{q_\Lambda\}}[\mathbb{K}_h]\{q_\Lambda\}\}\end{aligned} \tag{7.144}$$

7.8.1 Rigid elements

Differentiating the matrix $[\tilde{\mathbb{M}}_\Lambda]$ is differentiating separately each sub-matrix $[M_b]$ with respect to q_b, where the index b means any rigid body, component of the turbine. This differentiation becomes

$$\frac{\partial\{[M_b]\{\ddot{q}_b\}\}}{\partial\{q_b\}} = \frac{\partial}{\partial\{q_b\}}\begin{bmatrix} m_b[I] & 0 \\ 0 & [\bar{G}_b]^T[\bar{\mathbb{J}}_b][\bar{G}_b]\end{bmatrix}\left\{\ddot{q}_b\right\} \tag{7.145}$$

In sub-matrix $[M_b]$, the operation $m_b \frac{\partial}{\partial\{q_b\}}[I]\{\ddot{q}_b\}\}$ results in a null matrix. The bottom-right block is dependent only on the Euler parameters Θ_b. Then, one needs only to determine $\frac{\partial}{\partial\{\Theta_b\}}\left([\bar{G}_b]^T[\bar{\mathrm{J}}_b][\bar{G}_b]\{\ddot{q}_b\}\right)$. So,

$$\begin{aligned}&\frac{\partial}{\partial\{\Theta_b\}}\left([\bar{G}_b]^T[\bar{\mathrm{J}}_b][\bar{G}_b]\{\ddot{\Theta}_b\}\right) = \\ &\frac{\partial[\bar{G}_b]}{\partial\{\Theta_b\}}^T[\bar{\mathrm{J}}_b][\bar{G}_b]\{\ddot{\Theta}_b\} + [\bar{G}_b]^T[\bar{\mathrm{J}}_b]\left[\frac{\partial[\bar{G}_b]}{\partial\{\Theta_b\}}\{\ddot{\Theta}_b\}\right]\end{aligned} \tag{7.146}$$

The vector force $\{\mathbb{Q}_{v_b}\}$ is In the case of rigid body with the frame located at it center of mass all others have the same format given below

$$\{Q_{v_b}\} = \begin{Bmatrix}\{0\} \\ \{2[\dot{\bar{G}}_b]^T[\bar{\mathrm{J}}_b][\dot{\bar{G}}_b]\{\Theta_b\} + [\bar{G}_b]^T[\bar{\mathrm{J}}_b][\dot{\bar{G}}_b]\{\Theta_b\}\end{Bmatrix}.$$

whose derivative is

$$\frac{\partial\{Q_{v_b}\}}{\partial\{q\}} = \begin{bmatrix}[0] \\ 2[\dot{\bar{G}}_b]^T[\bar{\mathrm{J}}_b][\dot{\bar{G}}_b] + [\bar{G}_b]^T[\bar{\mathrm{J}}_b][\dot{\bar{G}}_b] + \frac{\partial}{\partial\{\Theta_b\}}[\bar{G}_b]^T[\bar{\mathrm{J}}_b][\dot{\bar{G}}_b]\{\Theta_b\}\end{bmatrix}.$$

The forces $\{Q_{v_b}\}$ must be performed for $\{\dot{\bar{q}}_b\}$ too. Recalling that $[\dot{\bar{G}}_b]\{\Theta\} = -[\bar{G}_b]\{\dot{\Theta}_b\} = \{\bar{\Omega}_b\}$ when using Euler parameters,

$$\frac{\partial\{Q_{v_b}\}}{\partial\{q\}_b} = \begin{bmatrix}[0] \\ -2\frac{\partial}{\partial\{\Theta_b\}}[\dot{\bar{G}}_b]^T[\bar{\mathrm{J}}_b]\{\bar{\Omega}_b\} - 2[\dot{\bar{G}}_b]^T[\bar{\mathrm{J}}_b][\bar{G}_b] - [\bar{G}_b]^T[\bar{\mathrm{J}}_b][\bar{G}_b]\end{bmatrix}.$$

The same systematic is used for differentiating the vector of external loads, $\{Q_{e_b}\}$, with respect to $\{q\}$ and $\{\dot{q}\}$. So, these derivatives limit to

$$\frac{\partial}{\partial\{q\}}\{Q_{e_b}\} = \begin{bmatrix}[0] \\ \frac{\partial[B_b]^T}{\partial\{\Theta_b\}}\{F_b\}\end{bmatrix} \tag{7.147}$$

and $\frac{\partial}{\partial\{\dot{q}\}}\{Q_{e_b}\} = [0]$ as $[B_b]$ is not function of $\{\dot{q}\}$.

7.8.2 Tower

The sub-matrices $[M_t]$ and $[K_t]$ have dimension $n_{dof} \times n_{dof}$ and are the result of finite element formulation. They are constant matrices (in this work), The the vector $\{q_t\} \equiv \{U\}$ is the vector of the nodal displacements with dimension $n_{dof} \times 1$. The external forces are considered only dependent on the time in this work, except for the non-linear force $\{N(\{\dot{U}\})\}$ which appears when considering the presence of surrounding water. With this information, it can be deduced that

$$\frac{\partial\left([M_t]\{\ddot{U}\}\right)}{\partial\{\ddot{U}\}} = [M_t] \tag{7.148}$$

$$\frac{\partial\left([M_t]\{\ddot{U}\}\right)}{\partial\{\dot{U}\}} = \frac{\partial\left([M_t]\{\ddot{U}\}\right)}{\partial\{U\}} = [0], \tag{7.149}$$

$$\frac{\partial\left([K_t]\{U\}\right)}{\partial\{U\}} = [K_t] \tag{7.150}$$

and

$$\frac{\partial\left([K_t]\{U\}\right)}{\partial\{\ddot{U}\}} = \frac{\partial\left([K_t]\{U\}\right)}{\partial\{\dot{U}\}}[K_t] = [0]. \tag{7.151}$$

Concerning to the nonlinear interaction between the tower and fluid, two forces arrive. One is linear and depends only on the time. The other is non-linear in $\{\dot{U}\}$, the nodal velocity vector. The interaction fluid-column force, $\frac{\partial}{\partial\{\dot{q}\}}\{N(\dot{q})\}$, will be performed below recalling Equation (3.32).

$$F_{d_{y,z}} = \int_0^L sign\left(W_{y,z}(x,t) - \dot{w}_{y,z}(x,t)\right) D(x)\, C_D(x)\rho_f \dot{w}_{y,z}(x,t)\psi(x)dx \tag{7.152}$$

$$N_{y,z} = \frac{1}{2}\int_0^L sign(W_{y,z}(x,t) - \dot{w}_{y,z}(x,t))D(x)\, C_D\rho_f(\dot{w}_{y,z}(x,t))^2\psi(x)dx \tag{7.153}$$

where $W_{y,z}$ and $\dot{w}_{y,z}$ are the water and tower transversal velocity vector components in a given section of the tower, $\psi(x)$ is the interpolating function. The non-linear vector load $\{N(\{\dot{U}\})$ is not dependent on the axial movement of the tower, so the degrees of freedom active are those associated to the transversal displacements. In element level the field of velocities in the domain is given using the interpolating functions as below

$$\{\dot{w}\} = \{\bar{\Psi}\}\{\dot{U}\} \tag{7.154}$$

where the vector $\{\bar{\Psi}\}$ contains the interpolating functions for transversal degrees of freedom of the tower, only (w_y and w_z). In an explicit form, for a generic finite element,

$$\begin{bmatrix} w_x \\ w_y \\ w_z \end{bmatrix} = \begin{bmatrix} 0 & 0 & 0 & 0 & 0 & 0 & 0 & 0 & 0 & 0 & 0 & 0 & 0 \\ 0 & \psi^1_{w_y} & 0 & 0 & \psi^1_{\theta_y} & 0 & 0 & \psi^2_{w_y} & 0 & 0 & \psi^2_{\theta_y} & 0 & 0 \\ 0 & 0 & \psi^1_{w_z} & 0 & 0 & \psi^1_{\theta_z} & 0 & 0 & \psi^2_{w_z} & 0 & 0 & \psi^2_{\theta_z} & 0 \end{bmatrix} \begin{Bmatrix} \{\dot{U}^1_x\} \\ \{\dot{U}^1_y\} \\ \{\dot{U}^1_z\} \\ \{\dot{U}^1_{\theta_x}\} \\ \{\dot{U}^1_{\theta_y}\} \\ \{\dot{U}^1_{\theta_z}\} \\ \{\dot{U}^2_x\} \\ \{\dot{U}^2_y\} \\ \{\dot{U}^2_z\} \\ \{\dot{U}^2_\theta\} \\ \{\dot{U}^2_\theta\} \\ \{\dot{U}^2_\theta\}, \end{Bmatrix} \tag{7.155}$$

recalling that the number of the degrees of freedom of the element used is 12.

$$F_{d_{y,z}} = \int_0^L sign\left(W_{y,z}(x,t) - \dot{w}_{y,z}(x,t)\right) D(x)\, C_D(x) \rho_f \dot{w}_{y,z}(x,t) \phi(x) dx \tag{7.156}$$

$$\dot{w} = \{\bar{\Psi}\}\{\dot{U}\} \tag{7.157}$$

$$F_{d_{y,z}} = sign\left(W_{y,z}(x,t) - \dot{w}_{y,z}(x,t)\right) \int_0^L D(x)\, C_D(x) \rho_f \{\bar{\Psi}\}^T \{\bar{\Psi}\}\{\dot{U}\} dx \tag{7.158}$$

then,

$$[C_{d_t}] = sign\left(W_{y,z}(x,t) - \dot{w}_{y,z}(x,t)\right) \int_0^L D(x)\, C_D(x) \rho_f \{\bar{\Psi}\}^T \{\bar{\Psi}\} dx \tag{7.159}$$

For the nonlinear case,

$$\dot{w}^2 = \{\dot{U}\}^T \{\bar{\Psi}\}^T \{\bar{\Psi}\}\{\dot{U}\}, \tag{7.160}$$

the i^{th} component, of the nonlinear load $\{N(\{\dot{U}\})\}$ is

$$N_i(\{\dot{U}\}) = \frac{1}{2} \int_0^L sign[W - \dot{w}] D\, C_D(x) \rho_f \dot{U}^T [\bar{h}] \dot{U} \bar{\psi}_i dx \tag{7.161}$$

and the derivative $\frac{\partial}{\partial(\{\dot{U}\})} N(\{\dot{U}\})$ is a matrix whose elements are

$$[C_{N_t}(\dot{U})] = \frac{\partial}{\partial \dot{U}_j} N_i(\{\dot{U}\}) = \int_0^L sign[W - \dot{w}] \rho_f D\, C_D(t) \bar{h}_{jk} \bar{\psi}_i \dot{U}_k dx \tag{7.162}$$

where $\bar{h} = \{\bar{\Psi}\}^T \{\bar{\Psi}\}$.

This operation is made in the element level and for each iteration. In this work the matrices $[C_{d_t}]$ and $[C_{N_t}(\dot{U})]$ are the only matrices associated to damping.

$\{F_t\}$ is the external time dependent force vector acting in the tower. The derivative $\frac{\partial}{\partial\{U\}}\{F_{e_t}\}$ is obviously a null.

7.9
Determination of the reactions at t=0

At the beginning of the analysis the constraints are already present. As the values for the reactions are unknown (the Lagrange parameters are unknown), they can be included in the formulation making use of the constraints themselves. In a problem of initial value, the velocities and positions are given at the beginning of the time. In order to include the influence of the constraints in the beginning of the analysis, consider the Equations presented in the Chapter 7.5.2 for the holonomic and non-holonomic constraints, 7.95 and 7.96, respectively. Differentiating the former twice with respect to time, one obtains [60]

$$\left[\frac{\partial\{\mathbb{G}_h\}}{\partial\{\breve{q}\}}\right]\{\ddot{\breve{q}}\} = -2\left[\frac{\partial^2\{\mathbb{G}_h\}}{\partial\{\breve{q}\}\partial t}\right]\{\ddot{\breve{q}}\} - \left[\frac{\partial}{\partial\{\breve{q}\}}\left\{\left[\frac{\partial\{\mathbb{G}_h\}}{\partial\{\breve{q}\}}\right]\{\dot{\breve{q}}\}\right\}\right]\{\dot{\breve{q}}\} - \left\{\frac{\partial^2\{\mathbb{G}_h\}}{\partial t^2}\right\} = \{\mathbb{Q}_{c_h}\} \quad . \tag{7.163}$$

Differentiating the latter once with respect to time, one obtains

$$\left[\frac{\partial\{\mathbb{G}_{nh}\}}{\partial\{\dot{\breve{q}}\}}\right]\{\ddot{\breve{q}}\} = -\left[\frac{\partial\mathbb{G}_{nh}}{\partial t}\right] = \{\mathbb{Q}_{c_{nh}}\}. \tag{7.164}$$

The right side of the equations 7.163 and 7.164 represents generalized forces due to the presence of the constraints. Considering that $\left[\frac{\partial\mathbb{G}_h}{\partial\{\breve{q}\}}\right] = [\mathbb{J}_h]$ and $\left[\frac{\partial\mathbb{G}_{nh}}{\partial\{\dot{\breve{q}}\}}\right] = \{\ddot{\breve{q}}\} = [\mathbb{J}_{nh}]$ and that the time is not explicit, that is the case in this work, the equations above become

$$[\mathbb{J}_{nh}]\{\ddot{\breve{q}}\} = -\left[\frac{\partial}{\partial\{\breve{q}\}}\left\{\left[\frac{\partial\{\mathbb{G}_h\}}{\partial\{\breve{q}\}}\right]\{\dot{\breve{q}}\}\right\}\right]\{\dot{\breve{q}}\} \tag{7.165}$$

and,

$$[\mathbb{J}_{nh}]\{\ddot{\breve{q}}\} = \{0\}. \tag{7.166}$$

The system of equation of motion for the turbine was given in 3.2.7 and is repeated here:

$$\begin{cases} [\mathbb{M}]\{\ddot{\breve{q}}\} + [\mathbb{J}_h]^T([\mathbb{P}_h]\{\mathbb{G}_h\} + [\mathbb{K}_h]\{\Lambda_h\}) + [\mathbb{J}_{nh}]^T([\mathbb{P}_{nh}]\{\mathbb{G}_{nh}\} + \\ [\mathbb{K}_{nh}]\{\dot{\Lambda}_{nh}\}) - \{\mathbb{Q}_c\} - \{\mathbb{Q}_k\} - \{\mathbb{Q}_v\} - \{\mathbb{Q}_f\} = \{0\} \\ [\mathbb{K}_h]\{\mathbb{G}_h\} = \{0\} \\ [\mathbb{K}_{nh}]\{\mathbb{G}_{nh}\} = \{0\} \\ \{\breve{q}(t_0)\} = \{\tilde{q}_0\} \\ \{\dot{\breve{q}}(t_0)\} = \{\dot{\tilde{q}}_0\} \\ \{\Lambda_h(t_0)\} = \{\Lambda_{0_{nh}}\} \\ \{\dot{\Lambda}_{nh}(t_0)\} = \{\dot{\Lambda}_{0_{nh}}\} \end{cases} \quad . \tag{7.167}$$

Substituting the initial conditions, the system becomes at the time $t = 0$

$$\begin{cases} [\mathbb{M}_0]\{\ddot{\breve{q}}_0\} + [\mathbb{J}_{h_0}]^T([\mathbb{P}_h]\{\mathbb{G}_{h_0}\} + [\mathbb{K}_{h_0}]\{\Lambda_{h_0}\}) + [\mathbb{J}^T_{nh_0}([\mathbb{P}_{nh}]\{\mathbb{G}_{nh}\} + \\ [\mathbb{K}_{nh}]\{\dot{\Lambda}_{nh_0}\} = \{\mathbb{Q}_0\} \\ [\mathbb{K}_h]\{\mathbb{G}_{h_0}\} = \{\mathbb{Q}_{h_0}\} \\ [\mathbb{K}_{nh}]\{\mathbb{G}_{nh_0}\} = \{\mathbb{Q}_{nh_0}\} \end{cases} \tag{7.168}$$

The second and third Equations of 7.168 are useless as they are identically null. But they can be substituted by Equations 7.165 and 7.166, then,

$$\begin{cases} [\mathbb{M}_0]\{\ddot{\breve{q}}_0\} + [\mathbb{J}_{h_0}]^T[\mathbb{K}_h]\{\Lambda_{h_0}\} + [\mathbb{J}_{nh_0}]^T[\mathbb{K}_{nh}]\{\dot{\Lambda}_{nh_0}\} = \{\mathbb{Q}_0\} \\ [\mathbb{J}_{nh}]\{\ddot{\breve{q}}\} = \{\mathbb{Q}_h\} = -\left[\dfrac{\partial}{\partial\{\breve{q}\}}\left\{\left[\dfrac{\partial\{\mathbb{G}_h\}}{\partial\{\breve{q}\}}\right]\{\dot{\breve{q}}\}\right\}\right]\{\dot{\breve{q}}\} \\ [\mathbb{J}_{nh}]\{\ddot{\breve{q}}\} = \{\mathbb{Q}_{nh_0}\} = \{0\} \end{cases} . \tag{7.169}$$

The unknowns are $\{\ddot{\breve{q}}_0\}$, $\{\Lambda_{h_0}\}$ and $\{\Lambda_{nh_0}\}$. The system 7.169 can that be written in the following way

$$\begin{Bmatrix} \{\ddot{\breve{q}}_0\} \\ \{\Lambda_{h_0}\} \\ \{\dot{\Lambda}_{nh_0}\} \end{Bmatrix} = \begin{bmatrix} [\mathbb{M}] & [\mathbb{K}_{h_0}][\mathbb{J}_{h_0}]^T & [\mathbb{K}_{nh_0}][\mathbb{J}_{nh_0}]^T \\ [\mathbb{K}_{h_0}][\mathbb{J}_{h_0}] & [0] & [0] \\ [\mathbb{K}_{nh_0}][\mathbb{J}_{nh_0}] & [0] & [0] \end{bmatrix}^{-1} \begin{Bmatrix} \{\mathbb{Q}\} \\ \{\breve{\mathbb{Q}}_{c_{h_0}}\} \\ \{\breve{\mathbb{Q}}_{c_{nh_0}}\} \end{Bmatrix} \tag{7.170}$$

where $\{\breve{\mathbb{Q}}_{c_{h_0}}\} = [\mathbb{K}_{h_0}]\{\mathbb{Q}_{c_{h_0}}\}$ and $\{\breve{\mathbb{Q}}_{c_{nh_0}}\} = [\mathbb{K}_{nh_0}]\{\mathbb{Q}_{c_{nh_0}}\}$.

In order to solve the system of equations 7.170, it must be first calculated the vectors $\{\mathbb{Q}_{c_{h_0}}\}$ which means determining the derivative $-\frac{\partial}{\partial\{\breve{q}\}}\left[\frac{\partial g_h}{\partial\{\breve{q}\}}\{\dot{\breve{q}}\}\right]\{\dot{\breve{q}}\}$. In the present work, $\{\mathbb{Q}_{c_{nh_0}}\} = \{0\}$ and the holonomic constraints are of the type

$$\{g_{h_{bi,bj}}\} = \{R_{bi}\} + [A_{bi}]\{_{bi}r\} - \{R_{bj}\} - [A_{bj}]\{_{bj}r\} \tag{7.171}$$

where the index bi and bj mean the bodies i and j. The Jacobian matrix for this constraint is

$$J_{h_{bi,bj}} = \begin{bmatrix} [I_{bi}] & \cdots & [B_{bi}] & \cdots & -[I_{bj}] & \cdots & -[B_{bj}] \end{bmatrix}, \tag{7.172}$$

where $[I_{bi}]$ and $[I_{bj}]$ are the identity matrix. $[B_{bi}]$ and $[B_{bj}]$ are given by 7.58 7.59. Then, considering only the constraints given by Equation 7.171, for two bodies ingle

$$-\frac{\partial}{\partial\{\breve{q}\}}\left[\frac{\partial g_h}{\partial\{\breve{q}\}}\{\dot{\breve{q}}\}\right] = -\frac{\partial}{\partial\{\breve{q}\}}\begin{bmatrix} [I_{bi}] & [B_{bi}] & [0] & [0] \\ [0] & [0] & -[I_{bj}] & -[B_{bj}] \end{bmatrix}\begin{bmatrix} \dot{R}_{bi} \\ \dot{\Theta}_{bi} \\ \dot{R}_{bj} \\ \dot{\Theta}_{bj} \end{bmatrix}, \tag{7.173}$$

then,

$$-\frac{\partial}{\partial\{\breve{q}\}}\left[\frac{\partial g_h}{\partial\{\breve{q}\}}\{\dot{\breve{q}}\}\right] = -\begin{bmatrix}[0] & \frac{\partial}{\partial\Theta_{bi}}\{[B_{bi}]\{\dot{\Theta}_{bi}\}\} & [0] & [0] \\ [0] & [0] & [0] & -\frac{\partial}{\partial\Theta_{bj}}\{[B_{bj}]\{\dot{\Theta}_{bij}\}\}\end{bmatrix}, \tag{7.174}$$

and $\frac{\partial(B_{ik}\dot{q}_k)}{\partial\Theta_m}$ is obtained by using Equation 7.61.

From this differentiations, a matrix with dimensions $3n_c \times 7n_b + n_{dof}$ is mounted considering the contribution of all bodies and then the vector $\{\mathbb{Q}_{c_h}\}$ can be calculated. Then, Equation 7.170 is solved and the initial generalized accelerations and Lagrange multipliers are obtained. In order to determine the overall reactions acting on the body in time, $\{\mathbb{Q}_{c_h}\}$ and $\{\mathbb{Q}_{c_{nh}}\}$ are determined as

$$\begin{aligned}\{\mathbb{Q}_{c_h}\} &= -[\mathbb{K}_h][\mathbb{J}_h)]^T\{\Lambda_h\} \\ \{\mathbb{Q}_{c_{nh}}\} &= -[\mathbb{K}_{nh}][\mathbb{J}_{nh}]^T\{\dot{\Lambda}_{nh}\} \quad .\end{aligned} \tag{7.175}$$

The actual resulting forces acting in the bodies are directly determined in the equations of movement and are represented by a vector in $\Re^3$. The torques are not represented this way if the generalized coordinates are the Euler parameters. In this case, some transformation must be made in order to obtain the actual torque. It can be demonstrated that the relation between the generalized torques and the real ones are given by

$$\begin{aligned}\{\bar{T}_{R_h}\} &= \frac{1}{4}[\bar{G}_b]\{Q_{c_{h_b}}\} \\ \{\bar{T}_{R_{nh}}\} &= \frac{1}{4}[\bar{G}_b]\{Q_{c_{nh_b}}\}\end{aligned} \tag{7.176}$$

where $\{\bar{T}_{R_h}\}$ and $\{\bar{T}_{R_{nh}}\}$ are the actual torques acting on a body of the system due to holonomic an non-holonomic constrains, respectively, $\{Q_{c_{h_b}}\}$ and $\{Q_{c_{nh_b}}\}$ are the generalized torques, for each body as well. The matrix $[\bar{G}]$ given in 7.55. The quantities above are represented with respect to the body frame and must be calculated for each body.

7.10 Uncertainty quantification

7.10.1 Maximum Entropy Principle

When the quantities involved in analysis have a random nature, this means that one can not predict the exact value of those quantities but only say that a given set of values has a probability of occurrence. Depending on the problem, available data are rare and incomplete so that the associated probability density function is not possible to be determined. However, based in the data available, it is possible to find the best PDF (which gives the most conservative result) with suits with the quality of the information contained in the data. This is due to the Principle of Maximum Entropy [61], [28]. This Principal states that, under to known constraints, the probability density function which best represents the current state of knowledge

is the one with the largest entropy [55]. The uncertainty of a random variable $\mathbf{X}$ is defined by

$$\mathbf{S}(f_{\mathbf{X}}) = -\int_D f_{\mathbf{X}} log(f_{\mathbf{X}}(\mathbf{X}))d\mathbf{X} \tag{7.177}$$

where $f_{\mathbf{X}}$ is the PDF of $\mathbf{X}$ and $\mathfrak{D}$ is the domain. Suppose that the only available information one has is that the random variable $\mathbf{X}$ exits only within a given range, say $[a \;\; b]$. Then, the Equation 7.177 leads to the following uniform PDF

$$f_{\mathbf{X}}(x|a,b) = \frac{1}{b-a}; \;\; a_u \leq x \leq b_u.0; otherwise. \tag{7.178}$$

If the constraints are the positiveness and bounded second moment, the Equation 7.177 indicates a gamma PDF. The gamma probability distribution function has two parameters a_g and b_g, so that $E(X) = ab$ and $\sigma_X^2 = ab^2$, and is given by

$$\begin{aligned} f_{\mathbf{X}}(x|a,b) &= \frac{1}{b^2\Gamma(a)}x^{(a-1)}e^{-\frac{x}{b}} \\ 0; &\quad otherwise. \end{aligned} \tag{7.179}$$

Still, from Equation 7.177 for given mean value $E(X) = \mu_{\mathbf{X}}$ and variation $\sigma_{\mathbf{X}}^2$, a Gaussian is obtained

$$f_{\mathbf{X}}(x|\mu_{\mathbf{X}}, \sigma_{\mathbf{X}}) = \frac{1}{\sigma_{\mathbf{X}}\sqrt{2\pi}}e^{-\frac{1}{2}(\frac{x-\mu_{\mathbf{X}}}{\sigma_{\mathbf{X}}^2})}. \tag{7.180}$$

Bibliography

ADHIKARI, S.; BATTACHARYA, S. Dynamic analysis of wind turbine towers on flexible foundations. **Shock and Vibration**, v.19, p. 37–56, 2012.

ALVES, J.; SAMPAIO, R. Dynamic analysis of a partially immersed wind turbine with lumped mass effect and flexible foundation. **Proceedings of the XVII International Symposium on Dynamic Problems of Mechanics - DINAME**, 2015.

ALVES, J. A. P.; ET AL. Analysis of a two bladed wind turbine under random loading. **Mecánica Computacional (AAMC)**, v.XXXII, p. 579–603, 2014.

AMARANTE, O. A. C.; ET AL. **Atlas do potencial eólico brasileiro**. Ministério de Minas e Energia, 2001.

AMARANTE, O. A. C.; ET AL. **Atlas eólico do Rio de Janeiro**. Secretaria de Estado de Energia da Indústria Naval e do Petróleo - RJ, 2002.

ANDERSEN, L.; NIELSEN, S. **Elastic Beams in Three Dimensions**. Aalborg, Denmark: Aalborg University, 2008. DCE Lecture Notes No. 23.

ANGULO, I.; ET AL. Impact analysis of wind farms on telecommunication services. **Renewable and Sustainable Energy Reviews**, v.32, p. 84–99, 2014.

ASHURI, T.; ET AL. Multidisciplinary design optimization of offshore windturbines for minimum levelized cost of energy. **Proceedings of the National Academy of Sciences of the United States of America**, v.111(42), p. 15126–31, 2014.

BAATH, L. B. Noise spectra from wind turbines. **Renewable Energy**, v.57, p. 512–519, 2013.

BATHE, K. J. **Finite element procedures in engineering analysis**. Prentice Hall, Inc., New Jersey, U. S., 428 p, 1982.

BENASSAI, G.; ET AL. Ultimate and accidental limit state design for mooring systems of floating offshore wind turbines. **Ocean Engineering**, v.92, p. 64–75, 2014.

BIERBOOMS, W. A gust model for wind turbine design. **JSME International Journal Series B**, v.47(2), p. 378–386, 2004.

BLEVINS, R. D. **Harrison 'Shock and Vibration Handbook 5^{th} ed.- Chapter 29 Part I**. USA: McGraw-Hill, 1982.

BORTOLINI, M. E. A. Performance and viability analysis of small wind turbines in the european union. **Renewable Energy**, v.62, p. 629–639, 2014.

BYRNE, B. W.; HOULSBY, G. T. Helical piles: an innovative foundation design option for offshore wind turbines. **Philosophical transactions. Series A, Mathematical, physical and engineering sciences**, v.373, 2015.

CASTRO, R. M. G. **Energias Renováveis e Produção Descentralizada - Introdução à Energia Eólica**. Universidade Técnica de Lisboa - Instituto Superior Técnico DEEC / Secção de Energia, 2003.

CHANG, J. Y.; HANG, L. Some studies on the natural frequencies of immersed restrained column. **Journal of Sound and Vibration**, v.130(1), p. 516–524, 1989.

CRYAN, P. M.; ET AL. Behavior of bats at wind turbines. **Proceedings of the National Academy of Sciences of the United States of America**, v.111(42), p. 15126–31, 2014.

DYRBYE, C.; HANSEN, S. O. **Wind loads on structures**. Baffins Lane, Chichester, West Sussex P019 1UD, England: Natl Council of Teachers, 1997.

FRØYD, L. Wind turbine design: Evaluation of dynamic loads on large offshore wind turbines. **Teknisk-Naturvitenskapelige Universitet, Fakultet For Ingeniørvitenskap Og Teknologi, Institutt For Energi- Og Prosessteknikk**, v.146, p. 1–10, 2015.

GÈRADIN, M.; CARDONA, A. **Multibody Flexible Dynamics - Finite Element Approach**. Susses, England: John Wiley and Sons, 2001.

HAN, S. M.; BENAROYA, H. ; WEI, T. Dynamics of transversely vibrating beam using four engineering theories. **Journal of Sound and Vibration**, v.225(5), p. 935–988, 1999.

HANSEN, M. O. L. **Aerodynamics of Wind Turbines - Second Edition**. Lindon-Sterling,VA, 2008.

HARTE, M.; BASU, B. ; NIELSEN, S. Dynamic analysis of wind turbines including soil-structure interaction. **Engineering Structures**, v.45, p. 509–518, 2012.

HOLM-JØRGENSEN, K.; NIELSENN, S. Nonlinear displacements of a wind turbine blade based on a multibody formulation with a local observer frame. **The Nordic Seminar on Computational Mechanics**, v. , p. 109–112, 2009.

HUGES, T. J. R. **The finite element method**. Dover Publications, Inc., Mineola, N.Y., USA, 682 p., 1987.

INMAN, D. **Engineering Vibration**, volume 1. Upper Saddle River, New Jersey, USA: Prentice Hall PTR, NJ, USA, 2003.

JAYNES, E. Information theory and statistical mechanics. **The Physical Review**, v.106(4), p. 1620–1630, 1957.

JIN, X. E. A. Multibody modeling of varying complexity for dynamic analysis of large-scale wind turbines. **Renewable Energy**, v.90, p. 336–351, 2016.

JONKMAN, J. Dynamics of off-shore floating wind turbine s- model development and verification. **Wind Energy**, v.12, p. 459–492, 2009.

KAIMAL, J. C. Turbulence spectra, length scales and structure parameters in the stable surface layer. **Boundary-Layer Meteorology**, v.4, p. 289–309, 1973.

KAIMAL, J. C. E. A. Spectral characteristics of surface-layer turbulence. **Boundary-Layer Meteorology**, v.4, p. 289–309, 1972.

KESSENTINI, S.; ET AL. Modeling and dynamics of a horizontal axis wind turbine. **Journal of Vibration and Control**, v.16(13), p. 2001–2021, 2010.

KRUG, F.; LEWKE, B. Electromagnetic interference on large wind turbines. **Energies**, v.2, p. 1118–1129, 2009.

KULUNK, E. **Aerodynamics of Wind Turbines, Fundamental and Advanced Topics in Wind Power**. Dr. Rupp Carriveau (Ed.), ISBN: 978-953-307-508-2, http://www.intechopen.com/books/fundamental-and-advanced-topics-in-wind-power/aerodynamics-of-windturbines, 2011.

KUSIAK, A.; ET AL. Dynamic control of wind turbines. **Renewable Energy**, v.35(2), p. 456–463, 2010.

LANZAFAME, R.; MESSINA, M. Fluid dynamics wind turbine design: Critical analysis, optimization and application of bem theory. **Renewable Energy**, v.32(14), p. 2291–2305, 2007.

LARSEN, J. W. **Nonlinear Dynamics of Wind Turbine Wings**. 2005. PhD thesis, Aalborg University.

LAURA, P. A. A.; GUTIERREZ, R. H. Vibrations of an elastically restrained cantilever beam of varying cross section with tip mass of finite length. **Journal of Sound and Vibration**, v.108(1), p. 123–131, 1986.

LEE, Y.-S.; ET AL. Reliability-based design optimization of monopile transition piece for offshore wind turbine system. **Renewable Energy**, v.71, p. 729–742, 2014.

LIECHTI, F.; ET AL. Modelling the spatial concentrations of bird migration to assess conflicts with wind turbines. **Biological Conservation**, v.162, p. 24–32, 2013.

LIU, Y. E. A. Advanced control design for wind turbines. **PAMM**, v.11(1), p. 823–824, 2011.

MAALAWI, K. Y. A model for yawing dynamic optimization of a wind turbine structure. **International Journal of Mechanical Sciences**, v.49(10), p. 1130–1138, 2007.

MANWELL, J. F.AND MCGOWAN, J. G.; ROGERS, A. L. **Wind Energy Explaned Theory, Design and Applications - Second Edition**. John Wlley and Sons Ltd, UK, 2009.

MÁRQUEZ-DOMÍNGUEZ, S.; SØRENSEN, J. D. Fatigue reliability and calibration of fatigue design factors for offshore wind turbines. **Energies**, v.5(6), p. 1816–1834, 2012.

MATHA, D.; ET AL. Efficient preliminary floating offshore wind turbine design and testing methodologies and application to a concrete spar design. **Philosophical transactions. Series A, Mathematical, physical, and engineering sciences, 28 Feb. 2015**, v.373(2035), 2015.

MEIROVITCH, L. **Principles and Techniques of Vibrations**. Prentice-Hall International, Inc., New Jersey, 1997.

NAGAYA, K. Transient response in flexure to general uni-directional loads of variable cross-section beam with concentrated tip inertias immersed in a fluid. **Shock and Vibration**, v.19, p. 37–56, 1986.

NEGRO, V.; ET AL. Uncertainties in the design of support structures and foundations for offshore wind turbines. **Renewable Energy**, v.63, p. 125–132), 2014.

PEDERSON, B. M.; SAYIGH, A. Wind turbine generators: state-of-the-art. **Solar & Wind Technology**, v.I(I), p. 37–48, 1984.

ROSE, S.; ET AL. Quantifying the hurricane risk to offshore wind turbines. **Proceedings of the National Academy of Sciences of the United States**, v.109(9), p. 3247–3252, 2012.

ROTH-JOHNSON, P.; ET AL. Structural design of spars for 100-m biplane wind turbine blades. **Renewable Energy**, v.71, p. 133–156, 2014.

SAAVEDRA-MORENO, B.; ET AL. Seeding evolutionary algorithms with heuristics for optimalwind turbines positioning in wind farms. **Renewable Energy**, v.36(11), p. 2838–2844, 2011.

SACHS, P. **Wind Forces in Engineering - 2nd Ed.** Oxford, U. K.: Pergamon Press, 1978.

SACRAMENTO, V.; ET AL. Integrity of an offshore structure subject to waves: a stochastic analysis. **Mecánica Computacional**, v.XXXII, p. 747–761, 2015.

SAMPAIO, R.; DE CURSI, E. S. **Uncertainty Quantification and Stochastic Modeling with Matlab®**. Elsevier, 2015.

SAMPAIO, R.; RITTO, T. G. **Short course on dynamics of flexible structures - Deterministic and stochastic analysis - Seminar on Uncertaity Quantification and Stochastic Modeling**, 2008.

SARKER, B. R.; FAIZ, T. I. Minimizing maintenance cost for offshore wind turbinesfollowing multi-level opportunistic preventive strategy. **Renewable Energy**, v.85, p. 104–113, 2016.

SEDAGHAT, A. Magnus type wind turbines: Prospectus and challenges indesign and modelling. **Renewable Energy**, v.62, p. 619–628, 2014.

SHABANA, A. A. **Dynamic of Multibody Systems**. New York: John Wiley and Sons, 1989.

SHANNON, C. A mathematical theory of comunications. **Bell System Tecnicall Journal**, v.27:379-423, p. 623–659, 1948.

SHEN, C.; MEISEN, P. **Various wind turbine technologies**. 1088 3rd Ave, San Diego, CA 92101, EUA: GENI - Global Energy Network Institute, 2012. 30p. Technical report.

STEPHEN, N. G. On the variation of timoshenko's shear coeffcient with frequency. **Journal of Applied Physics**, v.45, p. 695–697, 1978.

TAKAHASHI, K. Eigenvalue problem of a beam with a mass and spring at the end subject to an axial force. **Shock and Vibration**, v.71(3), p. 453–457, 1980.

THIEM, C. W. T.; ET AL. Stochastic analysis of wind turbine towers with lumped mass effect at the top on a flexible foundation. **Mecánica Computacional (AAMC)**, v.XXXIII, p. 1861–1875, 2014.

TIMOSHENKO, S. P. On the correction for shear of the differential equation for transverse vibrations of bars of uniform cross-section. **Philosophical Magazine**, v.744, 1921.

TIMOSHENKO, S. P. On the transverse vibrations of bars of uniform cross-section. **Philosophical Magazine**, v.125, 1922.

TOFT, H. S.; SØRENSEN, J. D. Probabilistic design of wind turbines. **Energies**, v.3(2), p. 241–257, 2010.

USLOWSKA, A.; KOLODZEJ, J. A. Free vibration of immersed column carrying a tip mass. **Journal of Sound and Vibration**, v.216(1), p. 147–157, 1998.

VEERS, P. Three-dimensional wind simulation. **SANDIA report, SAND88-0152 UC-261,Sandia National Laboratories - USA**, 1988.

VELDKAMP, H. F. **Chances in wind energy - A probabilistic approach to wind turbine design**. PhD. Thesis, Technische Universiteit Delft, Nederlands, 2006., 2006.

VISELLI, A. M.; ET AL. Estimation of extreme wave and wind design parameters for offshore wind turbines in the gulf of maine using a pot method. **Ocean Engineering**, v.August 1,104, p. 649–649, 2015.

WAKUI, T.; ET AL. Hybrid configuration of darrieus and savonius rotors for stand-alone windturbine-generator systems. **Electrical Engineering in Japan, (translated from Denki Gakkai Ronbunshi, Vol. 124-B, No. 2, February 2004, pp. 259-266)**, v.150(4), p. 13–22, 2005.

WANG, J.; QIN, D. ; LIM, T. Dynamic analysis of horizontal axis wind turbine by thin-walled beam theory. **Journal of Sound and Vibration**, v.329, p. 356–3586, 2010.

WANG, L.; ET AL. Comparative study on optimizing the wind farm layout using e design methods and cost models. **Journal of Wind Engineering & Industrial Aerodynamics**, v.146, p. 1–10, 2015.

WU, J.; CHEN, C.-T. An exact solution for the natural frequencies and mode shapes of an immersed elastically restrained wedge beam carrying an eccentric tip mass with moment of inertia. **Journal of Sound and Vibration**, v.286, p. 549–568, 2006.

WU, J.; HSU, S. An unified approach for the free vibration analysis of an elastically supported immersed uniform beam carrying an eccentric tip mass with rotary inertia. **Journal of Sound and Vibration**, v.291, p. 1122–1147, 2006.

YANG, H.; ; ET AL. Dynamic reliability based design optimization of the tripod sub-structure of offshore wind turbines. **Renewable Energy**, v.78, p. 16–25, 2015.

ZAAIJER, M. B. Foundation modeling to assess dynamic behavior of offshore wind turbines. **Journal of Applied Ocean Research**, v.28, p. 45–57, 2006.